

CONFIDENTIAL

**STEEL FIBRES FROM WASTE TYRES TO CONCRETE;
TESTING, MODELLING AND DESIGN**



BY

DIPL. - ING. HOUSSAM TLEMAT

A thesis submitted for the degree of Doctor of Philosophy in the faculty of
Engineering of the University of Sheffield

Centre for Cement and Concrete
Department of Civil and Structural Engineering
University of Sheffield

May 2004

Dedicated to my parents, my wife and my three children

ABSTRACT

The disposal of waste tyres and steel fibres from tyres is a serious worldwide environmental problem. This thesis examines the use of steel fibres extracted from waste tyres as reinforcement for concrete. Previous attempts to use such fibres with concrete ended up in balling of the fibres and wasting of the concrete.

Four concrete mixes using three different types of fibres (from shredded tyres, from pyrolysis and commercially available fibres) were developed. An optimisation procedure was used to maximise the amount of fibre used whilst maintaining a reasonable degree of workability.

Single and double sided pull-out tests were developed to determine the anchoring characteristics of fibres. Double-sided tests with multi-fibres were found to be the most reliable. The anchoring characteristics of tyre fibres were found to be as good as for commercially available fibres. Critical fibres lengths were determined for the different fibres used. A simple fibre pull-out model is proposed.

Flexural toughness tests were developed and optimised based on the ASTM and Japanese standards. The crack development, neutral axis depth and characteristic length were examined in detail. An examination of the RILEM σ - ϵ model has shown that the model can overestimate the flexural capacity of Steel Fibre Reinforced Concrete (FRC).

New σ - ϵ models were derived by adopting inverse analysis techniques on results from flexural tests on notched beams. These models when used with Finite Element Analysis (FEA) can predict the behaviour of the tested prisms accurately. For design purposes the models have been simplified. Parametric studies led to design equations which predict the design moment by using a fibre parameter (relating to length and bond) and the fibre amount by weight. The design equations are applied in several applications including the design of slabs on grade. The results compare favourably with existing design guidelines.

Finally, slabs for drainage covers were designed and tested, demonstrating that fibres from tyres can be used for industrial applications.

ACKNOWLEDGEMENT

I would like to express my deepest gratitude and appreciation to Professor Kypros Pilakoutas, for his supervision, continuous help, support, inspiration, encouragement and constructive criticism during the preparation of this thesis. I am also grateful to Dr Roger Crouch for his assistance in FE-Analysis and Dr Kyriacos Neocleous for his advises, cooperation and the joined publications.

I am grateful to all technical staff in the Structures Laboratory for their expert technical support. Particular thanks go to S. Smith, J. Wood, C. Todd and R. Grace for their support and help during the experiments.

I also wish to acknowledge the University of Sheffield and the UK Government's Department of Trade and Industry for the partners in Innovation project "Demonstrating steel fibres from waste tyres as reinforcement in concrete" (contract: CI 39/3/684, cc2227) for their financial support.

I am deeply indebted to my family, my wife and my children for their unconditional love, support and patience during the three years of research.

TABLE OF CONTENTS

ABSTRACT	I
ACKNOWLEDGMENTS	II
TABLE OF CONTENTS	III
ABBREVIATIONS	X
NOTATION	XI
TABLE OF CONTENTS	III
1 INTRODUCTION	1
1.1 Introductory Remarks	1
1.2 Aim and Objectives	5
1.2.1 Fibre Characterisation Tests	5
1.2.2 Fibre Reinforced Concrete	6
1.2.3 SFRC Characterisation Tests	6
1.2.4 Analytical Study	6
1.2.5 Testing of Prototypes	6
1.3 Research Method	6
1.3.1 Fibre Characterisation Tests	7
1.3.2 Fibre Reinforced Concrete	7
1.3.3 SFRC Characterisation Tests	7
1.3.4 Testing of Prototypes	8
1.3.5 Analytical and Numerical Work	8
1.4 Layout of the Thesis	9
2 LITERATURE REVIEW	11

2.1	Waste-Tyre Management and Recycling Techniques	11
2.1.1	Tyre Structure and Constituents	13
2.1.2	Tyre Recycling Techniques	14
2.1.2.1	Shredding Process	14
2.1.2.2	Microwave Induced Pyrolysis Process	16
2.2	SFRC Types and Applications	17
2.2.1	Types of Steel Fibres	18
2.2.2	Cast-in-situ Applications	19
2.2.3	Precast Applications	20
2.2.4	Sprayed Concrete Applications	21
2.2.5	Applications of Slurry Infiltrated Fibre Concrete	22
2.3	Mechanical Properties of SFRC	22
2.3.1	General	22
2.3.2	Properties of Freshly-Mixed SFRC	23
2.3.3	Behaviour under Compressive Force	24
2.3.3.1	Compressive Strength and Strain	25
2.3.3.2	Fibre Content and Aspect Ratio	26
2.3.3.3	Effects of Specimen Size, Shape and Mould Material	26
2.3.3.4	Process of Compressive Cracking in SFRC	27
2.3.4	Bond Behaviour of SERC	28
2.3.4.1	Interfacial Bond Stresses	29
2.3.4.2	Mechanical Behaviour of Pullout	29
2.3.4.3	Factors Affecting the Fibre-Matrix Bond	30
2.3.4.4	Analytical Models	32
2.3.4.5	Experimental Investigations on Pullout of SFRC	33
2.3.5	Behaviour under Direct Tensile Force	34
2.3.5.1	The Effect of Fibre Content	34
2.3.5.2	Critical Fibre Content	34
2.3.5.3	Experimental Evaluation	35
2.3.5.4	Theoretical Evolution of the Tensile-stress Curve	35
2.3.6	Flexural Behaviour and Testing	36
2.3.6.1	Flexure Toughness Standards and Guidelines	36
2.3.6.2	Discussion on Standards of Practice	40
2.3.6.3	Notched Beam Test for Toughness Characterisation	43
2.4	Modelling and Design of SFRC	44
2.4.1	Fracture Mechanics Models	44

2.4.1.1 Fictitious Crack Model (FCM)	44
2.4.1.2 Two Parameter Fracture Model (TPM)	45
2.4.1.3 Crack Mouth Opening Displacement (CMOD) Concept	45
2.4.1.4 Stress-block Models	47
2.4.2 Design Methods	48
2.4.2.1 Introduction	48
2.4.2.2 σ - ϵ Design Method	48
2.4.2.3 Finite Element Analysis of SFRC	52
2.5 Research and Development Needs	56
3 FIBRE CHARACTERISATION, CONCRETE MIX DEVELOPMENT AND OPTIMISATION	58
3.1 Introduction	58
3.2 Materials Used	59
3.2.1 Ordinary Portland Cement	59
3.2.2 Aggregates	60
3.2.3 Superplasticizer	61
3.3 Steel Fibres	62
3.3.1 Steel Fibres from Shredded Tyres	62
3.3.2 Steel Fibres from the Pyrolysis Process and Virgin Cord	64
3.3.3 Industrially Available Steel Fibres	64
3.3.4 Density of Steel Fibres	65
3.4 Production of FRC	66
3.4.1 Mix Design	66
3.4.2 Specimen Used and Curing Regimes	67
3.5 Mix Optimisation	68
3.5.1 Introduction	68
3.5.2 Compressive Tests	68
3.6 Results and Discussion	68
3.6.1 Fresh Concrete	68
3.6.1.1 Optimisation of Shredded Fibre Content	69
3.6.1.2 Optimisation of PRSF Fibre Content	71
3.6.1.3 Optimisation of VSF, ISF-1 and ISF-2 Fibres	74

3.6.1.4	Ultra High Strength Concrete with PRSF Fibres	75
3.6.2	Compressive Strength of the Mixes	75
3.7	Chapter Summary	77
4	PULL-OUT BEHAVIOUR OF RSF AND ISF	79
4.1	Introduction	79
4.2	Experimental Work	80
4.2.1	Single-sided Pull-out Tests	80
4.2.1.1	Specimen Preparation	82
4.2.1.2	Testing procedure	84
4.2.2	Double-sided Pull-out Tests	84
4.2.2.1	Specimen Preparation	85
4.2.2.2	Testing Apparatus	87
4.3	Results and Discussion	88
4.3.1	Single-sided Pull-out Tests	88
4.3.1.1	Pull-out Tests Using Load Spring	88
4.3.1.2	Pull-out Tests Using Load Cell	91
4.3.1.3	Comment on the Pull-out Behaviour	95
4.3.2	Double-sided Pull-out Tests	97
4.3.2.1	PRSF and ISF	97
4.3.2.2	SRSF	100
4.4	Theoretical Modelling of Bond-Slip	101
4.4.1	ISF Fibres	101
4.4.2	PRSF Fibres	102
4.5	Pull-out Test Conclusions	104
4.6	Summary	105
5	FLEXURAL TOUGHNESS BEHAVIOUR OF RSFRC	106
5.1	Introduction	106
5.2	Description of Flexural Toughness Tests	107
5.2.1	Unnotched Beams	108
5.2.1.1	Testing Procedure	108

5.2.2	Notched Beams	108
5.2.2.1	Specimen Preparation	109
5.2.2.2	Testing Procedure	110
5.3	Test Results	111
5.3.1	Compressive Strength	111
5.3.2	Flexural Strength - Unnotched Beams	112
5.3.2.1	Effect of Fibre Volume	114
5.3.2.2	Effect of Fibre Type	114
5.3.2.3	Effect of Concrete Strength	114
5.3.2.4	Effect of Fibre Length	115
5.3.3	Flexural Strength - Notched Beam	118
5.3.3.1	Flexural Strain and Crack Measurements	122
5.3.3.2	Position of Neutral Axis Depth	124
5.3.3.3	Parameters for the Determination of Stress-strain Relationship	126
5.3.3.4	Discussion on Parameters	130
5.4	Analytical Investigation of RILEM Stress-strain Approach	132
5.5	Conclusions	133
6.	ANALYSIS AND DESIGN	135
6.1	Introduction	135
6.2	Finite Element Analysis	136
6.2.1	Element Type Used	136
6.2.2	SFRC Model and Inverse Analysis	137
6.2.2.1	Compressive Characteristics	137
6.2.2.2	Shear Retention	138
6.2.2.3	SFRC Tensile Characteristics	139
6.3	FE Sensitivity Analysis and Results	140
6.3.1	Discussion on the SFRC tensile behaviour	142
6.3.2	Discussion on the Analytical Results	146
6.3.2.1	Deflection-strain, Deflection-neutral Axis	146
6.3.3	Mesh Independent Stress-strain Relationship	147
6.4	New Design Model	151
6.5	Design Tools	157

6.5.1	Stress Reduction Factors	157
6.5.2	Serviceability Limit State	158
6.5.3	Ultimate Limit State	160
6.6	Design of FRC Industrial Floor	162
6.6.1	Design Models for Sub-grade	163
6.6.2	Design of Sub-bases	164
6.6.2.1	Design Approach by Bekaert (1999)	164
6.6.2.2	Modified Design Approach	167
6.7	Conclusions	168
7	CONCRETE SLABS	170
7.1	Introduction	170
7.2	Experimental Program	171
7.2.1	Materials Used	172
7.2.2	Production of Slabs	174
7.2.2.1	Mix Design and Casting	174
7.2.2.2	Curing Regimes	178
7.2.3	Testing Procedure	178
7.3	Results and Discussion	179
7.3.1	Cube Test Results	179
7.3.2	Flexural Behaviour of SIScon Slab	180
7.3.3	Flexural Behaviour of Rcon Slabs	183
7.3.4	Flexural Behaviour of Pcon Slab	186
7.3.5	Flexural Behaviour of Scon Slab	187
7.4	Equivalent Flexural Strength	189
7.5	Conclusions	190
8.	CONCLUSIONS AND RECOMMENDATIONS	192
8.1	Conclusions	192
8.1.1	Part 1: Experimental Investigations	192
8.1.1.1	Fibre characterisation, Concrete Mix Development and Optimisation	192
8.1.1.2	Pull-out Tests	193

8.1.1.3	Flexural Toughness Tests Using Unnotched Beams	194
8.1.1.4	Flexural Toughness Tests Using Notched Beams	195
8.1.1.5	Concrete Slab Tests	196
8.1.2	Part 2: Analytical Study and Design	197
8.2	Recommendation for Further Study	198
8.2.1	Improving the Recycling Processes and the Quality of the Recycled Fibres	199
8.2.2	Improving The Experimental Data	199
8.2.3	Improving the Analytical Investigation and the Proposed Design method	200
REFERENCES		201
APPENDIX		A-1
Appendix A		A-1
A.1	Fresh and Hardened Properties	A-1
Appendix B		A-3
B.1	Data from Pull-out Tests	A-3
Appendix C		A-7
C.1	Load-deflection responses of the notched beam tests	A-7
C.2	Visual Basic Routine fro Data Filtering	A-11
C.3	Visual Basic Routine to Calculated the Average of Three Curves	A-12
C.4	Results of compressive tests for notched beams	A-13
Appendix D		A-14
D.1	Results of the FE analysis	A-14
D.2	ABAQUS input file for mesh (b), 25mm	A-17
D.3	Critical lengths	A-17
D.4	ABAQUS input file for mesh (c), 12.5 mm	A-19
D.5	ABAQUS input file for mesh (a), 50mm	A-21
D.6	ABAQUS input file for beam element	A-23
Appendix E		A-14
E.1	Images related to chapter flexural tests	A-14
E.2	Images relating to slab tests	A-29
Appendix F		A-31

ABBREVIATIONS

ACI	American Concrete Institute
ASTM	American Standards for Test Method
BOP	Bend-Over-Point
BS	British Standard
CMOD	Crack Mouth Opening Displacement
EC	Euro Code
FEM	Finite Element Method
FPcon	Flexural test for Pyrolysed Recycled Steel Fibre (PRSF) concrete slab
FScon	Flexural test for Shredded Recycled Steel Fibre (SRSF) concrete slab
FSIScon	Flexural test for Slurry Infiltrated Shredded concrete slab
ISF-1	Industrial Steel Fibres with a flatted end.
ISF-2	Industrial Steel Fibres with hocked end.
JSCE	Japan Society of Civil Engineers
OPC40	Ordinary Portland Cement, 40 MPa
OPC50	Ordinary Portland Cement, 50 MPa
OPC40S:	OPC40 reinforced with SRSF
OPC40A	OPC40 reinforced with PRSF
PRSF	Steel fibre from the pyrolysis process
Pcon	Concrete slabs reinforced with pyrolysed fibres
RSF	Recycled Steel Fibres
Rcon	Concrete slabs reinforced with Re-bars
Scon	Concrete slab reinforced with Shredded fibres
SFRC	Steel Fibre Reinforced Concrete
SIScon	Slurry infiltrated concrete slab reinforced with shredded fibres
SLS	Serviceability Limit State
ULS	Ultimate Limit State
SP	Superplasticizer
SPFA 40/30	Superpozzolan Fly Ash 40MPa / 30% by cement weight
SPFA/MS 120/20/10	Superpozzolan Fly Ash (20%) / Micro-silica (10%), 120 MPa
SRSF	Shredded fibre from shredded process.
Vol	Volume
VSF	Industrially available virgin tyre cord.

NOTATION

Forces

F_u	[kN]	Load at limit of proportionality
P_{peak}	[kN]	Load at peak load
P_s	[kN]	Load applied to the slab
M_0	[kNm]	Yield moment
m	[-]	Normalised moment
M_u	[kNm]	Moment at limit of proportionality
$D_{BZ,2}, D_{BZ,3}$	[Nm]	Energy absorption capacities
$A_{\sigma-\epsilon}$	[N/mm ²]	Area under the stress-strain curve
A_F	[Nm]	Area under the load deflection curve
f_{cm}	[MPa]	Measured mean compressive cube strength
f_{cd}	[MPa]	Design compressive strength of the concrete
f_{fcm}	[Mpa]	Mean compressive cylinder strength
$f_{fct,u}$	[N/mm ²]	Limit of proportionality
$f_{eq,2}, f_{eq,3}$	[N/mm ²]	Equivalent flexural tensile strengths
$f_{R,1}, f_{R,4}$	[N/mm ²]	Residual flexural tensile strengths at 0.5mm and 3.5mm crack width
$GF1$	[Nmm]	Fracture energy released rate
G_{F2}	[Nmm ⁻¹]	Surface fracture energy released per unit area
$\sigma'_{t,p}$	[N/mm ²]	Maximum tensile stress for plain concrete
$\sigma'_{t,inp}$	[N/mm ²]	Input ultimate tensile strength
σ_n	[N/mm ²]	Normalised against σ'_t

Stiffness and Strains

E_{cm}	[N/mm ²]	Secant modulus of concrete in compression,
E_f	[N/mm ²]	Effective young's modulus of fibre
E_s	[N/mm ²]	Modulus of soil elasticity
C	[N/mm ³]	Modulus of subgrade
G_C	[N/mm ²]	Shear modulus of intact concrete is
G_R	[N/mm ²]	Reduced shear modulus of cracked concrete
ϵ	[%]	Strain normal to the crack direction,
$\epsilon_{c1,ai}$	[%]	Compressive strain at first crack
ϵ_{max}	[%]	Strain at which the concrete tensile stress reduces to zero.

$\varepsilon_{i,inp}^u$	[‰]	Input ultimate tensile strain
$\varepsilon_{t1,si}$	[‰]	Tensile Strain at first crack
k	[N/mm ³]	Modulus of subgrade reaction

Geometric Values

A_f	[mm ²]	Effective cross-section area of the PRSF
b	[mm]	Width of the specimen
d	[mm]	Diameter of the slab
h	[mm]	Depth of the beam cross section
l_{ch}	[mm]	Characteristic length
h_{GP}	[mm]	Height of Gaussian point
L	[mm]	Support span
l_c	[mm]	Critical length
l_e	[mm ⁴]	Radius of elasticity for elastic subgrade
l_{GP}	[mm]	Length of Gaussian point
l_{el}	[mm]	Element length in crack direction
L_{emb}	[mm]	Fibre embedment length
l_{free}	[mm]	Fibre length between grip and specimens
h_{sp}	[mm]	Distance between the notch tip and the top of the cross section
s	[mm]	Length of the hinge.
δ	[mm]	Deflection
δ_{cal}	[mm]	Calculated deflection
δ_{el}	[mm]	Elastic deflection
δ_{exp}	[mm]	Measured deflection
δ_w	[mm]	Deflection after cracking
$w_{i,c}$	[mm]	Deformation measured after crack initiation,
y	[-]	Position of the normalised neutral axis
w	[mm]	Crack width

Factors

ρ^{close}		Full shear retention
θ		Reduction factor which represents the difference between the dislocation under the load and mid-span deflection
V	[%]	Fibre ratio by weight
ϕ		Stress reduction factor represents stress drop in the σ - ε curve

ξ	Factor reflects the influence of the fibre type on the tensile softening
α_{cl}^f	Durability reduction factor
α_{sys}	Size effect factor
γ_{cl}^f	Safety factor in tension
γ_c^f	Safety factor in compression
ν_s	Poisson ratio
a_r	Contact radius of load
$R_{e,3}$	Ductility factor
γ_p	Load safety factor

1 INTRODUCTION

1.1 INTRODUCTORY REMARKS

Disposal of used tyres constitutes a significant worldwide environmental problem. In particular illegal dumping and burning of tyres (Figure 1.1).



Figure 1.1 Illegal dumping and burning of tyres

Already identified as an EU priority waste stream, there are currently some 2.5M tonnes of used tyres arising per year in the EU. This amount is expected to rise to around 3.5M tonnes by 2008 (ETRA, 2001). The UK government developed a national waste strategy to comply with the requirement of the 1999 EU Landfill Directive, which prohibits the disposal of waste tyres to landfill since July 2003 and any part of used tyres by 2006 (Landfill Directive, 1999).

To deal with waste tyres, at the moment, there are a number of industrial reduction processes (e.g. pyrolysis and shredding process) which aim primarily to recover the

rubber, but do not make use of the steel extracted from the waste tyres (RSF) such as shown in Figure 1.2.



Figure 1.2 Steel fibres derived from used tyres (Left-Shredding process, Right-Pyrolysis)

It is estimated that up to 60,000 tonnes of high quality steel fibres from tyres are disposed annually in the UK alone. Hence, there is an urgent need for the development of products and markets which require steel fibres as a secondary raw material.

The construction industry is a possible market for these fibres. About 12M tonnes of reinforcement bar (re-bar) is used per annum by the EU concrete industry (1 M in UK). The use of steel fibres in the EU concrete market is currently 150-200k tonnes per annum (15-20k in UK), (SYEP, 2001). By proving that steel fibres from used tyres are fit for specific concrete reinforcement applications, they could be used in a range of existing applications (e.g. industrial floors, pre-cast concrete and foundations) to replace the commercially available steel fibres (ISF) or re-bar. In addition, they could provide an alternative to the use of virgin materials, assist in diverting waste from landfill and provide an incentive to reduce fly tipping.

Many types of materials have been used as fibre reinforcement in cement and concrete, such as glass, polymers, asbestos and ceramics. The low elastic modulus of these reinforcing materials means that they can predominantly only increase the toughness of the concrete, but not necessarily its strength. Steel, on the other hand, has a very high modulus of elasticity and better bond interaction with concrete, due to the good anchoring characteristics. Hence, steel fibres are used in many different

applications in concrete. Another benefit of adding steel fibres to concrete is crack control (structural as well as from plastic settlement and shrinkage), and enhancement of its surface characteristics. Other benefits include: lower permeability and increased freeze/thaw durability.

However, before fibres from waste tyres can be used in concrete several problems need to be addressed:

- high levels of impurities (either rubber or carbon black)
- fibres such as shredded fibres are tangled together, and are slightly magnetised
- the fibres come in a variety of different lengths, diameters, strength and ductility

The Centre for Cement and Concrete of the University of Sheffield is currently the only research establishment in Europe, working together with many industrial partners in this field, trying to demonstrate and encourage the use of RSF as reinforcement in concrete (Tlemat and Pilakoutas 2002(a, b), Tlemat, Pilakoutas and Neocleous 2003 (a, b, c), Tlemat, Pilakoutas and Neocleous 2004 (a, b, c, d), Neocleous, Pilakoutas and Tlemat 2004) and the University of Sheffield has applied for a patent to cover the use of tyre-RSF as concrete reinforcement (TWRC, 2001). The work is funded by the DTI Partners in Innovation programme and by the European Union Marie-Curie Programme. The DTI project funded part of the experimental work reported in this thesis.

The major scientific challenges being dealt with are categorising and characterising waste fibres in a consistent and reliable manner and the development of material laws for use in FEA.

Statistical techniques need to be adopted to sample and analyse the characteristics of fibres from various sources. These are needed not only to convince the industry to adopt these fibres in construction, but also to reduce the uncertainty later on in design.

The other major problem in making concrete with these fibres is minimising the “balling” of the fibres during mixing. This is an issue that will determine what percentage of fibre can be included in concrete. The higher the percentage of fibres, the better the quality of the concrete in respect to strength and toughness.

To achieve optimum fibre content, there is a need for two parameters to be identified. The first, relates to the optimum fibre length and the second to the density distribution of the length to diameter ratio. Long lengths are required to enhance fibre anchorage, but they also cause balling. Long fibres are the fibres that offer the most efficient control of concrete macro-cracks, but short fibres can help in controlling micro-cracks.

In addition to fibre characteristics, concrete characteristics also influence the behaviour of steel fibre reinforced concrete (SFRC). Larger aggregates restrict the arrangement of fibres and, hence, increase the tendency for balling. The introduction of fibres also reduces workability and fine particles in the form of “Pulverised Fuel Ash” can help to redress this problem.

Hence, to develop good SFRC mixes both suitable fibres and suitable concrete constitution needs to be determined. In both cases, experimentation needs to take place. This need to be done in a parametric manner.

The next stage should involve the development of tests that will classify the SFRC characteristics both at the fresh and hardened state. Standard tests already exist, but they are based on the use of industrial fibres. These tests have to be assessed and if necessary modified to accommodate the variety of different fibre characteristics that arise from tyres. This work will therefore try and build on existing knowledge so as to end up producing design guidelines for SFRC and RSF reinforced concrete (RSFRC).

Advanced analytical tools need to be developed to enable the use of SFRC in complex structures. For advanced analysis, accurate material constitutive models are required. A special FEA updating technique which uses experimental data to incrementally determine the material stress-strain relationship without

predetermining the shape is one way of progressing the state-of-the-art in this field. Such techniques are currently being used in the characterisation of structures through “Dynamic Updating”.

To validate the work undertaken, small demonstration products should also be designed and tested.

This is a highly original and innovative research, since for the first time waste tyre fibres are developed for use in the construction industry. The use of cord wire such as Pyrolysed RSF (PRSF) fibre or very thin steel fibres such as shredded RSF (SRSF) as reinforcement in concrete is not reported in the literature.

1.2 AIM AND OBJECTIVES

The overall objective of this research is to develop tests that will help enable a better understanding of bond and strength characteristics of RSF and the fresh and hardened properties of RSFRC, so as to ease the way for the use of steel fibres from waste tyres as reinforcement in concrete. Experimental investigations will provide data that can be used for the analytical studies and the development of design tools. Material laws will be developed for use in FEA which can then be used to design complex structural elements. The specific research objectives are the following:

1.2.1 FIBRE CHARACTERISATION TESTS

- Determine the fibre mechanical properties
- Develop pull-out tests for fibre anchorage in concrete
- Develop basic fibre characterisation procedures
- Propose fibre critical lengths

1.2.2 FIBRE REINFORCED CONCRETE

- Develop concrete mixes with different types of fibres
- Establish workability requirements and mixing procedures

1.2.3 SFRC CHARACTERISATION TESTS

- Examine the suitability of available standard flexural tests (RILEM, ASTM, JSCE)
- Adopt or propose tests for different types of fibres

1.2.4 ANALYTICAL STUDY

- Compare results with predictions using existing design equations
- Use experimental data to develop material laws for use in FE-analysis
- Validate the analytical tools

1.2.5 TESTING OF PROTOTYPES

Design and produce prototypes for testing and analysis

1.3 RESEARCH METHOD

The research adopts an intersectorial approach, since information needs to be gathered from policy makers, manufacturers of tyres, industry dealing with recycled tyres and environmental bodies as well as from the industry dealing with steel fibre reinforcement concrete.

1.3.1 FIBRE CHARACTERISATION TESTS

Statistical analysis was undertaken to determine the ranges of fibre diameters and lengths from at least two different processes (shredding and pyrolysis). Samples of fixed quantities were obtained from the factories at predetermined intervals.

The density of the steel fibre was determined using standard techniques. This helped determine the amount of impurities present with the fibre.

Special test-rigs were developed for the determination of the fibre properties and anchorage characteristics. The main problem with single fibre tests is their reliability, as well as the ability of conventional (for civil engineering purposes) instrumentation to measure small displacements at small loads.

To improve the reliability of pull-out tests, both single and multiple fibre pull-out tests were developed. To improve the accuracy of the results, suitable instrumentation was developed using load-cells of the requisite sensitivity.

1.3.2 FIBRE REINFORCED CONCRETE

The mix optimisation was undertaken by trying to incorporate as much fibre as possible without attaining fibre balling, and to maintain a slump value over 50 mm.

The concrete mix was varied and the main parameters included: aggregate type, size and proportion, PFA type and proportion, water cement ratio and fibre content. Different mixing sequences were studied, and trials were made on slurry infiltrated FRC.

1.3.3 SFRC CHARACTERISATION TESTS

The characterisation of the properties of SFRC is important for understanding the benefits of fibre reinforcement and for the development of design guidelines.

Although the addition of steel fibres results in strength enhancement of the tensile region of SFRC, direct tension tests are not always used to assess this enhancement. This is because these tests are not easy to perform and SFRC structural elements are rarely subjected to direct tension. Hence, the preferred tests for SFRC are in general flexural tests, through which the toughness of SFRC is measured. There are several international committees (such as RILEM, 2002, ASTM C1018, 1995 and JSCE-SF4, 1994), which have produced standards or recommendations for testing conventional steel fibres. These tests were assessed for suitability with recycled steel fibres.

The main problem of conventional tests is that they rely on specific key deformations on which the toughness characteristics are determined. These key deformations in some standards are arbitrarily selected based on calibration with test data on conventional fibres. Clearly there is a need to make these key deformations independent of the fibre characteristics and more reliant on key service deformations such as crack width.

The characterisation tests also need to have a direct link to design guidelines and this is done through the utilisation of guidelines already being developed at the University of Sheffield.

1.3.4 TESTING OF PROTOTYPES

To demonstrate that recycled steel fibres can be a viable alternative to manufactured fibres, manhole covers (with complicated geometry and reinforcement details) were designed and tested to destruction.

1.3.5 ANALYTICAL AND NUMERICAL WORK

The stress-strain characteristics of SFRC were considered to be unknown and were determined by back-analysis and updating. Stress-strain curves were obtained for all the tested fibres and this placed an extra demand for highly accuracy measurements.

The research aimed to de-couple the effect of various parameters (such as fibre type, concrete mix, fibre ratio by weight) and develop general material laws.

1.4 LAYOUT OF THE THESIS

The thesis is organised as follows

Chapter two, section one presents a state-of-the-art of issues relating to recycling of used tyres. The environmental impact of used tyres and the existing waste management of used tyres in the UK are presented. In addition, the barriers affecting the recycling of used tyres in the UK are examined.

The mechanical and chemical processes currently utilised for the recycling of used tyres are also elaborated.

The mechanical properties of SFRC are presented in section three of chapter 2. This includes the methods used for the experimental evaluation of these properties. Section four of chapter 2 presents the theoretical models developed for the modelling of the mechanical behaviour of SFRC. This section also includes a brief presentation of the design guidelines that are based on these theoretical models. The last section of chapter two discusses exciting numerical analysis methods.

Chapter three reports on the experimental investigation associated with fibre characterisation, mix methods and optimisation and fresh and hardened properties of SFRC using recycled steel fibres.

Chapter four describes the single-sided fibre pull-out tests (78 tests using load spring and 59 tests using load cell) and 81 double-sided pull-out tests (using plain concrete specimens) undertaken on industrial and recycled steel fibres.

The description of ten flexural toughness characterisation test series is presented in the first part of chapter five. This part mainly presents the methods of calculating the flexural toughness according to existing recommendations. In the second part of this

chapter ten series of tests on notched prisms reinforced with industrial and recycled steel fibres using four-point bending tests are presented. The load-deflection and load-crack width data obtained from these test are analysed and used in an analytical study.

Chapter six deals with the problems of current analytical techniques and identifies the need for stable numerical analysis to back calculate the uniaxial stress-strain curve for SFRC in tension. An FE package is used to simulate the behaviour of the notched beams. The predicted stress-strain curves are presented and a design model is proposed dealing with serviceability and ultimate limit states for flexural design. It is demonstrated that this model can be used to design a variety of elements including slabs on grade.

Chapter seven presents the design and manufacture of prototypes (manhole covers) as an example of SRSF in construction. Four sets of manhole slabs reinforced with re-bars and recycled fibres were tested.

Conclusions and recommendations for future research are presented in chapter eight.

2 LITERATURE REVIEW

This chapter presents relevant literature on tyre recycling and steel fibre reinforced concrete (SFRC) in six sections. In the first section, the tyre structure and tyre recycling techniques are examined, with the aim to introduce the sources of fibres used in this investigation. In the second section, a general presentation of SFRC and its applications is given. In the third section, the fresh and hardened mechanical properties of SFRC are reported. The standards tests used to identify those properties are also examined. In the fourth section, the available design recommendations and other theoretical models together with their limitations are presented and analysed. In the fifth section, an introduction is given of the Finite Element Analysis (FEM) for SFRC. Finally in the last section, the author identifies areas on the testing, design and modelling of SFRC that need further investigation.

2.1 WASTE-TYRE MANAGEMENT AND RECYCLING TECHNIQUES

The environmental impact of waste is high on the political agenda, and environmental legislation is being used as a means of reducing waste and its impact on the environment and to encourage recycling. Following EU directives, in particular the 1999 EU landfill directive (EULD, 1999), the United Kingdom (UK) government developed a new national waste strategy (WS-2000, 2000; Strategy Unit, 2002). The main aims of this strategy are to reduce the waste growth rate, to increase re-use, recycling, composting and to stimulate innovation in waste treatment. With regards to recycling, the new strategy aims to attain a national recycling rate of 45% by 2015 and thus, waste recycling presents a significant opportunity for making waste management processes more sustainable.

One type of waste considered by the UK government is that arising from used tyres (Fig. 2.1), since by 2006 no part of tyres would be allowed in landfill (EULD, 1999). The UK government and industry 'Used Tyre Working Group' (UTWG, 2001) estimates that more than 400,000 tonnes of used tyres are discarded annually in the UK; more than half of these tyres are either sent to landfill or used for energy recovery. The amount of used tyres in the UK is expected to increase further by 2008, as the EU end-of-life vehicle directive (EUELV, 2000) will be fully implemented.



Figure 2.1 Used tyres dumped in stockpiles (source: www.ntsua.org)

To comply with the two EU directives, the UK needs to develop markets (which will utilise used tyres as a secondary raw material) to accommodate the amount of tyres (around 130,000 tonnes for year 2000) that are not re-used or recycled. The need for developing new markets is also justified by the growing environmental concerns on the more popular option of energy recovery in cement kilns, due to the release of pollutants in the environment. A typical example of these concerns is the 2000 EU directive on waste incineration (EUWD, 2000), which aims at reducing by 90% the dioxin emissions of identified sources by 2005.

Whilst there is demand and established markets for the granulated rubber (Abbot, 2001; WasteGuide, 2003), which could be extracted by mechanical processes, the remaining steel is either being used as scrap feed in steel kilns or disposed to landfill due to health and safety issues regarding the storage of the steel fibres.

2.1.1 TYRE STRUCTURE AND CONSTITUENTS

A modern tyre consists of rubber compound usually reinforced with steel and textile. Until the 1970s, tyres were of cross ply construction, but they have now been almost completely replaced by the radial tyre (Fig. 2.2). Cross ply tyres have a number of layers of reinforcement arranged in criss-cross pattern at a particular angle, while in radial tyres the reinforcement layers run perpendicular to the travel direction. Radial tyres are more flexible, have a lower rolling resistance and are more durable than cross-ply tyres.

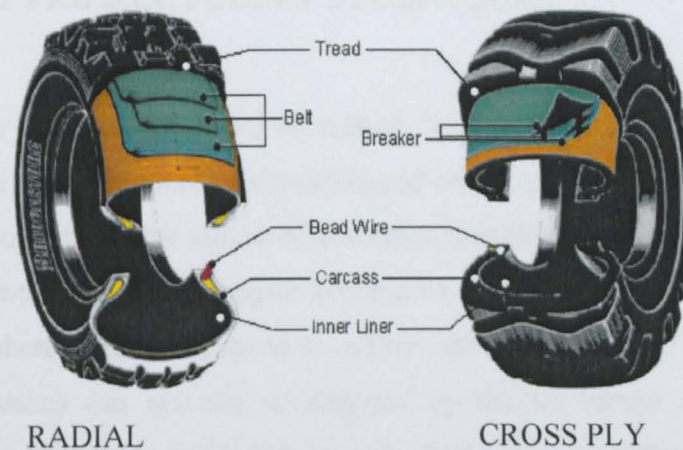


Figure 2.2 Types of tyres (source: www.bridgestone-eu.com)

Tyres vary in weight between 7 kg for a car to 60 kg for a truck or a lorry. The calorific value of a tyre is around 30 to 35 MJ per kg (8.3 to 8.5 kWh per kg), which means that used tyres have greater energy content than wood or coal.

The principal raw materials for modern tyre production are rubber compounds kept together with steel and textile reinforcement. The proportions of rubber, steel and textile vary with construction and tyre type (for example car or truck). Table 1 shows the approximate proportions of rubber, steel and textile in car and truck tyres (Department of the Environment and the Welsh Office, 1995).

Table 1 Main constituents of car and truck tyres by weight

Vehicle type	Tyre type	% Rubber	% Steel	% Textile
Car	Steel-braced radial	86	10	4
	Textile-braced radial	90	3	7
	Cross-ply	76	3	21
Truck	All-steel radial	85	15	< 0.5
	Cross-ply	88	3	9

Tyres contain different types of fibres according to the particular purpose of the tyre. Some tyres have cords made of nylon, polyester, and kevlar and other have steel.

2.1.2 TYRE RECYCLING TECHNIQUES

Used tyres are either reduced to rubber “crumb” and steel fibres by means of mechanical recycling (such as shredding and cryogenic processes) or reduced to their chemical constituents by means of anaerobic thermal degradation (such as pyrolysis and microwave induced pyrolysis processes). The feasibility of a new mechanical process (where tyres are reduced to rubber crumb and steel by means of ultra high water pressure) was recently investigated by the University of Salford (UTWG, 2001). However, there are not yet any published results regarding this process.

2.1.2.1 Shredding Process

The shredding process reduces tyres into rubber and steel through a number of stages, the number of which depends on the size desired for the rubber end-product. In the first stage of processing, a complete tyre is chopped or shredded until it is reduced to pieces ranging in size from about 50 to 150 mm (see Figure 2.2). The rubber, which still contains steel, can be used as tyre derived fuel (TDF) and possibly as fill to assist drainage. Unless destined for these limited uses, the rubber pieces are normally then fed into a second shredder which reduces them to smaller pieces. The rubber crumb is then fed into a knife or hammer mill where it is pulverised to approximately 1 to 10 mm in size.



Figure 2.2 First shredding processes (source Charles Lawrence Recycling Ltd)

By the second stage of shredding, the steel fibres have been subjected to the chopping, shredding, and pulverising operations. As a result, much of it will have been broken, and its thread or cord-like configuration destroyed. The broken, pulverised textile fibres form “fluff” that entraps and holds rubber particles and steel together. In order for the rubber to be usable, the steel and fluff need to be separated and removed. The use of magnets removes the free steel pieces, but the magnets also remove rubber particles, in which the rest of the steel is embedded (Recycling, 2001). To avoid substantial amounts of steel-bearing rubber, and to obtain finer rubber particles, the rubber must be subjected to a second re-grinding. This is normally done in a knife mill capable of disintegrating the rubber into smaller particles or in a hammer-mill (Recycling, 2001). Steel and fluff is extracted at this final stage as well (Figure 2.3).



Figure 2.3 Steel and fluff from final stage of shredding

The steel extracted after the second stage and the final stage of shredding differs in quality. The former contains large pieces of rubber as well as much of the textile wire in long lengths. The cord is sometimes undamaged, but most of it is deteriorated into individual wires. The latter is much finer, comprising mostly of thin individual steel wires, but still containing around 10% rubber and much fluff and as a result, it is considered a waste material and usually it is sent to landfill. The by-products at the different stages of shredding are shown in Figure 2.5.



Figure 2.5 From Tyre to crumb

2.1.2.2 Microwave Induced Pyrolysis Process

The microwave induced pyrolysis process, called “Advanced Molecular Agitation Technology” and patented by AMAT Ltd, optimises microwave power at the molecular level to thermally decompose tyres to their constituents. The microwaves excite the molecular bonds of the long-chain rubber hydrocarbons enough to break them into shorter hydrocarbons, which are released as volatile gases around 350° Celsius (AMAT-Ltd, 2003). Fig. 2.6a shows the prototype plant developed by AMAT Ltd; it is noted that the process can recycle shredded as well as whole tyres.

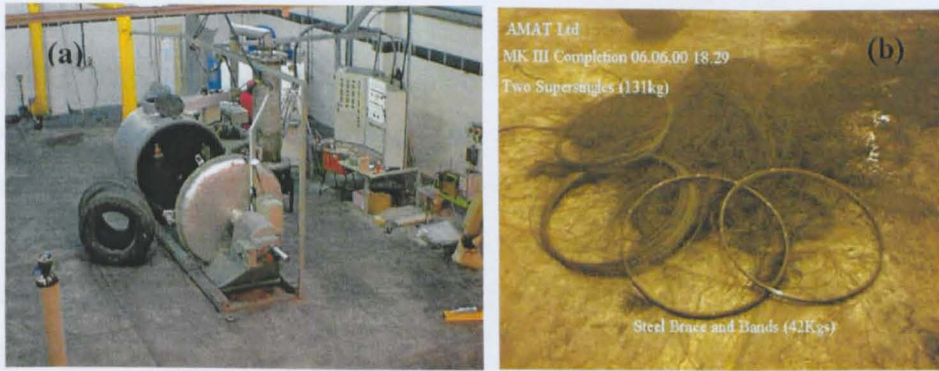


Figure 2.6 Pyrolysis process (AMAT-Ltd, 2003)

The process operates at relatively low temperature and hence, the derived steel cord and textile wire within the tyres remain intact (Fig. 2.6b), whilst the tyre rubber itself is converted to oil, gases and char. Similarly to the conventional pyrolysis process, the gases can be used for the energy requirements of the process.

The next section presents the available industrial fibres and the benefits of adding fibres to concrete. Possible applications of SFRC are also examined.

2.2 SFRC TYPES AND APPLICATIONS

Strengthening concrete with steel fibres is an old idea. Berard (1874) received a patent for the idea of improving concrete behaviour by introducing metallic wastes. However, for almost a century, SFRC was used very rarely. It was only in the 1960s, that the broad application of SFRC started. However, even today the large variety of steel fibres as well as the absence of unique design guidance still prevents the wider application of this type of concrete.

In the early stages of the development of SFRC, it was hoped that it would be possible to increase the relatively weak tensile strength of the concrete substantially. Until now, only small strength increases are possible. In addition, the flexural load-carrying capacity of reinforced concrete (RC) and pre-stressed concrete (PC) structural members cannot be substantially increased by fibre addition. However,

improvements in the behaviour of RC & PC structural members in some areas are possible, especially when there is ductility in demand in the tension zone. Moreover, steel fibres can increase the serviceability behaviour of RC and in some cases, when this limit state dominates, replace steel reinforcement altogether. The application of SFRC is particularly economical in those areas, where a relatively high compression stress is present in combination with a small bending load, such as in tunnel structures.

2.2.1 TYPES OF STEEL FIBRES

The bond strength between fibre and concrete is one of the major factors that determine the properties of the hardened concrete.

Steel fibres with a circular cross-section are produced by normal wire-drawing techniques, which are relatively inexpensive (Hannant 1978).

Other types of steel fibres shown in Figure 2.7 and 2.8 have been claimed by their manufacturers to give some extra benefits in bond when compared with plain round wire, but there can also be disadvantages associated with the mechanical deformations.

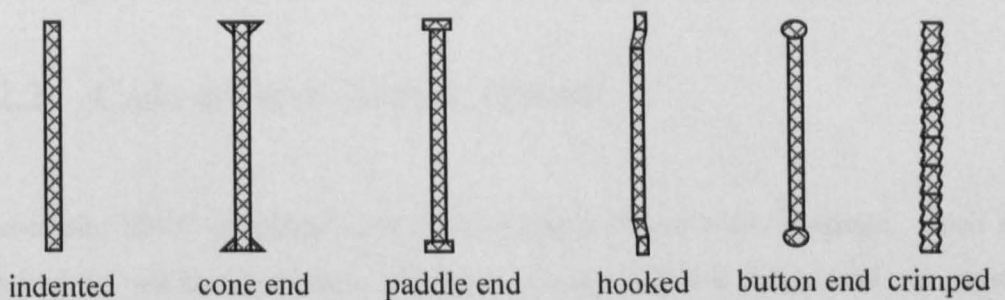


Figure 2.7 Different types of industrially produced steel fibres

For instance, the indentation process can weaken the fibre and make it more brittle, particularly in the case of the smaller diameter fibres. Also, stiff fibres combined

with a sinusoidal shape can cause local bursting of the matrix due to radial tensile stresses exerted on the concrete as the fibres pull out.

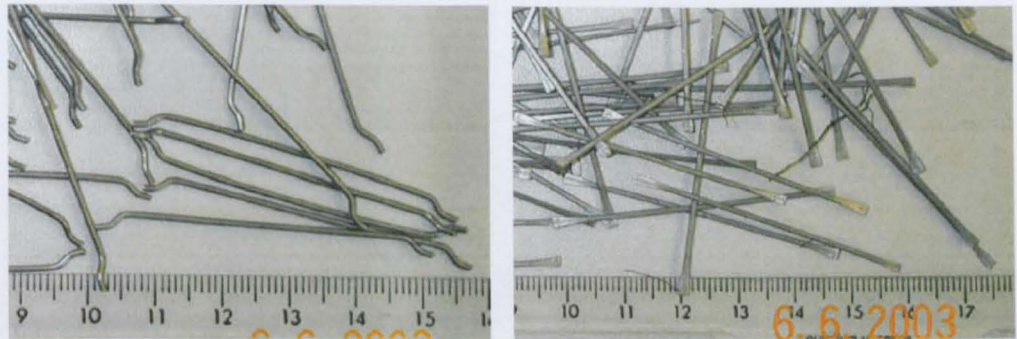


Figure 2.8 Industrial fibres with hooked and cone end

The ragged shape of fibres produced from the melt process can also cause problems if the bond is sufficiently good to cause fibre failure rather than pull out, because flexural strengthening relies on fibre slip occurring before failure (Hannant, 1978).

In addition to mechanically deforming the fibres, various chemical and physical treatments have been tried in an attempt to improve the fibre surface characteristics with respect to bonding with cement paste. These treatments have included degreasing, surface roughening, and surface coatings. Although the bond strength of single treated fibres can be considerably improved, the strength increase of SFRC containing treated fibres is known to be much less pronounced (Johnston, 1977).

2.2.2 CAST-IN-SITU APPLICATIONS

Cast-in-situ SFRC is mainly used in the construction of slabs-on-grade, which are required to withstand damage sustained by concentrated loads and to possess enhanced resistance to impact loading. The use of SFRC in this type of application is cost effective as it can decrease the thickness required for the slab and can reduce the lateral and longitudinal spacing of joints.

SFRC slabs-on-grade are mainly used for the construction of highway and pavements and industrial floors (Figure 2.9 a,b).



a. Industrial floor



b. Highway pavement

Figure 2.9 Cast-in-situ applications (after Fibermesh, 2003)

By 1990, over two million squared metres of industrial flooring were constructed in Europe (Robinson et al, 1991). A new cast-in-situ application area of SFRC was introduced in Berlin “Postamer Platz 1998”, where, for the first time, SFRC was used for the construction of an underwater slab (Falkner and Henke, 1998). Other applications of cast-in-situ SFRC are found in hydraulic and marine structures, retaining walls, overlays, foundations, bridge decks and composite construction (Bekaert, 2003; Hoff, 1985).

2.2.3 PRECAST APPLICATIONS

SFRC is used in many pre-cast applications as it can be an efficient and cost effective material. Its use in pre-cast construction reduces labour and material costs as pre-cast SFRC elements have enhanced mechanical properties and rarely require conventional rebar reinforcement. Examples include segmental shaft and tunnel lining, barrier segments, pipes, septic tanks, manholes, permanent formwork as well as tilt-up panels (Figure 2.10 a,b).



a. Barrier segments



b. Pipes

Figure 2.10 Pre-cast SFRC elements (after Fibermesh, 2003)

2.2.4 SPRAYED CONCRETE APPLICATIONS

Sprayed concrete, also referred as shotcrete, is mortar or concrete pneumatically projected at high velocity on to a surface (Ramakrishnan, 1985). Two methods are used in sprayed concrete: the dry and wet processes. The main difference between them is that, in the dry process, the material is batched and mixed without the addition of water until it reaches the nozzle. In the wet process, the material is already hydrated when it reaches the nozzle (Hannant 1978).

The mechanical properties of sprayed concrete are reported to be considerably improved by the addition of steel fibres (Ramakrishnan, 1985). Hence, the use of steel fibre reinforced sprayed concrete (SFRS) is efficient and cost effective, since it eliminates the use of conventional rebar or mesh reinforcement. SFRS can be sprayed to irregular surfaces and in almost any shape, and it does not require any formwork.

SFRS was first used in a commercial project in 1972 and it is now widely used in many applications. These include slope stabilisation, tunnel and mine support, soil nailing, decorative artificial work, retaining walls, repair and rehabilitation of existing concrete structures and seismic retrofitting (Ramakrishnan, 1985; Fibermesh, 2003).

2.2.5 APPLICATIONS OF SLURRY INFILTRATED FIBRE CONCRETE

Slurry infiltrated fibre concrete (SIFCON) is a variant of SFRC, which is made of randomly-orientated steel fibres, placed in a mould and infiltrated by cement-based slurry. When compared with conventional SFRC, SIFCON exhibits a superior strength and ductility, since it contains more steel fibres and its matrix consists of very fine particles (Van Mier et al, 1996).

Although SIFCON was first introduced in 1984 by Lancard (1984), there are very few commercial applications of this material. Krstulovic-Opara and Al-Shannag (1999) stated that this is due to the high costs involved in placing the fibres and the lack of uniformity in the fibre orientation. So far, SIFCON was mainly used in the repair of roads and overlay of industrial floors. It was also used in the construction of some military installations in the USA. Experimental studies also proposed the use of SIFCON in earthquake resistant construction and in the construction of structural systems made of linear elements (Van Mier et al, 1996).

A variant of SIFCON is slurry infiltrated mat concrete (SIMCON), which consists of continuous steel fibre-mats and cement-based slurry. The steel fibre mats are pre-woven in large rolls and hence, the placement of the fibres is simpler than those used in SIFCON.

2.3 MECHANICAL PROPERTIES OF SFRC

2.3.1 GENERAL

Cementitious materials such as concrete, mortar and cement paste have a weakness in resisting tensile, impact and other energy loadings. This weakness is due to the

inability of these materials to prevent small cracks, which can originate at a flaw or void in the materials, from becoming unstable under small tensile stresses.

The main objectives in attempting to modify the properties of cement or concrete through fibre reinforcement are: a) improvement of tensile or flexural strength, b) improvement of impact strength, c) control of cracking and mode of failure by means of post-cracking ductility.

The main factors controlling the theoretical performance of composite materials are the volume fraction of the constituent materials, physical properties of the fibres and matrix and the strength of bond between the two constituents.

2.3.2 PROPERTIES OF FRESHLY-MIXED SFRC

The main disadvantage of steel fibres is their tendency to ball together by means of fibre interlocking, when they are either moved from storage into the mixing system or during mixing. Balling prior to mixing can be controlled manually or mechanically by the use of dispensers and vibration screens. Whereas balling during mixing is influenced by fibre geometry, the relative volume proportions of fibre and coarse aggregate, the mixing sequence and duration of mixing. Experience shows that fibre balling can be avoided by adding the fibres after the concrete matrix is wet and by reducing the duration of the concrete-fibre mixing. As figure 2.11 shows (for a given size and shape of aggregate), the optimum fibre content, which can be embedded without getting fibre balling, decreases linearly as the aggregate volume fraction increases (Swamy and Mangat, 1974; Swamy, 1974).

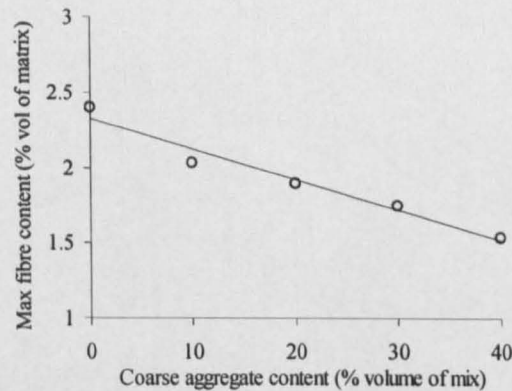


Figure 2.11 Effect of aggregate volume on fibre content (after Swamy and Mangat, 1974)

The aggregate volume fraction also affects the compactibility of SFRC, which reduces as the aggregate volume fraction increases. Consequently, to achieve the same compactibility level, the amount of fibres that can be incorporated without attaining fibre balling decreases as the aggregate volume fraction increases as shown in Figure 2.12 (Swamy, 1974).

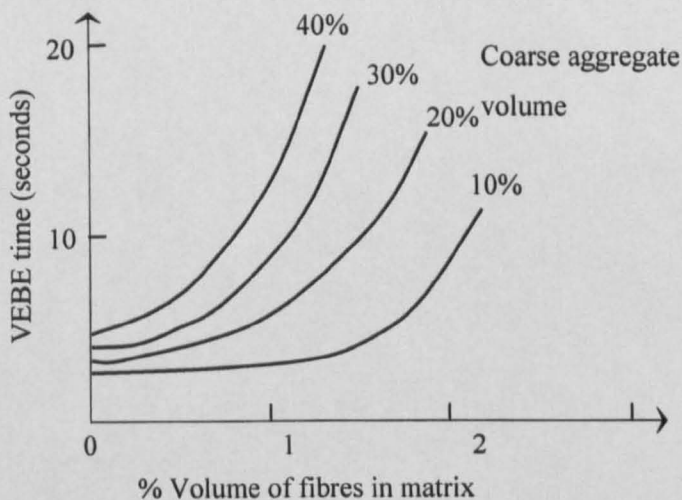


Figure 2.12 Aggregate-fibre interaction on SFRC compactibility (after Swamy, 1974).

Ramakrishnan (1987) and Mangat and Swamy (1974) reported that the compactibility of SFRC is also influenced by both the fibre diameter and length. It

was found that, for a given fibre diameter and content, the time required for compaction increases with the fibre length. Whereas, for a given fibre length and content, the time required for compaction increases as the fibre diameter decreases.

The fibre-aggregate interaction and rheology of the fresh SFRC matrix is also affected by the size and shape of coarse aggregate. This interaction becomes more problematic as the aggregate size increases and the surface texture of the aggregate becomes coarser. As the aggregate size is increased, it is generally advantageous to increase the fibre size (Swamy and Fattuhi, 1974).

2.3.3 BEHAVIOUR UNDER COMPRESSIVE FORCE

Concrete compressive strength is slightly enhanced by the addition of steel fibres, with observed increases ranging from 0 to 15% for up to 1.5% by volume of fibres (ACI 544.IR-XX, 1995). The presence of the fibres enables the concrete to keep its integrity even after failure, while normal concrete disintegrates directly after maximum load is reached.

2.3.3.1 Compressive Strength and Strain

After the peak-load, the SFRC compressive strength and deformation increase with the fibre content (Figure 2.13; Maidl, 1995). This increase in compressive strength depends on the direction of casting. The strength increase is slightly more, if specimens are tested in alignment with the casting direction (Bonzel and Schmidt, 1984).

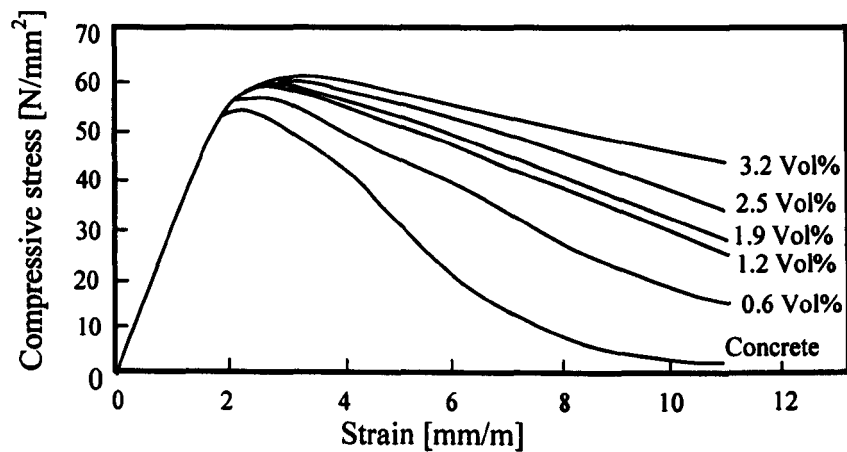


Figure 2.13 Compressive stress-strain curves for SFRC (after Maidl, 1995)

Compressive strength is very sensitive to density and the presence of voids, and SFRC may have more voids than normal concrete, if it is not properly compacted or the fibres can ball together and give a poorly compacted mix (Hannant, 1978). In addition, using very high ratios of fibres in concrete may lead to a lower density due to the presence of voids, which leads to lower compressive strength (Shommakhi, 2000).

2.3.3.2 Fibre Content and Aspect Ratio

Fanella and Naaman (1985) indicate that an increase in fibre content and aspect ratio (ratio of length to diameter) increase the energy absorption (the area under the compressive stress-strain curve), while the compressive strength is only slightly increased.

2.3.3.3 Effects of Specimen Size, Shape and Mould Material

The compressive strength decreases as the specimen size increases. On average, there is about a 5% reduction in the strength for each 50 mm increase of the cube size. The use of small specimens, such as 100 mm cubes or 100 mm x 200 mm cylinders, is suitable and recommended for testing high strength concrete (Imam, Vandewalle and Mortelmans, 1995).

In addition, the use of plastic moulds leads to concrete with strength lower than that of concrete cast in iron moulds. The drop in strength due to the effect of plastic moulds increases with an increase in the mould size. This may be attributed to: (a) the relatively lower smoothness of the internal surface of the plastic moulds that results in more voids, flaws, or even small convexities in the concrete and (b) to the lower energy transmitted inside the plastic moulds from the vibrating table to the concrete (Imam, Vandewalle and Mortelmans, 1995).

2.3.3.4 Process of Compressive Cracking in SFRC

Concrete undergoes three stages of cracking mechanisms when subjected to compressive loading: a) micro-cracking, b) macro-cracking and c) diagonal cracking (Rossi, Acker and Malier, 1987).

At the first stage of cracking (micro-cracking), cracks with length considerably smaller than the size of the concrete specimen are randomly generated within the specimen. The orientation of the micro-cracks is influenced by the stiffness difference between the cement paste and the aggregate particles in concrete, and by the fact that when concrete is subjected to longitudinal compression, tensile stresses develop perpendicularly to the direction of compression.

At the second stage of cracking, micro-cracks join together to form macro-cracks with length comparable to the size of the specimen. Eventually, the concrete specimen is divided into small columns of varying sizes and shapes. It is noted that macro-cracks always run parallel to the direction of compressive stress.

In the last stage of cracking, diagonal cracks appear within the small columns. These diagonal cracks are then joined together to create a diagonal sliding plane at the scale of the specimen.

By delaying the propagation of vertical cracks, fibres can delay the appearance of diagonal cracks and therefore increase the compressive strength of the concrete.

2.3.4 BOND BEHAVIOUR OF SERC

In fibre reinforced composites, the transmission of forces between fibres and matrix is achieved through interfacial bond. Bond is considered the weak link that governs most of the mechanical properties of FRC. The main bond components include physical and chemical adhesion, friction, mechanical anchorage, and fibre-to-fibre interlock. For steel fibres as well as a number of polymeric fibres (polypropylene, nylon, polyethylene, etc.), the adhesion component is weak if non-existent. However, it can be improved by the addition of adhesive agents such as latex (Hannant, 1978). Prior studies have shown that such additions, while improving the stress at first cracking, have little effect on the post-cracking response and toughness of the composite. They are also relatively costly.

The fibre-to-fibre interlock develops when fibres are in contact with surrounding fibres. It occurs only with very high fibre contents, such as in SIFCON or SIMCON. Thus, by disregarding adhesion and interlock, friction and mechanical anchorage are left as the main controlling bond parameters for a conventional FRC composite (Lankard, 1984; Mandel, 1985).

Frictional forces depend on the lateral surface of contact between fibre and matrix, the confinement of fibre by matrix, and the friction coefficient between them. For a given composite, the friction coefficient is constant. If confinement is considered to be constant, the lateral surface area is the only variable that can improve frictional forces.

2.3.4.1 Interfacial Bond Stresses

If a composite material reinforced with aligned fibres is stressed in the direction parallel to the fibres, different displacements occur in the fibre and matrix because of the differences in the elastic modulus of the two components. Thus, shear strains are produced along the length of the fibre. These strains and the resulting shear stresses

are the means by which the loads supported by the fibre and the matrix are distributed between the two components.

2.3.4.2 Mechanical Behaviour of Pullout

The mechanical behaviour of fibre pullout is considered to be the result of gradual debonding of an interface surrounding the fibre, followed by frictional slip and pullout of the fibre. A weak zone exists in the cement paste surrounding the steel fibre, which means that at debonding, the interfacial fracture occurs at a distance away from the fibre and not at the actual steel-paste contact surface. The reason for this phenomenon is that the porous layer around the steel fibre has a significantly different microstructure than the rest of the cement paste. This also means that material properties determined in normal testing such as Young's modulus and shear modulus do not apply (Wei, Mandel and Said, 1986).

The course of bond stress along the fibre during pulling out is shown in Figure 2.14a, b (Hartwich, 1986). The bond stress is a combination of shear and friction stresses. However, there are three characteristic sections that can be indicated in the pullout curve.

(1) Fibre and matrix deform elastically: At the first stage of pullout loading, induced shear stresses along the fibre do not exceed the bond strength between fibre and matrix. The shear stresses along the fibre interface have their maximum at the free end of the fibre, $x = l_f$ in curve 1. As the load P_v increases, the maximum shear stress also increases until the fibre-matrix bond breaks and an interfacial crack starts to appear (curve 1a). The frictional shear stress results from slip due to the elastic elongation of the fibre in the debonded zone. (2) Composite fracture: As the displacement (δ) at the fibre free end increases, the crack will progress and the load will either increase or decrease depending on the ratio between the bond strength and the frictional strength (curves 2.14, 2a). (3) Fracture: When the debonding has reached the end of the fibre, i.e. $x = 0$, pullout of fibre occurs under frictional resistance (curve 2.14, 3a).

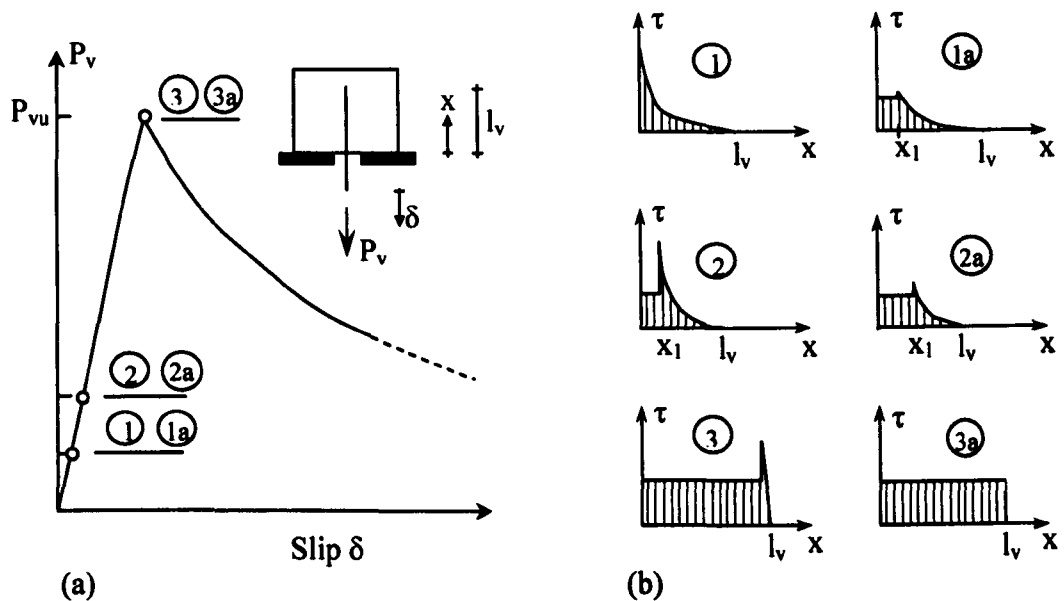


Figure 2.14 Qualitative representation of bond stress distribution in the fibre pullout test. (After Hartwich, 1986)

2.3.4.3 Factors Affecting the Fibre-Matrix Bond

The pullout characteristics of steel fibres embedded in cementitious matrix have been studied as a function of several variables, such as fibre geometry and dimension and concrete composition. Among the environmental characteristics, the curing temperature, curing type and test temperature also have an effect on the pullout characteristics. The rate at which the load is applied, and load cycling prior to a monotonic pullout may also affect the load-extension plot in a single fibre pullout test.

Matrix Properties: Chanvillard and Aitcin (1996) report that the displacement measured at fibre failure (for fibres with waved shape) increases with the water cement (w/c) ratio. This is explained by the size of the matrix cone that is crushed on each side of the crack when failure occurs. When the w/c ratio is high, the size of the cone is bigger so that the local straightening of the fibre is greater. On the other hand, the w/c ratio does not play a significant role during the slipping of the fibre.

The improvements in quality of the fibre-matrix bond due to the silica fume addition are significant (Banthia, 1990). In the case of excessively deformed fibres, silica fume addition also caused matrix brittleness, leading to matrix splitting prior to complete pullout.

Fibre Orientation: For the deformed fibres studied by Banthia and Trottier (1994), the peak loads supported by fibres that are aligned in the direction of loading are higher than those supported by fibres inclined with respect to the loading direction. The peak loads for the fibres aligned in the load direction also occur at smaller slips and absorb greater amounts of energy than the inclined fibres. A zero-degree inclination with respect to the loading direction is, therefore, the optimal inclination (Naaman and Shah, 1976). The tensile strength of a FRC is influenced by the fibre orientation factor (due to the randomness of the fibre orientation) which was found to vary between 0.41 and 0.82 with an average factor of 0.6 for all fibre types was determined by Parviz and Cha-Don (1990).

Fibre Shape, Surface and Embedment Length: The effectiveness of fibre deformation in improving the pullout resistance is well known (Banthia, 1990). Deforming a fibre along its length is necessary in order to maximise its resistance to pullout and properly utilise the potential of steel. However, there is a limit to deforming a fibre. An excessively deformed fibre may cause a premature matrix splitting and fracture in the process of pullout, leading to a considerable reduction in pullout energy consumption. Low fibre pullout energy is undesirable, because the prime motive behind adding fibre to concrete is energy absorption and not an increase in strength.

Chanvillard and Aitcin (1996) also investigated the pull-out behaviour of corrugated steel fibres. It was found that fibre debonding was the most frequent mode of failure for the one-and two-waves-long fibres. In case of the three-wave-long fibre, the pullout could have occurred according to two extreme modes. In the first mode, fibres could have kept their corrugated shape during the process, so that the matrix would have been completely destroyed in the fibre area during the pullout process. In

the second mode, if the matrix was not altered, the fibre was continuously deformed during its slipping until its final pullout within its initial print.

2.3.4.4 Analytical Models

The first analytical models describing the pullout behaviour of single fibre were elastic (Cox, 1952). Wang et al (1987) developed a theoretical model to predict the load-crack separation relationship for synthetic fibre reinforced concrete as a function of the slippage accumulation at that fibre segment. Gopalaratnam and Cheng (1987) assumed the local interfacial bond-slip relation to feature linear softening. Namur, Naaman and Clark (1987) and Namur and Naaman (1989) assumed that the fictional stress is constant and independent of the slip. However, accurately experimental measurements indicated otherwise (Naaman et al, 1991). Naaman et al (1991a) assumed that the bond stresses decreases according to an exponential function before reaching an asymptotic value as illustrated in Figure 2.15. These results were also reported by Fantilli and Vallini (2003).

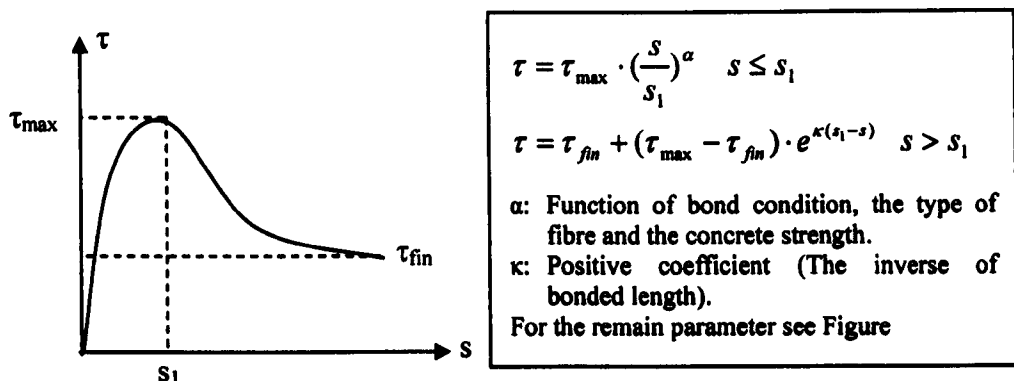


Figure 2.15 Bond-slip relationship (after Fantolli and Vallini, 2003)

2.3.4.5 Experimental Investigations on Pullout of SFRC

The test set-up and loading conditions, such as the speed of the test machine, holding the fibre with respect to the crack during casting, method of measurement and application of the external stress can strongly affect the results. Figure 2.16 shows that pullout tests have been carried out in a number of different ways to minimise the effect of parameters affecting the test. However, to this date, no standard method has been universally accepted.

Double-sided pullout tests using single and multi fibres were performed in a number of studies (Banthia 1990, Bindiganavile and Banthia 2001, Stoeven, Bouter and Shah 1978, Chanvillard, Aitcin 1996 and Groth 1996). It is noted that, when performing such tests, care should be taken to ensure that pullout only takes place at one of the two halves of the specimen. In the case of multiple fibres, all fibres must have the same embedded length and the total response be divided by the numbers of fibres used.

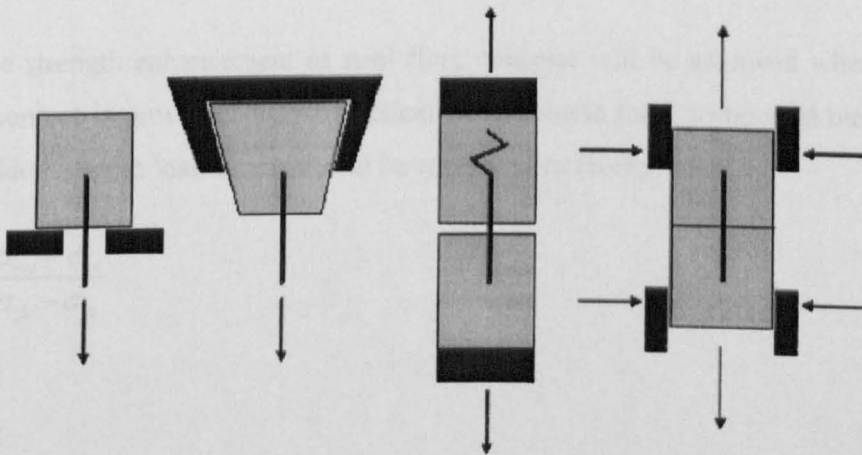


Figure 2.16 Different examples of pullout tests (after Groth, 1996)

2.3.5 BEHAVIOUR UNDER DIRECT TENSILE FORCE

Direct tension test data indicate that reinforcement by steel fibres increases the tensile strength of concrete and significantly improves the post-peak tensile behaviour.

2.3.5.1 The Effect of Fibre Content

The post-peak behaviour of SFRC subjected to a uniaxial tensile force is significantly dependent on the effective fibre crossing the crack. A linear dependence between the post-peak parameters and the number of fibres bridging the crack was identified by Gettu et al (2001), while the values of the maximum stresses were dominated basically by the matrix behaviour. On the other hand, RILEM (1972) indicates that the pre-peak behaviour and the maximum tensile stress reveal a great deal about the interaction of the two components of the materials.

2.3.5.2 Critical Fibre Content

Tensile strength enhancement in steel fibre concrete will be achieved when critical fibre content is provided. The theoretical fibre volume for a compound matrix with embedded fibre in load direction can be expressed as (Kelly, 1966):

$$V_{cr} = \frac{\sigma_{mu} - \sigma_m}{\sigma_{fu} - \sigma_m} \quad (2.1)$$

where:

σ_{mu} matrix tensile strength

σ_m concrete failure tensile stress

σ_{fu} fibre tensile strength

In the case of randomly oriented fibres, the critical fibre volume can be increased by 3 to 6 times depending on the fibre length and bond property. Such an increase of the fibre volume is usually not possible for economical and technical reasons (concrete workability).

2.3.5.3 Experimental Evaluation

No standard test exists to determine the stress-strain curve of SFRC in direct tension (ACI 544-4R, 1988). Common problems include: a) stress concentrations at the gripping point causing premature specimen failure; b) misalignment of the test specimen and test equipment centrelines causing eccentricities; c) the inability to obtain a stable post-peak response (Toutanji and El-Kochi, 1994). Different types of gripping devices were developed to overcome the stress concentrations as clamping by means of gluing (Karihallo 1995, Li, Stang and Krenchel 1993, Toutanji and EL-Korchi 1994, RILEM TC162-TDF 2001) and clamping by means of wedge action of friction (Philips and Binsheng, 1993). Some of these methods can reduce the stress concentration but none of them can totally eliminate these problems (Toutanji and El-Korchi 1994, Gettu et al 2001).

To obtain a stable post-peak response, a closed-loop testing system using notched beams was developed (Li, Stang and Krenchel 1993, RILEM TC162-TDF 2001).

The tensile stress-strain curve is also influenced by the method of strain measurement, the associated gauge length, loading rate (Glinicki, 1994) and specimen size (Neville, 1995). Gopalaratnam and Shah (1987) show that the total post-peak displacement is equal to the width of a widening crack regardless of the gauge length.

2.3.5.4 Theoretical Evolution of the Tensile-stress Curve

The stress-strain curve is associated with the non-uniform strain distribution occurring prior to peak load and the localised deformations in the post-peak region. To overcome the numerical problems Hillerborg (1980) considers a stress-strain

curve in the pre-peak region and a stress-crack width curve in the post-peak region. Phillips and Binsheng (1993) and Karihaloo (1995) assumed a straight line, with a gradient equal to the elastic modulus of the material for the stress-strain curve. The prediction of the stress-crack width curve for SFRC is not so simple, due to the influence of fibre ratio and type on the shape of the curve. Wecharatana and Shah (1983) proposed an empirical relationship as a function of the maximum tensile stress, maximum crack width (i.e. half the fibre length) and a constant depending on the geometry of the fibres. Other researchers (Li, Stang and Krenchel 1993, Gopalaratnam and Shah 1987, Hillerborg 1980) superimposed the fibre pull-out response curve on the stress-crack-width curve of a plain matrix.

Due to the problems associated with the direct tensile test, a flexural tensile test offers a suitable alternative to measure the post-cracking capacity (flexural toughness) of SFRC.

2.3.6 FLEXURAL BEHAVIOUR AND TESTING

The flexural test is widely used to measure the post-cracking capacity (flexural toughness) of SFRC, which can be represented through one of the following measures: a) absolute energy absorption, b) dimensionless indices related to energy absorption capacity and c) equivalent flexural strengths at prescribed post-cracking deflections (Gopalaratnam and Gettu, 1995).

2.3.6.1 Flexure Toughness Standards and Guidelines

The most widely recognised standard test methods are detailed below, all of them use unnotched beam specimens tested under a third-point configuration. Although these methods do not use the same specimen size, shape, span and load rate control, the greatest difference of these methods is in the manner in which toughness is defined and calculated.

North American and Japanese Standards

The flexural test adopted by the American Society of Testing and Materials (ASTM) uses a third-point loading configuration (ASTM C1018-94b, 1995). The test uses a 100mm square beam specimen. The span and overall length of the specimen are 300mm and 350mm respectively.

The flexural toughness of SFRC is characterised by energy dimensionless indices. These indices (I_5 , I_{10} and I_{20}) are computed at deflection limits of $3\delta_f$, $5.5\delta_f$ and $10.5\delta_f$ (Figure 2.17). The limiting deflections have been chosen to provide reference toughness index values of 5, 10 and 20 respectively, for an elastic-plastic material. The first crack is defined as the point on the load-deflection curve at which the form of the curve first becomes non-linear. Residual strength factor $R_{5,10}$ and $R_{10,20}$ are then calculated at the value of 20 ($I_{10}-I_5$) and 10 ($I_{20}-I_{10}$) respectively, as shown in Figure 2.17. When using this method, it is important to note that all three parameters (first-crack strength, toughness index and residual strength factors) are needed to fully define the toughness behaviour (Gopalaratnam and Gettu, 1995).

The American Concrete Institute seems to use the same basic idea as the ASTM (ACI 544, 1988). The significant difference is that the limiting deflection is up to a midpoint deflection of 1.9 mm. The main problem of this method is that the determination of the first crack deflection and choice of the deflection limits may not be reliable. Furthermore, ACI 544 recommends an alternate toughness index, I_t , that is defined as the ratio of the energy absorption capacity of an SFRC beam to that of its un-reinforced counterpart. The definition provides a fundamental measure of the effectiveness of fibre incorporation until complete failure. However, The ASTM C 1018 indices rely on the first-crack even more than the ACI 544 toughness index, since the limiting deflections are multiples of the first-crack deflections.

The Japanese Concrete Institute (JSCE-SF4, 1984) test is also based on the energy absorption capacity. The toughness definition, T_{JCI} , is calculated for a standard size beam ($b = d = 100 \text{ mm}$ for $l_{\text{fibre}} \leq 40 \text{ mm}$, $b = d = 150 \text{ mm}$ for $l_{\text{fibre}} > 40 \text{ mm}$ and span = $3d+80 \text{ mm}$), as the area under the load deflection curve up to a limiting deflection of $l/150$, as shown in Figure 2.17.

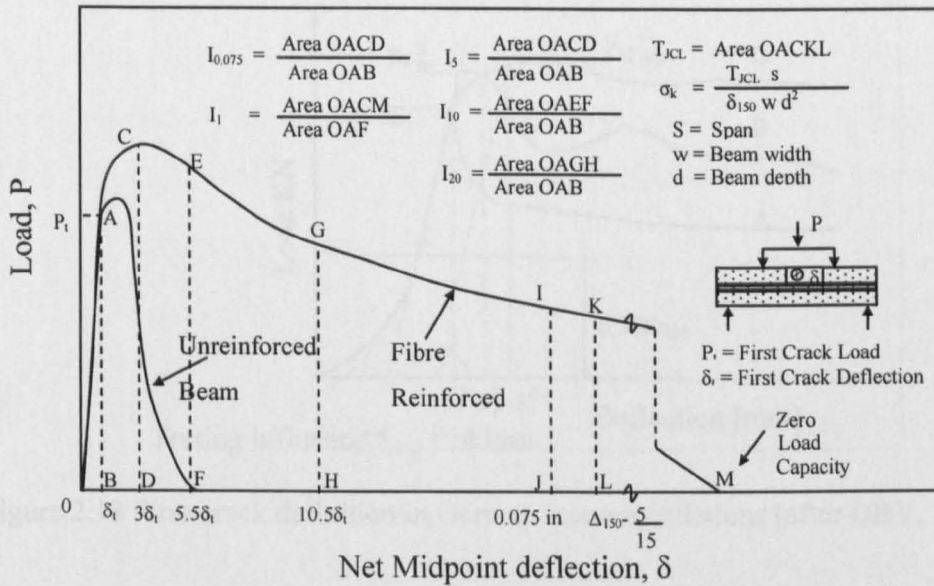


Figure 2.17 Toughness definitions from ASTM C1018, ACI 544 and JCI-SF4 Test Standards

European Standards

Similar indices to JSCE-SF4 have also been proposed in the Belgian, Dutch, German, RILEM and Spanish test specifications (Gopalaratnam and Gettu, 1995). They calculate the energy absorption at smaller deflection limits than those considered by JSCE-SF4 and those reflect a useful level of serviceability for many applications.

The German recommendations (DVB, 1991) specify energy absorption capacity that explicitly reflects the benefits of fibre incorporation. The basic idea has some similarities with the ACI 544 index I_t . Energy absorption capacity of a standard size FRC beam is calculated up to specified deflection limits by subtracting the idealised contribution of an unreinforced concrete beam of identical size, (Figure 2.18).

The standard also requires the calculation of the equivalent flexural strength at these two deflections (Figure 2.19), which offers perhaps one of the best ways to practically implement toughness-based design.

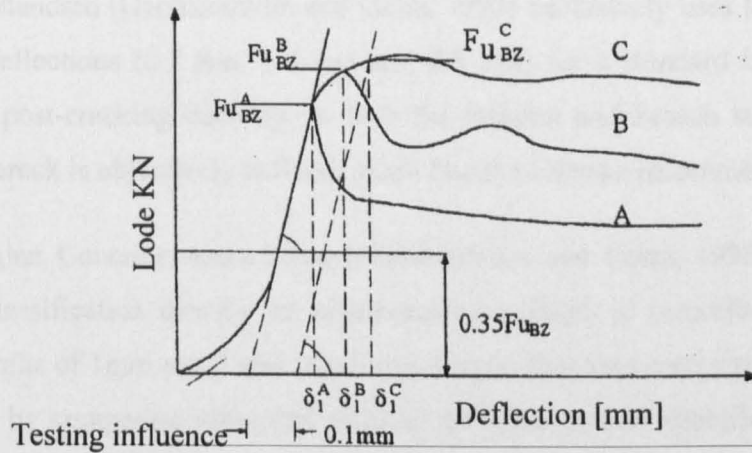


Figure 2.18 First-crack definition in German recommendations (after DBV, 1991)

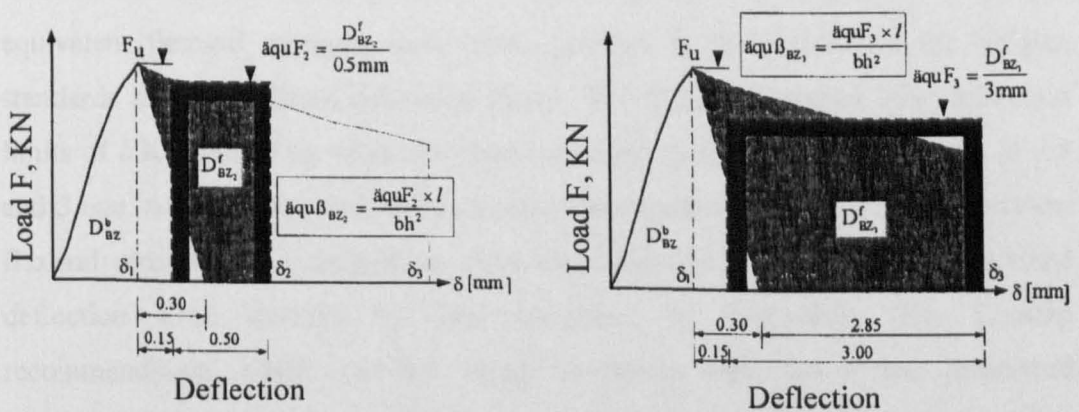


Figure 2.19 Toughness measures in German recommendations (after DVB, 1991)

The Spanish standard (Gopalaratnam and Gettu, 1995) requires computation of a dimensionless index equivalent to I_{30} of the ASTM C 1018 (calculated at a deflection limit of $15.5 \delta_f$) perhaps recognising that, at the smaller limiting deflections, such an index is not a sensitive toughness measure. It also requires reporting of the first-crack strength and the energy absorption capacity, as in the Japanese standard.

In addition to a toughness definition based on absolute energy, the Belgian specification uses dimensionless load ratios to characterise the shape of the load-deflection response in the post-cracking region. Deflection limits are specified as functions of the span, l/n (where $n = 600, 450$ and 150).

The French standard (Gopalaratnam and Gettu, 1995) exclusively uses load ratios at prescribed deflections (*0.7 mm*, *1.4 mm* and *2.8 mm*) for a standard beam size to characterise post-cracking ductility. In both the Belgian and French standards, the load at first-crack is objectively defined, much like the German recommendation.

The Norwegian Concrete Association (Gopalaratnam and Gettu, 1995) base their toughness classification directly on post-cracking strength at prescribed mid-span deflection limits of 1 mm and 3 mm measured on specified specimen size. Toughness is evaluated by comparing measured residual strengths against specified minimum requirements according to four toughness classes.

In addition to the energy-based toughness measure, T_{JCI} , the Japanese standard recommends the use of an equivalent flexural strength, σ_b , (Figure 2.14). Similar equivalent flexural strengths have been specified in the Dutch and the Belgian standards at two different deflection limits. The Belgian standard uses deflection limits of $l/300$ and $l/150$, while the Dutch standard specifies deflection limits of *1.5 mm* and *3 mm*. Additionally, the Dutch standard also requires reporting of the equivalent flexural strength ratio defined as equivalent flexural strength at the prescribed deflection limit divided by that computed at first-crack. The German recommendation, which uses the energy absorption capacities at two prescribed deflection limits, also requires the computation of the equivalent flexural strength at these two deflection limits in a manner somewhat similar to the JCI method.

2.3.6.2 Discussion on Standards of Practice

Current standards for the evaluation of the toughness of SFRC materials have a number of problems, as explained below.

Deflection measurement

In flexural toughness tests, the measured deflections must exclude any extraneous effects due to local deformations of the beam at the loading points, elastic and inelastic deformations at the supports and specimen rocking effects. Toughness characterisation methods that rely directly on first-crack deflections (e.g. ASTM

C1018 and JSCE-SF4) are significantly affected by errors in deflection measurement, due to gross overestimation of first crack deflections and, therefore, first crack energy (Banthia and Trottier, 1995). As shown in Figure 2.20, net deflection measurement can be achieved by using a “yoke”, which allows measurement of mid-span deflection in relation to the neutral axis of the beam at its supports.

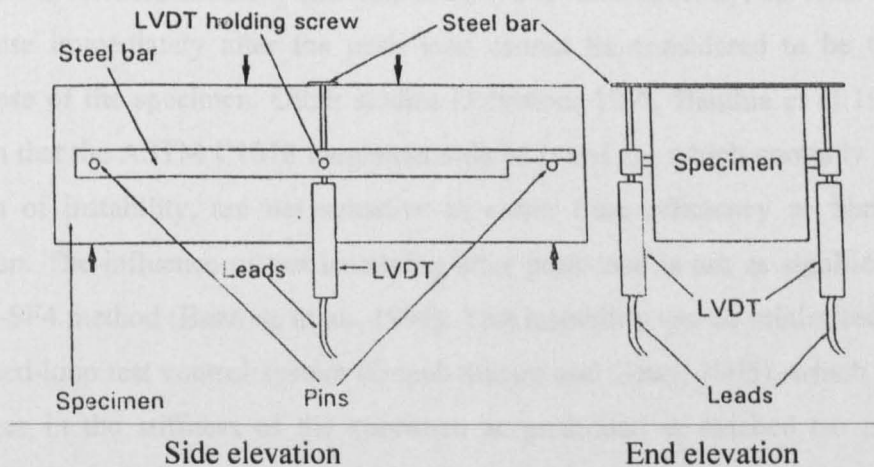


Figure 2.20 A schematic of the yoke loading system (Morgan, 1995)

Location of first-crack point

Any error in the location of the first-crack point on the load-deflection curve will lead to significant errors in the values of the various indices. In practice, the location of the first-crack point from the load-deflection curve can be highly subjective, resulting in variations in the measured index values (Gopalratnam and Gettu 1995, Banthia and Trottier 1995, Chen et al 1995). Morgan, Chen and Beaupre (1995) proposed that the difficulty in locating the first-crack is because there is no such thing as a discrete first-crack point in a flexural test. They suggest that progressive microcracking, which occurs as the beam deflects, causes substantial non-linearity in the load-deflection curve prior to peak load. As a result, the first-crack point can be almost impossible to locate accurately. In order to help locate and validate the first-crack point, a formula for estimating the first-crack deflection based on the elastic theory has been proposed (ASTM C108 1994, Chen et al 1995). However, a much

greater improvement could be achieved if an objective method of defining the first-crack point was adopted, as has been done in some European standards (Gopalaratnam and Gettu, 1995).

Instability after the peak-load

It is not uncommon in deflection controlled third-point flexural tests that the peak-load is followed by a temporary loss of stability, where the strain energy stored in the machine is released suddenly (Banthia et al, 1994). Consequently, the load-deflection response immediately after the peak load cannot be considered to be the actual response of the specimen. Other studies (Johnston, 1995, Banthia et al 1994) have shown that the ASTM C1018 toughness indices I_5 and I_{10} , which normally fall in the region of instability, are not sensitive to either fibre efficiency or fibre volume fraction. The influence of test instability after peak-load is not as significant in the JSCE-SF4 method (Banthia, et al., 1994). Test instability can be minimised by using a closed-loop test control system (Gopalaratnam and Gettu, 1995), which adjusts to changes in the stiffness of the specimen as peak-load is reached (to maintain a constant rate of mid-span deflection). This is more difficult to perform than cross-head control and requires sophisticated and expensive equipment.

Size and geometry effects

Any flexural toughness characterisation method based on a load-deflection response will be influenced by specimen size and geometry. Work by Chen, Mindess and Morgan (1994) has shown that the ASTM C1018 indices and the JSCE-SF4 toughness factor are dependent on the cross-sectional size and span of the test specimens. All the toughness parameters decreased with an increase in the span-to-depth ratio. In addition, where the depth and span were unchanged, toughness also appeared to increase with an increase in the width of the specimens. For these reasons, it is strongly recommended that flexural toughness testing should be conducted using standard size specimens (Morgan, Chen and Beaupre, 1995). A full account of these effects should be taken when attempting to extrapolate results from laboratory specimens to full-size structures (Gopalaratnam and Gettu, 1995).

Unsymmetrical cracking effects

Deflection is generally measured at the mid-span position, even though the crack can occur anywhere within the middle third of the beam. Therefore, the position of the crack relative to mid-span may influence the deflection measurement, and hence the shape of the load-deflection curves. However, none of the standard test methods appear to address this issue.

Shear effects

The extremely small shear span-depth ratio of 1, which is common to ASTM C1018 and JSCE-SF4, causes unusually high stresses in the shear spans, and may cause changes in the mode of failure (Gopalaratnam and Gettu, 1995).

Effects of testing directions

When the testing direction is perpendicular to the casting direction, specimens exhibit reductions in both flexural toughness (up to 30 % in case of high workability mixture and 14 % of low workability mixture) and strength compared to the case when testing and casting directions are parallel (Toutanji and Bayasi, 1998).

2.3.6.3 Notched Beam Test for Toughness Characterisation

As an alternative and possible improvement, to toughness characterisation, the use of notched beams has been investigated (Barr et al 1996, Gopalaratnam and Gettu 1995). This type of test specimen is controlled by the crack mouth opening displacement (CMOD) in place of the mid-span deflection. Lee and Barr (2003) report that the notched beam is a stable and reliable test and the variation in the results are significantly lower than the un-notched beams. It has been suggested that a load-CMOD approach to toughness characterisation has the following advantages.

CMOD measurement automatically excludes all extraneous deformations typically associated with deflection measurements, and is therefore less prone to errors.

CMOD can be readily related to crack-width limits and as a result to application specific levels of serviceability.

The results can be related to fundamental fracture mechanics and crack propagation behaviour of fibre reinforced concrete of the beam.

Unlike the unnotched beam, deformation behaviour in notched beams is always localised at the centre of the beam (i.e. at the notch).

To predict the load-deflection curve obtained from a bending test, two main analytical models are introduced in the literature. The first one is based on the determining the energy dissipated when a crack is formed (Fracture mechanics models), while the other is using the equilibrium conditions (Stress-block models).

2.4 MODELLING AND DESIGN OF SFRC

2.4.1 FRACTURE MECHANICS MODELS

This approach was originally developed for analysing materials with well defined crack tip during fracture (Glass and metals). Concrete is a quasi-brittle material and due to the micro-cracking, it develops an extensive fracture process zone (FPZ) ahead of the crack tip (Hillerborg 1983, Karrihaloo 1995). An additional fibre bridging zone enlarges the FPZ in the case of SFRC (Hillerborg, 1985).

2.4.1.1 Fictitious Crack Model (FCM)

The fictitious crack model (FCM) was first suggested by Hillerborg, Modeer and Peterson (1976) for modelling the fracture of plain concrete. The fictitious crack is thus a fracture zone which transfers stress according to the σ - w relationship and the concrete stress does not immediately fall to zero, but is assumed to gradually decrease with an increasing crack width (w). Hillerborg (1985) subsequently developed the FCM to predict the load-deflection curve of steel fibre reinforced concrete beams using non-linear fracture mechanics approach. Initially the σ - w curve is derived using the law of mixtures, by combining the σ - w curve of the plain

concrete matrix with a simplified theoretical σ - w curve from the pull-out stress. The model requires the use of four parameters: a) E-modulus, b) tensile strength, c) tensile stress – crack opening relationship and d) fracture energy. Unfortunately, the validation of the proposed model is not confirmed by experimental results. Bazant and Oh (1983) used the stress-strain relationship with an inelastic strain distribution over a band width, in place of the stress-crack-width curve. The inelastic strain is then related to inelastic deformation.

2.4.1.2 Two Parameter Fracture Model (TPM)

A two parameter fracture model (TPM) was proposed by Jenq and Shah (1985) to include nonlinear slow crack growth prior to peak load. A critical stress intensity factor is calculated at the tip of the effective crack (termed $k_{Ic,eff}$). The critical effective crack extension is dictated by the elastic critical Crack Tip Opening Displacement ($CTOD_c$). Based on tests on notched beams of three different sizes and five different material compositions, it was concluded that $K_{Ic,eff}$ and $CTOD_c$ as defined here, are size independent, but the flexural strength (modulus of rupture) is not. These two parameters, for any given geometry, can be calculated using Linear Elastic Fracture Mechanics (*LEFM*). From the proposed model, it is possible to calculate the peak load of structures with different geometries.

2.4.1.3 Crack Mouth Opening Displacement (CMOD) Concept

To calculate the flexural strength for unnotched beams in FRC, a tensile stress-crack opening relationship for FRC was adopted by Maalej and Li (1994). For a given value of $CMOD$ (Figure 2.21) and under the assumption of a linear crack opening distribution, the crack opening $w(x)$ in the process zone is determined as:

$$w(x) = CMOD \left(1 - \frac{x}{a}\right) \quad (2.2)$$

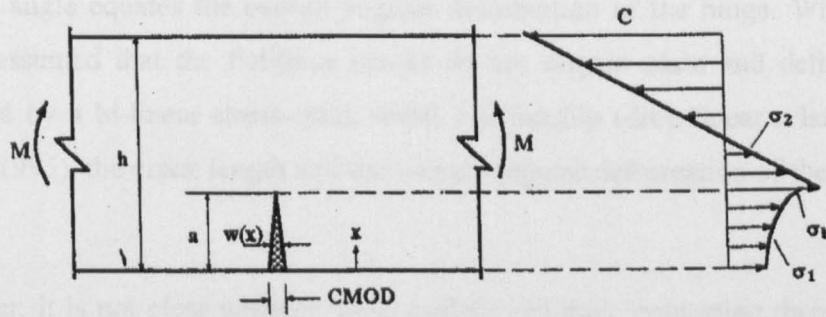


Fig. 2.21 Stress distribution in the cracked cross-section of an unnotched beam (Maalej and Li, 1994)

Related to the fictitious crack model described earlier determined by Maalej and Li, the crack opening $w = CMOD$ through the superposition of w_1 (crack opening under moment force) and w_2 (crack opening under compressive stress $\sigma = -\sigma_1$). The real crack opening is then $w = w_1 + w_2$ (Figure 2.22).

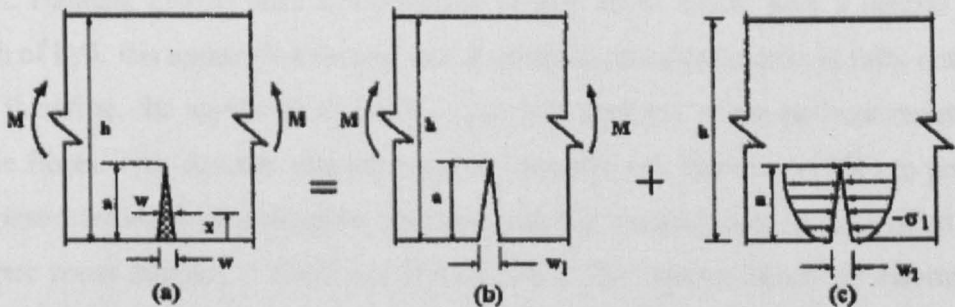


Fig. 2.22 $CMOD$ as a result of equivalent loading

The relationship between w_1 and M as well as w_2 and σ are given in Tada and Paris (1985). A relationship between M and crack length 'a', M and $CMOD$, respectively, derived by $\Sigma M = 0$, $\Sigma N = 0$ and the stress distribution shown in Figure (2.22) can be determined.

To predict the load-displacement curve a cross-sectional analysis of the cracked section is carried out by describing the cracked section as a non-linear hinge (RILEM 2002, Casanova and Rossi 1996 and 1997 and Olesen 2001). Casanova and Rossi (1996 and 1997) assumed that the fictitious crack surface remains plain and the crack

opening angle equates the overall angular deformation of the hinge. While Olesen (2001) assumed that the fictitious cracks do not remain plain and deformation is governed by a bi-linear stress-crack width relationship (drop-linear relationship by Ulkjar (1995), the crack length and the overall angular deformation of the non-linear hinge.

However, it is not clear whether these models and their supporting theories can be readily understood by civil engineers. Therefore, it is unlikely that a rational design procedure based on these models could be universally accepted in the foreseeable future.

2.4.1.4 Stress-block Models

Stress-block models use simple principles of mechanics to determine the moment of resistance (and hence flexural load capacity) of a steel fibre reinforced concrete beam. Hannant (1978) used a rectangular tensile stress block with a neutral axis depth of $D/4$. His approach assumed that at ultimate stress the matrix is fully cracked and, therefore, the tensile stress block is purely a function of the pull-out resistance of the fibres. This concept was extended by Armelin and Banthia, (1997) to predict the post-cracking load-deflection response and the cracked section is divided into discrete zones (similar to Swift and Smith, 1978). The section forces are determined by applying theoretical and experimental stress-strain relations to the respective zones. An iterative process is then used to determine the neutral axis position, crack-width profile and moment of resistance in relation to mid-span deflection, from an assumed value of maximum compressive strain. The process is repeated for a range of increasing compressive strain values in order to obtain points on the post-cracking load-deflection curve. However, the main limitation of the model is that crack-width profiles, neutral axis position and deflections are determined theoretically by assuming the strain values, without any apparent justification for their use, or accuracy.

2.4.2 DESIGN METHODS

2.4.2.1 Introduction

A current limitation in the structural use of fibre reinforced concrete is the lack of accepted design codes of practice; this has resulted in a general lack of confidence in its use as a permanent structural material. However, there is no recognised standard for structural applications involving axial and bending forces (ACI 544-4R, 1988). The most common design methods are based on the same fundamentals as the design of normal reinforcement concrete. Two design recommendations have been recently published (RILEM TC 162-TDF 2000 and DVB 1996) using the equivalent flexural tensile strength as a parameter to characterise the post-cracking behaviour.

2.4.2.2 σ - ϵ Design Method

The stress-strain (σ - ϵ) design guideline for SFRC was published by the RILEM technical committee on “Test and design methods of steel fibre reinforced concrete” (RILEM TC 162-TDF, 2000). This guideline is similar to previous design guidelines for SFRC that were developed for one specific type of industrial fibres (Nemegeer, 1996). The guideline utilises the design framework of Eurocode 2 (ENV 1992-1-1, 1992) and it contains design provisions for the ultimate limit states of bending and shear, and serviceability limit state of cracking.

Figure 2.23 shows the stress-strain relationship adopted by RILEM for SFRC. The compressive part of the stress-strain relationship is defined by using the model adopted by Eurocode 2 for plain concrete, whereas the tensile part of the stress-strain relationship is described in terms of the uni-axial tensile strength ($f_{ctk,ax}$) and the equivalent flexural tensile strength (f_{eq}). A new model for the tensile stress-strain relationship was recently developed on the basis of residual strengths (f_{res}) at a tensile strain of 25‰ (Brite-Euram, 2002).

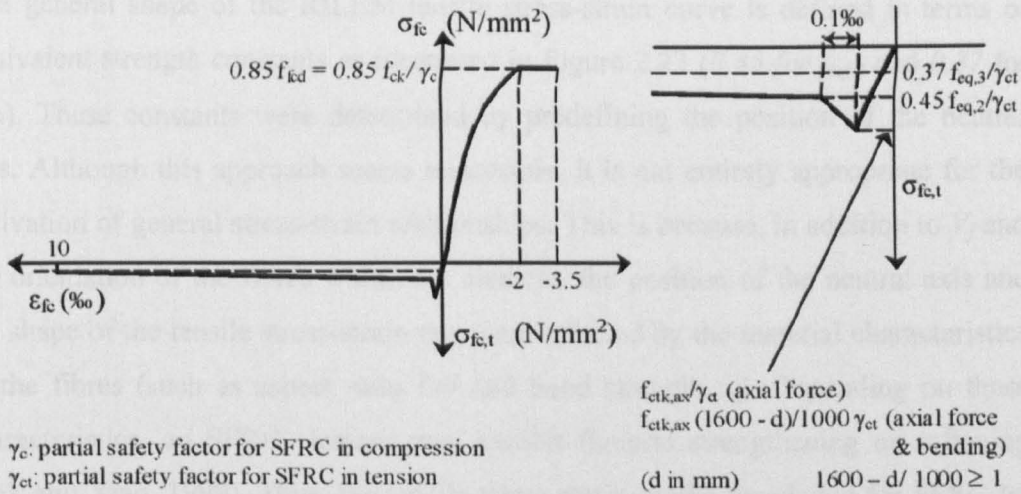


Figure 2.23 RILEM stress-strain model

The accuracy of the σ - ϵ model is still debatable. A recently completed study on SFRC reported that this guideline overestimates the bending resistance of deep beams (Brite-Euram, 2002). This was particularly observed for SFRC beams that did not contain any conventional steel reinforcement (Erdem, 2003). In addition, it was determined that, for SFRC beams containing conventional reinforcement, this inaccuracy increased with increasing fibre content (V_f). The study consequently proposed the use of reduction factors on the values of f_{eq} and f_{res} ; it is noted that these reduction factors are defined as a function of the element's depth. Erdem (2003) stated that, in addition to the size-effect, the overestimation of the bending resistance is caused by the application of the same tensile stress-strain relationship for the modelling of the bending behaviour of SFRC elements with different material characteristics. It was further stated that the effectiveness of the fibres, and consequently the bending resistance of SFRC, is influenced by the orientation of the fibres, which in turn is affected by the depth of the element. It was therefore proposed that the shape of the RILEM tensile stress-strain relationship is modified accordingly for each design case by considering the dimensions of the element. Reduction factors were probabilistically derived as a function of V_f and the dimensions of the element.

The general shape of the RILEM tensile stress-strain curve is defined in terms of equivalent strength constants as illustrated in Figure 2.23 (0.45 for $f_{eq,2}$ and 0.37 for $f_{eq,3}$). These constants were determined by predefining the position of the neutral axis. Although this approach seems reasonable, it is not entirely appropriate for the derivation of general stress-strain relationships. This is because, in addition to V_f and the orientation of the fibres within the element, the position of the neutral axis and the shape of the tensile stress-strain curve are affected by the material characteristics of the fibres (such as aspect ratio L/d and bond strength τ_d). Depending on these characteristics, an SFRC element may exhibit flexural strengthening or softening (Lok and Xiao, 1999). Thus, the tensile stress-strain model developed for SFRC by Lok and Xiao seems more appropriate for the codified design of SFRC.

Application of the σ - ϵ design guideline requires the evaluation of general material properties of SFRC, such as f_{eq} and f_{res} , which are essential for the characterisation of the post-cracking bending behaviour of SFRC. These material properties are in general determined by carrying out deformation-controlled bending tests on SFRC prisms. As shown in figure 2.24, the σ - ϵ design guideline uses a deformation-controlled bending test with a central-load arrangement (Vandewalle and Dupont, 2003). Consequently, due to this load arrangement, the test may overestimate the bending resistance of the element due to load spreading, which occurs at the point of load application (Timoshenko and Goodier, 1970). Hence, it may be more appropriate to use a third-point loading arrangement for the evaluation of the bending resistance, as this eliminates the load spreading effect and creates a region of constant moment.

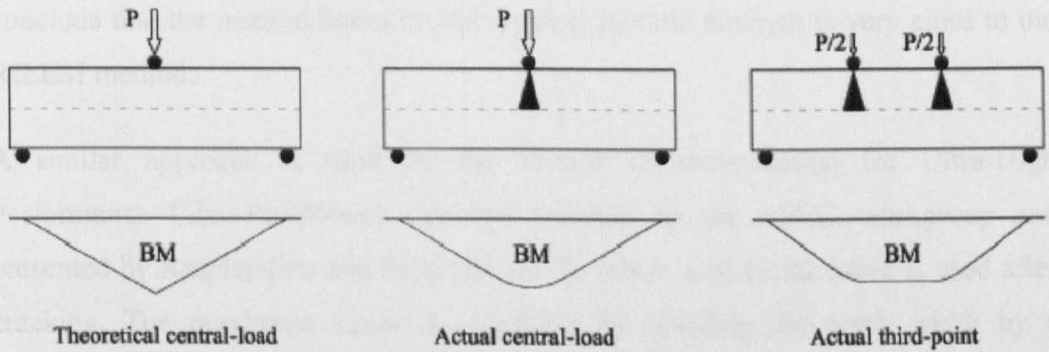


Figure 2.24 Bending tests – stress concentration.

The definition of the limit of proportionality (the point where cracking initiates) is one of the main problems encountered when evaluating the post-cracking behaviour of SFRC. Similar to other design guidelines, the bending test adopted by the σ - ϵ guideline defines the limit of proportionality (LOP) as the point of maximum load within a predefined deflection interval (RILEM uses the interval between 0.0 and 0.05 mm). This approach for defining the LOP can be subjective and it is therefore prone to errors. The recently completed Brite-Euram project on SFRC proposed the use of a more objective method, where the LOP is defined through an iterative procedure, whose aim is the evaluation of the correct slope at the limit of proportionality (Brite-Euram, 2002).

To solve this problem, Vandewalle (2003) uses the residual flexural tensile strength as design parameters instead of the equivalent flexural tensile strength. Those parameters are calculated from the experimentally determined load-CMOD curve at a crack width of 0.5 mm and 3.5 mm. The shape of the stress-strain curve is similar to that by RILEM. Dupont and Vandewalle (2002) presented a two-level stress-strain shape to distinguish between the pre- and post-peak behaviour. The limit strains, which related to a crack width of 0.5 mm and 3.5 mm, were determined by dividing the crack tip opening displacement (CTOD) by a characteristic length. This characteristic length is taken equal to two times the height of the tensile zone. The position of the neutral axis for a CMOD equal to 0.5 and 3.5 were approximately at 79% and 90% of the beam depth above the notch tip, respectively. The authors

conclude that the method based on the residual flexural strength is very close to the RILEM method.

A similar approach is used by the French recommendation for Ultra-High Performance Fibre-Reinforced Concrete (drafted by an AFGC workgroup and presented by Resplendino and Petitjean, 2003), where a tri-linear curve is used after cracking. The maximum strain is calculated by dividing the crack width by a characteristic length equal to $2/3$ of the depth of the beam section without any justification how the characteristic length was determined. The characteristic length (or the width of the fracture zone in a smeared tensile test) is defined by Bazant and Pijaudier-Cabot (1989) as the ratio G_F/W_F . The fracture energy G_F expresses the energy absorbed to create a unit crack area and W_F represents the energy absorbed by a volume of material during a smeared tensile test where a large number of microcracks are present. Both the surface fracture energy and the volumetric fracture energy were determined from the complete area enclosed by the stress-displacement or stress-strain curves. It seems intuitively appropriate that the fibre type and ratio and the maximum size of the aggregate limit the minimum crack spacing dimension in concrete. Clearly, it is not possible to give precise measures for the characteristic length due to the stochastic nature of this heterogeneous material.

2.4.2.3 Finite Element Analysis of SFRC

Commercially available FEA packages (e.g. DIANA, ATENA, ANSYS and ABAQUS) use the stress-crack width or stress-strain relationship to describe the tension softening of the concrete in the cracked region. The cracking process can be represented by two approaches.

The first approach uses the discrete crack representation model, which is based on the stress-displacement ($\sigma-w$) concept. This model was introduced by Ngo and Scordelis (1967). In general the location of the discrete crack need to be predefined (Hemmy, 2002). This method is more precise as far as local post-crack behaviour is concerned, but it is computationally more intensive and less useful when trying to

develop design models for practical applications. Hence, the more general smeared crack approach is adopted in this work.

The smeared crack approach assumes cracks to be smeared out over the element (σ - ε method). This model was first introduced by Rashid (1968) and then enhanced by Leibengood, Darwin and Dodds (1986) considering the effects of shear retention, Poisson's ratio and tension stiffening due to reinforcement. The main disadvantage of this model is that, in particular for small amounts of flexural reinforcement, it introduces mesh sensitivity in the analysis, since mesh refinement will lead to narrower crack bands.

To obtain the ideal stress-strain characteristics of concrete, an ideal uniaxial tensile test should be performed. However such a test is not easy to perform due to the localisation of the strain introduced by cracks. This approach also introduces the problem of crack spacing and, in general, a characteristic length of concrete needs to be chosen to reflect crack spacing.

A simple alternative to direct tensile tests is a displacement controlled flexural test, in which the strain across the crack can be controlled relatively easily by using the element stiffness.

Results from flexural tests can be used to develop the stress-strain or stress-crack width characteristics for FEA modelling.

Dupone and Vandewalle (2002a) used an iterative procedure to derive the σ - w characteristics by employing what they call "inverse analysis" of experimental results using the FEA package ATENA. The σ - ε characteristics were then determined by using the element length as the characteristic length. Figure 2.25 shows the experimental and calculated (by ATENA) load-deflection curves for beams of height *400 mm* and span of *2800 mm* reinforced with Dramix fibres (C25/30, 65/60 BN). A smeared crack model with a fine mesh (*25mm*) and course mesh (*100mm*) were used. It can be seen that ATENA overestimates the load-carrying capacity and the unloading of the load-deflection curve could not be followed. Furthermore, the results show that the FE analysis using this approach is almost mesh insensitive,

despite the fact that the course mesh is four times larger than the fine mesh. Mechtcherine (2000) studied the mesh sensitivity on a notched concrete beam under three-point loading using a smeared crack approach. It was confirmed that using a coarse mesh provided higher values of the net bending strength comparing to a finer mesh.

It is generally accepted that concrete models based on the stress-strain approach can lead to mesh sensitivity. The use of the element length as characteristic length is incorrect, but in this case it works because the overall result of scaling down was correct.

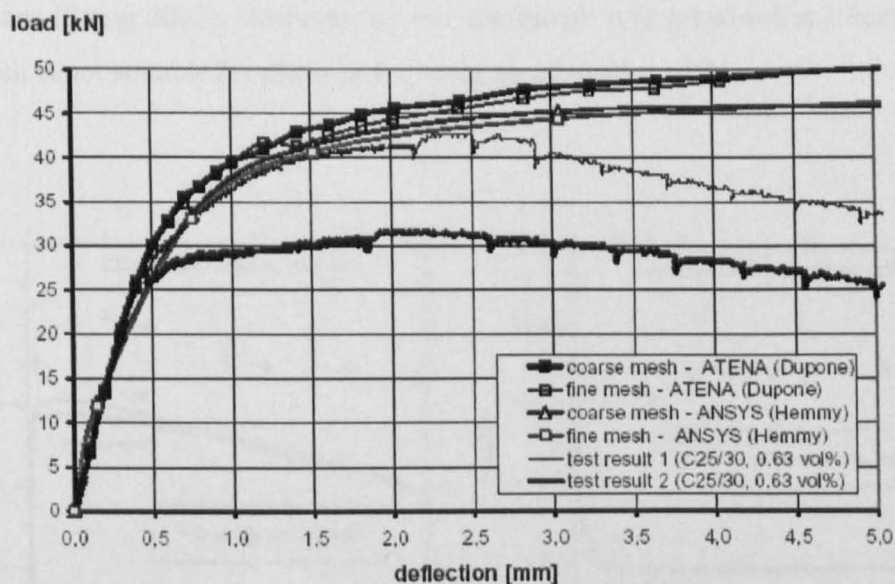


Figure 2.25 Load vs deflection calculated by Dupon and Vandewalle (2002) and Hemmy (2002)

Ostergaard et al (2002) also used an inverse analysis based on the bi-linear σ - w law model implemented in DIANA to establish the material parameters for simulating the non-linear behaviour of an imaginary hinge (hinge length = $0.5h$) in the crack zone by minimising the difference between the experimental results and hinge model prediction. This model was only tested on a wedge splitting test and was not demonstrated to simulate the behaviour of flexural elements.

Stang (2002) used non-linear springs between element nodes to simulate the crack within a non-linear hinge previously developed by Olesen (2001). The stress-crack opening relationship used as material law for the non-linear spring was measured directly through uniaxial tensile tests (Barr and Lee, 2001) and fitted with bi-linear relationships by Stang (2002). This model was used to predict the load-deflection curve of RILEM beam with various ratios of hooked fibres. Figure 2.26 compares the load-deflection responses predicted by Stang (2002) and the hinge model (Olesen, 2001) as well as the experimental results. It can be seen that the analytical models are similar but both are unacceptable compared to the experimental results. These poor predictions were attributed to the poor preparation of the uniaxial test specimens (Stang 2002). However, no σ - ε law model was proposed and hence, this approach is not suitable for use with the smeared cracked model.

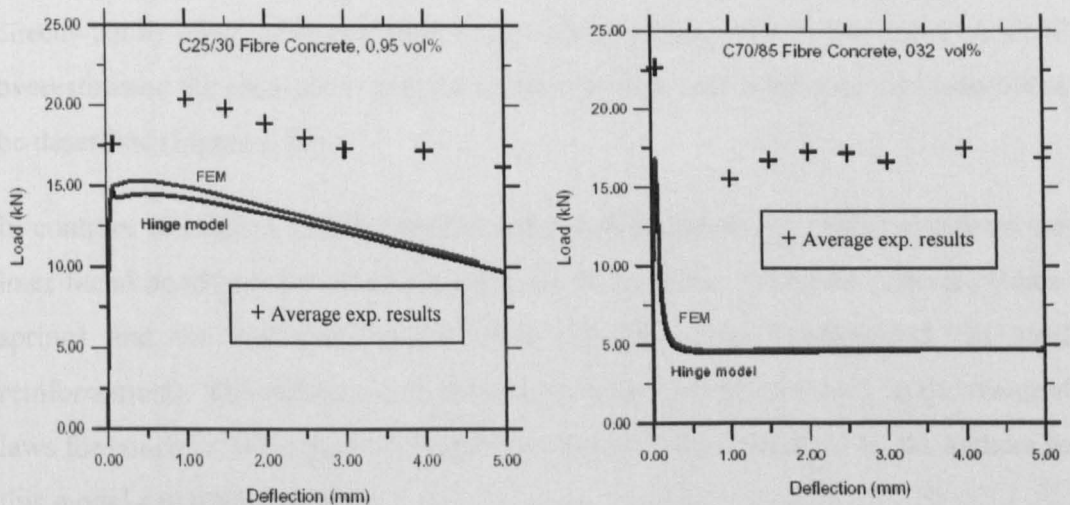


Figure 2.26 Load vs deflection responses after Oleson (2001) and Stang (2002)

Hemmy (2002), working in the same Brite Euram Project used ANSYS in his analysis. Since ANSYS does not allow much flexibility in defining the characteristics of concrete in tension, Hemmy added the effect of fibres by introducing smeared reinforcement in 3-D, by using a fictitious equivalent stress-strain relation as shown in Figure 2.27.

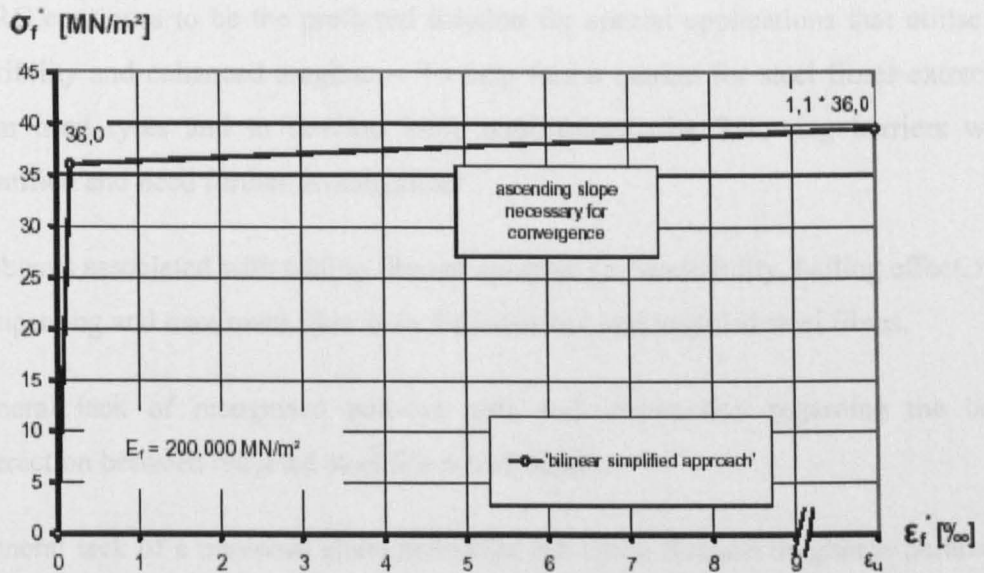


Figure 2.27: Equivalent Stress-strain relationship used by Hemmy (2002)

The tensile strength of the fibre reinforced beams was not derived from the RILEM beams directly but by using the inverse analysis developed by Stang (2000). The result obtained overestimated the load-carrying capacity and no post-peak behaviour was possible to be described (Figure 2.25).

In contrary to Hemmy (2002), Padmarajaiah and Ramaswamy (2002) simulated the inter-facial bond between fibre and concrete by using the “combine” element (linear spring) and the full stress-strain curve for fibre was implemented (as steel reinforcement). The references of the values of the parameters used in the material laws for concrete, fibres and the “combine element” were not given by the authors so this model can not be verified.

2.5 RESEARCH AND DEVELOPMENT NEEDS

Disposal of waste tyres is a world-wide problem and whilst there are uses for the rubber extracted from tyres, steel reinforcement is currently being disposed of in landfill. Demonstrating that the steel from tyres can be used as reinforcement in concrete will be of significant value to the UK and the world.

SFRC continues to be the preferred solution for special applications that utilise its flexibility and enhanced toughness. To help find a market for steel fibres extracted from used tyres and to develop more applications, the following barriers were identified and need further investigation:

Problems associated with adding fibre to concrete i.e. workability, balling effect, mix compacting and maximum fibre ratio for industrial and recycled steel fibres.

General lack of recognised pull-out tests and information regarding the bond interaction between recycled steel fibres and matrix.

General lack of a universal characterisation test and a flexural toughness parameter that can be used in design.

A lack of appropriate simple design methods that can be readily understood by practicing engineers.

A lack of appropriate finite element modelling of SFRC.

This thesis addresses these problems and presents the research done to overcome them.

3 FIBRE CHARACTERISATION, CONCRETE MIX DEVELOPMENT AND OPTIMISATION

3.1 INTRODUCTION

The main difficulty when a substantial amount of fibres are added to concrete is that the fibres tend to ball. The degree of the balling effect depends on the mix proportion and fibre types. This chapter presents the characteristics of four concrete mixes reinforced with five different types of fibres. The four mixes are:

- 1) **OPC40**: comprised coarse aggregate of maximum size 10 mm with Ordinary Portland Cement. The target compressive strength was 40 MPa.
- 2) **OPC50**: had a mix proportion (max size 10 mm)/(max size 20 mm) of 1/2 with Ordinary Portland Cement. The target compressive strength was 50 MPa.
- 3) **SPFA 40/30**: comprised coarse aggregate of maximum size 10 mm with 30% of Class F fly ash complying with ASTM 311, 1994. The mix with 30% fly ash content was expected to give the optimum strength and elastic properties (Swamy, R.N. and Stavridis, H., 1975). The target compressive strength was 40 MPa.
- 4) **SPFA/MS 120/20/10**: had a mix proportion (max size 10 mm)/(max size 20 mm) of 1/2 with 20% of Class F fly ash complying with ASTM 311 and 10% of Micro-Silica (MS) which was supplied as a 50/50 slurry with water by Elkem Materials Limited. The target compressive strength is 120 MPa.

The five types of fibre were:

- 1) **SRSF**: shredded fibre from shredded process.
- 2) **PRSF**: steel fibre from the Pyrolysis process.
- 3) **VSF**: industrially available virgin tyre cord.

4) ISF-1: industrial steel fibres with a flatted end.

5) ISF-2: industrial steel fibres with hocked end.

Though the exact amounts varied depending upon the concrete mix and fibre type, they included, for each mix of concrete, the maximum fibre content (defined as that quantity of fibres which, led to the desired slump without “balling”).

This chapter concentrates on the workability and compressive tests carried out on the plain and FRC mixes.

The principles described in this chapter were published by Tlemat and Pilakoutas (2002) and presented by the author at the International Conference on “Recycling and Reuse of Waste Material” in September 2003 (Tlemat et al., 2003).

3.2 MATERIALS USED

3.2.1 ORDINARY PORTLAND CEMENT

An Ordinary Portland cement type I, manufactured by the Rugby cement group in accordance to BS 12 (1996), class 42.5 N, was used throughout the study. The typical chemical and physical properties of the used binders are given in Table 3.1, (Kandie, 2001).

Table 3.1 Chemical and physical properties of the binders used in this work

Material Properties		Binder		
		OPC (%)	SPFA (%)	MS (%)
Silica	SiO ₂	20.5-21.8	53.5	94-98
Alumina	AlO ₃	5.1	34.3	0.1-0.4
Iron	Fe ₂ O ₃	3.7	3.6	0.02-0.15
Calcium	CaO	64.6	4.4	0.08-0.3
Potassium	K ₂ O	0.8	0.8	0.2-0.7
Magnesium	MgO	1.3	1.0	0.3-0.9
Sulphate	SO ₃	2.3-3.1	-	-
Titanium	TiO ₂	1.3	1.7	-
Alkalis		0.57-0.74	-	-
Loss on ignition		0.7	0.4	0.8%-1.5
Chlorides	Cl ⁻	< 0.02	-	-

Physical Properties			
Relative density	3.1	2.25	2.2
Theoretical surface area m ² /kg	3800	13000	20000
pH, in water	N/A	11-12	4.5-6.5
Moisture content (%)	N/A	< 0.2	< 1
Colour	Grey	light grey	Dark grey
Particle Shape	Crushed	Spherical	Spherical

3.2.2 AGGREGATES

The coarse and fine aggregate used in this work was fluvial dragged gravel. The shape of the aggregate was rounded (Figure 3.1a), fully water-worn or completely shaped by attrition, i.e. river or seashore gravel; desert, seashore and wind-blown sand (Figure 3.1b).

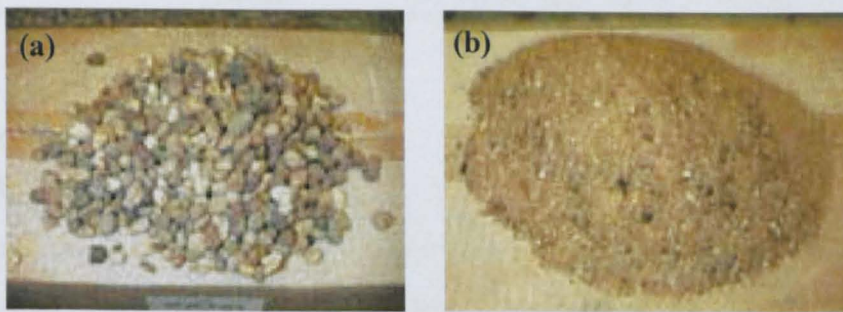


Figure 3.1 The aggregate used

The surface texture was smooth, water-worn, or smooth due to fracture of laminated or fine-grained rock, i.e. gravels, chert, slate, marble, some rhyolites. These classifications have been made according to the BS 812: Part 1 (1975). The results of this grading are shown in the Table 3.2a, and Table 3.2b.

Table 3.2a Coarse aggregate grading (Murguia, 2001)

Sieve size (mm)	20 mm Coarse aggregate Passing (%)	10 mm Coarse aggregate Passing(%)
37.5	100	100
20	98	100
14	57	100
10	12	95
5	05	7
2.36	-	0.65

Table 3.2b Fine aggregate grading (Murguia, 2001)

No. of Sieve	Weight (gr)	Sieve Analysis of Sand		
		Total	% retained	% Passing
4.75	8.9	8.9	1.5	98.5
2.36	72.3	81.2	14.1	85.9
1.18	56.8	138	23.9	76.1
600	79.2	217.2	37.6	62.4
300	243.1	460.3	79.8	20.2
150	84.7	545	94.5	5.5
75	32	577	100	0

The material density, water absorption and water content are shown in Table 3.2c.

Table 3.2c Density, water absorption and water content (Murguia, 2001)

	Material Data		
	Density	Water Absorption [%]	Water Content [%]
PC	3150		
Sand	2590	0.59	0.1
C. Agg. (20)	2600	0.58	0.09
C. Agg. (10)	2600	0.6	0.34

For practical mixes, the maximum size of coarse aggregate is recommended not to be larger than $2/3$ of the length of the steel fibre and should not exceed $1/5$ of the minimum size of the members to be placed (JSCE-SF1, 1984).

3.2.3 SUPERPLASTICIZER

The type of Superplasticizer used was sulphonated naphthalene- formaldehyde condensate complying with the BS 5075: Part 3, (1995) and ASTM C494-82 Type F, (1982). The properties are given in Table 3.3; the commercial name of the Superplasticizer is CONPLAST 501, supplied by FOSROC Ltd.

Table 3.3 Superplasticizer properties

Properties	CONPLAST 501
Appearance	Light Brown
Specific Gravity (at 200C)	1.123
Air entrainment	-
Chloride content	Negligible
Solid content (% by weight)	25
Recommended dosage (litre/50 Kg of cement content)	1.14-1.33

3.3 STEEL FIBRES

Five types of steel fibres were examined in this work, each type being determined by the process by which it was obtained.

3.3.1 STEEL FIBRES FROM SHREDDED TYRES

The shredded RSF (SRSF) were obtained from the third stage of mechanical shredding of discarded tyres and, hence, they were inconsistent in diameter and shape (Figure 3.2).

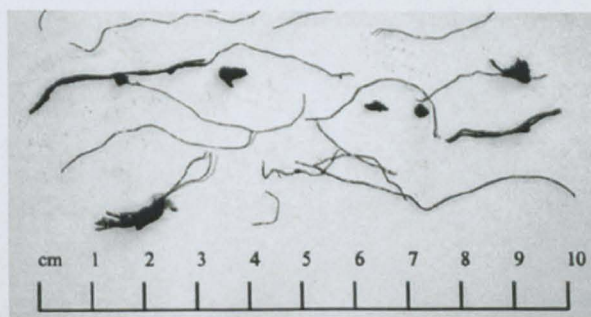


Figure 3.2 Un-sieved shredded steel fibres

The fibre characterisation is shown in Table 3.4 and 3.5

Table 3.4 Statistical analysis of length/diameter ratio of shredded steel fibres (Murguia, 2001)

Variable	Number	Mean	Median	3r mean	St deviation	Se mean
l/d	276	149.58	173.33	152.71	57.59	3.47
Variable	Minimum	Maximum	Q1	Q3		
l/d	25	218.75	100	190		

Table 3.5 Statistical analysis of length and diameter of shredded steel fibres (Murguia, 2001)

Variable	Number	Mean	Median	3r mean	St deviation	Se mean
Length	294	25.454	25	24.925	15.504	0.904
Thickness	294	0.15551	0.15	0.1503	0.1679	0.00396
Variable	Minimum	Maximum	Q1	Q3		
Length	1.4	70	11.78	37		
Thickness	0.04	0.37	0.1	0.2		

The SRSF were sieved to avoid using fibres containing rubber crumb on their surface and to remove the larger pieces of steel. In general, the sieved SRSF were more consistent in size and shape and had an average diameter of 0.23 mm, a length averaging over 20 mm and a tensile strength of around 2000 MPa. The proportions after sieving the steel fibres according to the ASTM A-820 are shown in Table 3.6.

Table 3.6 Shredded steel fibre grading (After sieving), (Murguia, 2001)

Sieve size	Mass retained grams	% retained	Cumulative % passing	Cumulative % retained
25.4 mm	0	0.0	100	0.0
19.05 mm	18	1.8	98.2	1.8
12.30 mm	106	10.6	87.6	12.4
6.35 mm	291	29.2	58.4	41.6
3.18 mm	213	21.3	37.1	62.9
2.40 mm	143	14.3	22.8	77.2
1.11 mm	85	8.5	14.3	85.7
< 1.11 mm	142	14.3	-	-
Total	998			

The sieve shredded fibres used in this study were the fibres passing the sieve 1.1 mm as shown in Figure 3.3.



Figure 3.3 Sieve shredded steel fibres passing the sieves 1) 6.35 mm, 2) 3.18 mm, 3) 2.40 mm and 4) 1.11 mm.

3.3.2 STEEL FIBRES FROM THE PYROLYSIS PROCESS AND VIRGIN CORD

The pyrolysed steel fibres (PRSF) were obtained by cutting recycled steel tyre-cord to 15 mm, 25 mm and 50 mm pieces. The cord was obtained from the microwave-induced pyrolysis of whole tyres (AMAT, 2003). The recycled cord was undamaged, since the tyres were decomposed at relatively low temperatures (about 350° C). However, it is noted that the cord was not entirely clean, as it contained a layer of carbon on its surface. In addition, the steel fibre diameter depends exclusively on the type of cord used in the tyre. The typical fibres, shown in Figure 3.4a, were obtained from super-single tyres. The fibres comprised 12 wires of 0.23 mm diameter, twisted together into a core strand of 0.85 mm diameter, and surrounded with another 15 twisted wires. On the cord surface there is a single twisted wire with a twist pitch of 5.33 mm. The fibre overall external diameter is 1.55 mm with effective diameter 1.16 mm and a tensile strength in excess of 1250 MPa. In general, the PRSF were not consistent in diameter (ranging 0.8 to 1.55 mm) and shape (Figure 3.4a,b).

The virgin steel fibres (VSF) were tested to examine the effect of carbon black on the surface of PRSF. VSF were obtained by cutting virgin steel tyre-cord to 50 mm pieces. The VSF fibres were free from any contaminates and had a consistent diameter of 1.55 mm. Their surface and tensile strength were similar to those of PRSF fibres (Figure 3.4a).

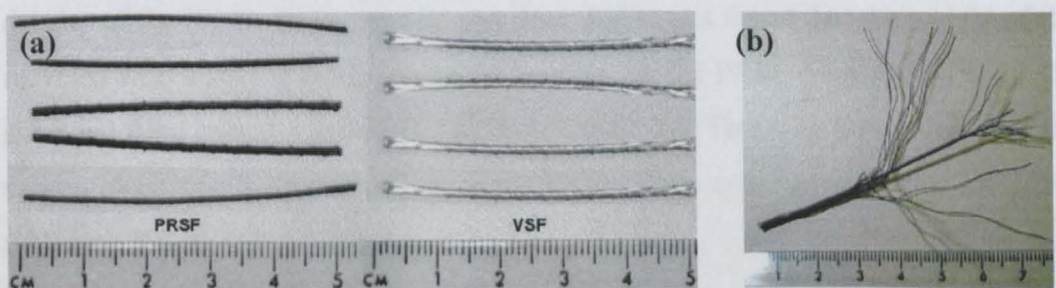


Figure 3.4 Pyrolysed and virgin steel fibres

Figure 3.4b Construction of one fibre

3.3.3 INDUSTRIALLY AVAILABLE STEEL FIBRES

Two types of industrially produced steel fibres (ISF) were used and both had a hooked end as illustrated in Figure 3.5. The fibres with a flattened end (Novotex, FE 1050, BRC 2003)), here called ISF-1, had a length of 50 mm and a nominal diameter

of 1mm and a tensile strength 1050 MPa. The ISF-2 fibres were made of cold drawn wires (Dramix, RL-45/50-BN, Bekaert, 2003)), 50 mm long, 1.05 mm thick, and a tensile strength 1050 MPa (Figure 3.5).

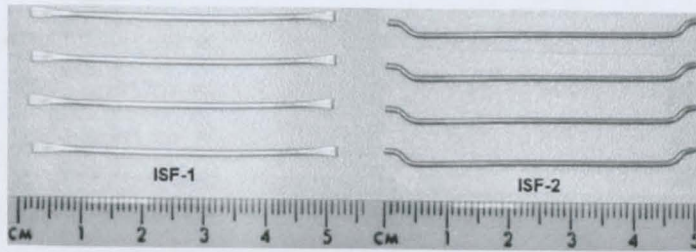


Figure 3.5 Types of industrially produced steel fibres

Figure 3.6 shows all the fibres used in this investigation.



Figure 3.6 Fibres used in this study

3.3.4 DENSITY OF STEEL FIBRES

In order to calculate the content of fibre by volume it is necessary to measure the density of the fibres. A density test was done and it was found that the weight of the recycled steel fibres in water increased by 29% for the PRSF fibre and 17% for the shredded fibre over the period of 183 min, Figure 3.7. This may be attributed to the carbon black found on the surface of the PRSF fibres and the impurities including rubber on the shredded fibres.

Density of PRSF fibres

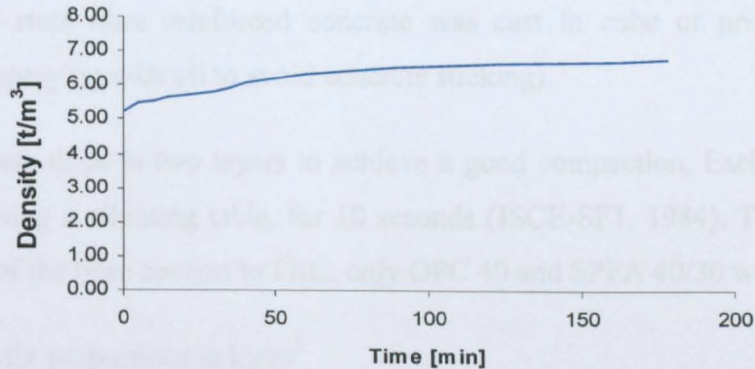


Figure 3.7 Density of PRSF fibres

The calculated density of the fibres is shown as follows:

PRSF fibre: 6725 [kg/m³]

SRSF: 6105 [kg/m³]

The above densities imply that the shredded fibre contained up to 25% rubber impurities (SG1) or 22% trapped air. It is most likely that the fibres trapped mostly air, since the rubber impurity was estimated at around 10%. The PRSF fibre also contained up to 18% carbon black (SG 1.8) or 14% air. Again it is most likely that the stranded wire trapped mostly air, especially in the inner cord.

3.4 PRODUCTION OF FRC

3.4.1 MIX DESIGN

The concrete mixing was done in either a 30 kg non-tilting drum mixer, or an 80 kg non-tilting mixer. The mixer availability or the size of the batch determined the mixer used.

There are no general rules on the order of feeding the ingredients into the mixer as this depends on the properties of the mixer. The order followed in this study was to feed the coarse and fine aggregate first, followed by approximately one third of the water, to ensure that the aggregates had a chance to wet. After the aggregates the cement was fed, followed by the rest of the water. Finally, the fibres and the

plasticizer were added in small amounts, to avoid balling. The mix proportions used in this study are given in Table 3.7.

The plain or steel fibre reinforced concrete was cast in cube or prism moulds (prepared by spraying with oil to avoid concrete sticking).

The casting was done in two layers to achieve a good compaction. Each layer was compacted, using a vibrating table, for 10 seconds (JSCE-SF1, 1984). To study the optimisation of the fibre content in FRC, only OPC 40 and SPFA 40/30 were used.

Table 3.7 Mix proportions in kg/m³

Mix Code	Cement			Water	W/B	Aggregate			Mass
	OPC	SPFA	MC			20mm	10mm	Sand	
OPC 40	346	0	0	180	0.52	0	1185	675	2386
OPC 50	394	0	0	177	0.45	770	340	715	2396
SPFA 40/30	236	101	0	155	0.46	0	1185	715	2392
SPFA/MS 120/20/10	367.5	105		105	0.2	770	340	730	2470

3.4.2 SPECIMEN USED AND CURING REGIMES

Two types of specimens were produced; cubes 100x100x100 to determine the compressive strength and prisms 100x100x500 mm for later testing. The specimens were demoulded and marked the day after casting (Figure 3.8).



Figure 3.8 The moulds used

Concrete curing was done according to the BS 1881- 111 (1983). Just after casting, the moulds filled with concrete were wrapped with polyethylene sheets (to avoid evaporation during hardening) in the laboratory for up to 24 hours after casting. After

removing the concrete from the moulds, the specimens were placed in a water tank at a temperature of 20°C.

3.5 MIX OPTIMISATION

3.5.1 INTRODUCTION

The mix optimisation was undertaken by trying to incorporate as much fibre as possible to maintain a slump value of 50 mm. Increasing the amount of fibre has a beneficial effect up to a certain point, beyond which there is too much air trapped and the compressive strength may decrease. Hence, in addition to a fresh concrete test (slump test according ASTM C143/C 143M – 98) a simple compressive strength test is required to determine the optimum mix.

3.5.2 COMPRESSIVE TESTS

The cube was placed according to BS 1881-116 (1983) with the cast faces not in contact with the platens of the testing machine i.e. the position of the cubes as tested is at right angles to the position as cast. The load was applied at a constant rate of stress within the range of 0.2 to 0.4 (kN / s) and the crushing strength was measured to the nearest 0.5 MPa.

3.6 RESULTS AND DISCUSSION

3.6.1 FRESH CONCRETE

The introduction of the five types of fibre, even at the lowest concentrations, produced concrete that was significantly more difficult to work with than the equivalent plain mix. The main cause for the reduced workability of FRCs is the increased internal friction which comes about because of fibre/fibre, fibre/matrix and fibre/aggregate interaction.

3.6.1.1 Optimisation of Shredded Fibre Content

The aim of the study was to produce mixes containing a maximum amount of shredded fibres without balling. The first mixing method was to start with mixes with high slump (coarse size $10 \text{ mm} \leq 2/3$ fibre length) as in OPC 40 and SPFA 40/30 with known slump and strength without fibre. Shredded fibres were added to the fresh concrete in 0.25% increments, measuring slump and making observations after each addition, until no more fibres could be incorporated to the mix without fibre balling. The results of this investigation are given in Table 3.8.

Table 3.8 Effect of incremental shredded fibre addition on slump to concrete

Fibres % (weight/vol)	Slump (mm)		Observations
	SPFA 40/30	OPC 40	
0.0/0.0	180-210	160-180	
0.25/0.1	140	150	
0.5/0.2	45	35	
0.75/0.3	40	20	Start of balling
1.0/0.4	20	10	slump too small
1.25/0.5	50	25	
1.5/0.6	45	10	badly balling

From Table 3.8, it can be seen that 0.5% (by weight) shredded fibres reduced the slump to 35 mm or less. However it was observed that the SPFA40/30 mixes had better slump and cohesivity than the pure OPC40 mixes. It is clear that to maximise the shredded fibre percentage whilst retaining a suitable workability for concrete, superplasticizer is needed.

In the second mixing method, plasticizer was added to the SPFA 40/30 mix with 1.5% (by weight) shredded fibres. After all the materials were mixed the plasticizer was added in dosages of 0.2% by cement content. This resulted in bad balling and segregation. This was attributed to the fibre geometry, mass and stiffness which prohibit dosages greater than 1.5% without balling as shown in Table 3.8. The use of the superplasticizer did not separate the balls once they formed in the mix. In fact, the superplasticizer created more, which means that the mixing of fibres should be kept to a minimum.

In the third method, all the materials were mixed, except the shredded fibres, including 2% superplasticizer by weight of cement content. After mixing for approximately 3 minutes, 1.5% shredded fibres were added to the concrete mix. The results were similar to the results obtained by the second approach. The reason is that by adding the superplasticizer to the concrete mix, the shear strength of the mix is reduced and the shredded fibres can travel freely through the mix, consequently forming fibre balls. After the balls are formed segregation occurs.

In the fourth method, all the dry materials were mixed first, including 1.5% shredded fibres. This was done to allow cement dispersion between the shredded fibres before adding any water or plasticizer. The results were such that even without adding the water or the plasticizer, some balls formed in the dry mixing process, and once the balls are formed there is no easy way to break them up.

The fifth method investigated the incremental addition of doses of 0.25% shredded fibres and controlling the slump and balling by adding incremental doses of 0.2% superplasticizer. This method proved effective and the results are given in Table 3.9.

Adopting this method seems to achieve an increased amount of shredded fibres (1.5%). However, in order to increase the amount of fibres further, another approach was tried.

The alternative approach was to use the sieved shredded fibres passing the 1.1 mm sieve (Figure 3.3).

Table 3.9 Effect of incremental addition of shredded fibre and superplasticizer on slump to SPFA40/30

Fibres (% by weight)	Fibre (% vol)	Slump (mm)	Superplasticizer (% by weight of cement)
0.00	0.0	210	0.0
0.25	0.1	140	0.0
0.50	0.2	75	0.0
0.50	0.2	90	0.1
0.75	0.3	70	0.1
0.75	0.3	95	0.2
1.00	0.4	65	0.2
1.25	0.5	60	0.3
1.50	0.6	75	0.4

The process used to investigate the effect of the sieved shredded fibres, was identical to those used for the un-sieved shredded fibres. The fibres were added in dosages of 0.25% and to control the slump and balling, superplasticizer was added in dosages of 0.20% by weight of cement, Table 3.10.

Table 3.10 Effect of incremental addition of sieved shredded fibre and superplasticizer on slump to SPFA40/30

Fibres (% by weight)	Fibre (% by vol)	Slump (mm)	Superplasticizer (% by weight of cement)
0.25	0.1	165	0.0
0.50	0.2	155	0.0
0.75	0.3	100	0.0
1.00	0.4	65	0.0
1.25	0.5	75	0.1
1.50	0.6	90	0.2
2.0	0.7	55	0.75

This last approach showed that the use of sieved shredded fibres reduced the amount of superplasticizer needed to achieve the slump required for concrete.

It was also found that the maximum amount of sieved shredded fibres that can be incorporated into a concrete without balling is around 2.0%.

3.6.1.2 Optimisation of PRSF Fibre Content

Fibre length of 15mm and 25mm: PRSF fibres were first cut in 15mm and 25mm similar to the length of the shredded fibre to study the fibre content due to the fibre type in FRC. The mixing methods used were similar to those for shredded fibres described in the previous section using OPC40 concrete. The mixing started with incremental fibre addition without superplasticizer (first mixing method). The results are shown in Table 3.11.

Table 3.11 Effect of incremental fibre addition on slump to OPC40 concrete

Fibres content % (weight/vol)	Slump (mm)		Observations
	15 mm	25mm	
0.0/0.0	130	135	highly workable
0.5/0.2	65	75	decrease of workability
1.0/0.35	25	20	further decrease of workability
1.5-4.0/0.5-1.4	5-0	5-0	low workability
4.5-5.0/1.6-1.8	-	-	balling initiates
5.5/1.9	-	-	badly balling

The balling initiates at approximately 5% of fibre content, but for that volume the mix was already too stiff. To increase the workability superplasticizer was added. The incremental addition of fibre and superplasticizer, according to the fifth method which provided the maximum amount of shredded fibre, was first used. The results of this trial mix are shown in Table 3.12.

Table 3.12 Effect of incremental fibre and superplasticizer addition on slump to OPC40

Fibres content %(weight/vol)	Slump (mm)		Superplasticizer (% by weight of cement)
	15 mm	25 mm	
0.0/0.0	120	135	0.0%
0.5/0.2	50	50	0.0%
0.5/0.2	70	70	0.2%
1.0/0.35	40	35	0.4%
1.5/0.5	100	90	0.6%
2.0/0.7	30	40	0.6%
2.5/0.9	25	30	0.8%
3.0/1.0	40	45	1.0%
3.0/1.0	60	70	1.2%

The fibre content was increased up to 3% (1.5% in the case of shredded fibre) without balling. In order to achieve a better dispersion of the superplasticizer in the mix a different mixing procedure was followed. Rather than pouring the superplasticizer straight into the concrete mix, it was initially dispersed into the water and then added to the mix (Manouselis, 2002). This mixing procedure gave better results as far as the workability of the mix was concerned. Different initial amounts of superplasticizer and fibres were also used, as for mixing method two. The amount of fibres was incrementally increased by 0.5% while the amount of superplasticizer remained constant. The results are shown in Table 3.13.

Table 3.13 Effect of incremental fibre addition on slump to concrete with SP

Fibres content %(weight/vol)	Slump (mm)			
	0.4% SP	0.6% Sp	0.8% SP	1% SP
0.5-2.0/0.2-0.7	>140	-	-	-
2.5/0.9	90*	-	-	-
3.0/1.0	-	>140	>140*	-
3.5/1.2	-	>140	105	>140
4.0/1.4	-	130	-	>140
4.5/1.6	-	-	-	>140
5.0/1.8	-	-	-	120*

* Partial collapse and shear in the slump test

From the above results the batch proportions adopted for the final mixes, comprised 5% of fibres (15mm or 20mm) and 1% superplasticizer. The FRC made by using such a mixing method can be used as pumped and sprayed FRC.

For conventional FRC in which less workability and higher flexural toughness is required, an FRC mix with longer fibres is required. For this purpose the PRSF fibre was cut to 50mm lengths.

Fibre length of 50mm: The mixes had in general very good workability, since the properties of the fibres (bundled fibres) did not permit the balling effect. It was decided to use OPC50 and SPFA40/30 for the studies involving the PRSF fibre. When OPC50 mix reached low workability (2% of steel fibres by weight), superplasticizer was added. Using this procedure it was possible to achieve a mix with 6% (by weight) fibres and 1% of superplasticizer (Zapnaris T.; 2001). However, it was difficult to place the mix into the moulds, which had a cross-section only two times the length of the fibre. In the case of SPFA40/30 the fibres were dispersed uniformly throughout the concrete at the end of the mix and mixed for only for one minute to avoid fibre balling. The resulting mix was consistent, had a good workability and no fibres were sticking out. Table 3.14 shows the workability of the mix with the addition of fibres and superplasticizer.

Table 3.14 Effect of incremental fibre and superplasticizer addition on slump

Mix type	Fibre (% by weight)	Fibre (%vol)	Superplasticizer (% by weight of Cement)	Slump (mm)
OPC50	1.0	0.35	0.08	75
	4.0	1.40	0.6	35
	4.5	1.57	0.8	45
	5.0	1.75	1	-
	5.5	1.90	1	60
	6.0	2.10	1	40
SPFA40/30	1.5	0.53	0.2	200
	3.0	1.0	0.4	150
	6.0	2.2	0.75	140

3.6.1.3 Optimisation of VSF, ISF-1 and ISF-2 Fibres

Since the fibres are mixed by weight and the PRSF fibres have carbon black, this means that less PRSF fibres are used in comparison to VSF. Only the SPFA40/30 mix was used to optimise the fibre content, since superpozzolan increases the workability and gives better concrete compaction. Three fibre ratios (1.5%, 3% and 6% by weight) of VSF and a high fibre ratio (6% by weight) of ISF-1 and ISF-2 were used, respectively. The optimal percentages of superplasticizer added to the mix are shown in Table 3.15. The mix procedure was similar to that of SPFA40/30 with PRSF fibres.

Table 3.15 Effect of fibre addition on slump to concrete mix SPFA40/30 with SP

Fibre type	Fibre (% by weight)	Fibre (%vol)	Superplasticizer (% by weight of cement)	Slump (mm)
VSF	1.5	0.46	0.2	160
	3.0	0.93	0.4	90
	6.0	1.9	0.75	70
ISF-1	1.5	0.46	0.2	160
	6.0	1.9	0.75	150
ISF-2	6.0	1.9	0.75	150

From Table 3.14 and 3.15 can be seen that SPFA40/30 mixed with PRSF fibres have better workability than with other fibres. It appears that the carbon black on the surface of PRSF increases the workability of the mixes. However, the diameter of

a fine powder with a large surface area. However, the diameter of this powder may be such that it leads to a better packing of the particles of wet concrete

3.6.1.4 Ultra High Strength Concrete with PRSF Fibres

The SPFA/MS 120/20/10 mix gave very good results utilising the properties of blended mixes. Taking into account the individual advantages of both SP and MS the two materials were blended successfully to produce very high strength concrete (Tsartsari, 2001). MS contributed to the high early strength, whilst SPFA improved the workability and gave higher late strength. The mix without fibres and superplasticizer was dry and not workable at all. Adding 1.2% superplasticizer (% binder) the plain mix became workable and the slump even exceeded the 60 mm. The optimum FRC mix was obtained by adding 5% of PRSF fibre and 1.5% superplasticizer. The use of superplasticizer was inevitable and the resulting slump was 60 mm.

3.6.2 COMPRESSIVE STRENGTH OF THE MIXES

The failure of plain concrete cubes is always due to abrupt crushing. In contrast, the inclusion of fibres allowed the reinforced cubes to deform significantly even after they had failed (with a noticeable bowing of their sides), without actually collapsing as shown in Figure 3.9.



Figure 3.9 Failure of plain and PRSF concrete cubes under compression.

However, the compressive strength of the FRCs was in general similar to that of plain concrete, as shown in Table 3.15 and Appendix (A.1). From Table 3.15 the following conclusions can be formulated:

Compressive strengths values of the OPC40 at seven days are much higher than those obtained from SPFA40/30. This is well documented in different works, and is because the hydration at early ages with SPFA is much slower than pure OPC concretes (Neville and Brooks, 1990). Compressive strength at 28 days is higher for SPFA40/30.

The overall trend is for an improvement in relative compressive strength with fibre volume; the highest increase around 10 % is achieved for fibre concentrations of 1% by weight. These observations are similar to other published works, as detailed in section 2 of the literature review.

Table 3.15 Effect of different type and amount of fibres on the concrete compressive strength

Mix code	Fibre type	Fibre content (% by weight)	Fibre content (% vol)	7 days	28 days
SPFA 40/30	Plain	0.0	0.0	39.5	42.6
	SRSF	1.0	0.4	30.6	48.8
		1.5	0.6	27.7	44.9
	SRSF(sieve)	1.5	0.6	27.4	-
	PRSF	1.5	0.52	27.8	-
	ISF	1.5	0.45	26.1	-
OPC 40	Plain	0.0	0.0	39.5	42.6
	SRSF	1.5	0.6	34.4	40.7
	PRSF (15mm/25mm)	1.5	0.5	31.5/30.7	43.0/42.5
		3.5	1.2	33.2/31.2	44.7/43.3
		5.0	1.8	33.2/35.4	43.8/47.3
OPC50	Plain	0.0	0.0	41.7	52.5
	SRSF	1.0	0.4	-	38.3
		1.5	0.6	-	40.8
	PRSF	0.0	0.0	41.7	53
		1.0	0.35	44.1	55.7
		2.0	0.52	41.0	51.7
SPFA/MS 120/20/10	Plain	0.0	0.0	79	113
	PRSF	5.0	1.3	103	120 (at 20d)

Increasing the shredded and PRSF (50mm fibre length) fibre over 1% can decrease the compressive strength. This can be related to the influence of fibre content and

fibre length on concrete compaction. These observations are similar to other published works, as detailed in section 2.3.3.

Increasing the fibre volume of PRSF with fibre length of 15mm or 25mm increases the compressive strength by values ranging between 25% for the 1.0% to 34% for the 5% of fibres due to the high workability of the FRC mix.

The compressive strength of FRC using normal shredded fibres is similar to that achieved using the same amount of sieved shredded fibres.

The performance of high strength concrete including SPFA/MS and fibres is significantly better than the concrete without fibres. By observations on the rate of strength gain, FRC strength of more than 120 MPa can be predicted for 28 days. The tested specimens in compression showed that not only first cracking was delayed, but the brittle explosive failure was avoided.

3.7 CHAPTER SUMMARY

This chapter demonstrated the use of steel fibres extracted from tyres as concrete reinforcement. Five types of fibres were selected for the mix development and optimisation. Four different mixes and different fibre ratios were mixed. Several mix methods were tried with the aim to optimise the mix with reference to workability, mix consistence and fibre volume. The main conclusions obtained are:

- Both types of SRSF and PRSF form a viable alternative for commercially-available steel fibres for use in steel-fibre-reinforced concrete.
- Incremental increase in fibre content is accompanied by reducing concrete slump and superplasticizers are needed to maintain workability.
- Maximum amount of SRSF that can be used in concrete mix without balling is 1.0% by weight of concrete and that increases to 2.0% if a superplasticizer is used.
- Use of sieved shredded steel fibres improves the workability of fresh concrete compared to a comparable mix made with un-sieved SRSF.

- Up to 6.0% by weight of concrete of PRSF, VSF, ISF-1 and ISF-2 fibres can be used in concrete without workability problems.
- The amount of PRSF fibres does not affect workability as much as SRSF fibres due to the fibre bundles remaining intact.

4 PULL-OUT BEHAVIOUR OF RSF AND ISF

4.1 INTRODUCTION

The characterisation of the properties of the SFRC resulting from the use of different fibres is important for an understanding of the behaviour of SFRC and the development of design guidelines.

To produce commercially and engineering viable recycled steel fibres (RSF), it is necessary to study the fibre material characteristics, such as the bond between fibre and concrete. Pull-out tests are the tests normally used in promoting the understanding of the bond characteristics of fibres and for the determination of the critical fibre length. Such tests are not always easy to perform on fibres, since the accuracy required is very high for very small displacements and loads. Pull-out tests were carried out in a number of different ways by different researchers (chapter 2), but to this date no method is accepted as standard. Test set-up and loading conditions can strongly influence the results. To obtain an accurate pull-out response, a suitable testing method must be developed and tested. Hence, in the study of the bond characteristic of RSF, several tests were developed to enhance the accuracy of the measurements.

This chapter presents a study on the bond characteristics of industrial steel fibres and steel fibres from used tyres. The current experimental program investigates the pull-out behaviour of different fibre types by using a single and double-sided pull-out test method (Figure 4.1 a, b). Single and multi-fibre pull-out set-ups are employed in these experiments.

The work described in this chapter was published and presented by the author at the International Conference on “Celebrating People and Concrete” held at Dundee University in September 2003 (Tlemat, Pilakoutas and Neocleous, 2003a) and at the

and Restoration, Lecce, Italy in June 2004 (Tlemat, Pilakoutas and Neocleous, 2004c) .

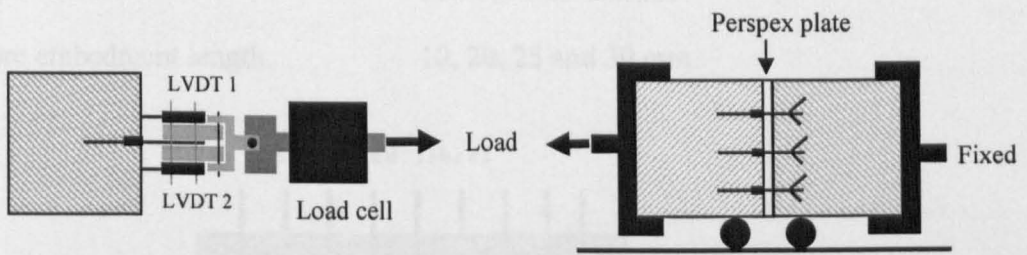


Figure 4.1a Single-sided pull-out test

Figure 4.1b Double-sided pull-out test

4.2 EXPERIMENTAL WORK

Fibres used in these experiments are the shredded fibres, PRSF and ISF-1 fibres described in chapter 3. The ISF-1 fibre will be called ISF in this chapter, because it is the only industrial fibre used in the pull-out tests. SFRC and plain concrete specimens were used to perform the single test and double-sided tests, respectively.

4.2.1 SINGLE-SIDED PULL-OUT TESTS

The single-sided pull-out test is the most common test method found in the literature due to its simplicity in set-up. The development of the test set-up was done in two phases:

Phase 1 (using spring calibrated to measure load): The specimen was prepared as shown in Figure 4.2(a). Single fibres were pulled out from fibre reinforced concrete specimen. The protruding end of the steel fibre was fastened to a specially prepared grip that allows a secure hold without deforming the fibre end (to reduce the risk of fibres breaking at the grip). This grip is held by a calibrated spring that is attached to the test machine as shown in Figure 4.2(b). The load was applied by pulling the spring (measured by LVDTs 1 and 2) and the slip of the fibre from concrete was measured by LVDTs 3 and 4. The calibrated spring was used for the measurement of the very small loads applied, since no load cells were available in our laboratories at the time that were sensitive enough for this job.

The variables examined in this phase included:

Type of fibre SRSF, PRSF and ISF

Fibre embedment length 10, 20, 25 and 30 mm

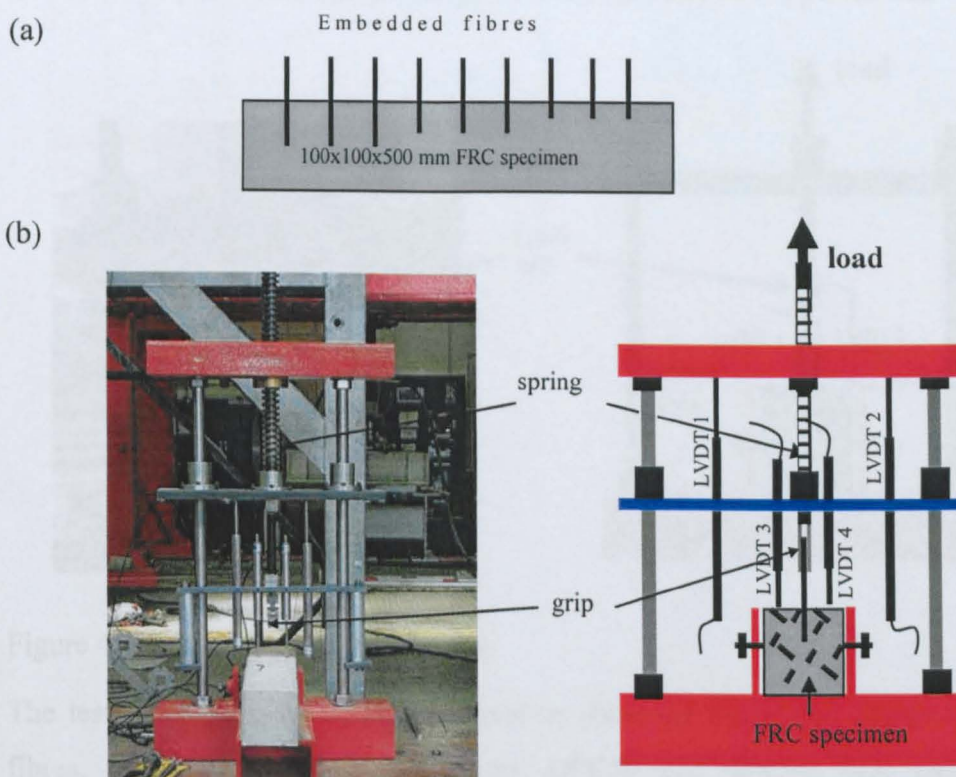


Figure 4.2 SFRC specimen and set-up pull-out test

The test programme comprised of 48 tests using shredded fibres, 21 tests using PRSF fibres and 9 tests using ISF fibres, as shown in Table 4.1. Mix OPC50 was used in this investigation.

Table 4.1 Pull-out test programme using load spring

Fibre code	Fibre content (% vol)	Tests per embedded length			
		10 mm	20 mm	25 mm	30 mm
PRSF -2%	0.7%	7	9		5
ISF-2%	0.6%	3	3		3
Shredded – 0.5%	0.2%		6		
Shredded – 1%	0.4%	7			11
Shredded – 2%	0.8%		15	9	-

Phase 2 (using load cell): The pull-out tests were carried out in the test-rig shown in Figure 4.3. Two transducers were used for measuring the slip of the fibre from the concrete prism. A load cell (range 500N), purchased specifically for this test was used for the measurement of the force required to pull-out (or fracture) the fibres. The concrete prism was clamped in place while the fibres were pulled-out.

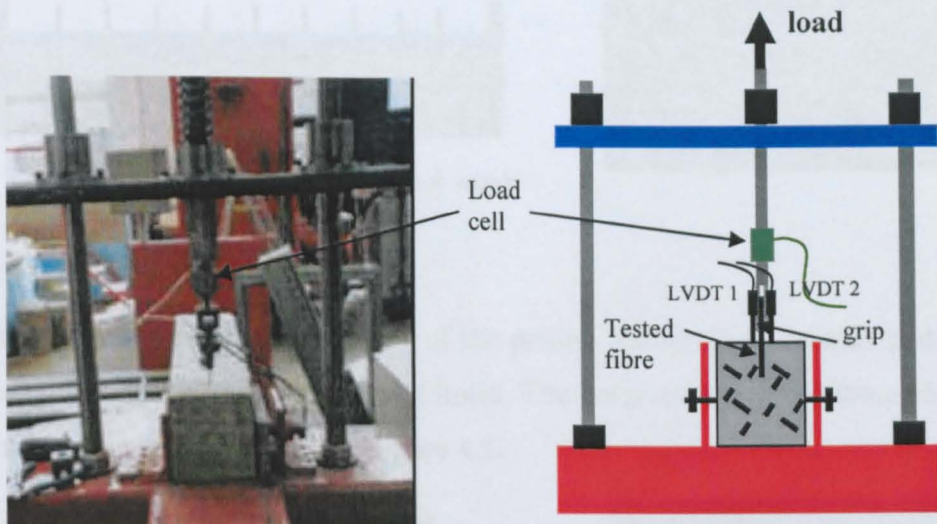


Figure 4.3 Test set-up using load cell

The test programme comprised 26 tests on shredded fibres and 33 tests on PRSF fibres, as shown in Table 4.2. Mixes OPC40 and OPC50 were used in this investigation.

Table 4.2 Pull-out programme using load cell

Fibre codes	Mix design	Fibres content by volume %	Number of tests for each fibre embedded length		
			10 mm	20 mm	30 mm
PRSF -1.86%	OPC40	1.86%	3	9	3
PRSF-0.5%	OPC50	0.5%	3	3	3
PRSF - 0.33%	OPC50	0.33%	3	3	3
Shredded - 1.86%	OPC40	1.86%	3	3	3
Shredded - 0.5%	OPC50	0.5%	3	3	2
Shredded - 0.33%	OPC50	0.33%	3	3	3

4.2.1.1 Specimen Preparation

The steel moulds used for casting the specimens were the standard moulds 100 x 100 x 500 mm used for testing the FRC flexural strength. The mould had three

compartments. Since the fibre was inserted in the side of the specimen, the middle compartment was left empty as shown in Figure 4.4.

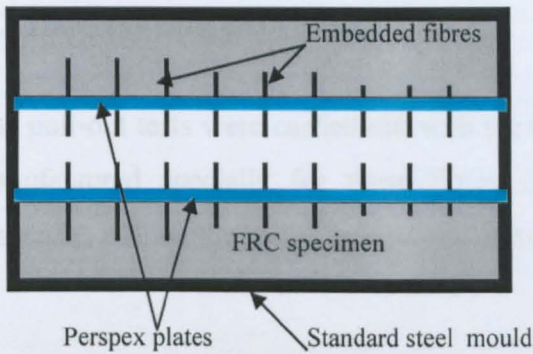


Figure 4.4 Standard steel mould

Instead of the steel plate separators of the prisms, 20mm thick Perspex plates were used. Each had 9 small equi-distant holes. The holes were placed 50mm above the bottom of the moulds as seen in Figure 4.5.

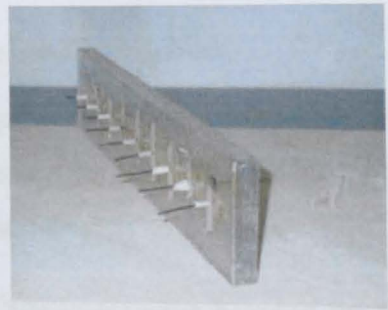


Figure 4.5 Perspex plate with 9 holes

Adhesive tape was used to prevent the concrete from coming out of the holes and sticking to the steel fibres. This was done so that it will be easier to pull out the plates once the concrete has hardened. Heat shrinkage wire (shrinks with heat) was also used and placed around fibres at the side of the concrete in order to avoid surface effects during tests. This procedure required about 5 hours for every 18 fibres, because it was very difficult to put the fibres with the right embedment length in the moulds and ensure that no concrete escaped and got stuck onto the fibres. The mould was filled in three layers, i) bottom layer approximately 35mm thick with 15 second vibration, ii) middle layer for another 15 seconds. However, the final layer was vibrated for a longer period to remove all air bubbles. The specimens were left under

polyethylene sheets in the laboratory for 24 hours after casting and then they were stripped from the moulds. Curing took place in the mist room until testing.

4.2.1.2 Testing procedure

The pull-out tests were carried out with the test-rig shown in Figure 4.6, which was manufactured specially for these fibres. The screw arrangement was operated manually, pulling the spring or load cell in a controlled manner.



Figure 4.6 Pull-out specimen and testing machine used in this work

However, it was found that energy stored in the spring was released suddenly when the fibre started pulling out. To improve the measurements after the peak load, it was decided to replace the spring with a load cell attached directly to the grip.

The other factor affecting measurements was the fibre extension between the FRC prism and the grip, which means that the measured displacement includes two components, fibre extension and fibre slip. To arrive at the fibre slip the fibre extension needs to be eliminated, something which is not always easy, especially if there is slip in the grip, or the wire stiffness is not known. To eliminate these problems the double sided pull-out test, described below, was developed.

4.2.2 DOUBLE-SIDED PULL-OUT TESTS

To investigate the bond strength and the pull-out behaviour of steel fibres in a matrix a new type of test was devised, in which fibres in the simulated cracked surfaces were subjected to essentially uniaxial tensile stresses. The specimens were cast in two parts separated by a perspex plate 4 mm thick. The fibres were inserted through a central series of holes in the perspex plate. A multitude of fibres (3 or 5) can be

used instead of a single fibre. Concrete prisms were subjected to uniaxial tension at a constant rate of displacement. This test method is used to determine the critical length, which is the maximum length that a fibre can be embedded without breaking during pull-out. In this method all fibres have the same embedded length and the total response is divided by the number of fibres used.

The variables used were:

Type of fibre: SRSF, ISF, PRSF and PRSF with a blob at the end

Fibre embedded length: 10, 20, and 30 mm

Number of pulled fibres: 1 and 3

The test programme comprised 54 test specimens, as shown in Table 4.3. Mix OPC50 was used in this investigation.

Table 4.3 Double sided pull-out test programme

PRSF Fibre codes	ISF fibre codes	SRSF fibre codes	Number of pulled fibres	Number of tests for each fibre embedded length		
				10 mm	20 mm	30 mm
A1	I1-10	-	1	3	3	3
A1*	-	-	1	3	3	3
A3	I3-10	S3-10	3	3	3	3

A1*: PRSF fibres with a blob at the end

A more stable load-displacement control test rig (based on a Tensometer) was adopted in this work to eliminate instability after reaching the peak load (Banthia and Trottier, 1994).

4.2.2.1 Specimen Preparation

Standard steel moulds were used for casting the specimens; the moulds were divided into two sections by a wooden partition. In each section a pull-out specimen is cast in two blocks, each block being separated by a Perspex plate located in the middle of the specimen. The nominal size of each half is 100 x 100 x 80 mm, as shown in Figure 4.7a.



Figure 4.7a Moulds used

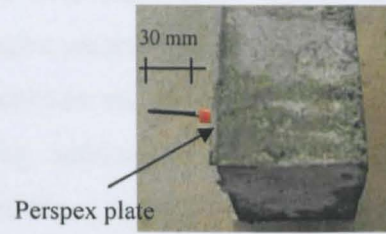


Figure 4.7b Fibre embedded length

In the Perspex plate, holes in the centre allow the fibre to go through to the other side. To prevent bond forming between the plate and the concrete, oil spray was applied to the side of specimen which contains the fibre to be pulled out. To prevent surface cracking near the top of the embedded fibre, every fibre was covered with a 10 mm plastic tube filled with silicon over the initial fibre length in concrete. In this way the bond length is determined exactly and in the experiment this was varied from 10 to 30 mm (Figure 4.7b)

To anchor the fibre securely in the fixed half of the specimen, the ISF end was welded to a deformed metal stick (Figure 4.8a). In the case of the PRSF, a steel stick was threaded through the cord (Figure 4.8b). Whereas for the shredded fibre, the end was tied in a knot.

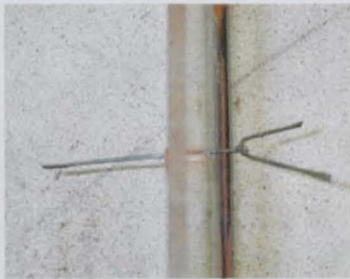


Figure 4.8a Anchoring of ISF

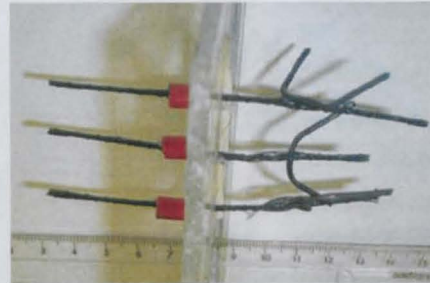


Figure 4.8b Anchoring of PRSF

Specimens were cast in two stages (Figure 4.7a). To ensure the accurate position of the tested fibre, the half of the specimen containing the anchored fibre was cast first. The mould was left to cure for 24 hours, and the second half was cast the following day. Once hardened, the completed specimens were carefully demoulded and placed in a curing tank for 7 days and then kept in air at approximately 70% RH and 18° C for 3 days before testing.

Before testing, specially made steel clamps were fixed at the ends of each block as shown in Figure 4.9a. At this stage, the displacement transducers were also fixed on the sides, as shown in Figure 4.9b. The specimen was then pinned to the spherically mounted shuck attachments in the testing apparatus to ensure axial alignment (Figures 4.10). To avoid any damage to the fibre-concrete interface during handling of the specimen prior to testing, a metal strip was fixed on the clamps. The two halves of the specimen were therefore temporarily supported by the metal strip rather than by the fibre.

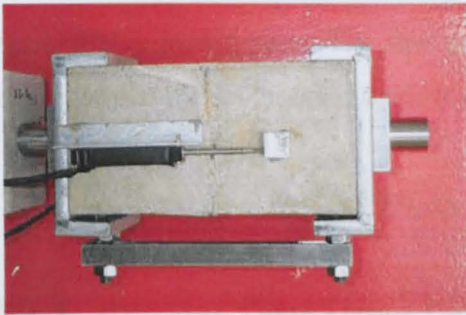


Figure 4.9a Metal clamps

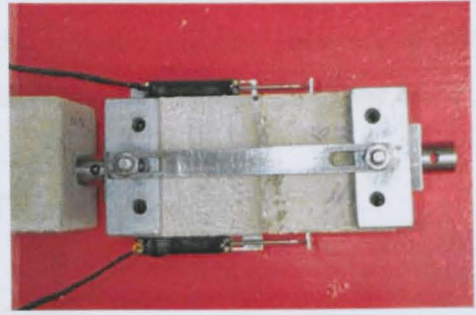
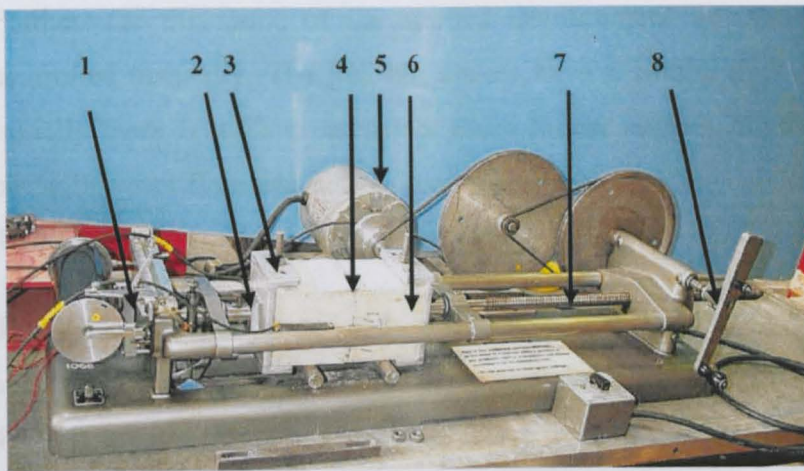


Figure 4.9b Location of transducers

4.2.2.2 Testing Apparatus



1. Spring beam with two strain gauges.
2. Chuck attached to the clamp with a pin.
3. Metal clamp
4. Perspex plate
5. Electric motor
6. Pulled part of the specimen
7. Cross-head attached to motor
8. Manual handles

Figure 4.10 Testing apparatus

The tests were performed by using a modified tensometer with a 5 kN strain gauged spring beam. The pull in the test specimen is transmitted through a tension head to the spring beam. Specimen deformations and crack widths were measured over a gauge length of 50 mm using two transducers mounted on each side of the specimen to enable an average deformation reading to be determined (Figure 4.9a, b). The load (measured by the two strain gauges) and deformations (measured by the two

transducers) were digitally recorded using a four channel data acquisition system. An electric motor, fitted with a 3-step pulley, drove the cross-head at a speed of 0.2 mm/min at the debonding phase and 1.5 mm/min at the pull-out phase (Figure 4.10).

4.3 RESULTS AND DISCUSSION

The data from each pull-out test were initially processed to determine the applied load versus slip. In each section the pull-out behaviour of the tested steel fibres is described here in two parts. The first part deals with the pull-out behaviour of PRSF and ISF, whilst the second part deals only with the pull-out behaviour of the SRSF.

4.3.1 SINGLE-SIDED PULL-OUT TESTS

4.3.1.1 Pull-out Tests Using Load Spring

All load-slip curves were unstable after the occurrence of the peak load. The measured load undergoes sudden unloading to zero and releases all energy. Furthermore the speed of the applied displacement was not constant, as it was controlled manually. The pull-out curves have a similar appearance (Figure 4.11). Initially there is a fibre extension phase (linear region), followed by a debonding phase between fibre and matrix (non-linear region). This debonding process ends at the peak load.

The peak load increases with the embedment length. In addition, the energy absorption (area under the load-slip curve) for a fibre slip less than 1mm (Figure 4.11) is greater in the case of PRSF fibre than for ISF. This shows that the PRSF fibre has good bond characteristics.

On the other hand, the peak loads for the PRSF fibres with all embedded lengths occur at a fibre slip less than 2 mm, whilst in the case of ISF fibres this takes place after 2 mm as shown in Figure 4.12. It seems that the PRSF fibre will be better at bridging cracks earlier whilst the ISF fibre appears to be relying on a frictional mechanism from its end anchorage during pull-out. This mechanism is capable of dissipating energy, but not to arrest cracks at an early stage.

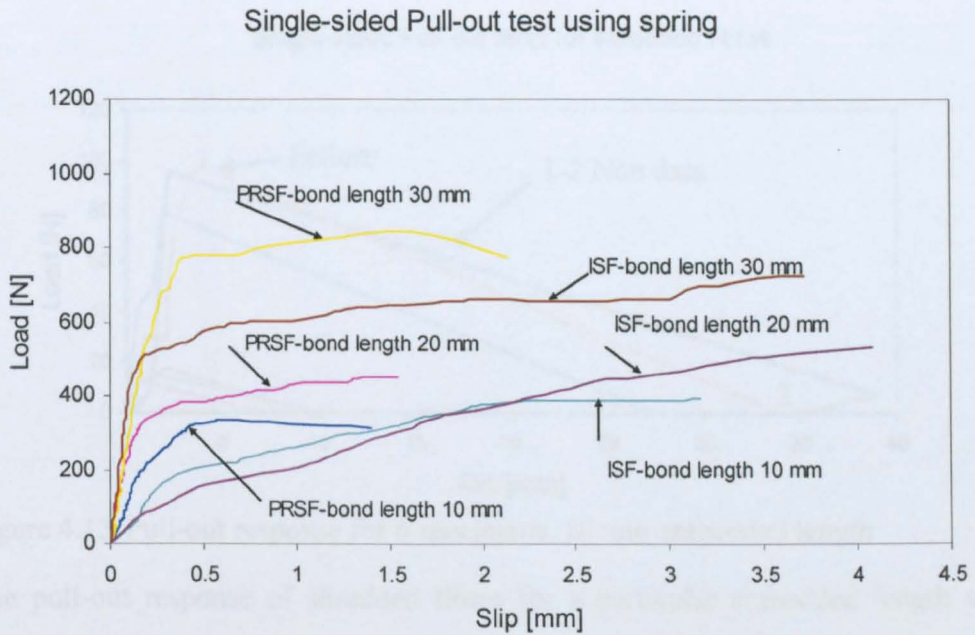


Figure 4.11 Pull-out response for PRSF and ISF fibres

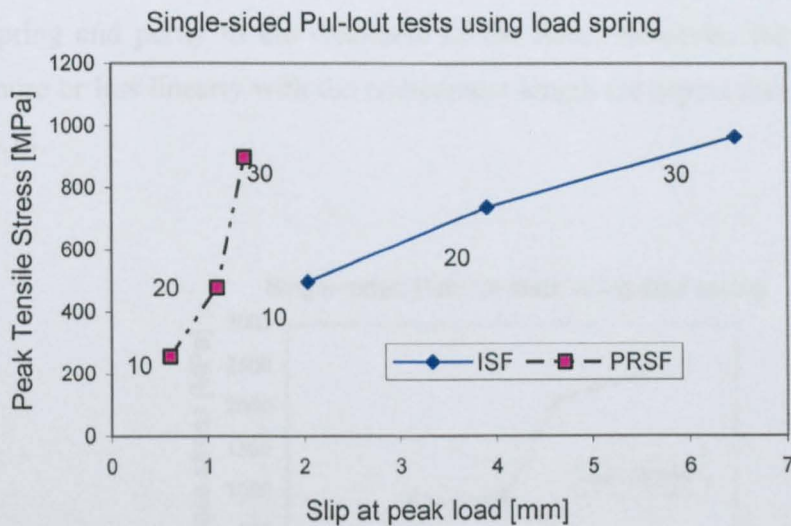


Figure 4.12 The effect of fibre shape on the pull-out response; bonded length 10, 20, 30 mm

In the case of shredded fibres, as shown in Figure 4.13, the initial linear phase of the pull-out curve is relative long with a short debonding phase between fibre and surrounding matrix.

Table 4.4 Results of single-sided pull-out tests

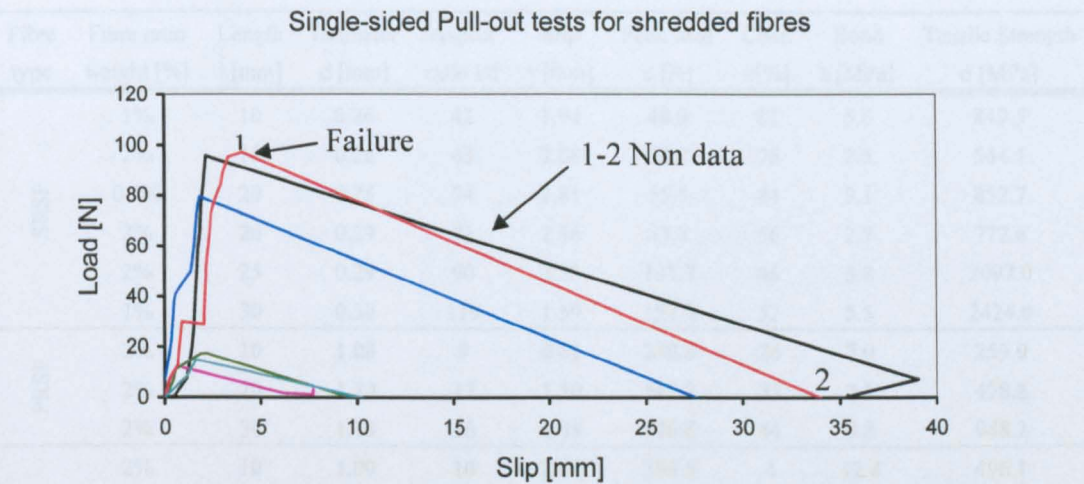


Figure 4.13 Pull-out response for 6 specimens, 10 mm embedded length

The pull-out response of shredded fibres for a particular embedded length varies considerably in energy and strength. This scatter of results (see coefficient of variation in Table 4.4) is partly related to the inaccuracy of the measurements via a spring and partly to the weakness of the fibre. However, the peak load increases more or less linearly with the embedment length (or aspect ratio) as shown in Figure 4.14.

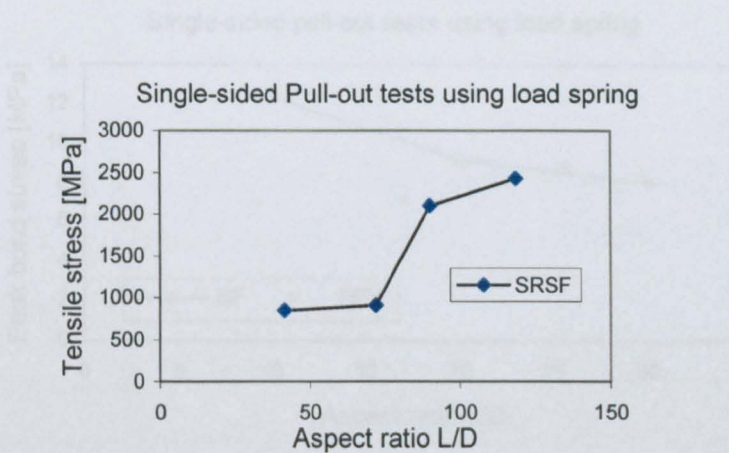


Figure 4.14 Tensile stress vs aspect ratio

Table 4.4 shows the average peak load and the corresponding bond and tensile strength for the tested fibres. It can be seen that the increase in fibre content in the FRC does not increase the bond stress, which means that the pull-out strength of the shredded fibre is not influenced much by macro-cracking of the surrounding matrix. The summary of all results is shown in tables in Appendix B.

Table 4.4 Results of single-sided pull-out tests

Fibre type	Fibre ratio weight [%]	Length l [mm]	Diameter d [mm]	Aspect ratio l/d	Slip s [mm]	Peak load n [N]	Coef. v[%]	Bond t [MPa]	Tensile Strength σ [MPa]
SRSF	1%	10	0.26	42	1.94	48.9	81	5.6	849.5
	2%	15	0.26	63	2.08	32.9	76	2.5	544.1
	0.5%	20	0.28	74	1.81	55.5	44	3.1	852.7
	2%	20	0.29	71	2.16	47.8	56	2.7	772.6
	2%	25	0.29	90	2.23	131.7	46	5.8	2097.0
	1%	30	0.30	119	1.59	159.9	52	5.5	2424.0
PRSF	2%	10	1.08	9	0.61	238.8	26	7.0	259.9
	2%	20	1.20	17	1.10	545.3	33	7.1	478.8
	2%	30	1.18	26	1.39	996.8	44	8.8	948.2
ISF	2%	10	1.00	10	2.00	389.5	4	12.4	496.1
	2%	20	1.00	20	3.81	579.0	23	9.2	737.2
	2%	30	1.00	30	6.43	757.6	5	8.04	964.5

Figure 4.15 shows a comparison between the maximum stress achieved in the ISF and PRSF fibres. It is clear that the better bond of the PRSF fibre is surpassed at the end by the anchorage detail of the ISF fibre.

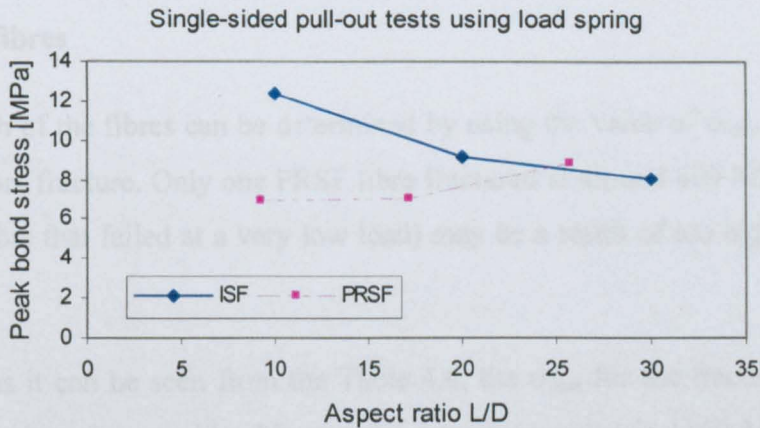


Figure 4.15 Tensile stress vs aspect ratio

4.3.1.2 Pull-out Tests Using Load Cell

Results of PRSF and shredded fibre pull-out tests are listed in Tables 4.5 and 4.6 respectively.

Table 4.5 Results of PRSF fibre pull-out tests

Fibre type	D_{eff} [mm]	L_{emb} [mm]	Mix type	P_{max} [N]	τ_{max} [MPa]	$\tau_{max,ave}$ [MPa]	σ_{max} [MPa]	σ_{ave} [MPa]	σ	P/F*
PRSF	1.41	10	OPC40	950	21.45	-	608.41	-	-	P
	1.39	30	OPC40	1190	9.08	-	784.20	-	-	P
	1.41	10	OPC50	700	15.80	-	448.30	-	-	P
	1.39	10	OPC50	525	12.02	-	345.97	-	-	P
	1.41	10	OPC50	690	15.58	14.47	441.90	412.06	57.32	P
	1.38	20	OPC50	920	10.61	-	615.09	-	-	P
	1.40	20	OPC50	1205	13.69	12.15	782.78	698.94	118.57	P
	1.34	30	OPC50	1080	8.55	-	765.82	-	-	P
	1.36	30	OPC50	1010	7.88	-	695.27	-	-	P
	1.39	30	OPC50	1220	9.31	8.58	803.97	755.02	55.15	F
	1.31	10	SPFA40/30	210	5.10	-	155.81	-	-	P
	1.34	10	SPFA40/30	262.5	6.24	-	186.14	-	-	P
	1.36	10	SPFA40/30	725	16.97	9.44	499.08	280.34	190.04	P
	1.37	20	SPFA40/30	410	4.76	-	278.13	-	-	P
	1.36	20	SPFA40/30	890	10.42	7.59	612.66	445.40	236.55	P
	1.36	30	SPFA40/30	975	7.61	-	671.18	-	-	P
	1.39	30	SPFA40/30	890	6.79	-	586.50	-	-	P
	1.39	30	SPFA40/30	51.5	0.40	4.93	34.27	430.65	345.88	F

- P = Pull-out, F = Failure

Failure of fibres

The strength of the fibres can be determined by using the value of σ_{max} when failure is due to fibre fracture. Only one PRSF fibre fractured at around 800 MPa. This (and the other fibre that failed at a very low load) may be a result of too high pressure in the grip.

However, as it can be seen from the Table 4.6, the σ_{max} for the fractured shredded fibres strength varies considerably and the maximum value is 1150 MPa. Some of the fibres that were pulled-out show an even higher strength of nearly 1400 MPa. This indicates that the fibres that fractured did not reach their real strength but a reduced one, most likely due to damage inflicted during the shredding process possibly due to notches inflicted by the knives.

Table 4.6 Results of shredded fibres pull-out tests

Fibre type	D_{eff} [mm]	L_{emb} [mm]	Mix type	P_{max} [N]	τ_{max} [MPa]	$\tau_{max,ave}$ [MPa]	σ_{max} [MPa]	σ_{ave} [MPa]	σ	P/F
SRSF	0.21	10	OPC50S*	17.2	2.61	-	496.59	-	-	P
	0.22	10	OPC50S	33.75	4.88	-	887.85	-	-	P
	0.22	10	OPC50S	43.75	6.33	4.61	1150.91	845.12	329.25	F
	0.21	20	OPC50S	39.5	2.99	-	1140.43	-	-	P
	0.22	20	OPC50S	45.0	3.26	3.13	1183.80	1162.12	30.67	P
	0.23	30	OPC50S	32.0	1.47	-	770.20	-	-	P
	0.23	30	OPC40S	58.0	2.68	-	1396.0	-	-	P
	0.21	30	OPC40S	(13.9)	-	2.07	-	1083	703.35	P
	0.22	10	OPC40A*	8.4	1.22	-	220.98	-	-	P
	0.19	10	OPC40A	11.2	1.88	1.55	395.02	308.0	123.06	P
	0.22	20	OPC40A	36.25	2.62	-	953.61	-	-	P
	0.22	20	OPCA40	1.89	0.137	1.38	49.72	501.67	639.15	F
	0.22	30	OPCA40	34.0	1.64	-	894.42	-	-	F

S*: Mix contains shredded fibres; A*: Mix contains PRSF fibres

Comments on the results:

Figures 4.16 and 4.17 show that although there is not much difference in the results, a slight increase in bond strength is noticeable with an increase in the effective diameter. Furthermore, as far as bond strength is concerned in Figure 4.6, OPC50S (SRSF) seems to give a better performance whilst in Figure 4.17, OPC40S seems to be better. Hence, it is concluded that the main parameters affecting bond strength are the mix type and the embedment length rather than the diameter.

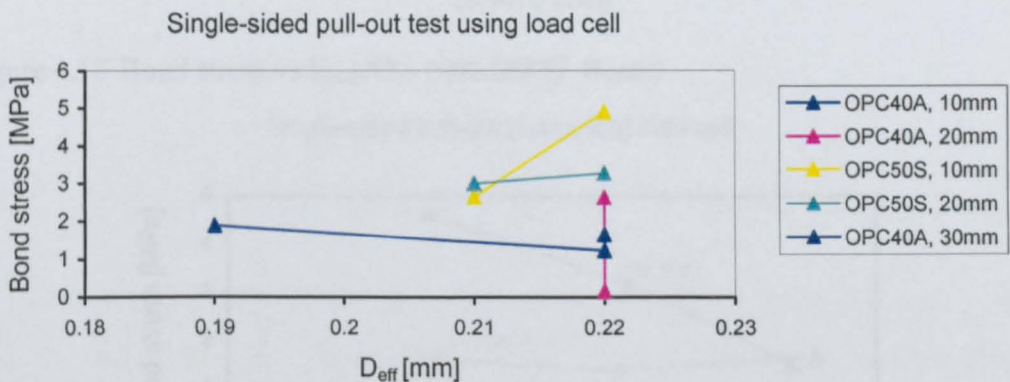


Figure 4.16 Bond stress vs effective diameter for various embedded shredded fibre length

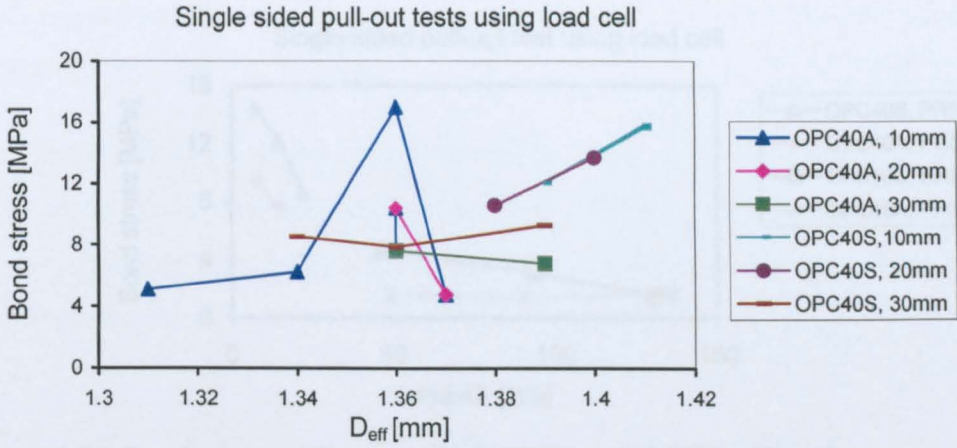


Figure 4.17 Bond stress vs effective diameter for various embedded PRSF fibre length

Although it seems that shredded fibres develop lower bond strengths than PRSF fibres, the two cannot be compared directly as the L/d ratio of the shredded fibres is much higher than the one of the PRSF fibres. This can be clearly observed from Figures 4.18, 4.19 and 4.20.

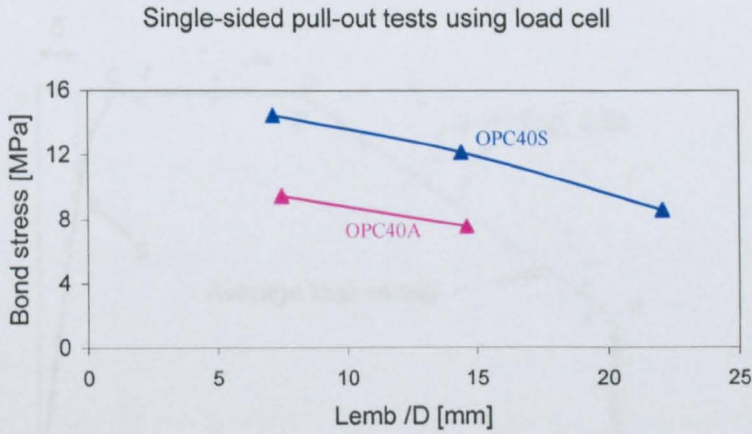


Figure 4.18 Bond stress vs L_{emb}/D_{eff} ratio (PRSF fibres)

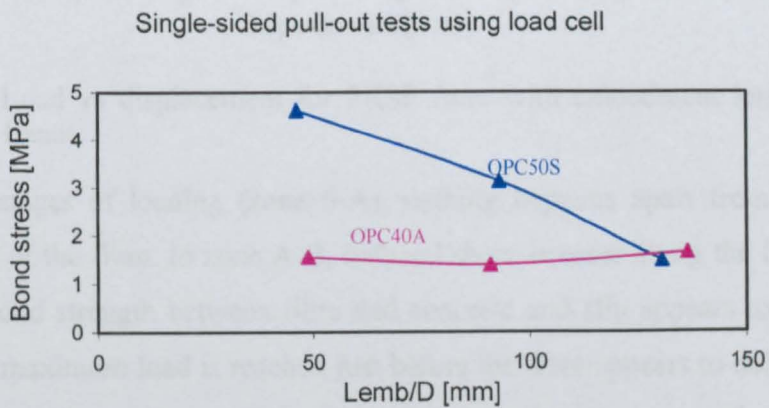


Figure 4.19 Bond stress vs L_{emb}/D_{eff} ratio (shredded fibres)

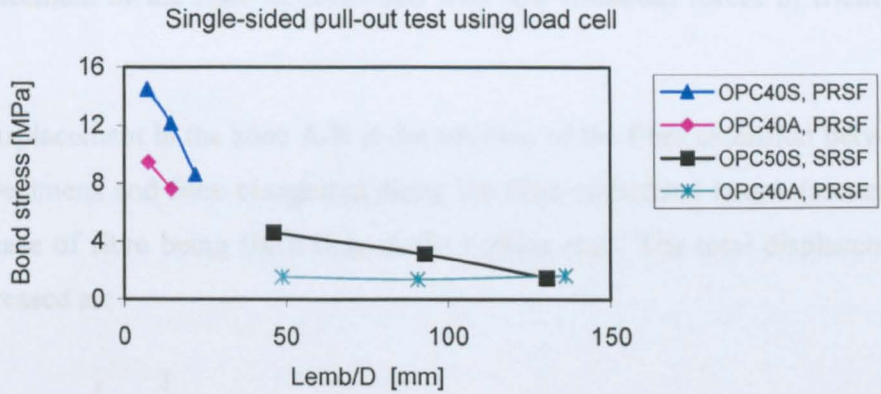


Figure 4.20 Bond stress vs D_{eff} ratio (both PRSF and shredded fibres)

4.3.1.3 Comment on the Pull-out Behaviour

The pull-out behaviour of SFRC is examined in further detail by studying the load-slip curves for pull-out test shown in Figure 4.21.

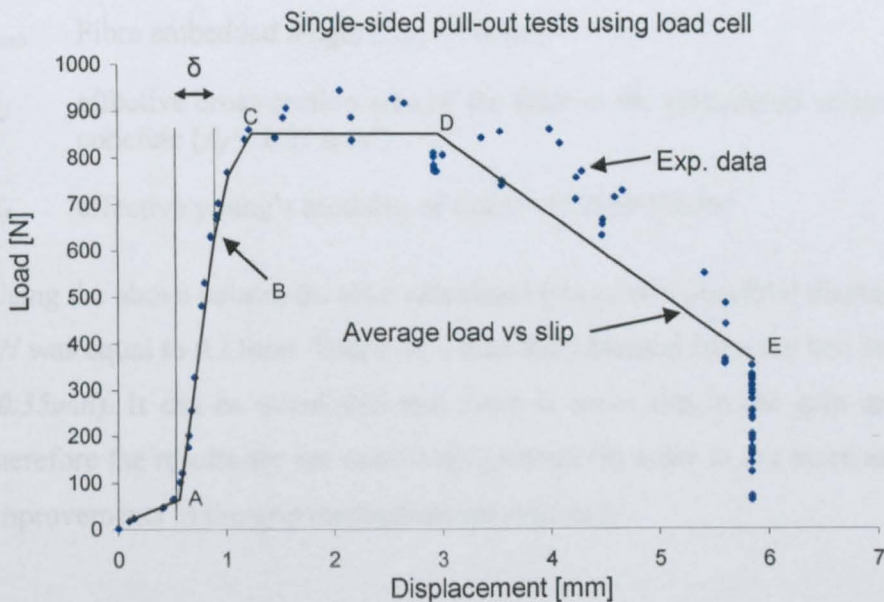


Figure 4.21 Load vs displacement for PRSF fibre with embedment length, $L_{emb} = 10\text{mm}$

At the first stages of loading (zone 0-A), nothing happens apart from the initial straightening of the fibre. In zone A-B, induced shear stresses along the fibre do not exceed the bond strength between fibre and concrete and slip appears to be elastic. The point of maximum load is reached just before the fibre appears to debond and at the point where shear stresses become greater than the bond strength (debonding zone B-C). The pull-out of fibre occurs against frictional resistance in zone C-D. The

main displacement of the fibre is developed with low frictional forces in frictional zone D-E.

The total displacement in the zone A-B is the addition of the fibre extension between grip and specimens and fibre elongation along the fibre embedded length (assuming the worst case of fibre being fixed only at the bottom end). The total displacement can be expressed as:

$$\delta = P_{cr} \left[\frac{l_{free}}{A_f E_f} + \frac{l_{emb}}{A_f E_f} \right] \quad [\text{mm}] \quad (4.1)$$

where

P_{cr} The load before debonding accrues (point B in Figure 4.21, $P_{cr} = 630 \text{ N}$)

l_{free} Fibre length between grip and specimens ($l_{free} = 25 \text{ mm}$)

l_{emb} Fibre embedded length ($l_{emb} = 10 \text{ mm}$)

A_f effective cross-section area of the fibre in the considered volume of the fibre concrete ($A_f = 1.01 \text{ mm}^2$)

E_f effective young's modulus of fibre = 150000 N/mm^2

Using the above values, the total calculated (maximum possible) displacement at 630 kN was equal to 0.15 mm . This is less than that obtained from the test in the zone A-B (0.35 mm). It can be concluded that there is some slip in the grip mechanism and therefore the results are not extremely accurate. In order to get more accurate results improvements in the grip mechanism are required.

4.3.2 DOUBLE-SIDED PULL-OUT TESTS

4.3.2.1 PRSF and ISF

The average of three test results for the PRSF and ISF tests is shown in Table 4.6. The values of coefficient of variations calculated for peak loads shown in the Table are lower than in the case of single-sided pull-out test, which indicate the better accuracy of the double-sided pull-out test.

Table 4.6 Average test results for PRSF and ISF

Fibre type	Length l [mm]	Diameter d [mm]	Effective d [mm]	Aspect ratio l/d	Aspect ratio eff l/d	Slip s [mm]	Peak load [N]	Coef of v. v[%]	Single fibre [N]	Bond τ [MPa]	Tensile σ [MPa]
ISF	10	1.00		10.00		4.47	231	28		7.36	295
	20	1.00		20.00		10.60	370	22		5.89	471
PRSF 1-fibre	10	1.55	1.18	6.45	8.47	3.25	359	31		7.37	328
	20	1.55	1.18	12.90	16.95	0.88	443	20		4.55	405
	30	1.55	1.18	19.35	25.42	1.44	653	8		4.47	633
PRSF 3-Fibres	10	1.55	1.18	6.45	8.47	0.75	800	31	267	5.48	244
	20	1.55	1.18	12.90	16.95	1.58	1640	14	547	5.61	500
	30	1.55	1.18	19.35	25.42	0.19	2015	6	672	4.60	643
PRSF 1-fibre with blob	10	1.55	1.18	6.45	8.47	0.58	875	42		17.96	800
	20	1.55	1.18	12.90	16.95	1.53	1290	23		13.25	1180
	30	1.55	1.18	19.35	25.42	0.83	1375	20		9.41	1257

Figure 4.22 represents a typical pull-out load versus slip response of PRSF and ISF fibres. It can be seen that the PRSF appears to be debonding gradually until end slip takes place (initial linear region A-B1) followed by a change in the slope, which characterises the formation and propagation of a stable debonding process (region B1-C1). This debonding process ends near the maximum load. Finally, the third region (C1-D1) corresponds to the failure of the bond mechanism. The ISF has no bond along its length, hence resistance is provided only by end anchoring slip. That means a softer response in the region A-B2.

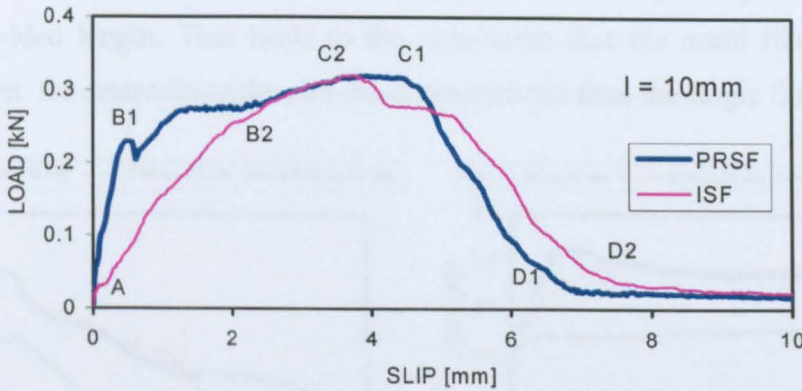


Figure 4.22 Load vs slip response for PRSF and ISF fibres

Effect of Fibre Shape

The response in regions A-B and B-C is of great interest. This is because in SFRC when the crack-width is greater than 1mm, the fibre is in general not relevant for flexural toughness and design purposes. The gradient of the curve of the PRSF fibre in the linear region is much steeper than that of the ISF fibre which reflects the better bond characteristics of a fibre with distributed bond. This is expected to lead to better flexural characteristics.

Effect of Fibre Embedment Length

The effect of the embedment length is of great importance to the pull-out behaviour and its understanding can lead to fibre length optimisation. It can be seen from Figure 4.23 that the pull-out load increases with increased embedment length. A better investigation of this loading region is achieved by the multi-fibre test, as shown in Figure 4.24 for three fibres.

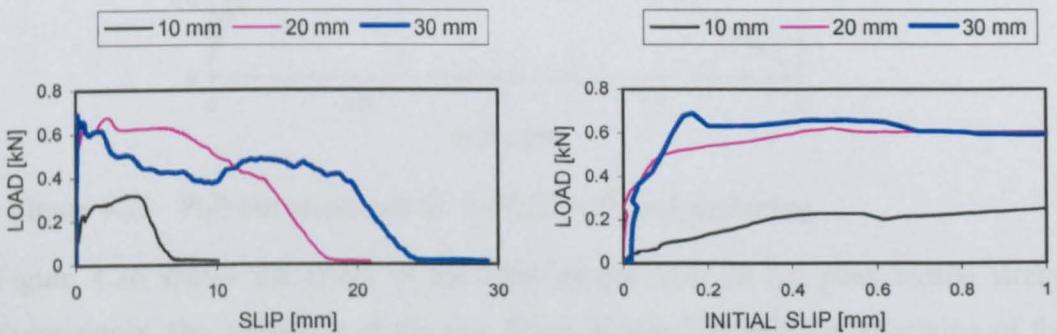


Figure 4.23 The total and the initial pull-out response of 1-PRSF fibre

Figure 4.24 shows more stable initial load-slip behaviour, especially for fibre with low embedded length. That leads to the conclusion that the multi fibre test is a suitable test for determining the pull-out characteristics than the single fibre test.

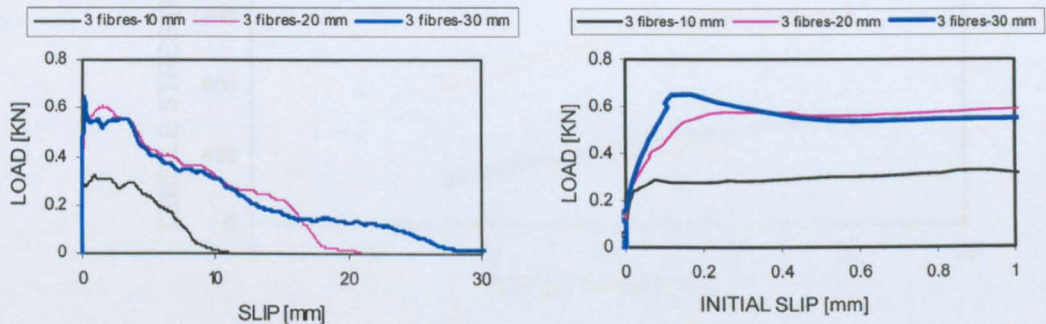


Figure 4.24 The total and the initial load vs slip response for 3-PRSF fibre

Effect of anchoring detail

To improve the pull-out behaviour of the PRSF, it was decided to weld a blob with a nominal diameter of 2.5 mm at the fibre end. Again, single fibres with 3 different embedment lengths were tested. Figure 4.25 shows the load-displacement curves for the three embedment lengths. The shape of the three curves is similar, comprising of an ascending part that curves until the maximum load. Throughout this process, the fibres appear to be fully bonded until the welding between the fibre and the blob breaks. A maximum tensile strength of 1257 MPa is achieved.

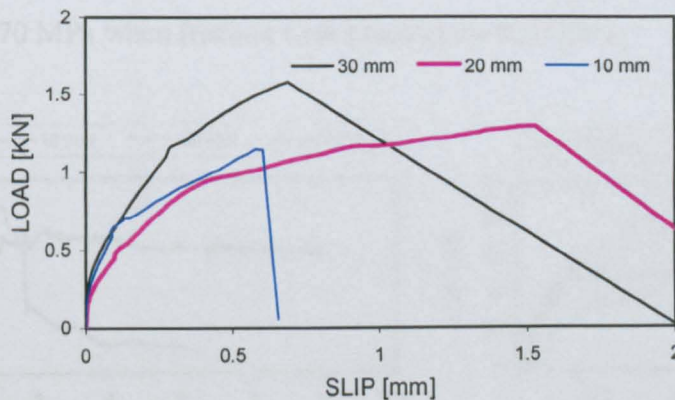


Figure 4.25 Pull-out responses for 1-PRSF with end anchoring

Figure 4.26 shows the effect of the fibre aspect ratio on the peak tensile stress. Surprisingly, the behaviour of the two fibres is identical with the exception of the PRSF fibre with blob which gives better results. The peak stress increases more or less linearly with the aspect ratio.

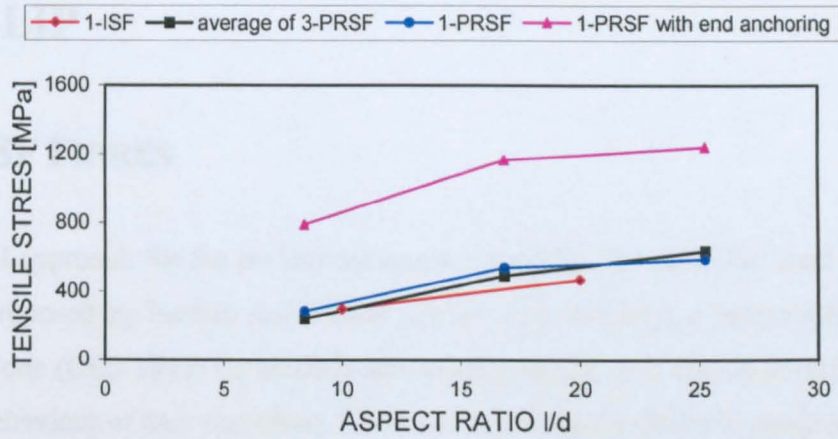


Figure 4.26 Tensile stress vs aspect ratios for PRSF and ISF fibres

4.3.2.2 SRSF

The tested 0.23 mm diameter SRSF were obtained from twisted tyre cord strands. These fibres are fragile which makes the handling and placing of the specimen difficult and, hence, some fibres were broken in the specimen before testing. It was decided to test multi fibres to ensure specimen stability. As shown in Figure 4.27, all of the fibres with 20 mm embedment length broke during loading. In the case of the 30 mm fibre embedment length, two fibres were broken and one was pulled out. Only the fibres with 10 mm embedment length were pulled out. The recorded load for 3 fibres, at failure, was approximately 84 N. This load corresponds to an average stress of 670 MPa when fracture took place in the first fibre.

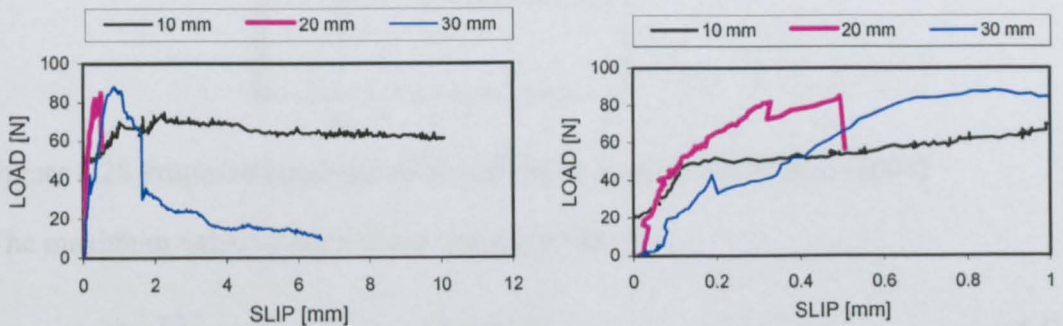


Figure 4.27 The total and the initial pull-out response of 3-SRSF

4.4 THEORETICAL MODELLING OF BOND-SLIP

4.4.1 ISF FIBRES

A theoretical approach for the pullout mechanism used for the industrial steel fibres (ISF) was proposed by Fantilli and Vallini (2003). This model is an improvement to the Model Code (CEB 1993) for smooth steel reinforcement. It is able to describe the post-peak behaviour of bars and fibres. The τ - s relationship for fibres is composed by the following branches:

$$\tau = \tau_{\max} \cdot \left(\frac{s}{s_1} \right)^\alpha \quad s \leq s_1 \quad (4.2)$$

$$\tau = \tau_{fin} + (\tau_{\max} - \tau_{fin}) \cdot e^{k(s_1-s)} \quad s > s_1 \quad (4.3)$$

Parameters τ_{\max} , s_1 and τ_{fin} are illustrated in Figure 4.28.

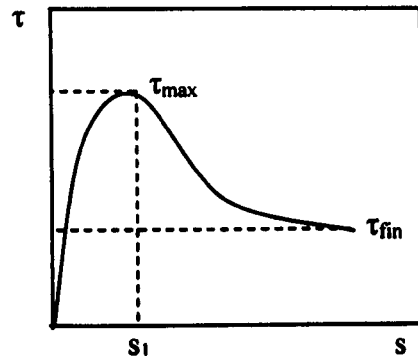


Figure 4.28 Proposed bond-slip relationships by Fantilli and Vallini (2003)

The maximum value of bond stress was expressed as:

$$\tau_{\max} = 1.65 \cdot \sqrt{f_c} \quad [\text{N/mm}^2] \quad (4.4)$$

The ultimate bond stress was expressed for all types of fibres as:

$$\tau_{fin} = 0.067 \cdot \sqrt{f_c} \quad [\text{N/mm}^2] \quad (4.5)$$

where

f_c concrete compressive strength $f_c = 40$ [N/mm²]

Φ Fibre diameter $\Phi = 1.0$ [mm]

The parameters s_l and k are affected by the experimental evaluation of slip (Wang, Li and Backer 1988). The position of the peak bond stress s_l can be evaluated from experiments while the value of k is in the range of 1 ~ 4 per mm, independently of the fibre diameter and of the strength of surrounding concrete. The exponent $\alpha = 0.5$ is suggested by the Model Code.

By adopting suitable parameter values for the τ -s relationship, the numerical best fit pullout load-slip curve is compared with the experimental results in Figure 4.29. It is clear that this approach simulates the behaviour of the ISF very well. However, since most of the parameters seem to be determined experimentally, this approach is not much different to curve fitting.

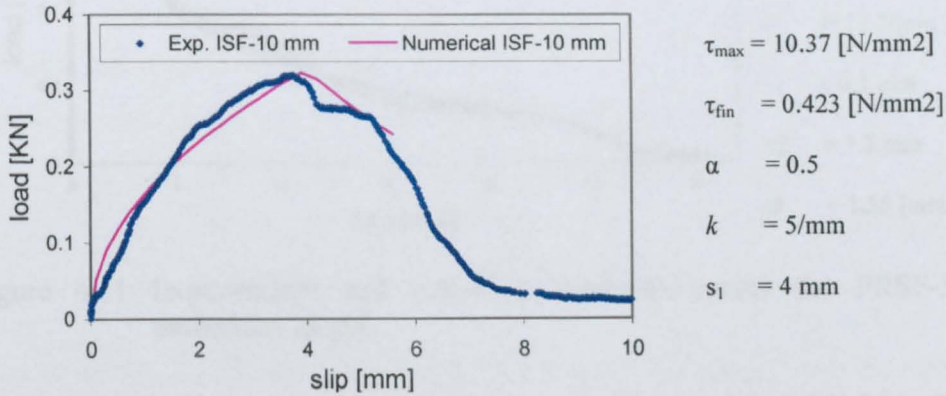


Figure 4.29 Comparison between exp. and numerical load-slip results for ISF

4.4.2 PRSF FIBRES

The pullout response of the PRSF fibres differs from that of the ISF fibres due to the surface of the PRSF fibres and it shows a stiffer initial response and a larger plateau at pull-out load. The Fantilli model on its own can not represent this behaviour and here it is modified by combining it with the CEB (1993) model between the CEB (1993) and the model proposed by Fantilli and Vallini (2003) as illustrated in figure 4.30.

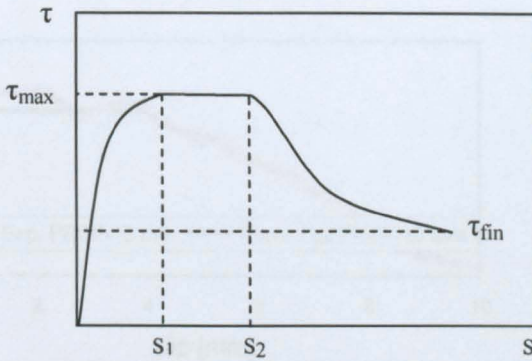


Figure 4.30 Modified Bond-slip curves for PRSF fibres

Equations 4.2 and 4.3 can be used for $s \leq s_1$ and $s > s_2$. The parameters for the model and the comparison between numerical and experimental pullout tests are illustrated in Figures 4.31 to 4.33.

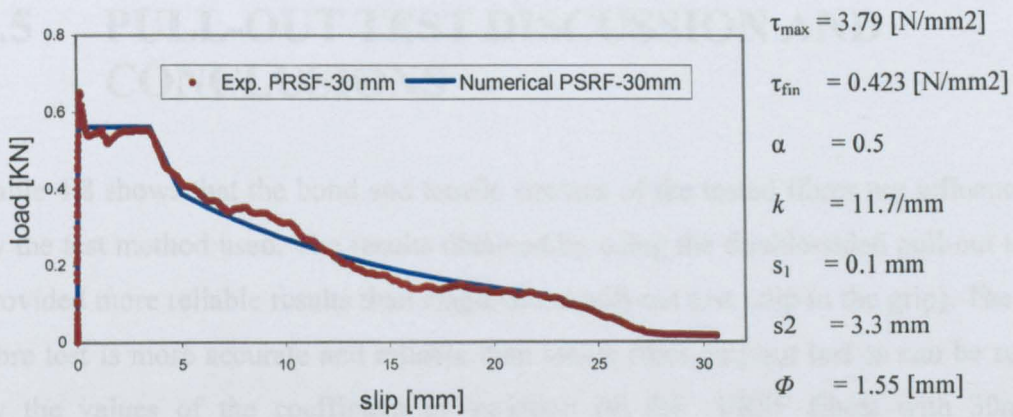


Figure 4.31 Experimental and numerical load-slip curves for PRSF-30 mm embedded length.

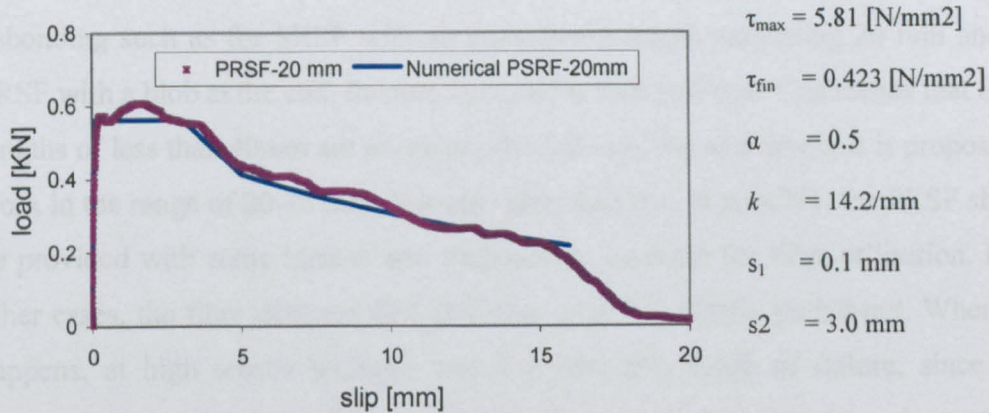


Figure 4.32 Experimental and numerical load-slip curves for PRSF-20 mm embedded length.

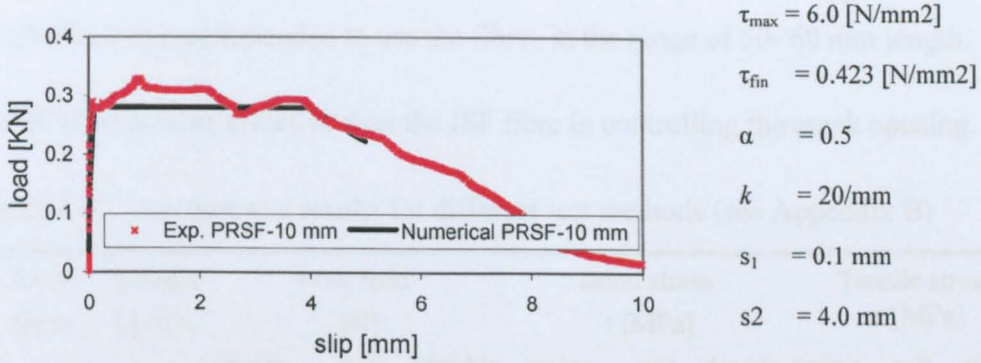


Figure 4.33 Experimental and numerical load-slip curves for PRSF-10 mm embedded length.

The modified model appears to provide curves that fit the experimental results well, but as with the original Fantilli model, is not really a predictive model.

4.5 PULL-OUT TEST DISCUSSION AND CONCLUSIONS

Table 4.8 shows that the bond and tensile stresses of the tested fibres are influenced by the test method used. The results obtained by using the double-sided pull-out test provided more reliable results than single-sided pull-out test (slip in the grip). The 3-fibre test is more accurate and reliable than single fibre pull-out test as can be seen by the values of the coefficient of variation (v) for PRSF fibres with 30mm embedded length (8.4% for single fibre and 6.6% for three fibres).

Two modes of failure are observed. In some cases, the fibres were broken before debonding such as for SRSF with an embedment length exceeding 20 mm and for PRSF with a blob at the end, fracture occurred before pull-out. This means that SRSF lengths of less than 40mm are necessary for full bonding and hence, it is proposed to work in the range of 20-25 mm. It is also proposed that, if possible, the PRSF should be provided with some kind of end treatment to increase the fibre utilisation. In all other cases, the fibre debonds first and slips until it is finally pulled-out. When this happens, at high tensile stresses, this is a desirable mode of failure, since it is expected to require high fracture energy. However, when it takes place at low stresses, the utilisation of the fibre strength is inefficient.

As far as the PRSF fibres are concerned, when an end anchorage detail is not available, it is recommended to use the fibres in the range of 50- 60 mm length.

PRSF fibre is more effective than the ISF fibre in controlling the crack opening.

Table 4.8 Average test results for different test methods (see Appendix B)

Fibre types	Length L[mm]	Peak load [N]			Bond stress t [MPa]			Tensile stress σ [MPa]		
		spring	cell	double	spring	cell	double	spring	cell	double
ISF	10	389.5	-	231	12.4	7.36	7.36	496	-	295
	20	578.9	-	370	9.21	5.89	5.89	737	-	471
PRSF 1- fibre	10	238.8	690	359	6.96	14.47	7.37	256	412	328
	20	545.3	1205	443	7.09	12.15	4.55	479	699	405
	30	996.7	1220	653	8.84	8.58	4.47	897	755	633
PRSF 3-Fibres	10	-	-	267	-	-	5.48	-	-	244
	20	-	-	547	-	-	5.61	-	-	500
	30	-	-	672	-	-	4.60	-	-	643
SRSF	10	48.9	31.6	84	5.56	4.61	13.4	849	845	670
	20	49.0	42.3	-	2.74	3.13	-	908	1162	-
	30	159.9	45	-	5.50	2.07	-	2424	1083	-

The load versus displacement curves obtained from this chapter are used again later on in a proposed stress-block model. The maximum tensile strength of SRSF and PRSF were about 2400MPa and 1500MPa. These values were recorded in the single-sided pull-out test using load-spring (Appendix B).

5 FLEXURAL TOUGHNESS BEHAVIOUR OF RSFRC

5.1 INTRODUCTION

The first of two phases of tests investigates the first crack values and toughness indices of SFRC according to ASTM C1018 (1995) and toughness factor according to JSCE-SF4 (1994) with different matrix strength, fibre volume content and type using unnotched beams. This phase aims to study the characteristic of ISF-RC, SRSF-RC and PRSF-RC.

The second phase of tests investigates the parameters affecting the stress-strain characterisation of SFRC (crack propagation and location of neutral-axis depth), along the lines of the RILEM design model described in section 2.4.2. The second phase of tests was necessary because an initial attempt to use the RILEM design model (RILEM, 2000 and 2002) in Finite Element Analysis (FEA) simulation for the derivation of flexural behaviour of RSFRC was not successful because the model considers a constant uniaxial tensile stress in the fracture zone, which is clearly not the case for most fibres, since failure is mainly through pull-out and not yield.

The determination of the design parameters such as the limit of proportionality, f_{ct} , the equivalent flexural strength, f_{eq2} and f_{eq3} , are directly dependent on the value chosen for the load at the limit of proportionality F_u , which is difficult to determine by using the RILEM procedure (Barr and Lee, 2000). Finally, a fixed value is considered for the neutral axis depth after cracking, independent of the amount and type of fibre reinforcement (Vandewalle 2003). The tests in this second phase were carried out on notched prisms by utilising the RILEM bending test (RILEM, 2002). It is noted that a four-point load arrangement was used instead of three-point load. The use of four-point load arrangement created a region of constant moment and, hence, minimised the overestimation of bending resistance, caused at the point of load application by the load-spreading effect (Timoshenko, 1970).

The work described in the first phase of this chapter was published and presented by the author at the International Conference on “Celebrating People and Concrete” held at Dundee University in September 2003 (Tlemat, Pilakoutas and Neocleous 2003b) and at the conference in Innovation Materials and Technologies for construction and Restoration, held in Lecce, Italy (Tlemat, Pilakoutas and Neocleous 2004c). The results of the second phase were submitted for publication to the Journal of Materials and Structures (Tlemat, Pilakoutas and Neocleous 2004a).

5.2 DESCRIPTION OF FLEXURAL TOUGHNESS TESTS

5.2.1 UNNOTCHED BEAMS

Two recycled steel fibres (PRSF and SRSF) and one industrial fibre (ISF-1) were used. Three specimens were tested for each series shown in Table 5.1. The size of the specimen was 100 x 100 x 500 mm.

Table 5.1 Flexural test programme for unnotched beams

Mix code	Fibre type and length	Fibre content (% by weight)	Fibre content (% by vol)
SPFA 40/30	SRSF (20mm)	1.0	0.4
		1.5	0.6
	SRSF; sieve (20mm)	1.5	0.6
	PRSF(50mm)	1.5	0.52
	ISF-1 (50mm)	1.5	0.45
OPC 40	SRSF (20mm)	1.0	0.4
		1.5	0.6
	SRSF ;sieve (20mm)	1.5	0.6
	PRSF ; 28days (15mm and 25mm)	1.5	0.5
	3.5	1.2	
5.0	1.8		
OPC50	SRSF (20mm)	0.5	0.2
		1.0	0.4
	2.0	0.8	
	PRSF (50mm)	1.0	0.35
	2.0	0.52	
6.0	1.6		
SPFA/MS 120/20/10	PRSF (50mm)	5.0	1.3

5.2.1.1 Testing Procedure

The test prisms prepared for the single-sided pull-out tests were used in this test series.

The prisms of FRC were tested in flexure using the four-point loading arrangement specified in ASTM C1018-94. The specimens were tested at the age of 7 days and 28 days. Three LVDTs mounted on a supporting frame were positioned along the centreline of the top surface of the test specimen, one at the mid-span (LVDT1) and one at each support (LVDT 2,3 in Figure 5.1). The net mid-span deflection is obtained by subtracting the average of the measured support deflection from the measured mid-span deflection. The specimens were tested in a 250 kN Screw Jack testing machine. The initial loading rate was approximately 0.5 kN/min.



Figure 5.1 Flexural test set-up according to ASTM C1018

5.2.2 NOTCHED BEAMS

The fibres used in the notched beam tests were the PRSF, SRSF, VSF, ISF-1 and ISF-2.

Six groups of prisms were cast for this study (see Table 5.2). In these groups, all sets comprised of three specimens. Group one comprised one set of plain concrete prisms, which were used as control specimens. Group two included three sets of prisms containing SRSF for three fibre ratios (0.5%, 1% and 2% by weight). Groups three and four included three sets of prisms reinforced with PRSF and VSF, respectively, having fibre ratios of 1.5%, 3% and 6% by weight. Groups five and six

each comprised of one set of prisms reinforced with high fibre ratio (6% by weight) of ISF-1 and ISF-2, respectively.

The aggregates used for the plain and SRSF specimens had a maximum size of 10 mm. Two sizes of coarse aggregates were used for the remaining fibres: a) one with a maximum size of 10 mm, and b) one with a maximum size of 20 mm.

To improve workability, 30% (by cement weight) of a special PFA (superpozzolan) and various percentages of superplasticizer were used. Each mix resulted in a set of three prisms and six cubes.

As expected, Table 5.2 shows that increasing the fibre ratio reduces the workability as measured by the slump test. To obtain a reasonable workability the superplasticizer was increased when the fibre ratio was increased.

Table 5.2 Result of slump tests

Groups	Fibre ratio by weight [%] ¹	Fibre diameter/ Fibre length [-]	Superplasticizer by cement weight [%]	Slump test [mm]
Plain	0.0	-	0.1	200
SRSF	0.5	≤87	0.2	160
	1.0	≤87	0.4	150
	2.0	≤87	0.75	55
PRSF	1.5	≈32	0.2	200
	3.0	≈32	0.4	150
	6.0	≈32	0.75	140
VSF	1.5	32	0.2	160
	3.0	32	0.4	90
	6.0	32	0.75	70
ISF-1	6.0	50	0.75	150
ISF-2	6.0	48	0.75	150

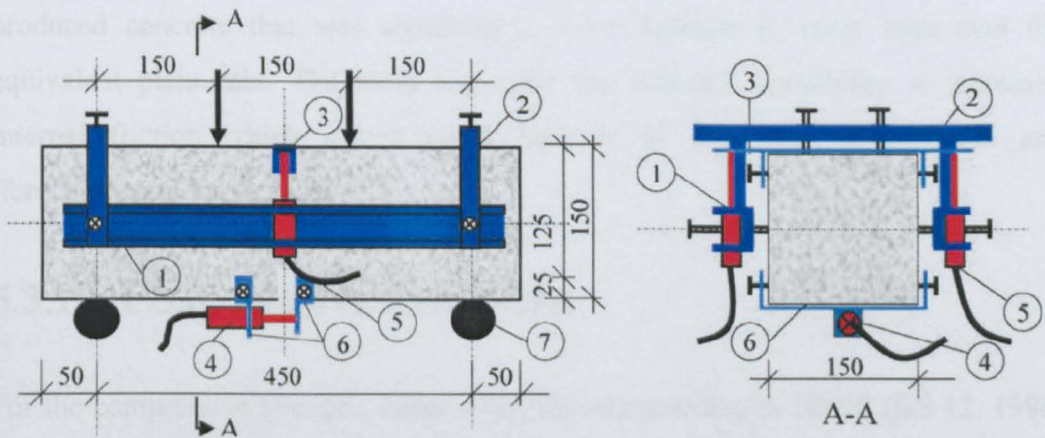
5.2.2.1 Specimen Preparation

The prismatic specimens (150 mm deep, 150 mm wide, and 550 mm long) were cast in timber moulds. The specimens were cast in two layers, and were vibrated in the moulds during casting. A day after casting, the specimens were demoulded and then placed in the mist room until the day of testing. A notch (25 mm high and 5 mm

thick) was sawn at mid-span, a day before testing, using rotating diamond blades into the tensile face of each beam (perpendicular to the top casting surface) (Tlemat et al, 2003b). The purpose of the notch was to act as a crack inducer. All tests were performed at an age shown later on in Table 5.5.

5.2.2.2 Testing Procedure

Results from flexural tests on such concrete prisms are prone to significant experimental errors (due to spurious support displacements, machine stiffness and load rate) and, hence, accurate deflection measurements need to be made (Copalaratnam, 1995). To avoid these errors and eliminate the effect of torsion on the deflection measurements, it was decided to use a yoke (Figure 5.2) as specified by the Japanese standard (JSCE SF4, 1994). The specimens were tested in a 100 kN servo-hydraulic machine under displacement control at a constant rate of 0.2 mm/min. Average mid-span beam deflections were measured on both sides of the beam (δ_1 and δ_2) using two transducers fixed to the yoke (LVDT5).



1- Steel bar; 2- clamps with pins; 3- steel plate; 4,5- LVDT; 6- clamps for LVDT; 7- supports

Figure 5.2 Specimen and test set-up

One transducer (LVDT4) was mounted across the notch mouth to monitor the crack mouth opening displacement (CMOD). Furthermore, three transducers were used to measure the crack propagation at different height locations, and one transducer was used on the compressive face to measure the compressive strain (Figure 5.3).

One transducer (LVDT) was mounted across the notch mouth to monitor the crack mouth opening displacement (CMOD). Furthermore, two LVDT's were used to

measure the crack propagation at different height locations and one LVDT was used on the compressive face to measure the compressive strain (Figure 5.3).

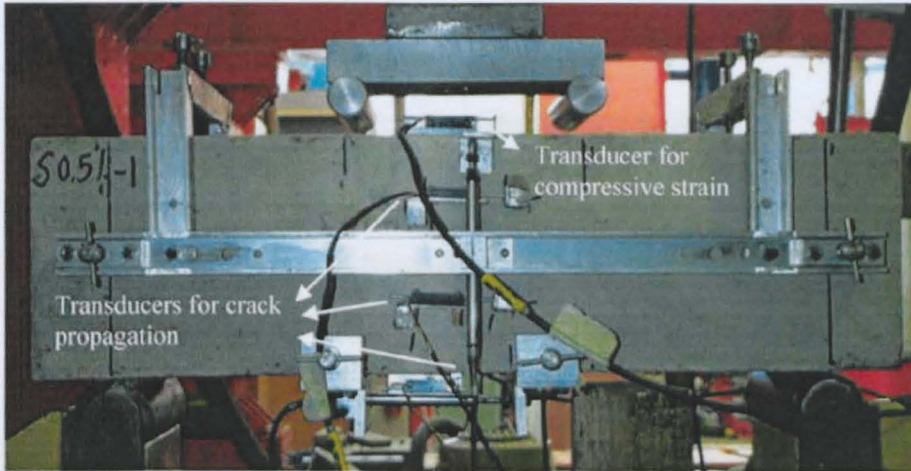


Figure 5.3 Testing arrangement and instrumentation

5.3 TEST RESULTS

The introduction of the five types of steel fibres, even at the smallest proportions, produced concrete that was significantly more difficult to work with than the equivalent plain mix. The main cause for the reduced workability is increased internal friction which comes about because of fibre/fibre, fibre/matrix and fibre/aggregate interaction.

5.3.1 COMPRESSIVE STRENGTH

For the compressive strength, cubes were placed according to BS 12 (BS 12, 1996) with the cast face not in contact with the platens of the testing machine. The load was applied at a constant rate of stress within the range of 0.2 to 0.4 (kN / s), and the compressive strength was measured to the nearest 0.5 MPa.

The cylinder compressive strength and the secant modulus needed for the subsequence analysis were calculated according to EC 2 (ENV 1992-1-1) as follows.

$$f_{fc} = 0.85 * f_{cm}, \quad [\text{MPa}] \quad (5.1)$$

$$E_{cm} = 9500 f_{fc}^{1/3} \quad [\text{MPa}] \quad (5.2)$$

Where:

- E_{cm} secant modulus of concrete in compression,
 f_{cm} mean compressive cylinder strength in SFRC,
 f_{cm} measured mean compressive cube strength in SFRC.

Table 5.3 shows the cube compressive strength as the average of four cubes tested at 7 and 28 days in the case of tests with unnotched beams. For the notched beams, four specimens were tested on the same day as the corresponding set of prisms (Table 5.5, details values are presented in Appendix C4). Since different constituents are used in the different mixes, a direct comparison between groups is not easy to make. However, within groups, increased fibre reinforcement appears to increase the compressive strength in all fibres except SFRC. The reduction of strength shown for SFRC 2% may be associated with the reduced workability in that set. Between groups there is only one direct comparison that can be made relating to the sets having 6% fibres. If date of testing is taken into account, no major differences are noted.

5.3.2 FLEXURAL STRENGTH - UNNOTCHED BEAMS

The ASTM C1018 standard method is based on determining the amount of energy required first to deflect and crack an SFRC beam ($100 \times 100 \times 500 \text{mm}$) loaded at its third points, and then to selected multiples of the first crack deflection. The calculation of toughness indices I_5 , I_{10} , I_{20} (etc), requires an accurate assessment of the elastic energy at first-crack, which constitutes the denominator in the definition of the respective indices (see Figure 5.4). Any error in the measurement of elastic energy will lead to a significant error in the values of the respective indices. According to ASTM C1018, first crack is the point where the load-deflection curve first becomes non-linear. Locating the point on the load-deflection curve where the first crack occurs is not so simple and sometimes has to be estimated (Banthia and Trottier, 1995). Figure 5.4 shows a typical load-versus-deflection curve for a low-fibre volume SFRC specimen. The initial shape of the curve, up to 30%-40% of the peak load, is caused by extraneous deformations due to local crushing deformations of the specimen at the loading points.

The first-crack in the SFRC specimen occurs at point B, after which the fibres bridging the crack are activated and carry additional load until the bond between fibre and concrete fails (point C). The energy up to point B is related to some extent to the fibre volume in concrete. The peak load point C, is a point of instability where the loading machine and specimen undergo sudden unloading and release large amounts of energy (point E). It is proposed that the area CDE in Figure 5.4 should not be considered in the calculation of the toughness indices.

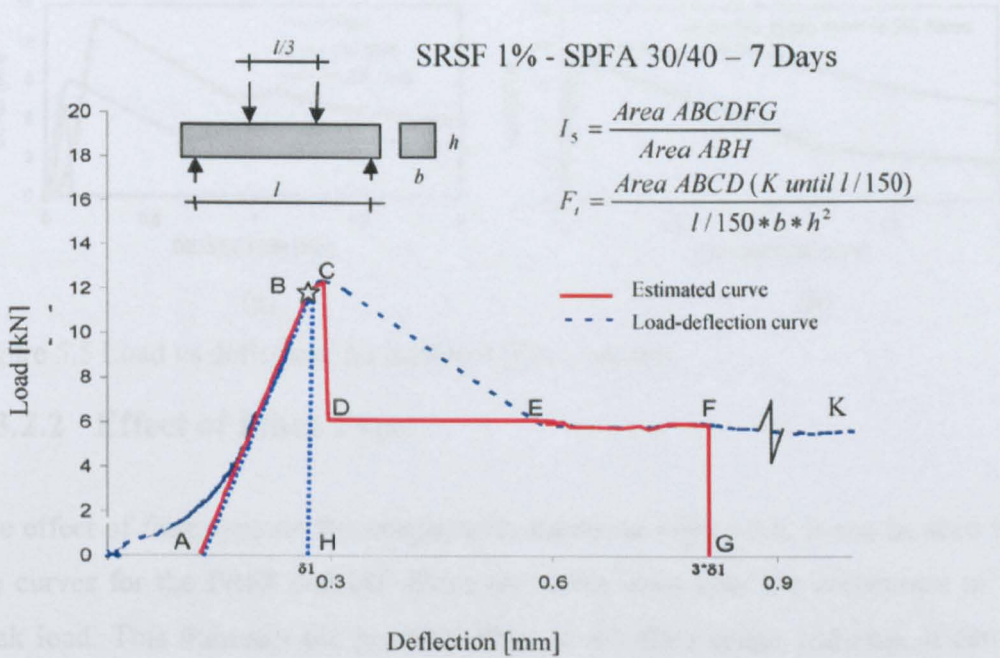


Figure 5.4 Load-deflection curves for SFRC beams

The curve should be considered to follow the path A-B-C-D-E and the toughness index I_5 calculated as the area under the path A-C-D-F-G divided by the area under the path A-B-H (first crack toughness).

In this procedure, the area under the load-versus-deflection curve is obtained up to a deflection (K) of $span/150$. From this a flexural toughness factor F_t is calculated as shown in Figure 5.4.

The load-displacement curves using a yoke give much better results at the early stages, since the local crushing effects are eliminated as shown in Figure 5.5b

5.3.2.1 Effect of Fibre Volume

Figure 5.5 shows that an increase in the fibre volume, not only increases the peak strength but also the residual strength after cracking. This was observed for all the fibre types considered in this investigation.

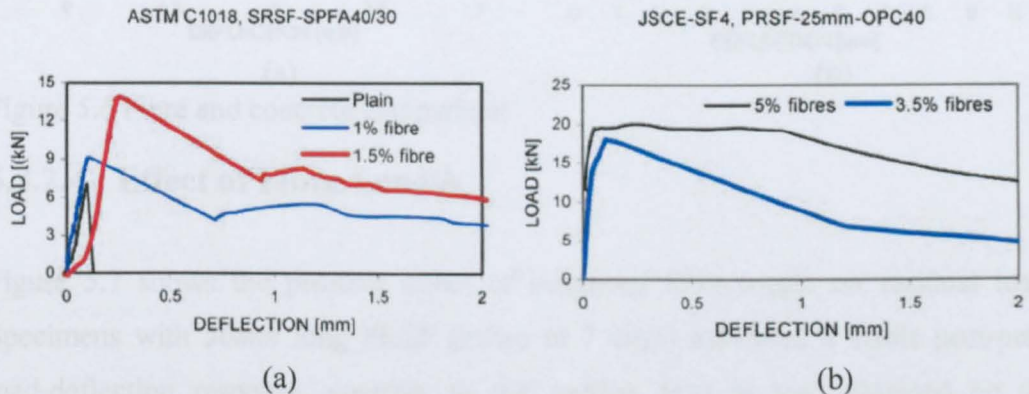


Figure 5.5 Load vs deflection for different fibre volumes

5.3.2.2 Effect of Fibre Type

The effect of fibre type on the toughness is shown in Figure 5.6. It can be seen that the curves for the PRSF and ISF fibres are stable even after the occurrence of the peak load. This indicates the positive effect of the fibre shape and size. It can be deduced that both fibres are slipping, but at the same time offering higher resistance, through the mobilisation of more and more fibres.

For a similar design mix and fibre content, the PRSF demonstrated a higher peak load and better ductility than the ISF-1 and SRSF. The twisted form of the PRSF appears to have a good influence on the bond, and increases the SFRC ductility.

5.3.2.3 Effect of Concrete Strength

By comparing the flexural results obtained for the normal strength concrete (with 6% fibres) and the high strength concrete (with 5% fibres), it is clear that the high strength concrete achieves a much higher flexural capacity as well as residual strength (Figure 5.6b).

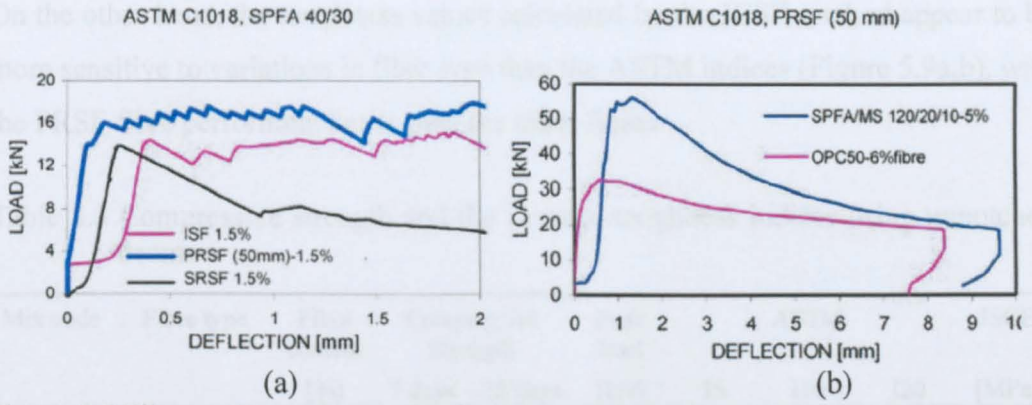


Figure 5.6 Fibre and concrete comparison

5.3.2.4 Effect of Fibre Length

Figure 5.7 shows the positive effect of increased fibre length on residual load. Specimens with 50mm long PRSF (tested at 7 days) exhibited a stable post-peak load-deflection response, contrary to the sudden drop in load obtained by the specimens with 15mm and 25mm long fibres (tested at 28 days).

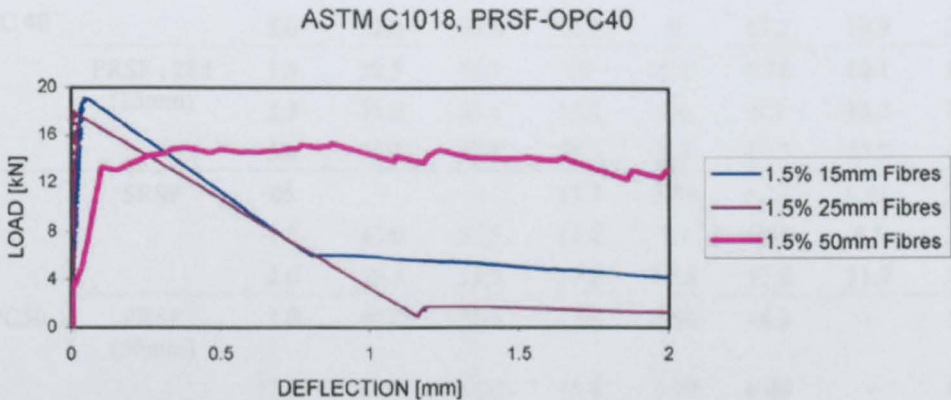


Figure 5.7 Effect of fibre length on the flexural toughness

Table 5.3, summarises the concrete compressive strength and average toughness indices, which were determined for each fibre type and concrete mix by utilising the ASTM and JSCE flexural tests (for more details see Appendix A.1).

The toughness indices were calculated using the criterion illustrated in Figure 5.4. It can be seen that index I_5 is relatively insensitive to the fibre type (for the same fibre volume Figure 5.8).

On the other hand, the toughness values calculated by the JCSE method appear to be more sensitive to variations in fibre type than the ASTM indices (Figure 5.9a,b), with the PRSF fibre performing better than the other fibres.

Table 5.3 Compressive strength and the average toughness indices using unnotched beams

Mix code	Fibre type	Fibre content [%]	Compressive Strength		Peak load [kN]	ASTM			JSCE [MPa]	
			7 days	28 days		I5	I10	I20		
SPFA 40/30		1.0	30.5	49.0	10.7	2.58	4.44	8.37	1.56	
	SRSF	1.5	27.5	45.0	12.2	4.75	8.34	14.46	1.88	
	SRSF ;sieve	1.5	27.5		17.7	4.60	10.9	23.4	2.24	
	PRSF(50mm)	1.5	27.5		16.4	4.62	10.1	20.35	4.50	
	ISF-1	1.5	26.0		14.5	5.97	12.2	24.48	3.82	
OPC 40		1.0			16.4	4.66	6.26	9.01	1.90	
	SRSF	1.5	34.5	40.5	10.1	1.38	1.62	2.07	2.08	
	SRSF ;sieve	1.5			11.2	4.49	8.49	18.71	2.48	
	PRSF ; 28d (15mm)	1.5	31.5	43.0	17.9	1.3	1.7	2.6	0.46	
		3.5	33.0	44.5	15.8	1.92	2.9	5.1	0.91	
		5.0	33.0	44.0	10.9	6	13.2	19.9	2.83	
	PRSF ; 28d (25mm)	1.5	30.5	42.5	18	5.1	6.78	10.1	1.72	
		3.5	31.0	43.5	13.3	5.6	8.3	13.7	1.98	
		5.0	35.5	47.5	15.5	6.3	11.3	23.2	4.82	
		SRSF	05			13.7	2.85	5.27	9.91	2.55
OPC50		1.0	43.0	55.5	17.2	3.7	6.88	8.5	2.43	
		2.0	39.5	51.5	17.0	11.6	17.6	31.9	3.14	
	PRSF (50mm)	1.0	44.0	55.5	18.4	6.96	14.2	-	1.69	
		2.0	44.0	52.0	15.9	3.79	6.26	-	4.43	
		6.0			30.4	4.31	8.29	14.6	9.45	
		SRSF	05			13.7	2.85	5.27	9.91	2.55
		1.0	43.0	55.5	17.2	3.7	6.88	8.5	2.43	
	2.0	39.5	51.5	17.0	11.6	17.6	31.9	3.14		
SPFA/MS 120/20/10	PRSF (50mm)	5.0	103	120	37.7	14.7	29.4	48.1	11.36	

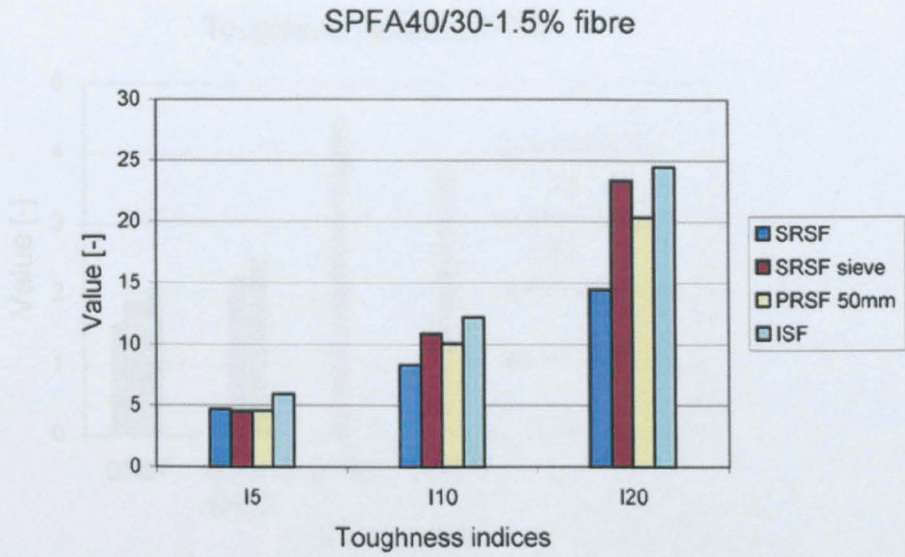
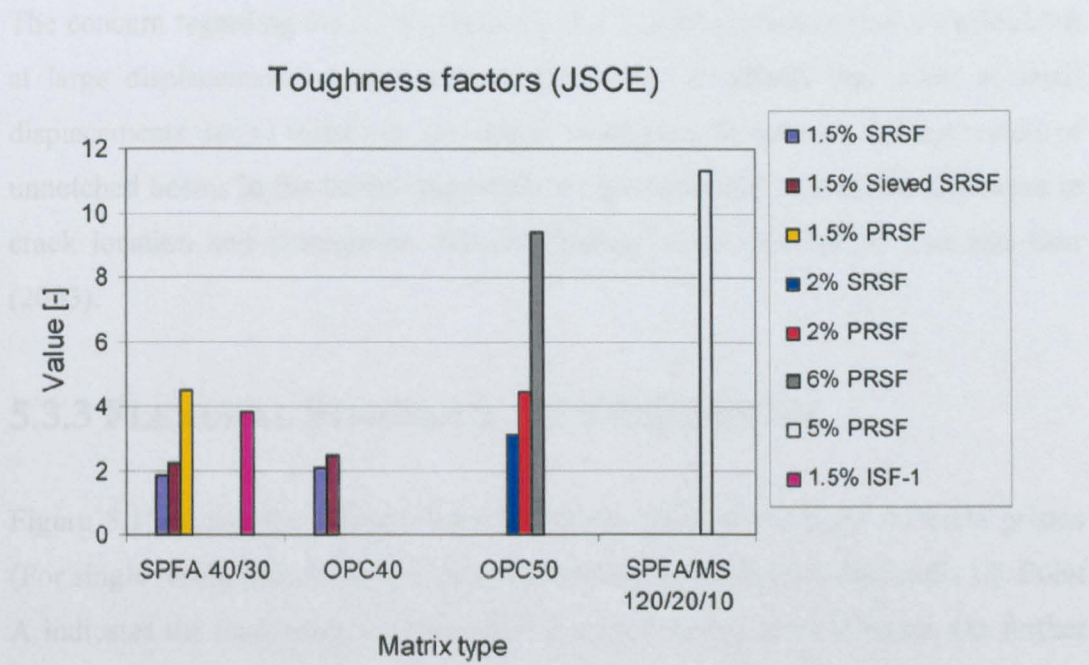
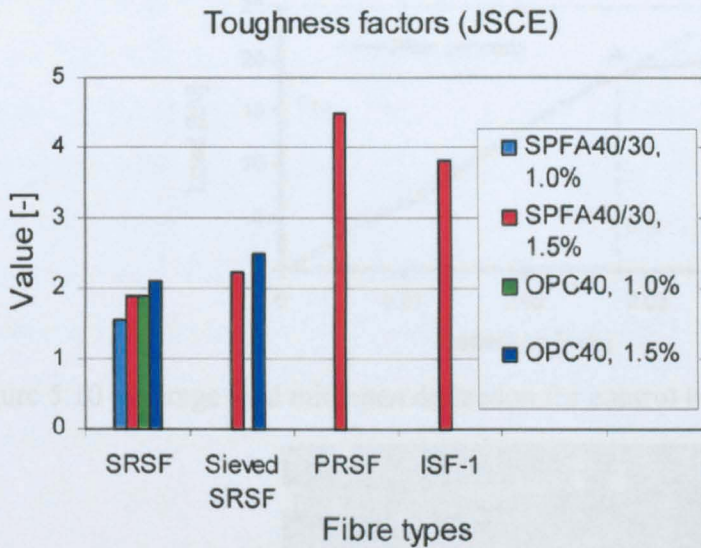


Figure 5.8 ASTM toughness indices for different fibres

Figure 5.9 JSCE



(a)



(b)

Figure 5.9 JSCE toughness factors for different fibre types and matrix types

The concern regarding the JSCE method is that toughness factors that are calculated at large displacements do not account for all of the effects that occur at small displacements due to instability and matrix brittleness. In general, the test results of unnotched beams in the initial stage show a high variability due to the difference in crack location and propagation. Similar findings were reported by Lee and Barr (2003).

5.3.3 FLEXURAL STRENGTH - NOTCHED BEAM

Figure 5.10 shows the average load-deflection curve of the plain concrete prisms (For single result, data filtering routine and averaging routine see Appendix C). Point A indicates the load when the first crack is considered to have initiated. On further loading, the plain concrete prism broke suddenly in two halves (Fig. 5.11). The testing machine was not stiff enough to measure the softening region of plain concrete and no further measurements were recorded.

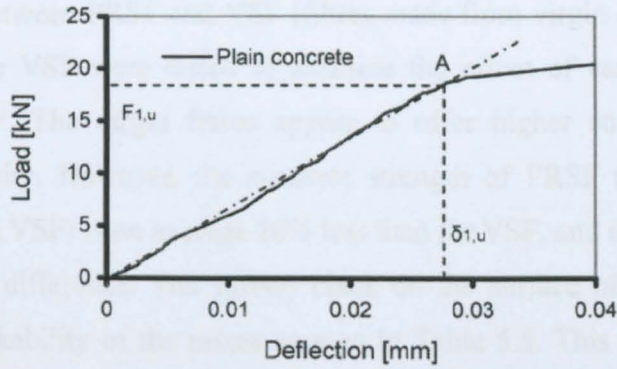


Figure 5.10 Average load mid-span deflection for control beam



Figure 5.11 Fracture of plain concrete prism

Fig. 5.12 shows the average load versus average mid-span deflection for all the SRSF prisms. As expected, the flexural behaviour of the prisms improves as the fibre fraction increases. Fibres act as crack arrestors, giving a substantial increase in toughness, even when fibres debond and are pulling out. In the case of 0.5% fibre ratio, only the toughness was increased. The peak load is 10% lower than of plain concrete, but that can be attributed to the lower compressive strength. However, overall the peak load and the toughness increase with the amount of fibres used.

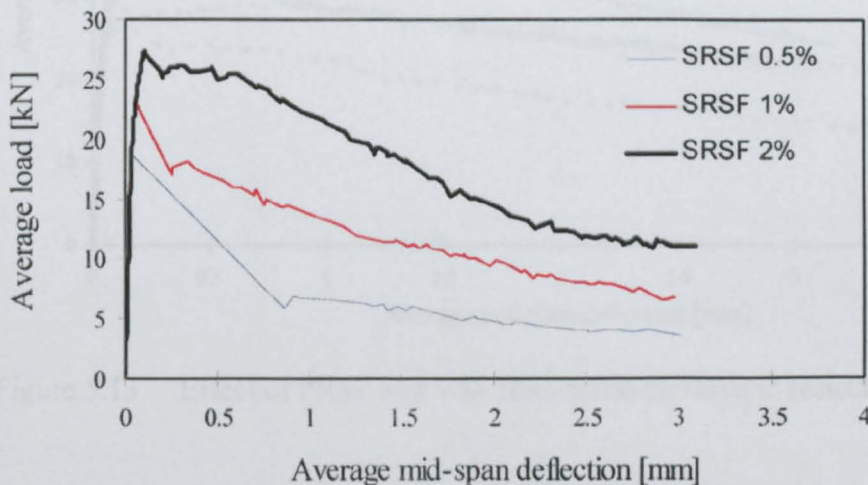


Figure 5.12 Flexural behaviour of SRSF prisms with different % of fibres

A comparison between PRSF and VSF (fibres made from virgin cord) is shown in Figure 5.13. The VSF were tested to examine the effect of carbon black on the surface of PRSF. The virgin fibres appear to offer higher strength and energy absorption capacity. However, the concrete strength of PRSF (which was tested much earlier than VSF) is on average 20% less than for VSF, and this on its own may account for this difference. The carbon black on the surface of PRSF appears to increase the workability of the mixes as seen in Table 5.5. This is surprising since carbon black is a fine powder with a large surface area. However, the diameter of this powder may be such that it leads to a better packing of the particles of wet concrete. The carbon black may also have an effect on the bond strength of the fibres. However, there is no physical evidence to support that. Since the fibres are mixed by weight and the PRSF fibres have carbon black, this means that less PRSF fibres are used in comparison to VSF. A density examination shows a difference between the two fibres at up to 15%. As less PRSF fibres are used in comparison to VSF, this may explain both the small reduction in energy absorption capacity and the increase in workability.

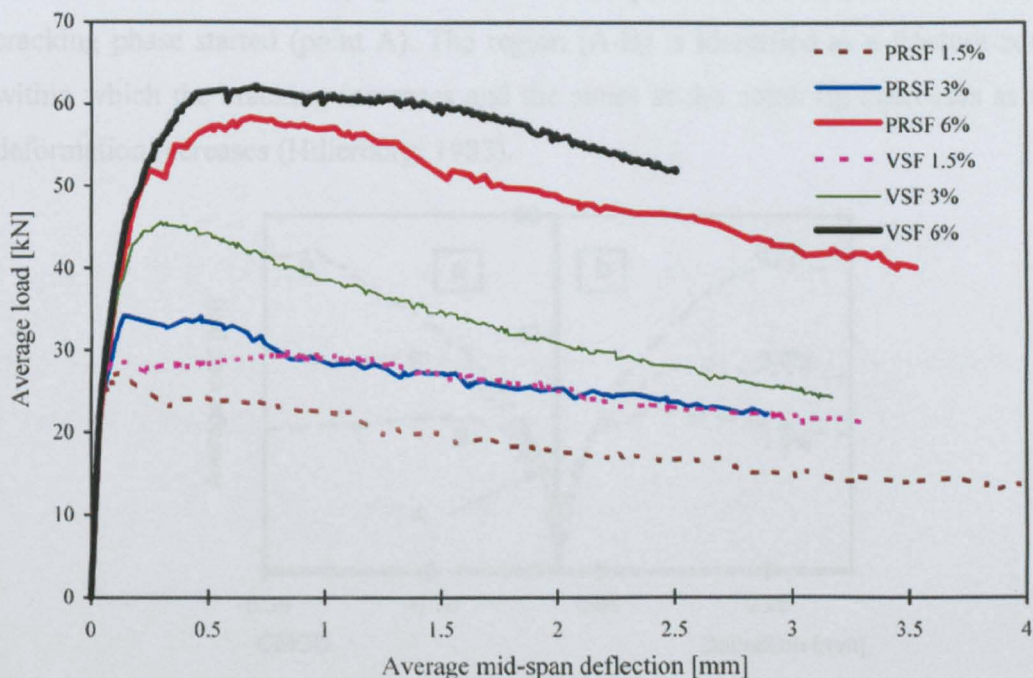


Figure 5.13 Effect of PRSF and VSF fibre ratios on flexural resistance

Figure 5.14 shows that the behaviour of the prism reinforced with 6% ISF-1 and ISF-2 fibres is similar to that of VSF and PRSF prisms. This is surprising considering the very different nature of the fibres.

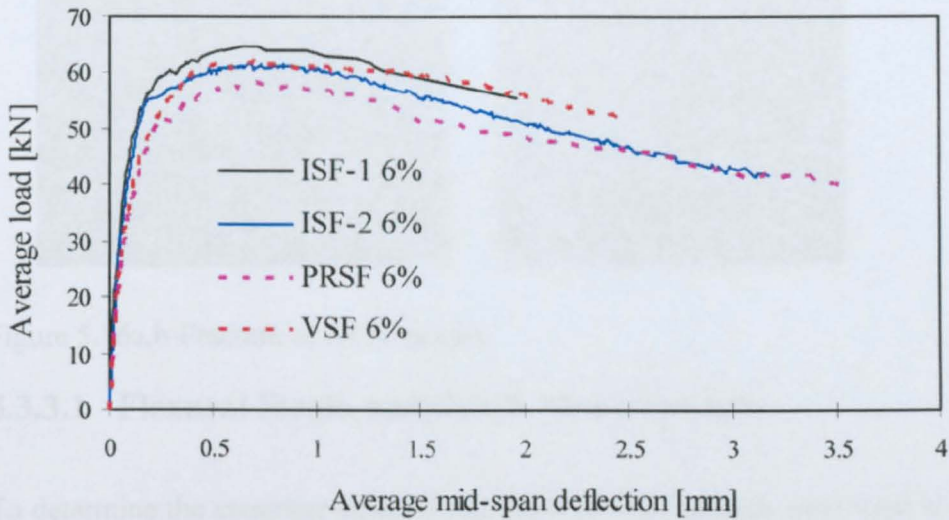


Figure 5.14 Results for prism containing 6% ISF, PRSF, and VSF

Fig. 5.15a shows that the initial load-CMOD behaviour of prisms containing various ratios of PRSF was linear (region 0-A) until the point of fracture, when the micro cracking phase started (point A). The region (A-B) is identified as a fracture zone, within which the cracking increases and the stress at the notch tip decreases as the deformation increases (Hillerborg, 1983).

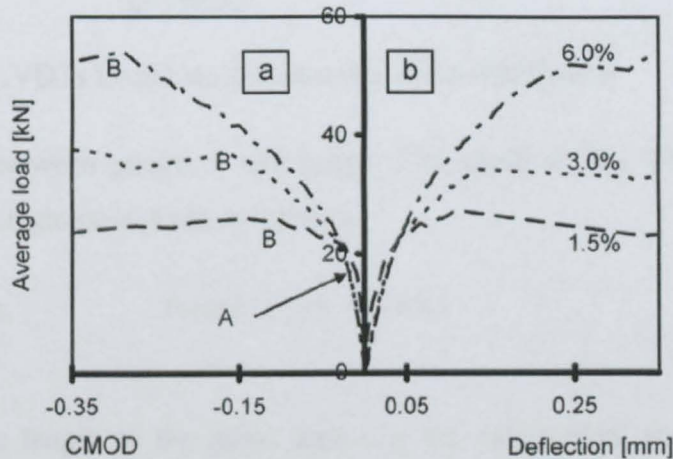


Figure 5.15a,b Initial behaviour for prisms containing PRSF

On further deformation, the load also decreases due to complete fibre pull out. The experiments were stopped after the crack exceeded 4 mm. On unloading, the cracks were still visible as shown in Fig. 5.16a. Even for the same fibre amount, the crack

propagation is not always vertical, indicating high variability in material properties (Figure 5.16b). For more images see Appendix E.

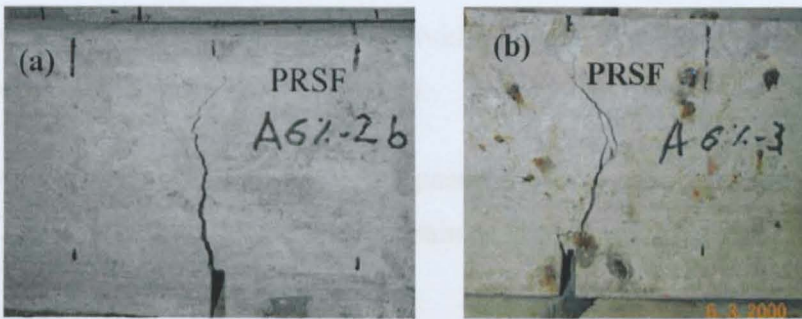


Figure 5.16a,b Fracture of PRSF beams

5.3.3.1 Flexural Strain and Crack Measurements

To determine the complete strain/crack-width profiles, gauges were used to measure the displacement at fixed points along the depth at mid-span as shown in Fig. 5.17.

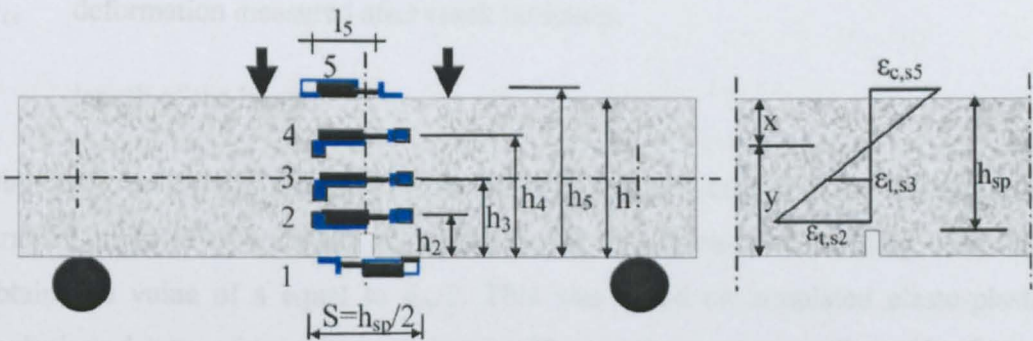


Figure 5.17 LVDTs Locations and assumed strain distribution

The distance between gauge 5 and gauge 2 is equal to h_{sp} . The displacement measured at each gauge is given as follows.

$$u_i = w_{i,el} = l_i \cdot \varepsilon_i \quad \text{Prior to crack initiation} \quad (5.3)$$

Where l_i is the length of the gauge and ε_i is the longitudinal strain. After crack initiation, the displacement may be obtained as the sum of the elastic displacement and the crack opening (equation 5.4).

$$u_{(i)} = w_{i,el} + w_{i,c} \quad \text{After crack initiation} \quad (5.4)$$

The compressive strain can be determined by dividing the displacement measured by gauge 5 by the length of the gauge length l_5 (50mm). The tensile strain prior to crack initiation, at locations h_2 , h_3 and h_4 (30, 66 and 117 mm from the bottom surface) respectively, can be determined by dividing the displacement measured by gauges 2, 3 and 4 by the gauge length of 55mm.

Using the cracked hinge model proposed by Ulfkjar et al (1995) and adopted for FRC, by Olesen (2001), the tensile strain can be obtained by equation 5.5.

$$\varepsilon_{i,j} = \frac{\sigma_{i,max}}{E} + \frac{w_{i,c}}{s} \quad (5.5)$$

Where:

$\sigma_{i, max}$ maximum stress at first crack,

$w_{i,c}$ deformation measured after crack initiation,

s length of the hinge.

Obviously, the determination of the length of the hinge is critical in the calculation of strain. Ulfkjar (1995) applied the hinge model to a three-point bending beam and obtained a value of s equal to $h_{sp}/2$. This was based on simulated elasto-plastic analysis and comparison with experiments. This result was also confirmed by Olesen (2001).

Figure 5.18 shows the load versus mid-span deflection and strain at locations 2, 3, 4 and 5 versus mid-span deflection. It can be seen that the compressive strain $\varepsilon_{c0,s5}$ and the tensile strain $\varepsilon_{t0,s2}$ prior to crack initiation (at a deflection corresponding to point A) are more or less equal. The crack at gauges 2, 3 and 4 was initiated at a load $P_{0,s2}$, $P_{0,s3}$ and $P_{0,s4}$ of 21.4, 28.5 and 32.0 kN, respectively. After crack initiation, the tensile strain $\varepsilon_{t1,s2}$; $\varepsilon_{t1,s3}$; $\varepsilon_{t1,s4}$ at peak load (at a deflection corresponding to point B) were 1.31, 0.84 and 0.03 ‰, respectively.

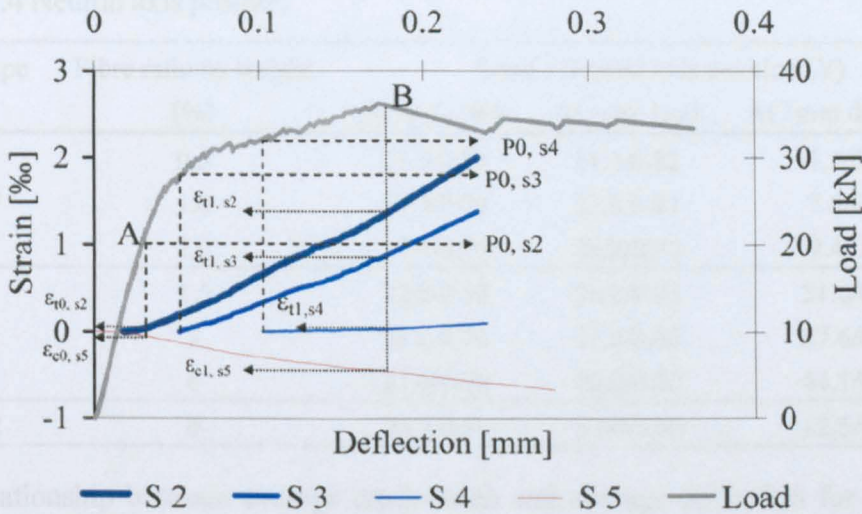


Figure 5.18 Strain measurements for VSF 1.5%

5.3.3.2 Position of Neutral Axis Depth

The position of the normalised neutral axis ($y = 1-x/h$), shown in Figure 5.19 for a prism reinforced with 1.5% VSF fibres, was calculated using the assumption plane sections remain plane (Bernoulli). This position varied between 0.61 and 0.82 at first micro crack and peak-load, respectively. The maximum depth of the neural axis was 0.97h at a deflection of 3mm. For prisms with low fibre ratios such as SRSF, the depth of the neutral axis at first crack was lower with higher fibre ratio (Table 5.4). Similar results were reported by Schnuetgen (1994). It is clear from the above discussion, that the simple approach taken by the RILEM model (RILEM TC 162-TDF, 2002) that the value of y is independent of the fibre volume is not right.

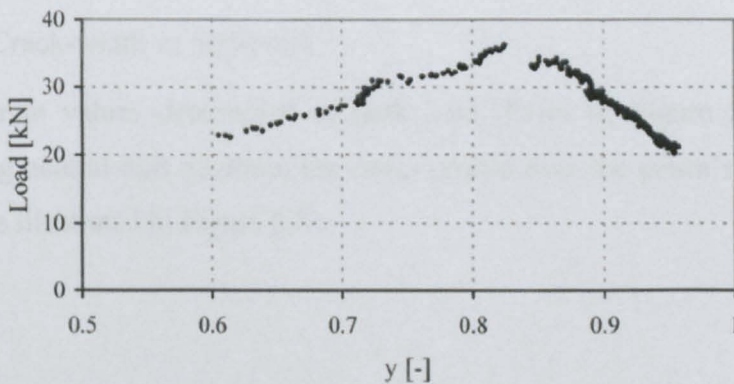


Figure 5.19 Variation of the neutral axis depth for VSF 1.5%

Table 5.4 Neutral axis position

Fibre type	Fibre ratio by weight [%]	Load / Neutral axis position (Y)		
		At first crack	At peak load	At 3mm deflection
SRSF	0.5	13.9/0.81	14.3/0.82	1.7/0.84
	1.0	17.4/0.79	23.0/0.81	7.8/0.92
	2.0	23.1/0.76	29.3/0.83	9.4/0.93
VSF	1.5	22.8/0.58	36.2/0.83	21.0/0.97
	3	23.0/0.70	51.8/0.80	27.6/0.93
	6	23.6/0.76	49.7/0.90	44.1/0.91
ISF-2	6	26.7/0.64	59.4/0.90	42.6/0.93

The relationship between average crack-width and average deflection for different fibre types is shown in Figure 5.20. This relationship is independent of fibre ratio and fibre type.

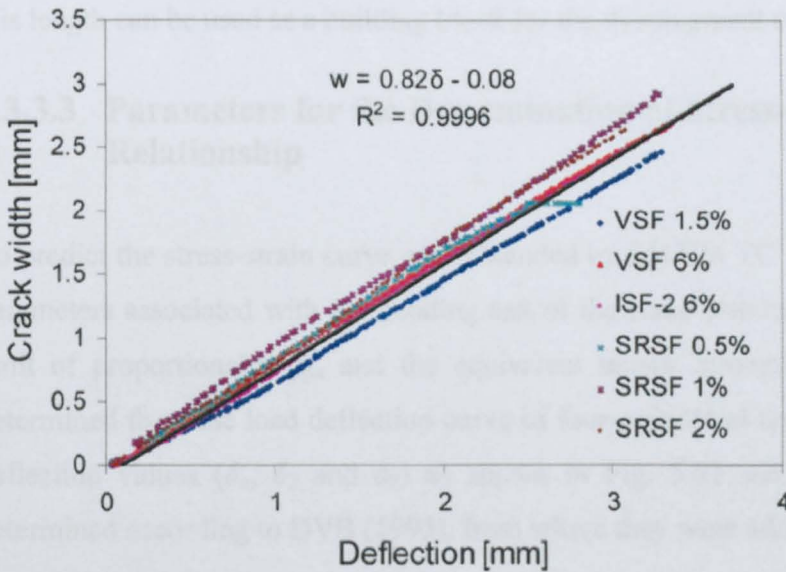


Figure 5.20 Crack-width vs deflection

Using the strain values determined at peak load (Point B, Figure 5.18) and the corresponding neutral axis position, the strain profile over the prism's depth can be determined as illustrated in Figure 5.21.

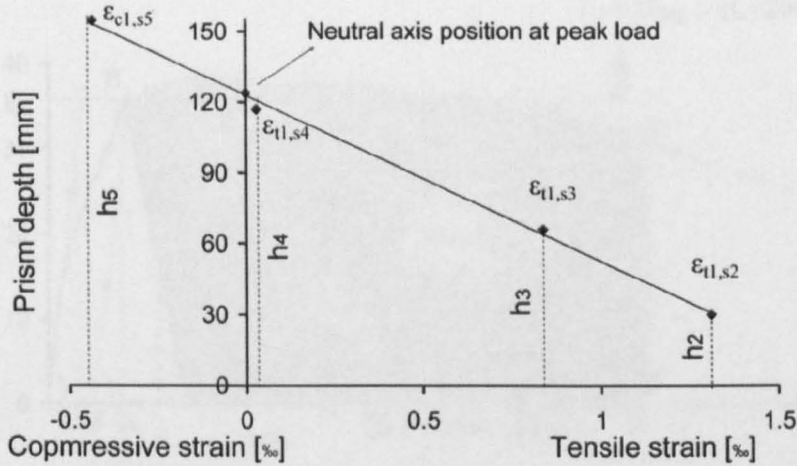
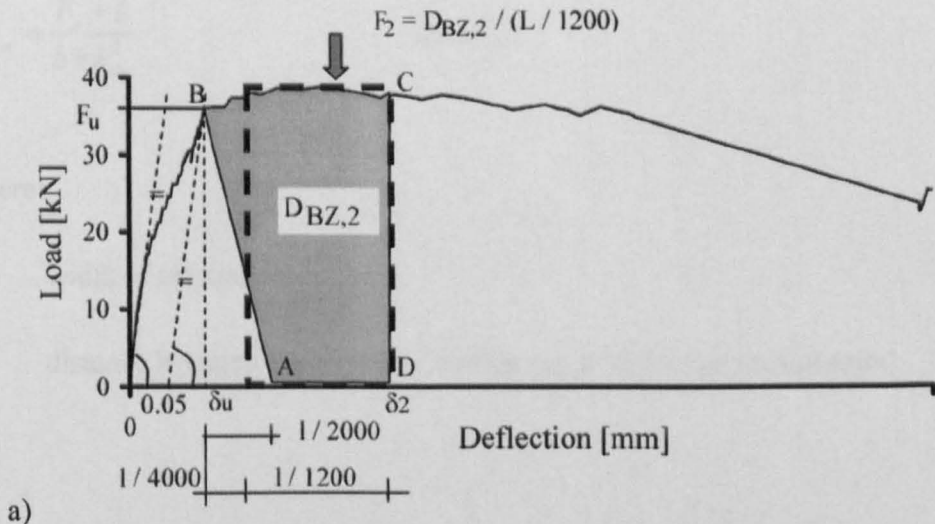


Figure 5.21 Strain profile over the prism depth

It can be seen that the method to determine the strains and neutral axis position was accurate. This indicates that the choice of hinge length of $h_{sp}/2$ was satisfactory and this length can be used as a building block for the development of design models.

5.3.3.3 Parameters for the Determination of Stress-strain Relationship

To predict the stress-strain curve recommended by RILEM TC 162-TDF (2002), the parameters associated with the bending test of the same standard were studied. The limit of proportionality f_{fct} and the equivalent tensile strength, f_{eq1} and f_{eq3} were determined from the load deflection curve of four-point load tests at several specific deflection values (δ_u , δ_2 and δ_3) as shown in Fig. 5.22 a,b. These values were determined according to DVB (1995), from where they were adopted by RILEM.



a)

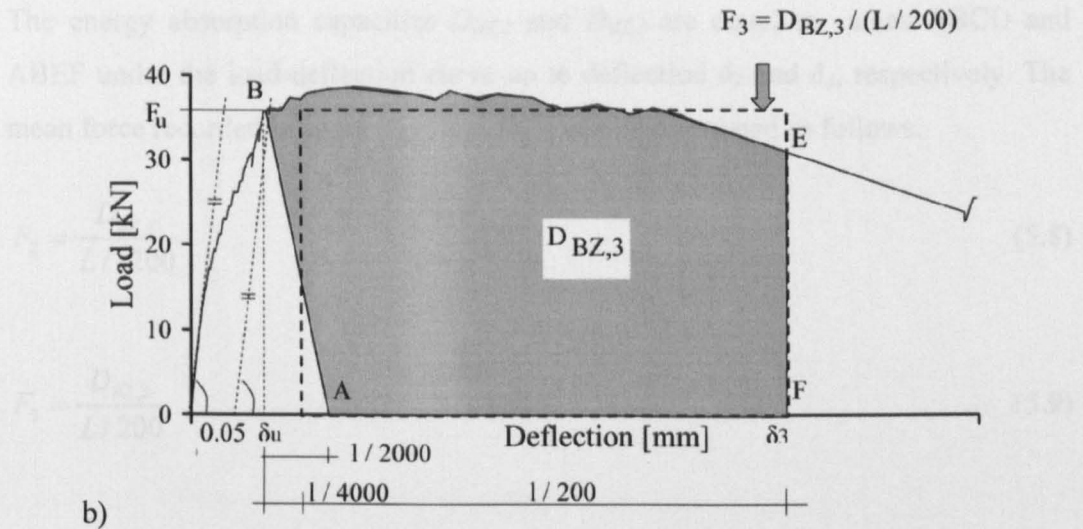


Figure 5.22 a,b Determination of F_u and equivalent tensile strength.

F_u is the highest value of the load when deflection δ_u does not exceed 0.05mm . The moment at mid span for the four point test arrangement corresponding to F_u is as follows:

$$M_u = \frac{F_u}{2} * \frac{L}{3} \quad [\text{Nmm}] \quad (5.6)$$

Where:

L Support span (mm),

Assuming a linear stress distribution, the limit of proportionality $f_{fct,u}$ can be calculated by equation 5.7.

$$f_{fct,u} = \frac{F_u * L}{b * h_{sp}^2} \quad [\text{N/mm}^2] \quad (5.7)$$

Where:

b width of the specimen (mm),

h_{sp} distance between the notch tip and the top of the cross section (mm).

The energy absorption capacities $D_{BZ,2}$ and $D_{BZ,3}$ are equal to areas ABCD and ABEF under the load-deflection curve up to deflection δ_2 and δ_3 , respectively. The mean force recorded in areas $D_{BZ,2}$ and $D_{BZ,3}$ can be calculated as follows.

$$F_2 = \frac{D_{BZ,2}}{L/1200} \quad [\text{N}] \quad (5.8)$$

$$F_3 = \frac{D_{BZ,3}}{L/200} \quad [\text{N}] \quad (5.9)$$

The moment at mid span of the corresponding to F_2 and F_3 are determined by equations 5.10 and 5.11 respectively.

$$M_2 = \frac{F_2}{2} * \frac{L}{3} = \frac{D_{BZ,2}}{L/1200} * \frac{L}{6} \quad (\text{Nmm}) \quad (5.10)$$

$$M_3 = \frac{F_3}{2} * \frac{L}{3} = \frac{D_{BZ,3}}{L/200} * \frac{L}{6} \quad (\text{Nmm}) \quad (5.11)$$

The equivalent flexural tensile strength $f_{eq,2}$ and $f_{eq,3}$ can be determined by means of the following expressions.

$$f_{eq,2} = \frac{M_2}{bh_{sp}^2/6} = \frac{F_2 L}{bh_{sp}^2} \quad (\text{N/mm}^2) \quad (5.12)$$

$$f_{eq,3} = \frac{M_3}{bh_{sp}^2/6} = \frac{F_3 L}{bh_{sp}^2} \quad (\text{N/mm}^2) \quad (5.13)$$

In addition, the residual flexural tensile strengths $f_{R,1}$ and $f_{R,4}$ were calculated from the load-CMOD curve at CMOD equal to 0.5mm and 3.5mm , respectively as shown in Figure 5.23.

$$f_{R,i} = \frac{F_{R,i} L}{bh_{sp}^2} \quad (\text{N/mm}^2) \quad (5.14)$$

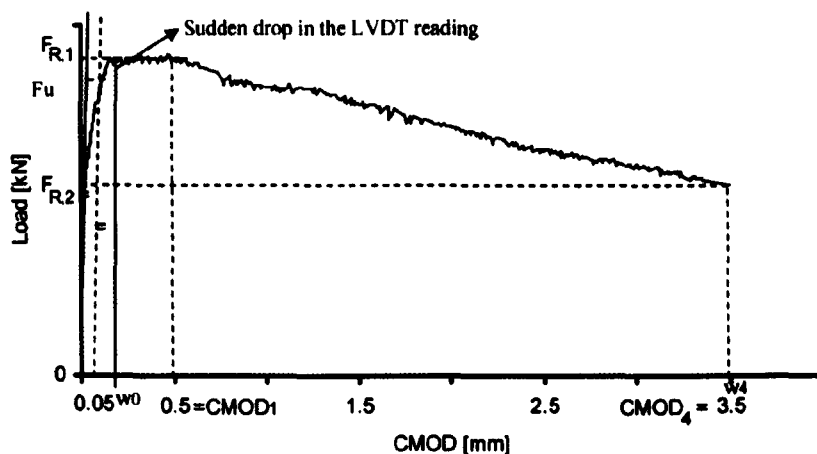


Figure 5.23 Determination of F_u and residual tensile strengths

It should be noted that the CMOD at the bottom surface is calculated using CMOD1, measured at a distance ζ (5mm) below the prism (equation 5.15, Barr and Lee, 2002).

$$CMOD = CMOD_1 \frac{h}{h + \zeta} \quad [\text{mm}] \quad (5.15)$$

$f_{eq,2}$ or $f_{R,1}$ are used in the verification of the serviceability limit states, while $f_{eq,3}$ or $f_{R,4}$ are taken into account at the ultimate limit state. The average design parameters were determined for all tested specimens as shown in Table 5.5.

Table 5.5 Test results and design parameters

Groups	Fibre ratio	f_{cm}	Age	F_u	P_{peak}	δ_u	$f_{fc1,u}$	$f_{eq,2}$	$f_{eq,3}$	$f_{R,1}$	$f_{R,4}$
	[%] ¹	[MPa]	[Day]	[kN]	[kN]	[mm]	[MPa]	[MPa]	[MPa]	[MPa]	[MPa]
Plain	0.0	51.5	101	18	18	0.03	3.45	-	-	-	-
	0.5	49.5	90	18.5	18.5	0.046	4.26	1.4	1.6	1.1	0.8
SRSF	1.0	50.0	94	23.1	23.1	0.064	5.32	2.0	2.8	3.9	1.7
	2.0	45.0	105	27.1	27.1	0.08	6.24	2.4	4.1	6.0	2.5
PRSF	1.5	44.0	112	25.1	27.1	0.07	5.78	3.3	4.6	5.4	3.7
	3.0	38.5	113	31.7	34.0	0.11	7.30	4.3	6.1	7.8	5.8
	6.0	50.0	115	37.4	58.3	0.11	8.62	6.3	11.0	12.6	11.2
VSF	1.5	54.1	163	28.7	28.6	0.09	6.61	3.2	5.8	6.6	4.3
	3.0	62.0	162	33.4	40.7	0.07	7.7	5.2	7.7	10.2	5.2
	6.0	66.2	161	41.6	61.6	0.07	9.6	5.9	12.6	14.1	10.4
ISF-1	6.0	52.9	66	44.8	64.6	0.09	10.3	6.6	12.4	14.1	12.7
ISF-2	6.0	63.9	196	46.8	61.3	0.118	10.78	5.6	11.8	13.8	11.5

The results shown in Table 5.5 indicate that the equivalent tensile strengths ($f_{eq,2}$, $f_{eq,3}$) or the residual strengths ($f_{R,1}$, $f_{R,4}$) of PRSF are slightly lower than for VSF (due to reasons explained earlier). However, the strength characteristics of prisms reinforced with 6% VSF are similar to those for prisms containing 6% of ISF-1 or ISF-2. This can lead to the conclusion that cleaned PRSF fibres are as good as industrial fibres.

The $f_{eq,2}$ and $f_{R,1}$ values for the prism reinforced with 2% SRSF are comparable to those obtained for prisms reinforced with 1.5% of the other types of fibres. However, this is not true for $f_{eq,3}$ or $f_{R,4}$. This indicates that SRSF can be used in applications where bridging of micro cracks is more important than flexural strength.

5.3.3.4 Discussion on Parameters

The results in Table 5.5 suggest that the relationship between the equivalent flexural tensile strength ($f_{eq,2}$ and $f_{eq,3}$) and the residual flexural tensile strength ($f_{R,1}$ and $f_{R,4}$) differs significantly. The residual flexural tensile strength values ($f_{R,1}$) were higher than the values obtained for the equivalent flexural tensile strength $f_{eq,2}$. This difference ranged from 1.6 to 2.5 times. This means that the use of both parameters for design purposes, in a similar way as recommended by RILEM, can lead to different results. This problem is related to the fact that the RILEM method for determining the load at the limit of proportionality F_u and the corresponding δ_u is not consistent. Therefore, the evaluation of $D_{BZ,2}$ is inaccurate. The effect of errors in the determination of the initial slope on $f_{eq,3}$ is minor.

Figure 5.24 shows the relationship between $f_{eq,2}$ and $f_{eq,3}$, and between $f_{R,1}$ and $f_{R,4}$.

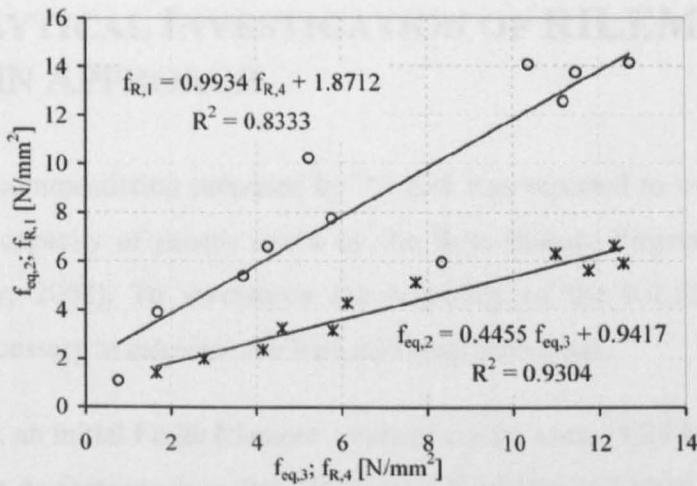


Figure 5.24 Correlation between equivalent tensile strength and residual tensile strength parameters

Fig. 5.25, on the other hand, reveals that the residual tensile strength parameter $f_{R,4}$ and equivalent tensile strength $f_{eq,3}$ have similar values but $f_{R,1}$ is greater than $f_{eq,2}$. This indicates that $f_{R,4}$ and $f_{eq,3}$ parameters are insensitive to initial errors and are more appropriate for design purposes.

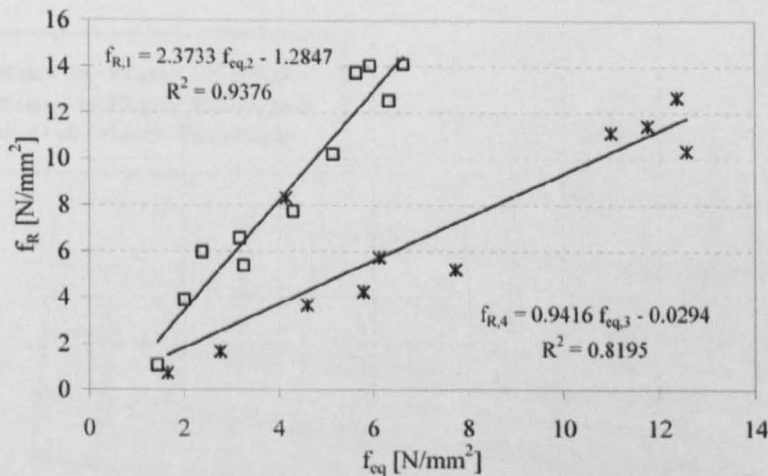


Figure 5.25 Correlation between f_R and f_{eq} .

It is clear from the above that the determination of the stress-strain curves for SFRC using the RILEM approach is not that reliable and a more robust approach needs to involve more extensive analytical investigations. An extensive analytical investigation is beyond the scope of this chapter, but a further demonstration of the problems associated with the RILEM model is given in the following.

5.4 ANALYTICAL INVESTIGATION OF RILEM STRESS-STRAIN APPROACH

The design recommendation proposed by RILEM was reported to overestimate the load-carrying capacity of prisms tested by the Brite-EuRam Project BRPR-CT98-0813 (Hemmy, 2002). To investigate the reliability of the RILEM stress-strain model, it is necessary to calculate the load mid-span deflection.

In this chapter, an initial Finite Element Analysis for the tested VSF beam with 1.5% fibre ratio was performed using the ABAQUS FE-package (Hibbitt, 2000). Due to the symmetric boundary, only one half of the prism was analysed. The tension stiffening effect was modified using the stress-strain curve based on the RILEM design parameters provided in Table 5.3. Figure 5.26 shows the distribution of the principal stresses at peak load. The position of the neutral axis is about $0.8h_{sp}$ at a peak load of 35 kN. This load is higher than that achieved experimentally (Table 5.5 and Figure 5.26).

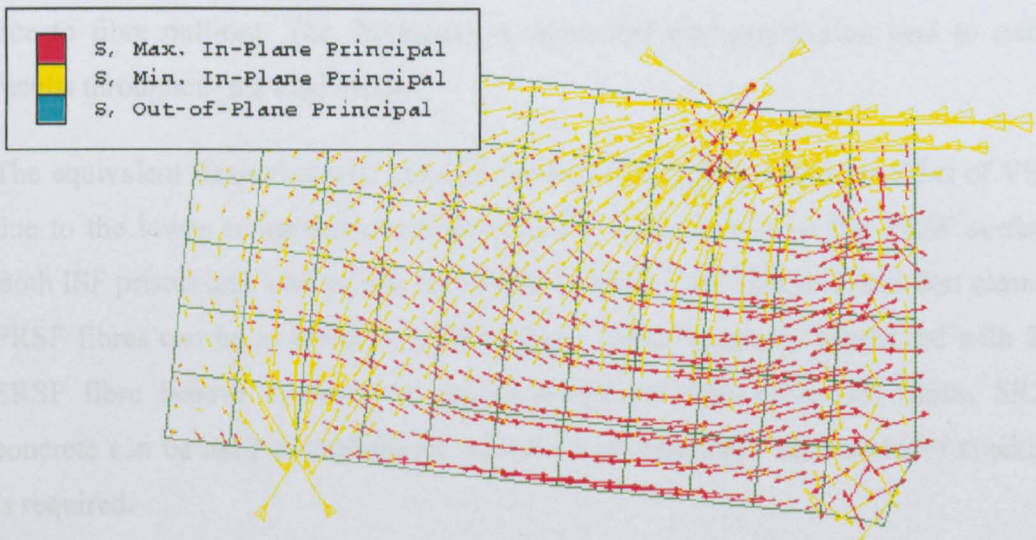


Figure 5.26 Distribution of the principal stress.

A comparison of the load-deflection curves obtained experimentally and analytically, is shown in Figure 5.27. The use of the RILEM stress-strain approach leads to an overestimation of the peak response. In addition, the FE-program was not able to converge after a deflection of 0.12 mm. The overestimation of the load-carrying

capacity highlights the deficiencies of the RILEM model identified earlier and underlines the need for the development of more robust models.

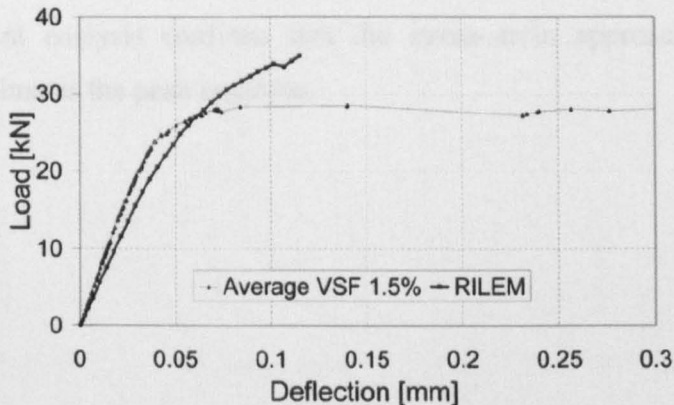


Figure 5.27 Load-deflection behaviour (result of testing and FEA)

5.5 CONCLUSIONS

The SRSF and PRSF can form a viable alternative to commercially-available steel fibres for use in SFRC. All steel fibre reinforced concrete specimens failed in flexure due to fibre pull-out. The displacement controlled load application lead to stable results throughout the load history.

The equivalent flexural tensile strength for PRSF is slightly lower than that of VSF, due to the lower compressive strength and the black carbon on the PRSF surface. Both ISF prisms and VSF prisms are similar in behaviour. This indicates that cleaned PRSF fibres can be as effective as ISF fibres. Concrete prisms reinforced with 2% SRSF fibre behave similarly to prisms reinforced with 1.5% ISF fibres. SRSF concrete can be used in applications where a high resistance against micro cracking is required.

It is demonstrated here that the neutral axis depth of SFRC migrates with load and should differ for different types and amounts of steel fibres.

The equivalent hinge length of $h_{sp}/2$ was shown to lead to reasonable results when converting displacement measurements to equivalent strains.

The load at limit of proportionality can not be accurately determined and its use can lead to erroneous estimation of $f_{eq,2}$. The parameter $f_{eq,3}$ can be determined with

greater accuracy and is a better parameter for design. The values of the parameters $f_{eq,2}$ and $f_{R,1}$ have great differences contrary to $f_{eq,3}$ and $f_{R,4}$.

A finite element analysis confirms that the stress-strain approach proposed by RILEM overestimates the peak response.

6. ANALYSIS AND DESIGN

6.1 INTRODUCTION

The design method for SFRC recommended by RILEM (2002) is based on the traditional section-analysis method used for normal reinforced concrete (RC) and, hence, offers a convenient means for designing SFRC elements (Vandewalle and Dupont 2003). The difference between the two design methods is that the stress-strain model used for the design of SFRC does not ignore tension and takes into account the tension stiffening due to the steel fibres. In the previous chapter it was shown that the main problem of the RILEM method is in the accuracy of the procedure adopted for the selection of the initial slope of the load-deflection curve. The procedure used is subjective and, hence, it may not lead to the correct value of F_u . The determination of f_{ct} , f_{eq2} and f_{eq3} is not accurate either, since the values of these parameters are influenced directly by the value adopted for F_u . As a result, a 10% variation in the calculation of f_{ct} may be obtained due to the subjectivity of the procedure (Barr and Lee 2002).

Another disadvantage of the RILEM model is found in the assumption used for the calculation of the tensile stresses in the cracked SFRC section. These stresses are calculated by using equivalent elasto-plastic stress diagrams, which are determined by assuming specific values for the neutral axis depth ($0.66h_{sp}$ and $0.9h_{sp}$, at f_{eq2} and f_{eq3} , respectively) (Vandewalle and Dupont 2003). As a result of this latter assumption, the SFRC tensile strength is overestimated and as shown in the previous chapter this leads to an overestimation of the load-carrying capacity of SFRC.

The aim of this section is to determine a more accurate tensile stress-strain relationship for SFRC by using step-by-step numerical analysis. The ABAQUS finite element package (Hibbitt, Karlsson and Sorensen 2000) is used to perform the analysis, since ABAQUS allows the user to define the strain-softening behaviour for cracked concrete in as many stages as needed.

The objective is to optimise the stress-strain model input until the analytical load-deflection curve fits experimental results.

It should be mentioned that the experimental work used in this chapter included tests on notched beam using conventional industrial steel fibres (ISF-1 and ISF-2), as well as on chopped tyre wire (VSF) and two types of recycled fibre (PRSF and SRSF) (see chapter 5).

The work described in this chapter is included in a journal paper submitted in April 2004 for publication in Materials and Structures.

6.2 FINITE ELEMENT ANALYSIS

6.2.1 ELEMENT TYPE USED

A two-dimensional solid biquadratic element (CPS4) with eight-nodes having two degrees of freedom per node (X,Y) was chosen. A 3x3 Gaussian integration rule over the element plane was adopted (see input file in Appendix D). The Gaussian element length is measured perpendicular to the crack direction (as illustrated in Fig. 6.1) by assuming that the element is a rectangle, and the crack propagation is perpendicular to the tensile surface of the beam.

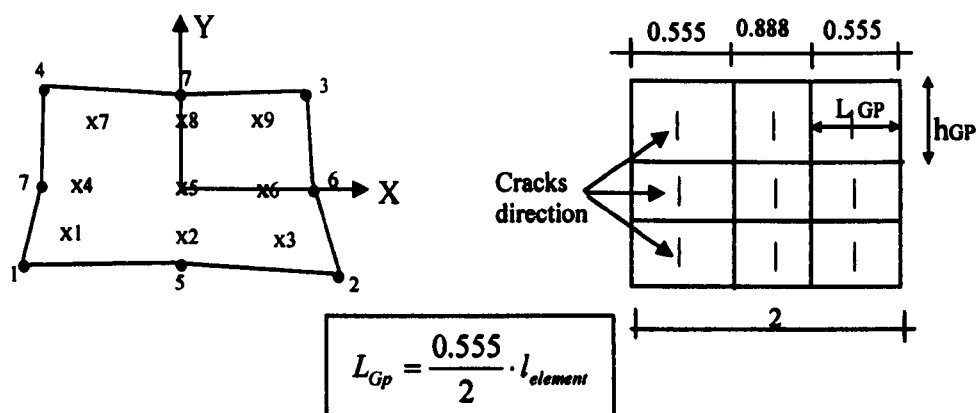


Figure 6.1 Element used in ABAQUS

The analysis is performed by incremental loading, with integration in each increment. Since considerable nonlinearity is expected in the response of the analysed beam (including the possibility of instability as the concrete cracks), the

load magnitudes are covered by a single scalar parameter. The modified Riks algorithm with automatic increments is used (Hibbitt, Karlsson and Sorensen 2000). This method uses the “arc length” along the static equilibrium path in load-displacement space. This provides a solution regardless of whether the response is stable or unstable.

6.2.2 SFRC MODEL AND INVERSE ANALYSIS

6.2.2.1 Compressive Characteristics

In ABAQUS, the concrete model developed by Kupfer, Hilsdorf and Rusch (1973) is used. A Mohr–Coulomb type compression surface combined with a crack detection surface is used to model the failure surface of concrete (Figure 6.2).

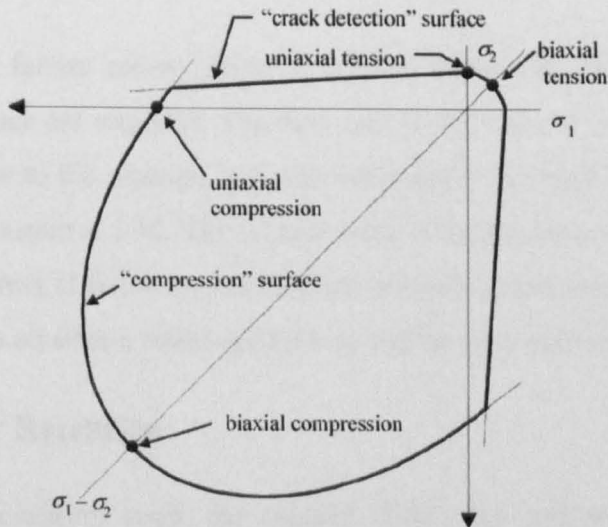


Figure 6.2 Concrete failure surfaces in plane stress (after Kupfer, Hilsdorf and Rusch 1973).

When the principal stress components of concrete are predominantly compressive, the response of the concrete is modelled by the elastic-plastic theory with associated flow and isotropic hardening rule.

The previous chapter indicated that the compressive strain measured at peak load for SFRC containing 1.5% virgin steel fibres (VSF), during third-point bending tests, is around 0.4%. This strain is considered to be in the linear elastic region. However, for SFRC with higher fibre ratios and at post-peak load displacement, the strain

magnitude could fall in the non-linear region. To cover all possibilities, the uniaxial non-linear stress-strain relationship for concrete in compression, as defined by Eurocode 2 (1991) and adopted by RILEM (2002), is used in the analysis (Figure 6.3).

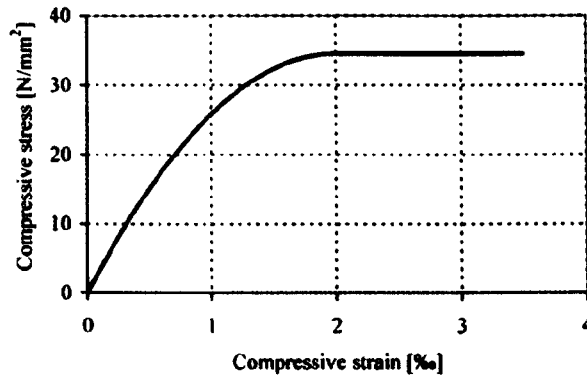


Figure 6.3 Compressive stress-strain curve implemented in ABAQUS

In ABAQUS the failure ratios option is used to define the shape of the failure surface. Two values are required. The first one is the ratio of the ultimate biaxial compressive stress to the ultimate uniaxial compressive strength (Figure 6.2). This value was kept constant at 1.15. The second value is the absolute value of the ratio of uniaxial tensile stress at failure to the ultimate uniaxial compressive stress. In SFRC this value depends on fibre content and type as will be discussed later.

6.2.2.2 Shear Retention

During the post cracking stage, the cracked SFRC can still retain shear through transfer of shear forces through aggregate interlock or shear friction through fibres. Assuming that the shear modulus of intact concrete is G_c , then the reduced shear modulus G_R of cracked concrete can be expressed by;

$$G_R = \rho^{close} G_c \quad (6.1)$$

and

$$\rho^{close} = 1 - \varepsilon / \varepsilon_{max} \quad (6.2)$$

where:

- ε strain normal to the crack direction,
 ε_{max} strain at which the concrete tensile stress reduces to zero.

In ABAQUS, a very large value is usually assumed for ε_{max} , which is automatically invoked with default data value ρ^{close} equal to 1.0 (full shear retention). In this investigation the values for shear retention parameter $\rho^{close} = 0.1$ and 1.0 (full shear retention) were used. The overall deformation was very similar for the two solutions. Since this parameter did not make much difference in this flexure dominated problem, the value of $\rho^{close} = 1.0$ was chosen for further analysis since it gives more stable results.

6.2.2.3 SFRC Tensile Characteristics

In tension, once cracking is defined to occur (by the crack detection surface), the orientation of the cracks is stored, and fixed. Damaged elasticity is then used to model existing cracks.

Due to the random orientation of fibres in concrete, the behaviour of SFRC in tension can be assumed to be similar to the one of plain concrete, but with improved tension stiffening. By changing the tensile softening characteristics step-by-step, a stress-strain relationship can be found that will equate the analytical load-deflection curve with the experimental one. This method is called “back-calculation” or “inverse analysis” for the determination of the stress-strain characteristics.

The tension softening of concrete after cracking is simulated by a multi-linear descending curve. The gradient of the stress-strain curve along the softening region is varied as illustrated in Figure 6.4.

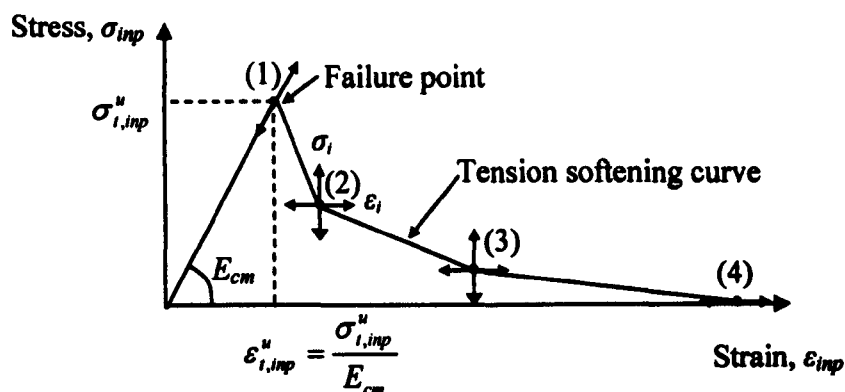


Figure 6.4 Tension stiffening model

Up to point (1), the concrete is considered to be uncracked having an elastic modulus of E_{cm} (same as initial modulus in compression). This point is established by determining the first deviation from linearity of the load deflection curve. After this stage, subsequent points (2), (3) and (4) are obtained by iteration, until the complete load deflection curve is followed relatively accurately.

6.3 FE SENSITIVITY ANALYSIS AND RESULTS

Taking advantage of symmetry, only half of the beam is modelled. To simulate the notch along the symmetry axis, nodes within the notch's height are unrestrained. A mesh sensitivity study was performed using three meshes as shown in Figure 6.5.

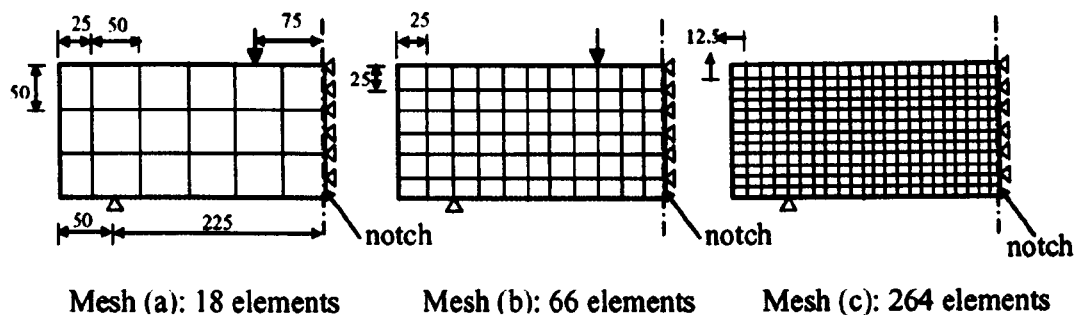


Figure 6.5 FE model with coarse, middle and fine meshes

Mesh (b) was used to optimise the initial results. The input tension stiffening curve was modified until the calculated load versus mid-span-deflection curve agreed with the experimental results, as shown in Figure 6.6 for the integration point nearest to the crack. This stress-strain response was used to describe the SFRC characteristic for all meshes. The load-deflection curves obtained from analysis and experiments are shown in Figure 6.7.

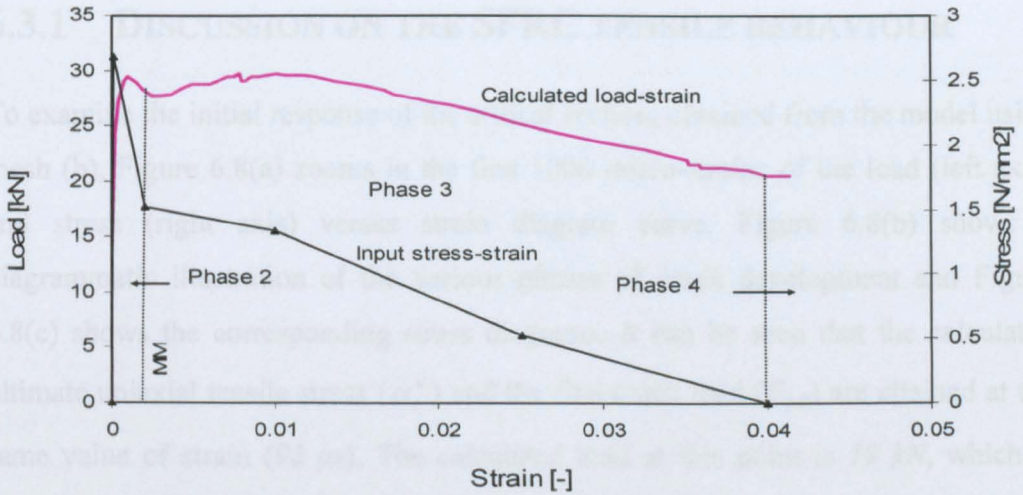


Figure 6.6 Input and output stress-strain relationship (1.5% VSF)

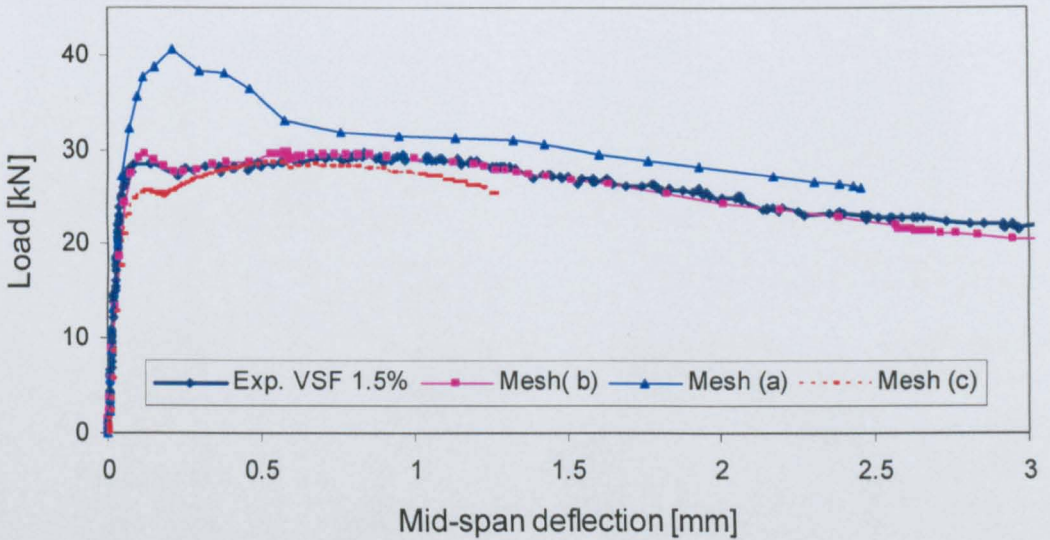


Figure 6.7 Predicted load-displacement curves for beam with 1.5% VSF

As expected, mesh (a) leads to an increase in the post-crack energy absorption capacity, whilst mesh (c) underestimates the capacity after cracking. The results also showed that the FE analysis for mesh (c) is unstable at a deflection of 1.25 mm . This is because the post-crack energy is too low, causing local cracking failure in the SFRC and leading to unstable behaviour in the overall response of the model. To get larger deflections, it is necessary to increase the post-crack energy input.

6.3.1 DISCUSSION ON THE SFRC TENSILE BEHAVIOUR

To examine the initial response of the critical section, obtained from the model using mesh (b), Figure 6.8(a) zooms in the first 1000 micro-strains of the load (left axis) and stress (right axis) versus strain diagram curve. Figure 6.8(b) shows a diagrammatic illustration of the various phases of crack development and Figure 6.8(c) shows the corresponding stress diagrams. It can be seen that the calculated ultimate uniaxial tensile stress (σ_t^u) and the first crack load ($F_{l,u}$) are attained at the same value of strain ($92 \mu s$). The calculated load at this point is 19 kN , which is equivalent to the load obtained from the tests (Chapter 5).

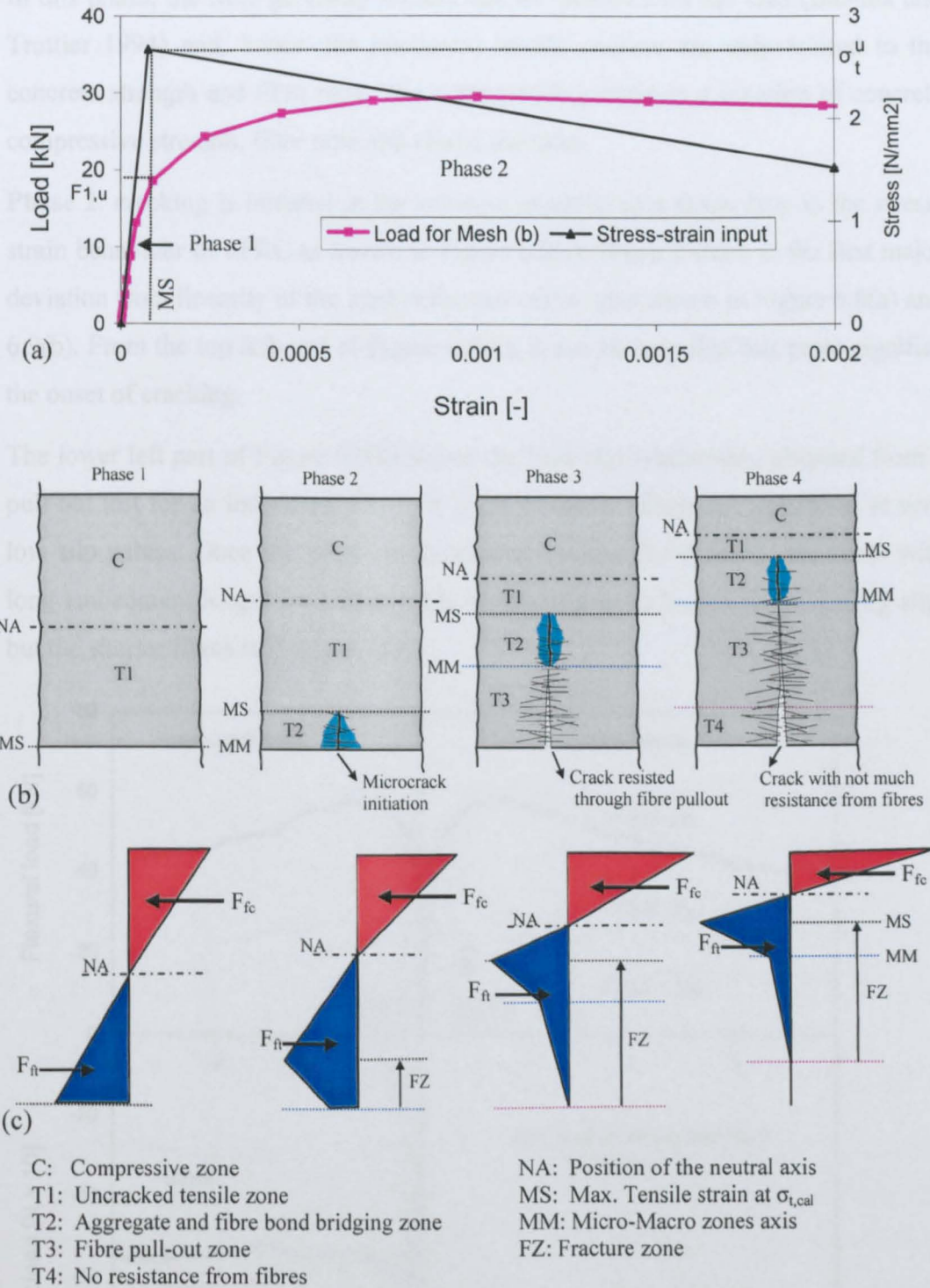


Figure 6.8 Initial load vs stress, stress vs strain and stress distribution.

By considering the above, the load-stress relationship can be described in four phases.

Phase 1: the load-stress relationship can be idealised as linear elastic. There is no crack in the tensile zone (T1) and the maximum tensile stress is reached at strain MS.

In this phase, the fibre geometry usually has no influence on the load (Banthia and Trottier 1994) and, hence, the maximum tensile stresses are only related to the concrete strength and fibre ratio. The corresponding strain is a function of concrete compressive strength, fibre ratio and elastic modulus.

Phase 2: cracking is initiated in the concrete resulting in a sharp drop in the stress-strain behaviour of SFRC as shown in Figure 6.8(a). Phase 2 starts at the first major deviation from linearity of the load-deflection curve, also shown in Figure 6.8(a) and 6.9(b). From the top left part of Figure 6.9(b), it can be seen that this point signifies the onset of cracking.

The lower left part of Figure 6.9(b) shows the load-slip relationship obtained from a pull-out test for an individual PRSF. It is clear that the fibres are mobilised at very low slip values. Once the crack starts opening (around $0.1\text{--}0.2\text{mm}$), the fibres with long embedment length are still capable to carrying extra load with increasing slip, but the shorter fibres start to pull-out.

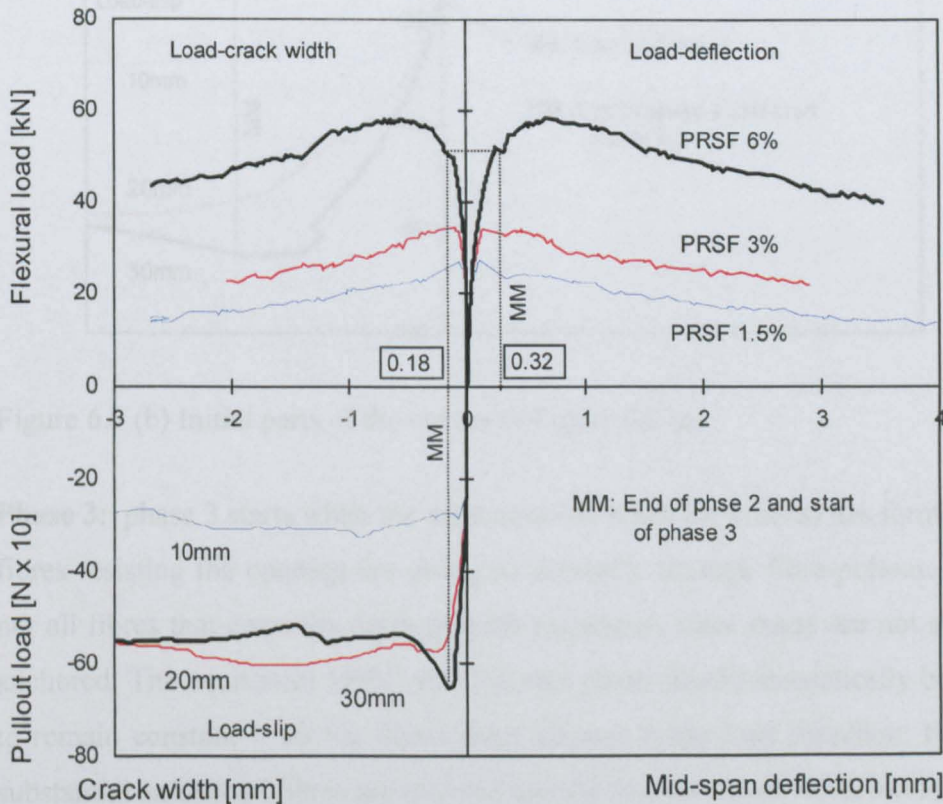


Figure 6.9 (a) Relationship between load-crack width, load-slip and load-deflection.

By the end of phase 2, the crack is well established (the concrete tensile contribution is lost) and most fibres have exceeded their peak loads and are beginning to slip at more or less constant loads.

On the element level, by the end of phase 2, the deflection behaviour of the prism changes from elastic to more or less elasto-plastic, with a hinge developing in the mid-span.

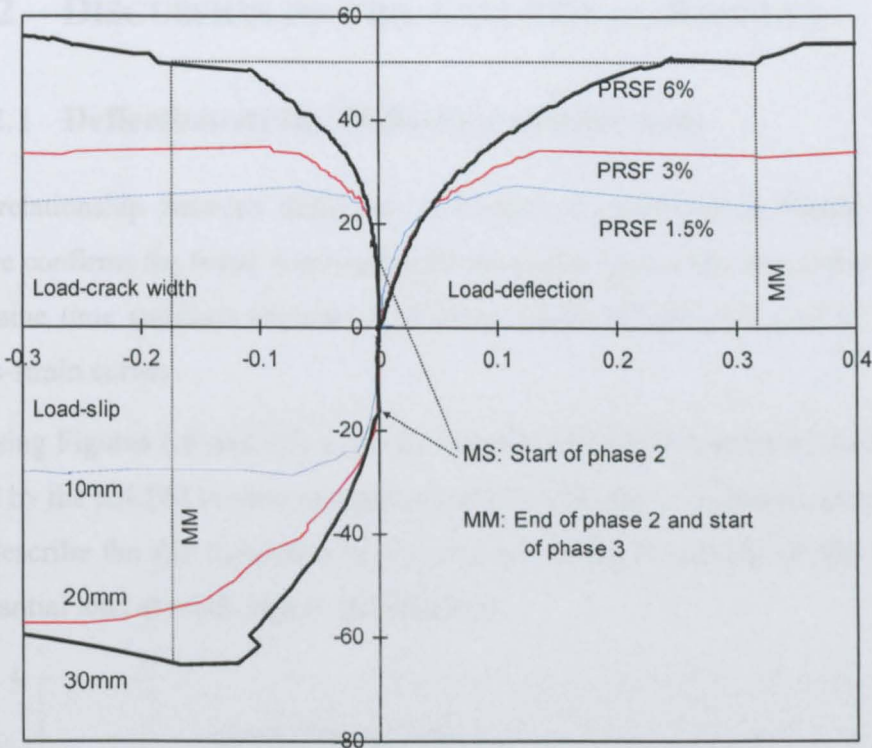


Figure 6.9 (b) Initial parts of the curves of Figure 6.9 (a)

Phase 3: phase 3 starts when the main concrete crack (or cracks) has formed and the fibres resisting the opening are doing so primarily through fibre-pullout. Naturally, not all fibres that cross the crack provide resistance, since many are not sufficiently anchored. The equivalent SFRC stress in this phase should theoretically be expected to remain constant if all the fibres were aligned in the load direction. However, a substantial amount of fibres are inclined and are less activated. With increasing crack opening, the inclined fibres will crush the concrete between the fibre and the crack, as they try to straighten out (Chanvillard and Aitcin 1996). This will decrease the effective stress across the crack during the middle stage of phase 3 as shown in Figure 6.8. However, it is possible that the contribution of inclined fibres increases

later on, when they are re-engaged by the uncrushed concrete. Eventually, with increasing crack opening, most fibres will pull-out with no residual force and that brings phase 3 to an end.

Phase 4: during phase 4, the concrete near the notch carries no tensile stress, but the load is carried by the part of the section in which the fibres are still engaged and the neutral axis depth moves closer to the compressive zone.

6.3.2 DISCUSSION ON THE ANALYTICAL RESULTS

6.3.2.1 Deflection-strain, Deflection-neutral Axis

The relationship between deflection and strain is examined in Figure 6.10. The Figure confirms the linear relationship between mid-span deflection and strain and at the same time validates the choice of hinge length (Chapter 5) used to derive the stress-strain curves.

By using Figures 6.6 and 6.7, it can be determined that the maximum strain of 10‰ (used by the RILEM model) corresponds only to 0.8 mm in deflection and hence, can not describe the full behaviour of the element which is capable of still resisting a substantial load at much higher deformations.

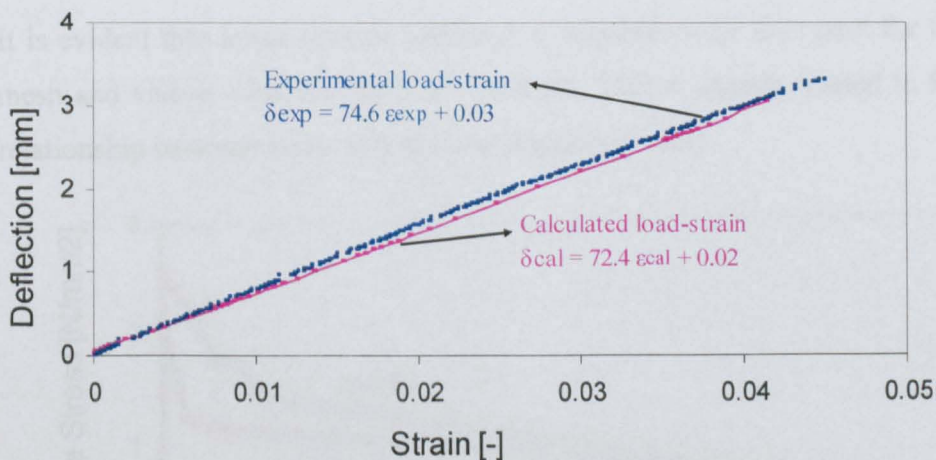


Figure 6.10 Numerical mid-span deflections versus tensile strains (1.5% VSF)

Figure 6.11 shows the shift of the calculated normalised neutral axis depth from the notch tip (y) for a prism reinforced with 1.5% VSF. The positions of the neutral axis are 0.58, 0.83 and 0.97 at first crack, peak load and 3 mm deflection, respectively.

These values agree with experimental results reported previously by the author (Chapter 5).

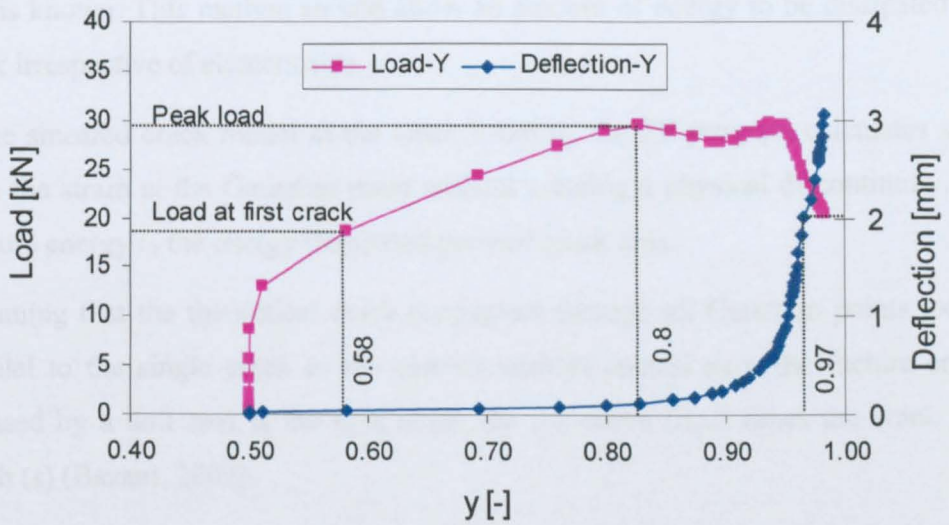


Figure 6.11 Deflection vs normalised neutral axis

6.3.3 MESH INDEPENDENT STRESS-STRAIN RELATIONSHIP

To get the numerical results for any mesh (here mesh (a) is used as an example) to agree with the experimental results, the tension softening has to be reduced (σ - ϵ (a)) as shown in Figure 6.12.

It is evident that lower tension softening is required to fit the result for the coarser mesh and vice-a-versa for the finer mesh (c). This is clearly related to the inverse relationship between strain and element length ($\epsilon = \Delta l/l$).

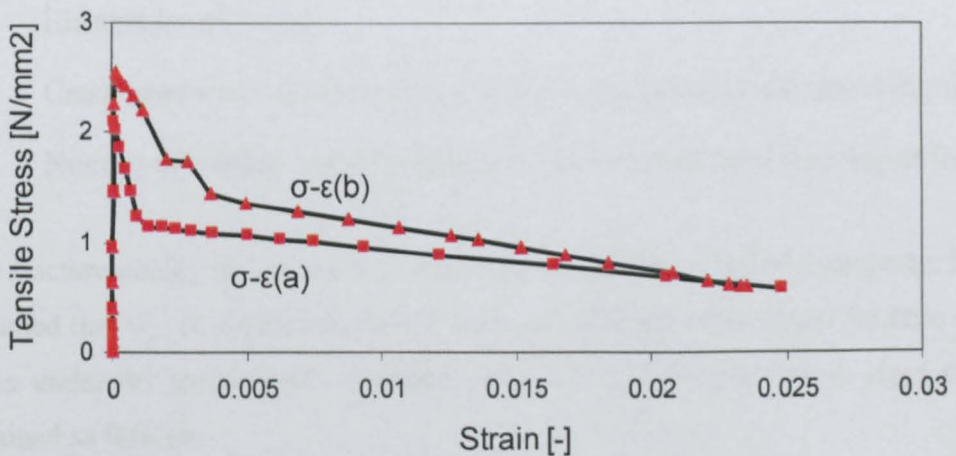


Figure 6.12 Tension softening for mesh (a) before and after modification.

It is necessary to develop a method, which will be able to derive the stress-strain curves for any mesh sizes, when the optimum stress-strain curves for a given mesh size is known. This method should allow an amount of energy to be dissipated in a crack irrespective of element size.

In the smeared crack model at the crack location, the FE program calculates stress from the strain at the Gaussian point without creating a physical discontinuity. The fracture energy is the energy dissipated per unit crack area.

Assuming that the theoretical crack propagates through all Gaussian points located parallel to the single crack in the beam's vertical central axis, the fracture energy released by a unit area is the area under the σ - ε curve ($A_{\sigma-\varepsilon}$) times the crack band width (s) (Bazant, 2002).

$$G_{F1} = A_{\sigma-\varepsilon} \cdot s \quad [\text{Nmm}^{-1}] \quad (6.3)$$

$$s = l_{GP} \cdot n_c \quad [\text{mm}] \quad (6.4)$$

$$l_{GP} = \frac{0.555}{2} \cdot l_{el} \quad [\text{mm}] \quad (6.5)$$

where

$A_{\sigma-\varepsilon}$ Area under the stress-strain [N/mm^2]

l_{GP} Length of Gaussian point [mm] (Figure 6.1)

l_{el} Element length [mm]

s Crack band width or plastic hinge length in a smeared crack model [mm]

n_c Number of cracked Gaussian points within the crack band (see Appendix D)

The fracture energy dissipated in a single crack is purely a material property. If it is assumed that G_{F1} is approximately the same for different mesh sizes, the ratio of the areas under the stress-strain softening curve for two different mesh sizes can be obtained as follows.

$$\frac{A_{\sigma-\varepsilon}}{A'_{\sigma-\varepsilon}} = \frac{l_{el}}{l'_{el}} \quad (6.6)$$

By assuming that the pre-crack part of the stress-strain relationship remains elastic, the strain values for the stress-strain curves for a new element length can be expressed by equation 6.7 (Figure 6.13).

$$\frac{\varepsilon_n - \varepsilon'_i}{\varepsilon'_n - \varepsilon'_i} = \frac{A_{\sigma-\varepsilon}}{A'_{\sigma-\varepsilon}} \quad (6.7)$$

where

- ε Strain for new element size
- ε' Strain from initial element size
- n Number of linear portions

The element length in a finite element analysis, along the crack path should not be greater than $0.3-0.4l_c$ (Hillerborg, 1983). l_c is the critical length or the length of the fracture zone in a smeared tensile test. Bazant and Pijaudier-Cabot (1989) defined l_c as the ratio:

$$l_c = \frac{G_{F2}}{W_F} \quad [\text{mm}] \quad (6.8)$$

The surface fracture energy, G_{F2} , expresses the energy dissipated to create a unit crack area (N/mm). W_F represents the energy released by a volume (N/mm²) of material during a smeared tensile test, where a large number of micro-cracks are created. Both the surface fracture energy and the volumetric fracture energy are determined from the complete area enclosed by the stress-displacement or stress-strain curves. The external work-done at the applied load in a four point loading test can be considered to be mostly due to energy dissipated in the fracture zone. This energy can be calculated for a notched beam by the following expression.

$$G_{F2} = \theta \cdot A_F / b \cdot yh \quad [\text{Nmm}^{-1}] \quad (6.9a)$$

$$W_F = A_{\sigma-\varepsilon} \quad [\text{Nmm}^{-2}] \quad (6.9b)$$

where:

- $\theta = 2/3$ Represent the difference between the dislocation under the load and mid-span deflection
- A_F Area under the load deflection curve after first crack initiation [Nmm]
- h Depth of the beam cross section [mm]
- y Position of the normalise neutral axis [-]

From equations 6.3 and 6.9a it can be seen that the critical length (l_c) is equal to the crack band width (s). Hence, the calculated average critical length (69.0mm for 50mm long fibres and 65.0mm for SRSF, see Appendix D.3) of the tested beams was about that by Ulfkjar (1995) assumed hinge length of $hsp/2$ (62.5mm).

The σ - ε diagram used in ABAQUS for further FE analysis is shown in Figure 6.13. The strains ε_1 , ε_2 and ε_3 were determined at values of 2%, 10% and 25%, respectively. The mesh size (b) was used through the analysis.

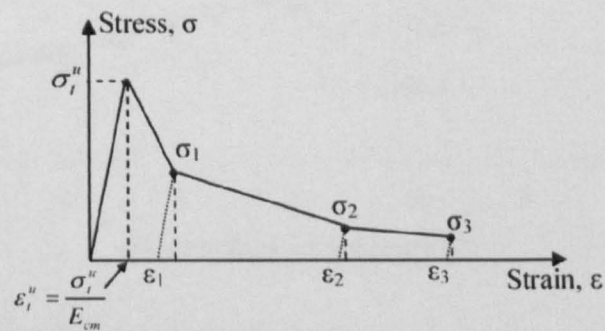


Figure 6.13 Determination of the strain values for the a given element size

The input parameters for the tested fibres shown in Table 6.1 were determined for element length 25mm . The values shown in the table for σ_{n1} , σ_{n2} and σ_{n3} are normalised against σ_t^u .

Table 6.1 Input parameters for the tested fibres

Type	Fibres	Material input		Element input $l_{el} = 25 \text{ mm}$				
		E_{cm}	σ_t^u	σ_{nt}^u	ε_t^u	$\sigma_{n1}/\varepsilon_1$	$\sigma_{n2}/\varepsilon_2$	$\sigma_{n3}/\varepsilon_3$
-	%	[N/mm ²]	[N/mm ²]		[‰]			
Plain	0	33400	1.9	1	0.06	-	-	-
VSF	1.5	34000	2.68	1.4	0.07	0.57/2	0.50/10	0.20/25
	3.0	35500	4.2	2.2	0.10	0.70/2	0.33/10	0.05/25
	6.0	37500	5.5	3.0	0.13	0.70/2	0.65/10	0.40/25
PRSF	1.5	31000	2.6	1.36	0.08	0.55/2	0.30/10	0.15/25
	3.0	30000	3.4	1.78	0.11	0.60/2	0.35/10	0.25/25
	6.0	33000	5.3	2.78	0.16	0.70/2	0.60/10	0.35/25
ISF-1	6.0	33500	6.0	3.10	0.17	0.70/2	0.60/10	0.35/25
ISF-2	6.0	36000	5.7	2.94	0.15	0.70/2	0.60/10	0.35/25
SRSF	0.5	33000	2.03	1.07	0.06	0.30/2	0.15/10	0.05/25
	1.0	33000	2.41	1.26	0.07	0.40/2	0.25/10	0.10/25
	2.0	32000	2.7	1.42	0.08	0.50/2	0.30/10	0.15/25

6.4 NEW DESIGN MODEL

The values of maximum tensile stress σ_{nt}^u , normalised against the strength of plain concrete, are plotted against fibre ratios in Figure 6.14.

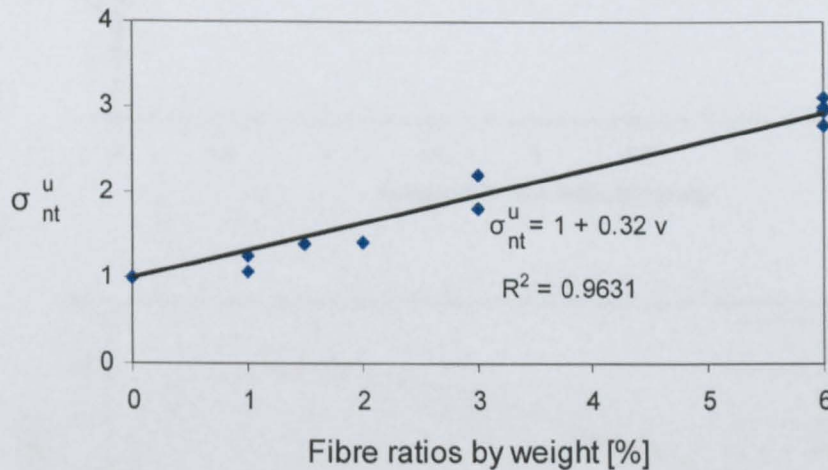


Figure 6.14 Normalised strength vs fibre ratio

It is clear that a linear function best describes this relationship. The expected maximum tensile stress can be determined as a function of fibre ratio as follows.

$$\sigma_i^u = \sigma_{i,p}^u (1 + 0.32 \cdot v) \quad [\text{N/mm}^2] \quad (6.10)$$

where:

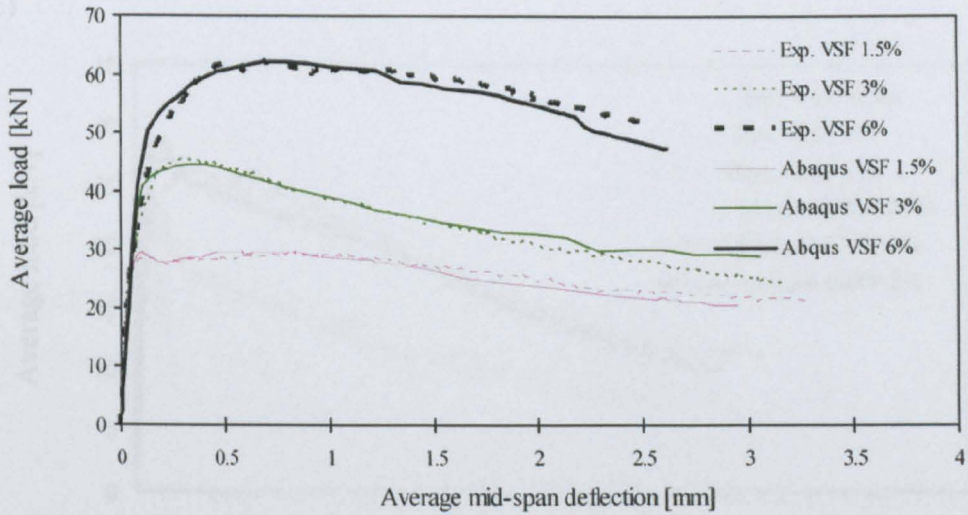
$\sigma_{t,p}^u$ Maximum tensile stress for plain concrete

v Fibre ratio by weight [%]

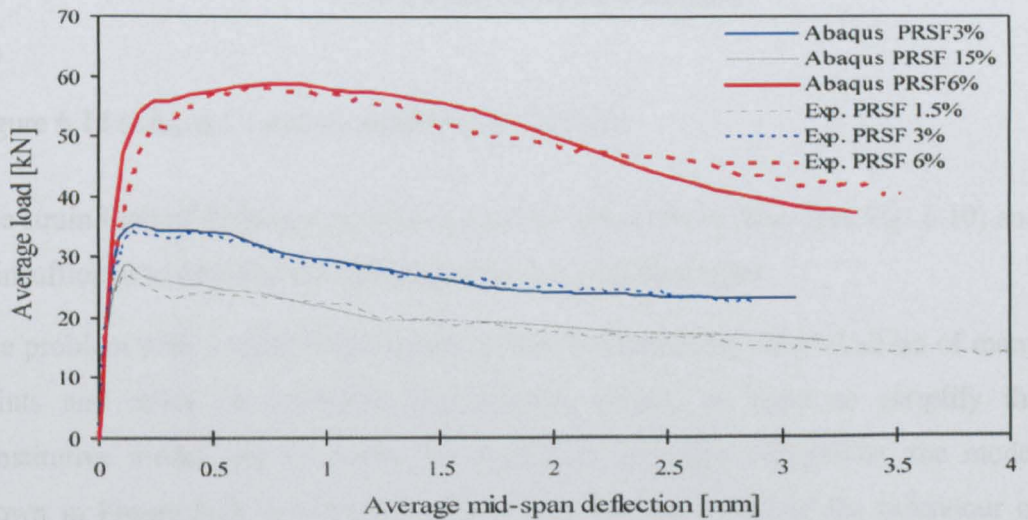
The strain corresponding to σ_t^u can be expressed as

$$\varepsilon_t^u = \sigma_t^u / E_{cm} \tag{6.11}$$

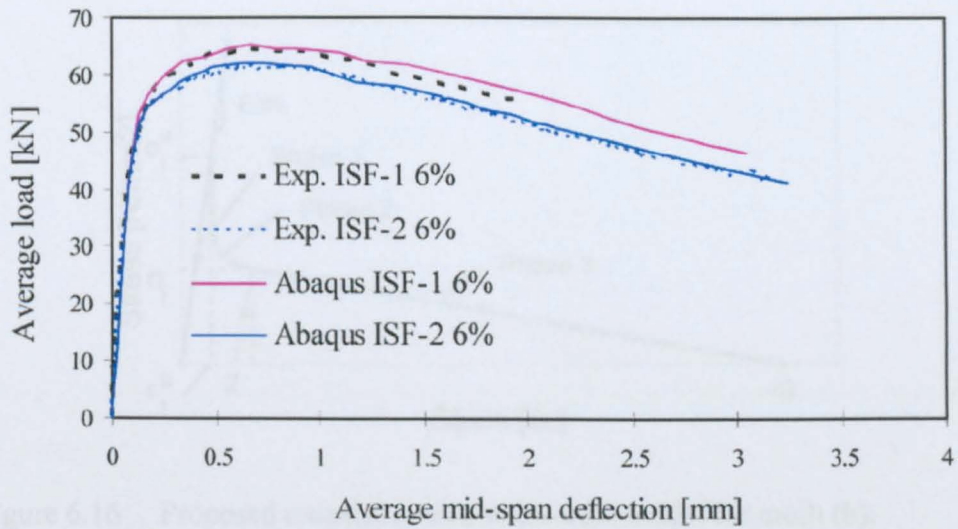
Using the values of the normalised stresses (σ_{n1} , σ_{n2} and σ_{n3}) and the corresponding strains (2‰, 10‰ and 25‰) shown in Table 6.1, the load-deflection curves calculated by using ABAQUS were in good agreement with the experimental results for all fibre ratios and fibre types as seen in Figure 6.15 (a,b,c,d).



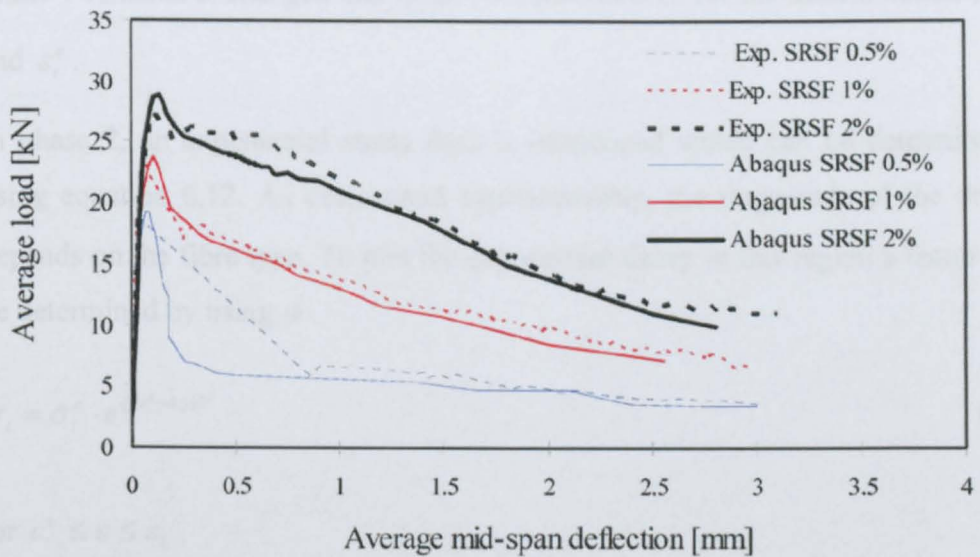
(a)



(b)



(c)



(d)

Figure 6.15 (a,b,c,d,) Load vs deflection predictions

The strain limit of 25‰ corresponds to a deflection of about 2mm (see Fig. 6.10) and is insufficient to describe the full load deflection characteristics.

The problem with a multi-linear model is that it requires the determination of many points and relies on extensive experimental results. In order to simplify the constitutive model and to enable the prediction of larger deflections, the model shown in Figure 6.16 is proposed. This model aims to represent the behaviour of SFRC in a more realistic manner, following the phases described in section 6.3.1.

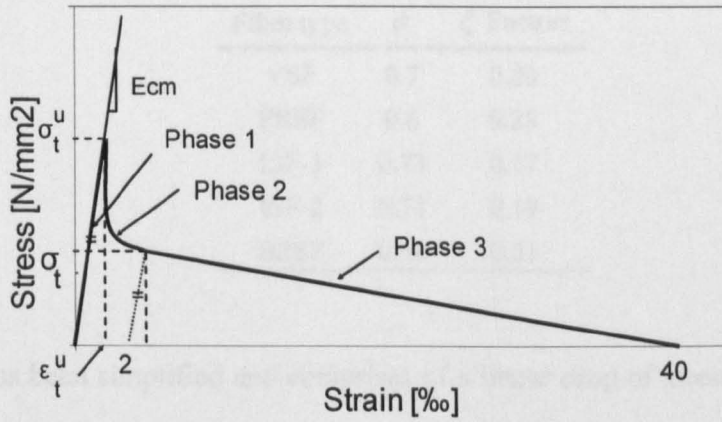


Figure 6.16 Proposed uniaxial tensile stress-strain model for mesh (b).

Phase 1 remains unchanged and relies on equation 6.12 for the determination of σ_t^u and ε_t^u .

In phase 2, an exponential stress drop is introduced which can be determined by using equation 6.12. As determined experimentally, the magnitude of the drop ϕ depends on the fibre type. To plot the exponential decay in this region a factor ξ can be determined by using ϕ .

$$\sigma_t = \sigma_t^u \cdot e^{\xi(\varepsilon_t^u - \varepsilon) \cdot 10^3} \tag{6.12}$$

for $\varepsilon_t^u \leq \varepsilon \leq \varepsilon_1$

where:

$$\phi = \frac{\sigma_1}{\sigma_t^u} \tag{6.13}$$

ξ Factor reflects the influence of the fibre type on the tensile softening (Table 6.2).

ε_1 equal to 2%

$$\sigma_t = \sigma_t^u \cdot e^{\xi(\varepsilon_t^u - 0.002) \cdot 10^3} \tag{6.14}$$

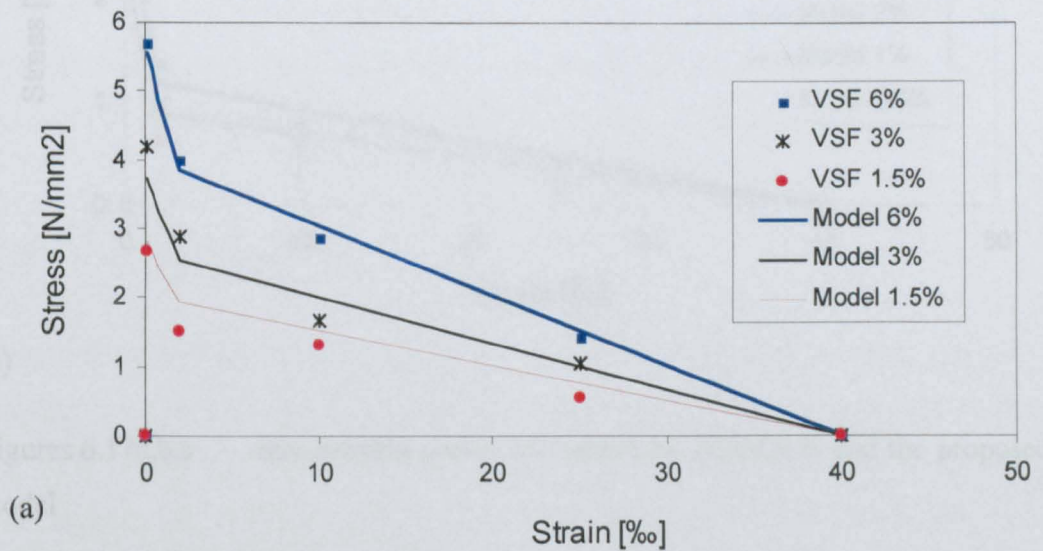
Table 6.2 Factors for the proposed model

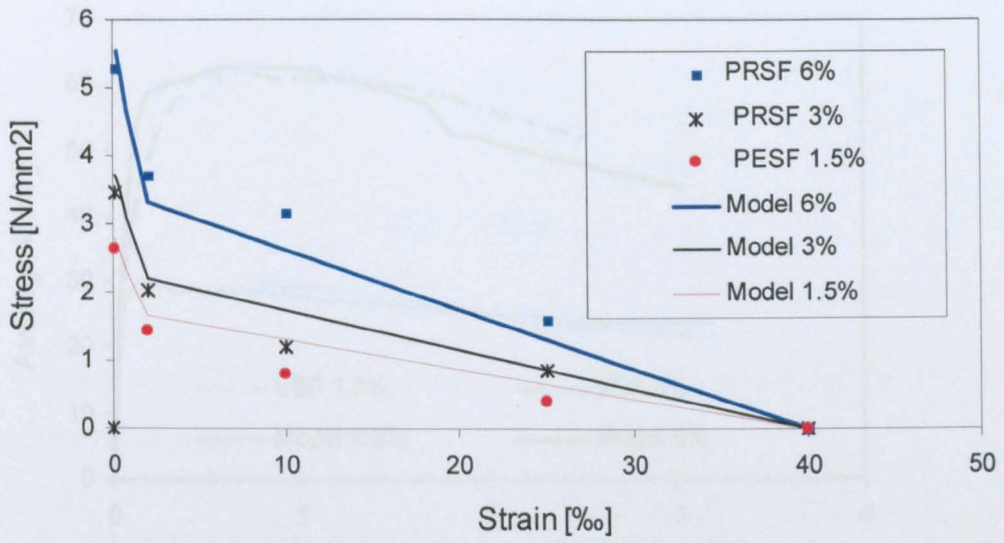
Fibre type	ϕ	ξ Factors
VSF	0.7	0.20
PRSF	0.6	0.28
ISF-1	0.73	0.17
ISF-2	0.71	0.19
SRSF	0.38	0.51

Phase 3 has been simplified and comprises of a linear drop of stress to zero at strain ε_4 (40‰).

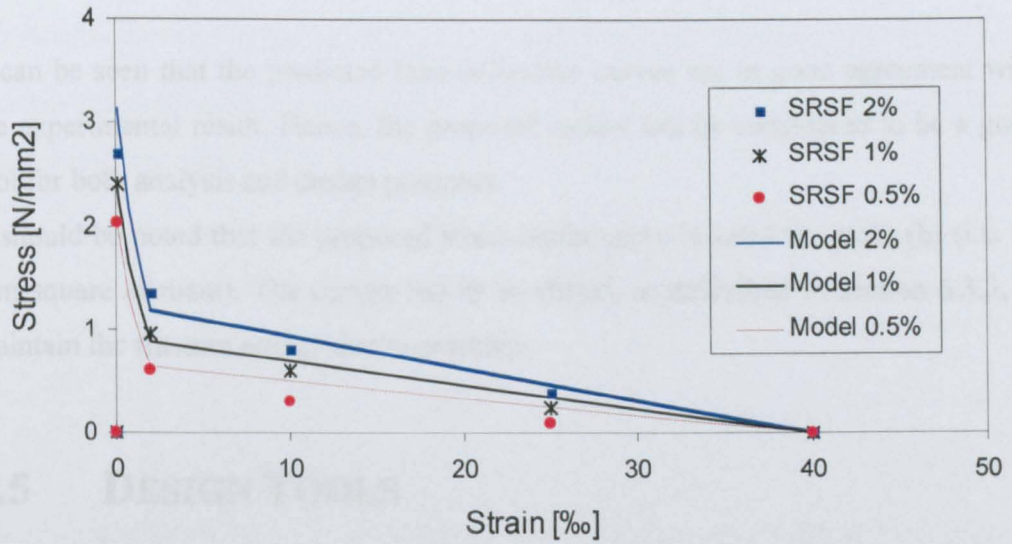
For each fibre type ϕ has to be determined by performing bending tests. An accurate evaluation of ϕ requires FE back analysis. A simplified procedure for determining the value ϕ is given in Appendix F.

Figures 6.17(a-c) show the prediction of the proposed model (indicated by solid lines) in comparison with the results obtained from the ABAQUS back analysis (indicated by points).





(b)



(c)

Figures 6.17a,b,c Stress-strain curves calculated by ABAQUS and the proposed model

Figure 6.18 shows the predicted load-deflection curves for VSF fibres using the proposed model and the experimental results.

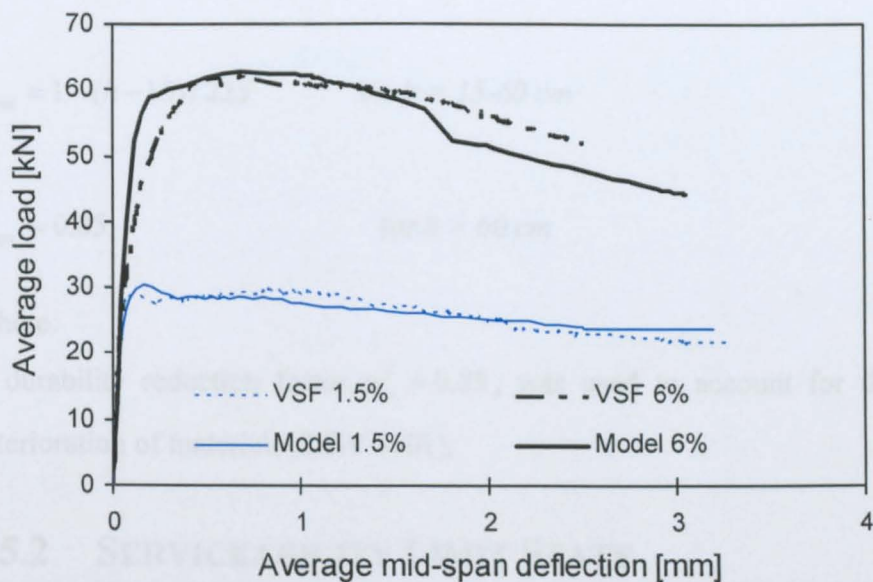


Figure 6.18 Predicted load-deflection curves using the proposed model.

It can be seen that the predicted load-deflection curves are in good agreement with the experimental result. Hence, the proposed model can be considered to be a good tool for both analysis and design purposes.

It should be noted that the proposed stress-strain curve is valid for mesh (b) (i.e. 25 mm square element). The curves can be modified, as described in section 6.3.3, to maintain the fracture energy due to cracking.

6.5 DESIGN TOOLS

Simplified equations and charts are often used in reinforced concrete design to simplify the design procedure for practicing engineers. A similar design procedure can be developed for SFRC. The aim of this section is to provide design equations and diagrams that can be used for design in the serviceability limit state and ultimate limit state.

6.5.1 STRESS REDUCTION FACTORS

Two beam sizes, 100x100x500 and 150x150x550 and concrete C40/50 were used for the development of the σ - ε model and experimental studies (Chapter 5).

To account for the size effect the following stress reduction factor should be used as proposed by DBV (2001).

$$\alpha_{sys} = 1 - (h - 15) / 225 \quad \text{for } h = 15-60 \text{ cm} \quad (6.15)$$

$$\alpha_{sys} = 0.85 \quad \text{for } h > 60 \text{ cm} \quad (6.16)$$

Where:

A durability reduction factor, $\alpha_{ct}^f = 0.85$, was used to account for the long-term deterioration of materials (DBV 2001).

6.5.2 SERVICEABILITY LIMIT STATE

In an uncracked flexural element, the full section is active and the steel fibre reinforced concrete can be considered to be elastic in both compression and tension.

For the calculation of deflections, the elastic modulus can be calculated by using equation 5.2 (in chapter 5).

For example, the elastic deflection of the tested prisms in the uncracked stage can be determined using the linear elastic theory as shown in equation 6.17.

$$\delta_{el} = \frac{Pl^3}{48EI} \quad [\text{mm}] \quad (6.17)$$

The tensile strength (σ_t^u), at which cracking takes place, can be determined by using equation 6.10. In the case of a cracked section, the compressive zone can initially be assumed to remain elastic. The tensile stress (σ_1), at a plastic strain of 2‰, can be expressed by equation 6.14. Using the proposed stress reduction factors, the stress-strain model can be simplified as shown in Figure 6.19.

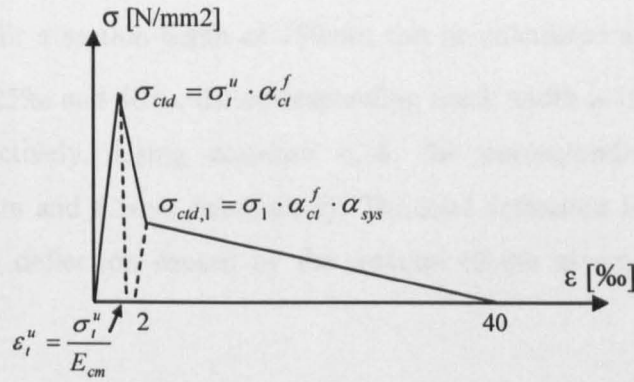


Figure 6.19 Stress-strain model at SLS

After cracking, the deflection is a function of crack width. Assuming that the two parts of the beam behave as rigid body, as shown in Figure 6.20, the deflection can be expressed as shown in equation (6.18).

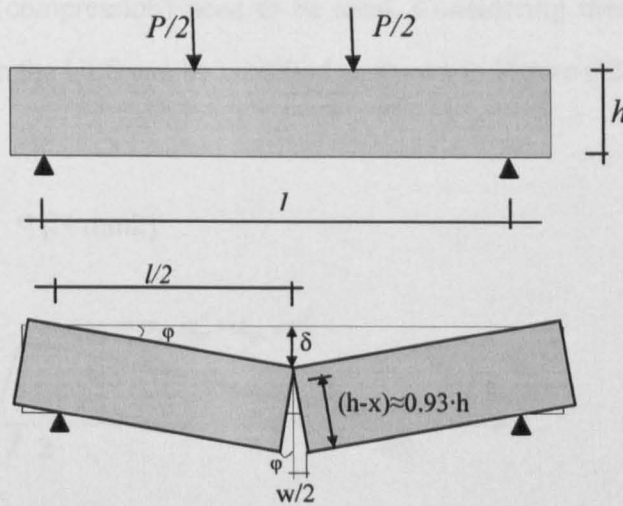


Figure 6.20 Relationship between deflection and crack width

$$\delta_w = \frac{w \cdot l}{4 \cdot (h - x)} \tag{6.18}$$

where:

The crack width can also be determined according to RILEM (2000) as

$$w = \epsilon_i \cdot (h - x) \tag{6.19}$$

Assuming an average crack width of $0.93h$, a relationship between crack width and tensile strain for a section depth of 150mm can be calculated as $w = \varepsilon_t / 7.1$. For a strain at 2‰, 25‰ and 40‰, the corresponding crack width is 0.28mm, 3.5mm and 5.6mm, respectively. Using equation 6.18, the corresponding deflections are 0.22mm, 2.8mm and 4.5mm respectively. The total deflection is the sum of elastic deflection and deflection caused by the rotation of the assumed plastic hinge as follows:

$$\delta = \delta_{el} + \delta_w \quad (6.20)$$

6.5.3 ULTIMATE LIMIT STATE

For design at the ultimate limit state (ULS), the safety factor $\gamma_{ct}^f = 1.3$ (tension) and $\gamma_c^f = 1.5$ (compression) need to be used. Considering these factors, the stress-strain model in the ULS can be modified as shown in Figure 6.21.

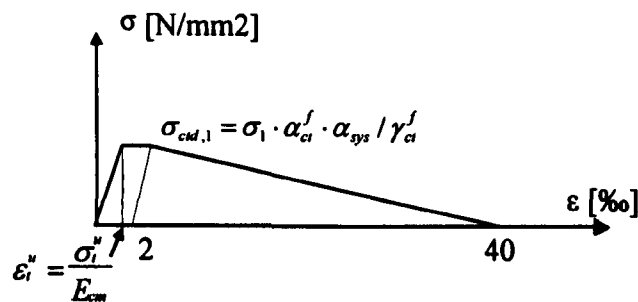
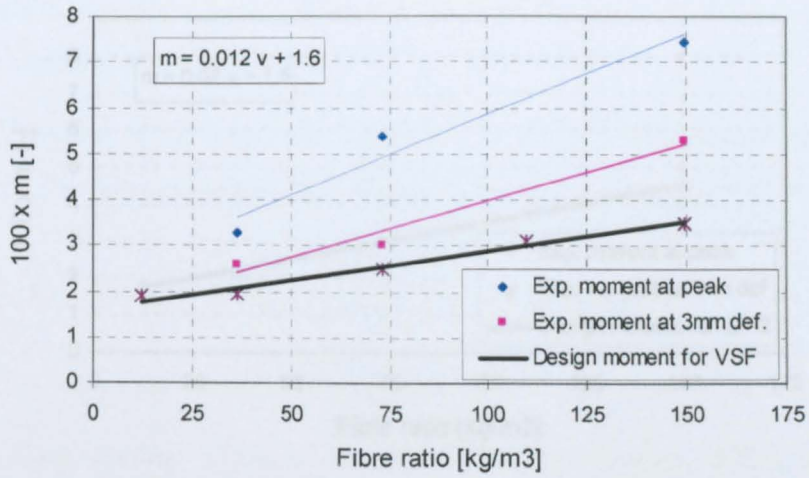
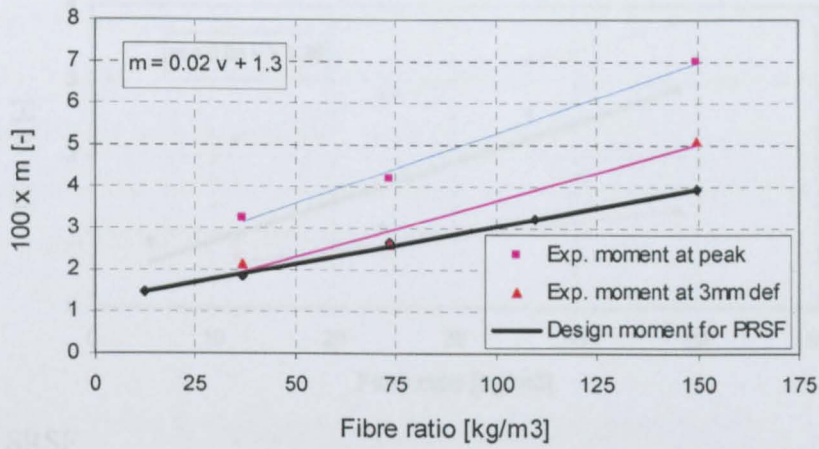


Figure 6.21 Tensile design stress-strain model for ULS

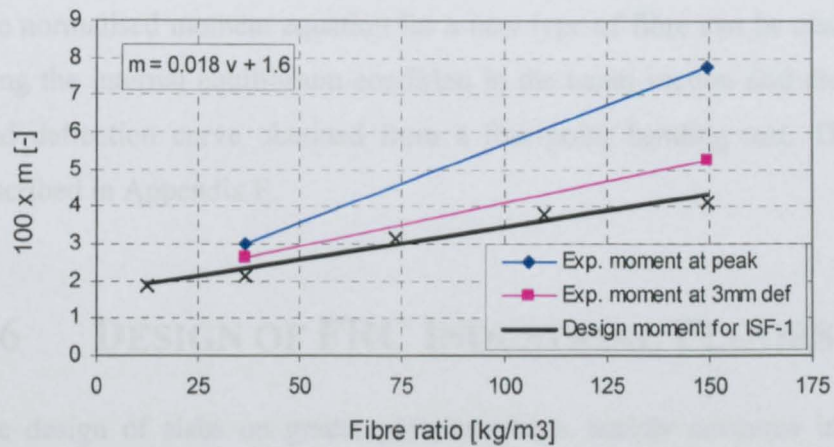
Using this model, the relationship between normalised moment ($100m = M / b \cdot h^2 \cdot f_{cd}$) and fibre ratio were determined (by using ABAQUS) as shown in Figures 6.22 (a, b, c, d and e).



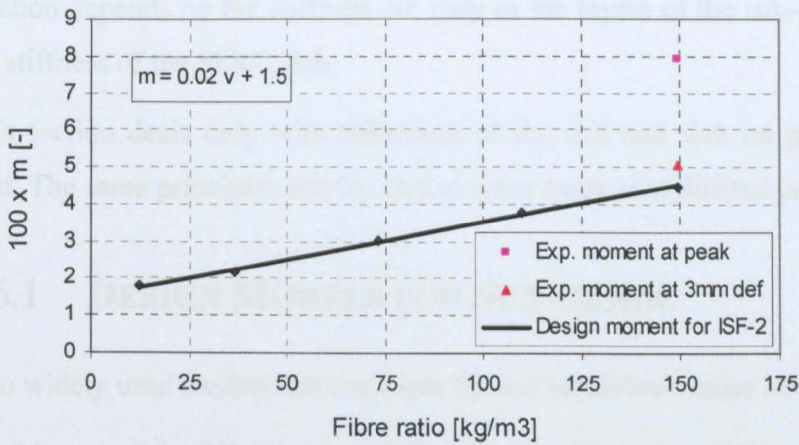
(a) VSF



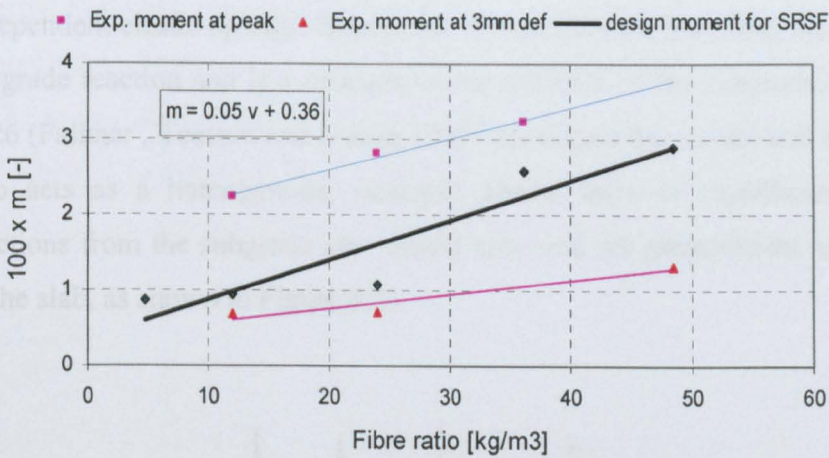
(b) PRSF



(c) ISF-1



(d) ISF-2



(e) SRSF

Figure 6.22a,b,c,d,e Normalised moment vs fibre ratio

The normalised moment equation for a new type of fibre can be also determined by using the internal equilibrium condition in the beam section and the area under the load deflection curve obtained from a four-point bending test. The procedure is described in Appendix F.

6.6 DESIGN OF FRC INDUSTRIAL FLOORS

The design of slabs on grade, presented here, mainly concerns industrial ground slabs, which carry heavy concentrated loads from machinery and machine parts. Structurally speaking, these are slabs on elastic foundations. A vertically applied load causes stresses and deformation both in the slab and the sub-grade. The sub-grade

reaction depends on the stiffness not only of the layers of the sub-grade, but also on the stiffness of the SFRC slab.

This section deals only with behaviour of the soil and slab on grade under single load. The same principles can be used to solve more complicated problems.

6.6.1 DESIGN MODELS FOR SUB-GRADE

Two widely used models can represent the soil behaviour under load.

Winkler model: Winkler in 1867 (Concrete Society, 2003) assumed that the subgrade may be considered to act as if it were rows of closely spaced, but independent elastic springs. Hence, the spring constant describes the modulus of the subgrade reaction and is a measure of the stiffness of the subgrade. Westergaard in 1926 (Falkner , Teutsch and Huang 1995) developed this model and assumed that the slab acts as a homogenous, isotropic elastic solid in equilibrium and that the reactions from the subgrade are vertical only and are proportional to the deflections of the slab, as shown in Figure 6.23.

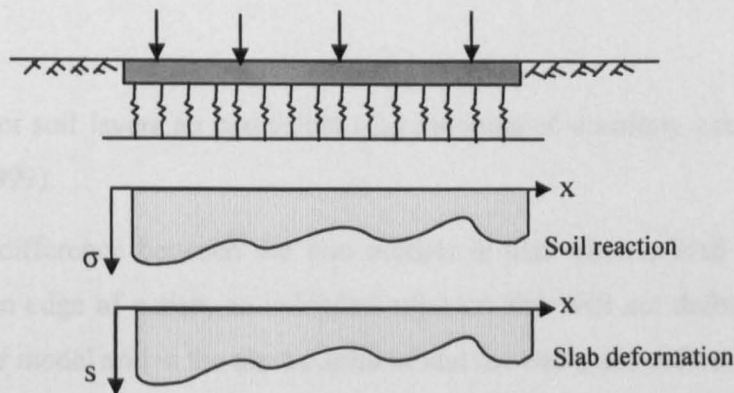


Figure 6.23 Winkler model (after Falkner , Teutsch and Huang 1995)

This soil characteristic was termed by Westergaard as the “modulus of subgrade reaction (k) or “resilience modulus”, which is the load per unit area causing unit deflection as expressed in equation 6.21.

$$k = \frac{P_s}{W} \quad [\text{N/mm}^3] \quad (6.21)$$

where:

$$W = \frac{\pi \cdot d^2}{4} \cdot 1.25 \quad [\text{mm}^3] \quad (6.22)$$

P_s Load applied to the slab [N]

d Diameter of the slab (mm)

Due to soil consolidation under loading, k values do not reflect long-term settlement. However, low values represent the plastic behaviour of near to surface soils as indicated in the design manual of Bekaert (Bekaert, 1999).

Elastic Solid Model: It assumes that the subgrade is an elastic, isotropic and homogeneous body of semi-infinite extent. This means that a vertical force applied to the surface of the foundation produces a continuous and infinite deflection basin. The soil reaction is described by a modulus of soil elasticity (E_s) and a Poisson ratio for ground of (ν_s). The modified modulus of elasticity can be expressed as:

$$C = \frac{E_s}{(1 - \nu_s^2)} \quad (6.23)$$

where:

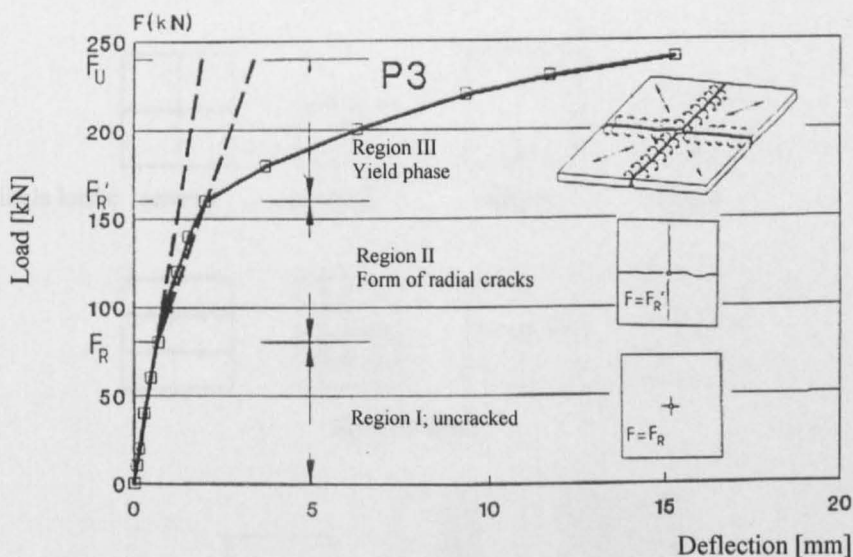
For different soil layers an equivalent (E_g) modulus of elasticity can be determined (Bekaert 1999).

The main difference between the two models is that when a load is applied to a corner or an edge of a slab, an unloaded adjacent slab will not deform according to the Winkler model and in the elastic solid model the two slabs deflect together.

6.6.2 DESIGN OF SUB-BASES

6.6.2.1 Design Approach by Bekaert (1999)

Falkner, Teutsch and Huang (1995) investigated the influence of the modulus of the subgrade, steel fibre type and content on the ultimate bearing load. It was found that the load-displacement behaviour of an FRC slab resting on an elastic subgrade can be separated into three regions (Figure 6.24):



- F_R : The load at first crack appearance
 F'_R : The load when the crack reaches the slab boundary
 F_U : Ultimate load

Figure 6.24 Slab on grade behaviour under single load (after Falkner, Teutsch and Huang, 1995)

Region I: the load-carrying capacity and displacement can be described by the elastic theory.

Region II: radial cracks propagate from the applied load to the boundary of the slab.

Region III: plastic hinge lines (yield lines) are formed along the radial cracks.

Essentially, the value of F_R depends solely on the value of the flexural strength of concrete. On the other hand, the first crack load (F'_R) and the ultimate load (F_U) are a function of the equivalent flexural strength, modulus of the subgrade and slab geometry.

The theory of elasticity gives excellent results for loads at or less than initial yield. For higher loads, however, the theory of elasticity becomes less and less applicable and the plastic analysis method can be used (Falkner, Teutsch and Huang 1995). The ultimate bearing capacity of RC slab, estimated on the basis of a rigid-plastic slab resting on an elastic subgrade, can be evaluated by the yield-line theory.

The yield line propagation depends on the applied load location and slab geometry, as shown in Figure 6.25 (Falkner, Teutsch and Huang 1995).

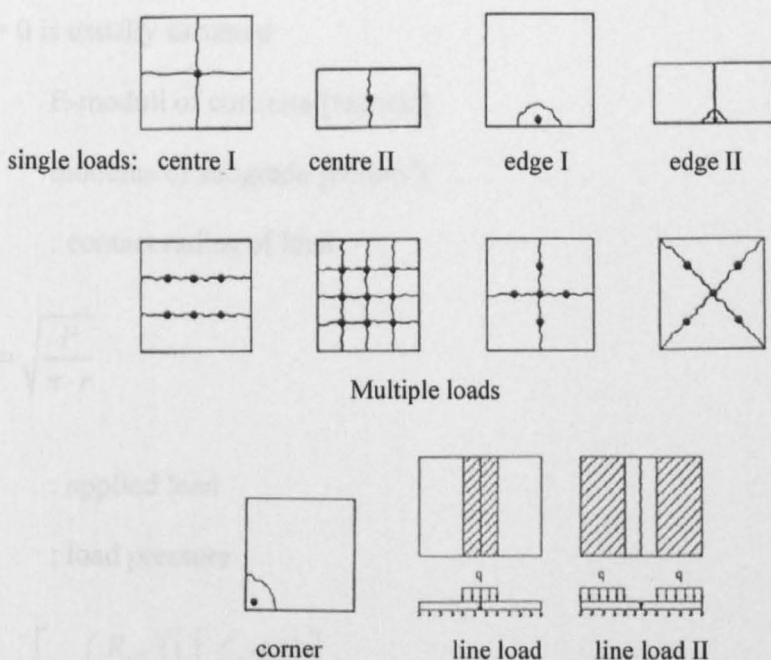


Figure 6.25 Propagation of the Yield lines versus the load locations

There are two factors influencing the bearing capacity of the slab on grade. The first one is the yield line length, which is a function of the slab geometry, load area and modulus of subgrade. The second factor is the plastic moment of the section along the yield line, which is influenced by the tensile strength, equivalent flexural strength and thickness of the FRC slab.

Meyerhof (1962) developed semi-empirical formulas for collapse loads of infinitely large plates under single load in the centre as follows (Bekaert, 1999):

$$P_0 = 6 \left[1 + \left(\frac{2a_r}{l_e} \right) \right] M_0 \quad (6.24)$$

where:

$$l_e = \sqrt[4]{\frac{D}{k}} \quad (6.25)$$

$$D = \frac{EI}{(1-\nu_c^2)} \quad [\text{Nmm}] \quad (6.27)$$

l_e radius of elasticity for elastic subgrade

$\nu_c = 0$ is usually assumed

E E-moduli of concrete [N/mm²]

C modulus of subgrade [N/mm³]

a_r : contact radius of load

$$a_r = \sqrt{\frac{P}{\pi \cdot r}} \quad (6.28)$$

P : applied load

r : load pressure

$$M_0 = \left[1 + \left(\frac{R_{e,3}}{100} \right) \right] \cdot \left[\frac{f_{ct} \cdot bh^2}{6} \right] \quad (6.29)$$

f_{ct} flexural stress of un-reinforced concrete

$$f_{ct} = 0.393 \cdot \sqrt[3]{(f_{cu})^2} \quad (6.30)$$

f_{cu} Characteristic compressive strength of cube (150 x 150 x 150) at 28 days

b 1 m

h thickness of the slab

$R_{e,3}$ ductility factor (Table in Bekaert, 1999) or the equivalent flexural ratio between the equivalent flexural strength and concrete strength at which the first crack occurs (Smorgon ARC, 1998).

6.6.2.2 Modified Design Approach

The theoretical concept of design for a slab on grade developed by Bekeart (1999) is adopted in this study. However, the design moment for a slab on grade M_d can be determined by using the normalised moment (see section 6.5) as follows:

$$M_d = m \cdot h \cdot b \cdot f_{cd} \cdot \alpha_{ys} \quad (6.31)$$

where:

- m Normalised moment Figure 6.22
 h thickness of the slab
 b 1 m
 f_{cd} design compressive strength of the concrete

According to Bekaert the design moment can be expressed as:

$$M_d = M_0 \cdot \alpha_{ct}^f / \gamma_p \quad (6.32)$$

where

- M_0 Yield moment (equation 6.22)
 α_{ct}^f Durability factor ($\alpha_{ct}^f = 0.85$)
 γ_p Load safety factor ($\gamma_p = 1.5$ according to Bekaert)

For comparison purposes, the moment capacity for a slab on grade with a thickness of 300mm, concrete class C 40/50 and ISF-2 was calculated. Figure 2.26 shows a very good agreement between both methods.

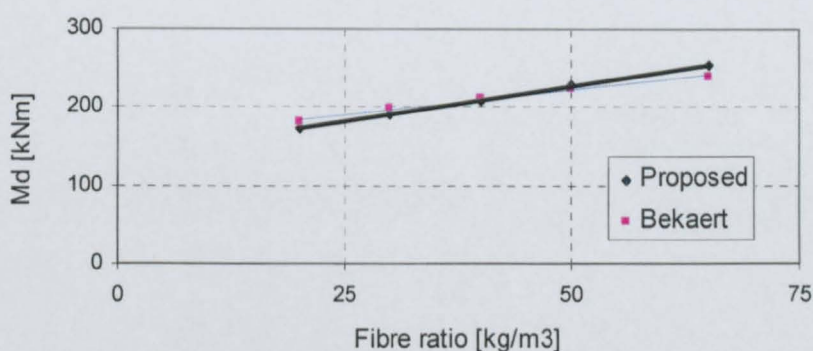


Figure 2.26 Design moment vs fibre ratio

6.7 CONCLUSIONS

The RILEM model describing the behaviour of SFRC is shown to be inaccurate due to some fundamental problems in the procedure of determining key parameters.

This chapter presents a model for determining the stress-strain characteristics of SFRC by using experimental data and FE back analysis. This model describes the behaviour of SFRC in three phases and gives good results for a range of fibres tested.

A general design procedure in the serviceability and ultimate limit state for structural element was proposed and charts and equations describing the relationship between moment and fibre ratios for different fibre types were developed.

For design of slab on grade, a modified design method, based on the proposed moment vs fibre ratios relationship was proposed. The results obtained from this method are in agreement with the design manual by Bekaert (1999).

7 CONCRETE SLABS

7.1 INTRODUCTION

The previous chapters demonstrated that recycled steel fibres can be used effectively to produce laboratory SFRC. Tests on full-scale slabs were undertaken to demonstrate the use of fibre as reinforcement in a practical application. It was decided to use one of the Decathlon system drainage cover slabs manufactured by Hodkin and Jones Ltd (Hodkin and Jones, 2003). Decathlon is a reinforced concrete surface-water drainage system. Its most common applications are in road carriageways, hard shoulders and parking areas for all types of vehicles. The steel mould used for casting the slabs was provided by Hodkin and Jones Ltd (Figure 7.1).



Figure 7.1 Mould and Slab preview

The drainage slab is one metre long and 450 mm wide. The depth of the central strip (hole region) is 163 mm, while the depth at the support region is only 100 mm. As shown in Figure 7.2, the slab has ten inclined slotted holes. The holes are only 6 mm wide to avoid the problem of shoe heels being stuck in the holes. The holes are inclined so that water running perpendicular to the direction of the drainage-system will always find a hole to drain. This creates an interesting engineering design problem, since the slab is left with inclined beams in the critical region of its centre.

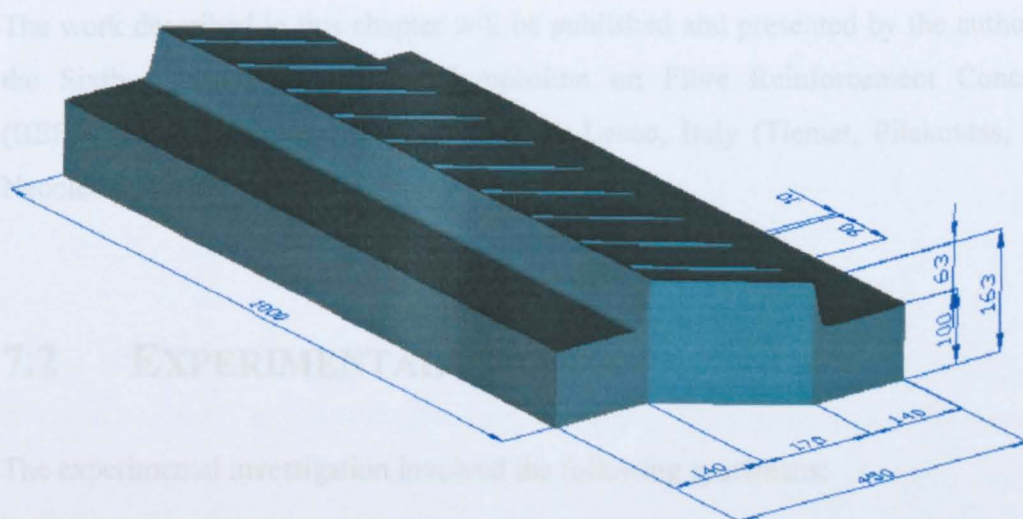


Figure 7.2 Slab dimensions

To make matters worse, a recent change of the design of this slab has introduced recesses on either side of the holes. The recesses are covered by block-paving or black-top so that the drain cover integrates well with the surrounding environment.

The slab is normally reinforced with nine ordinary steel bars, 12 mm in diameter (Figure 7.3), to satisfy the EN 124 (1994) loading condition C250. This reinforcement is replaced in this work by recycled tyre steel fibres.



Figure 7.3 Slab made with steel bar reinforcement

Steel fibre reinforced cover slabs containing shredded, pyrolysed steel fibre or slurry infiltrated slab reinforced are examined. Prisms were also tested in third-point bending to evaluate the flexural characteristics of each concrete mix used in the study.

The work described in this chapter will be published and presented by the author at the Sixth International RILEM Symposium on Fibre Reinforcement Concrete (BEFIB 2004) in September 2004, Varenna-Lecco, Italy (Tlemat, Pilakoutas, and Neocleous, 2004).

7.2 EXPERIMENTAL PROGRAM

The experimental investigation involved the following specimens:

Rcon slabs: concrete slabs reinforced with re-bars

Pcon: concrete slabs reinforced with pyrolysed fibres

Scon: concrete slab reinforced with shredded fibres

SIScon: slurry infiltrated concrete slab reinforced with shredded fibres

To determine the flexural characteristics of each concrete mix, three control prisms (100x100x500 mm) and four cubes (100x100x100 mm) were cast from each slab series. The test programme is shown in Table 7.1.

Table 7.1 Slab test programme

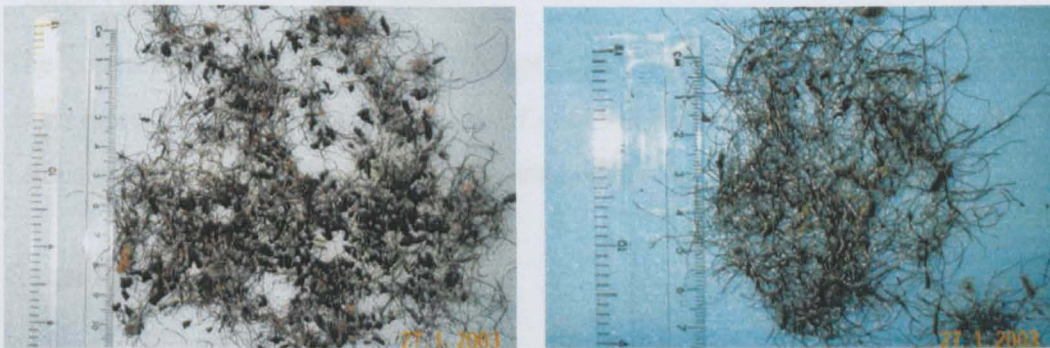
Mix code	Test type	Concrete type	Reinforcement type	Fibre content (% by weight)
Rcon	Two Slabs	OPC 40	conventional	-
Pcon	Two slabs, prisms and cubes	SP 40/30	PRSF	6%
Scon	Slab, prisms and cubes	SP 40/30	Sieved SRSF	2%
SIScon	Slab, prisms and cubes	Slurry	SRSF	17.5%

7.2.1 MATERIALS USED

The cement, aggregate and superplasticizer used are similar to those presented in chapter 5.

The steel fibres from the pyrolysed process were delivered containing wires from different tyres. It was necessary to clean and to sort the wire before cutting it to 50 mm lengths. For this purpose, a machine was developed in the laboratory to cut the fibre to the required length. The diameters of the PRSF fibres used are in the range of 0.8-1.5 mm.

The shredded steel fibres, used in the Scon slab, were obtained from the third shredding process, as reported previously in chapter 3 and contained a high amount of rubber (Figure 7.4a). To obtain a cleaner and more consistent in size and diameter steel fibre, it was decided to use only the fibre that passed through the 8.0 mm sieve and that which remained in the 6.3 mm sieve (Figure 7.4b). The average diameter of the shredded fibre remaining is around 0.23 mm. The proportions after the sieving of the steel fibres (according to ASTM A-820) are shown in Table 7.2.



a) Un-sieved fibres with rubbers

b) Sieved fibres

Figure 7.4 Shredded fibres from third shredding process

Table 7.2 Shredded steel fibres grading (after sieving)

Sieve size	Mass retained grams	% retained	Cumulative % passing	Cumulative % retained
19.05 mm	0	0.0	100	0.0
9.60 mm	12	1.2	98.8	1.2
8.0 mm	66	6.6	92.2	7.8
6.3 mm	70	7.0	85.2	14.8
4.70 mm	242	24.2	61.0	40.0
< 4.70 mm	610	61.0	-	-
Total	1000			

7.2.2 PRODUCTION OF SLABS

7.2.2.1 Mix Design and Casting

In selecting the mix proportions, some modifications were made from the mixes reported in chapter 3, so as to improve the cohesion and workability of the mixes. The mix proportions used in this series of tests are shown in Table 7.3.

Table 7.3 Mix proportions in kg/m³

Mix Code	Cement		fibre	Water	W/B	Aggregate			Mass	WR** (%)
	OPC	SP*				20mm	10mm	Sand		
Rcon	346	0	0	180	0.52	0	1185	675	2386	0
Pcon	236	101	149	155	0.46	690	345	807	2483	0.75
Scon	236	101	48.4	155	0.46	0	1035	844	2420	0.75
SIScon	1084	464	363	390	0.25	0	0	0	2301	0.81

* Supper Porzz

** Water Reducer

The concrete mixing for all slabs (except Rcon) was done in a 170 kg non-tilting drum mixer. The Rcon Slabs were mixed in the Sheffield factory of Hodkin & Jones Ltd using the actual ready mix concrete used in production.

Rcon Slabs

To measure the strain of the reinforcement bars, six strain-gauges (Table 7.4) were fitted in the bottom of the bars (where the maximum strain was expected), as shown in Figure 7.5.

Table 7.4 Data for the strain-gauges used

Type	KFG-10-120-C1-11	Gauge factor	2.11 ± 1.0
Temperature compensation	Steel	Adoptable Expansion	11.7
Gauge length	10 mm	Transverse sensitive	0.20
Gauge resistance	120.2 ± 0.2	Tolerance	± 0.85 [(μm/m/°c)]

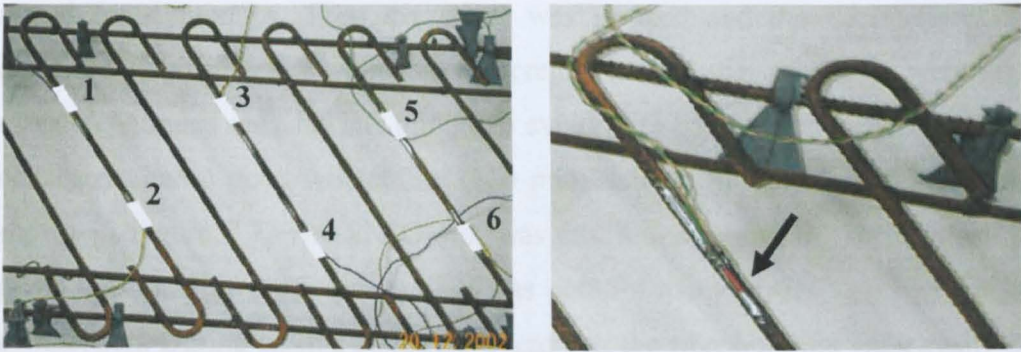


Figure 7.5 the location of the strain-gauges on the reinforcement bars

The steel rebar was ground and cleaned thoroughly before the strain-gauges were glued. To identify the location of the individual strain-gauges, colour coded wires were used. The ready mixed concrete was cast in the steel slab mould (prepared by spraying it with demoulding oil) as shown in Figure 7.6. The Rcon slab was reinforced in the bottom. The mix is designed for a characteristic strength of 45 kN/mm^2 . The slab was tested more than 28 days after the day of casting.



Figure 7.6 Casting of the Rcon slab

Pcon slabs

The mixing was performed in the heavy structures laboratory of the department, using the 170 kg mixer. The coarse and fine aggregates were fed first, followed by approximately one third of the water, to ensure that the aggregates had a chance to wet. After permitting the mixer to turn a few revolutions, the mixer was stopped and the top of the mixer was covered for approximately 8 minutes to prevent evaporation during the rest period. Cement and superpozzolan (ash) were added and the mixer was started again. The remainder of the water was mixed with the superplasticizer and added to the mix during the batching. All the ingredients were mixed for 4

mixed for 4 minutes. Then the mixer was stopped and the PRSF fibres were dispersed uniformly throughout the concrete. Finally, after the fibres were added, mixing continued only for one minute to avoid fibre balling. The resulting mix was consistent, had a good workability (110 mm) and no fibres were sticking out, as shown in Figure 7.7. The SFRC mix was cast and vibrated in the prepared slab, prism and cube moulds. The casting was done in many layers to achieve a good compaction. During casting it was observed that the fibres did not enter easily in to the central slots. This is expected to cause problems during testing.

SFScon Slabs



Figure 7.7 FRC slab with 6% PRSF fibres

Scon Slab

The above mix proportion and procedure were adopted for the Scon slab as well. Because of the length of the shredded fibre (< 20 mm) the coarse aggregate size used had to be less than 10 mm (JSCE-SF1, 1994). To avoid fibre balls being generated and to disperse the steel fibres into the concrete uniformly, the shredded fibres were added incrementally to the mixer by using a sieve. During the addition of the fibres, the concrete was mixed manually. Finally, the mixer was rotated for 30 seconds to ensure a uniform fibre distribution (Figure 7.8). It is noted that some fibre balling was initiated even before the final mixing.



Figure 7.8 casting of SFRC with 2% shredded fibres

SIScon Slabs

Slurry-infiltrated-shredded fibre reinforced concrete (SIScon) is a new type of high-performance FRC, made by infiltrating high fibre-volume fractions of discontinuous short steel fibre (from the third shredding process, Figure 7.4a) with a specially designed cement-based slurry. After preparing the moulds, the fibres were manually placed in the mould, up to its top (Figure 7.9).



Figure 7.9 Shredded fibres placed in the moulds

The cement and superpozzolan were first added to the mixer. Water was first mixed with the superplasticizer and, then, it was slowly added to the mixer for approximately 2 minutes. The slabs, cubes, and prisms were cast by pouring the slurry from the mould top (as demonstrated in Figure 7.10 for the slab). The specimens were vibrated during casting to ensure a good penetration of the slurry.



Figure 7.10 Pouring of the slurry in the moulds

7.2.2.2 Curing Regimes

Just after casting, the specimens were covered with a wet burlap textile and a plastic sheet, and were left in the mould for one day. After demoulding, all slabs and control specimens were moist cured and left in the laboratory environment ($20\pm 3^\circ\text{C}$, 60% RN) until the day of testing.

7.2.3 TESTING PROCEDURE

The slabs were simply supported on two opposite steel beam supports. To avoid stress concentrations within the support line, 5 mm thick dental plaster was placed on a plywood base (Figure 7.11).



Figure 7.11 Slab supports

All slabs were tested according to BS-EN-124 (1994) under single point loading, which was acting on a 250 mm steel plate through a 500 kN Screw Jack displacement controlled machine. Slab deflections were measured using LVDTs (Figure 7.5). One LVDT was fixed underneath the centre of the slab to measure the

total mid-span displacement, two on the support edges and two on the corners of the slab to measure the support uplift. To measure the crack width, two LVDTs were fixed on the side of the concrete slab (Figure 7.12). To record the initial hysteresis loops and stabilise the slab, each slab was subjected to five load cycles up to 2/3 of the design load at a rate of up to 5 kN/s. After that, the load was increased to failure.

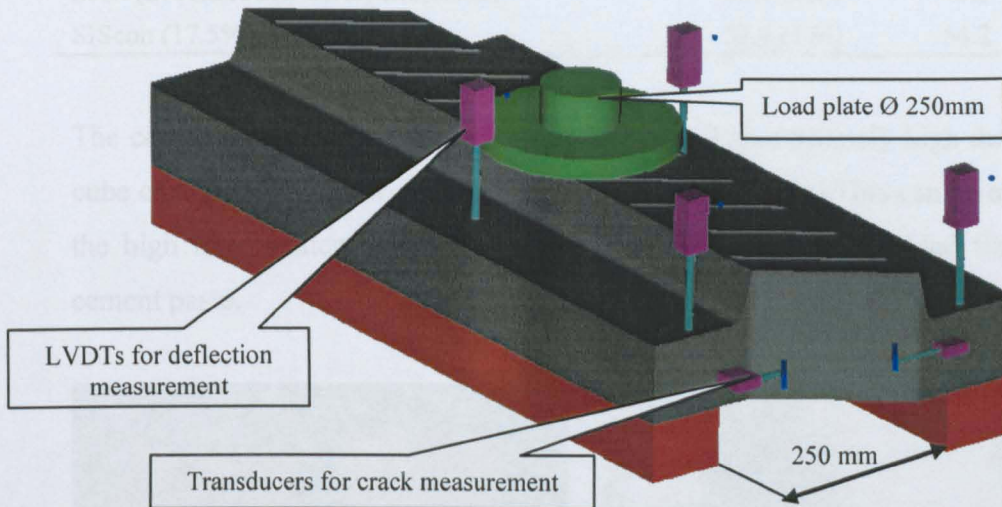


Figure 7.12 Test set-up

Table 7.5 Data for the LVDTs used for crack measurement

Model	8FLP10A	Electrical Stroke	11 ± 0.5 mm
Total Resistance Tolerance	± 15%	Power Rating	0.2 W
Contact Resistance Variation	Below 0.2%	Resolution	Essentially Infinite

7.3 RESULTS AND DISCUSSION

7.3.1 CUBE TEST RESULTS

Cubes were tested on the day of slab testing and 28 days after casting. As expected, adding fibre to concrete reduces the workability (Table 7.6). Fibres with low aspect ratio (e.g. shredded fibres) reduce the workability even further. The compressive strength decreased when the fibre by weight increased to 6% (pyrolysed fibres).

Table 7.6 Cube and slump test results

Mixes	Cube strength [N/mm^2]		Slump [mm]
	(day of test)	(28 d)	
OPC40 (Rcon slab)	47.0(40d)	45.0	80
SP 40/30 (Control specimen, Pcon slab)	-	59.0	200
Pcon (6% pyrolysed fibres, Pcon slab)	46.8 (19d)	54.4	110
SP 40/30 (Control specimen, Scon slab)	-	43.6	180
Scon (2% shredded fibres, Scon slab)	35.9 (19d)	45.3	60
SIScon (17.5% shredded fibres)	52.8 (17d)	54.2	-

The compressive test of the SIScon cube indicated an extremely high ductility. The cube changed in shape without total collapse (Figure 7.13a). This can be attributed to the high fibre content and a very good bond between the shredded fibre and the cement paste.



Figure 7.13 a) Compressive test

b) Crack in the bottom of the SIScon slab

The behaviour of the tested slabs is described in the following sections. The description begins with the SIScon slab which was tested last, since more instrumentation was used to examine a peculiarity in initial slab behaviour.

7.3.2 FLEXURAL BEHAVIOUR OF SISCON SLAB

To classify the SIScon slab according to BS 124 (1994), it was decided to test the slab first for B125 class, and when the applied load passed the mark of 150 kN, the slab was tested for the class of C250.

The stiffness of the slab across its cross-section is not constant. Hence, the deformation behaviour of the slab in the central cross-section can not be similar to a slab with a constant stiffness. To study the influence of the slab stiffness and the support deformation on the slab deformation, two more LVTDs (7&8) were fixed on the support edge as shown in Figure 7.14.

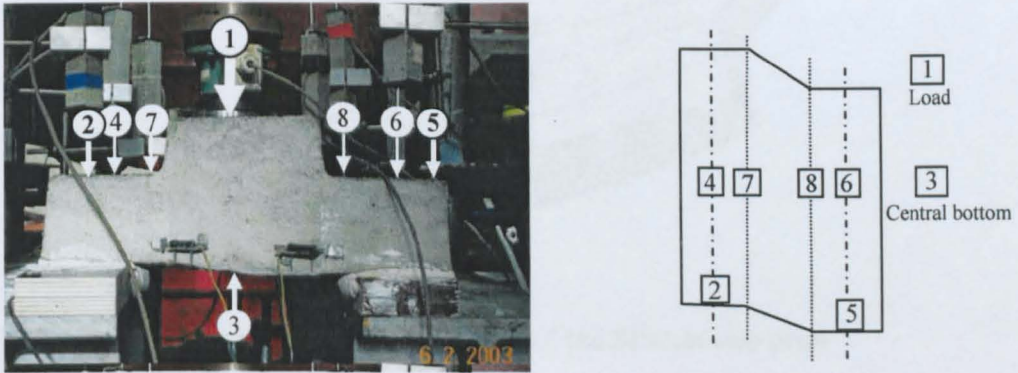


Figure 7.14 LVDTs position

Figure 7.15 shows the average deflection of LVDTs 4 and 6, 7 and 8, 2 and 5 and the absolute deflection of No.3 (it should be noted that LVDT No.3 was reading in the opposite direction of the other LVDTs). Due to reduced sectional stiffness of the slab at the supports, the initial deflection for 4 and 6 is greater than for No 3.

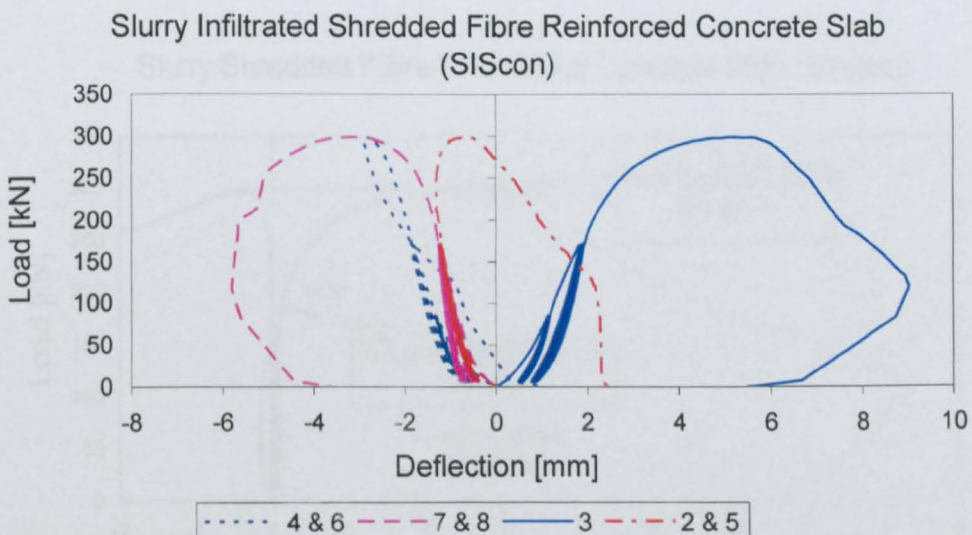


Figure 7.15 Average load-deflection registered by the used LVDTs

To understand the initial behaviour of the slab, the slab deformation is illustrated in Figure 7.16. The slab deformation in the span-direction is smaller than the deformation of the support. The support is deforming, as if it was supported on an

elastic foundation. However, the central stiffer part of the slab is not as deformable, hence the centre of the slab, initially deforms less than its central support.

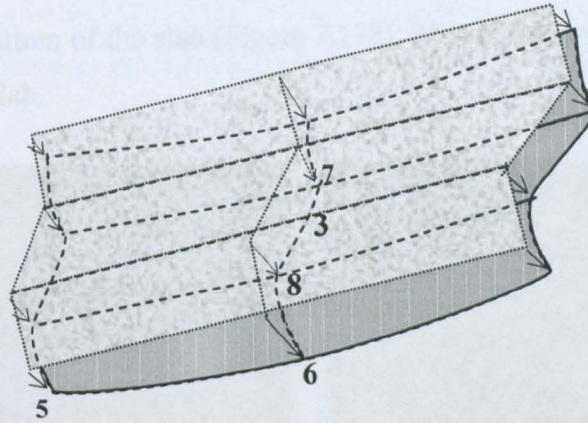


Figure 7.16 Displacement and deformation of the SIScon slab print

Figure 7.17 shows the relative load-deflection behaviour (after subtracting the average deflection of the support) of the SIScon as well as the crack-opening. As mentioned above, the shape of the initial curve is influenced by the high initial deflection of the support. The transition from the uncracked behaviour is very gentle and the curve then continues in a smooth way. This indicates a favourable crack development and good anchoring of the fibres.

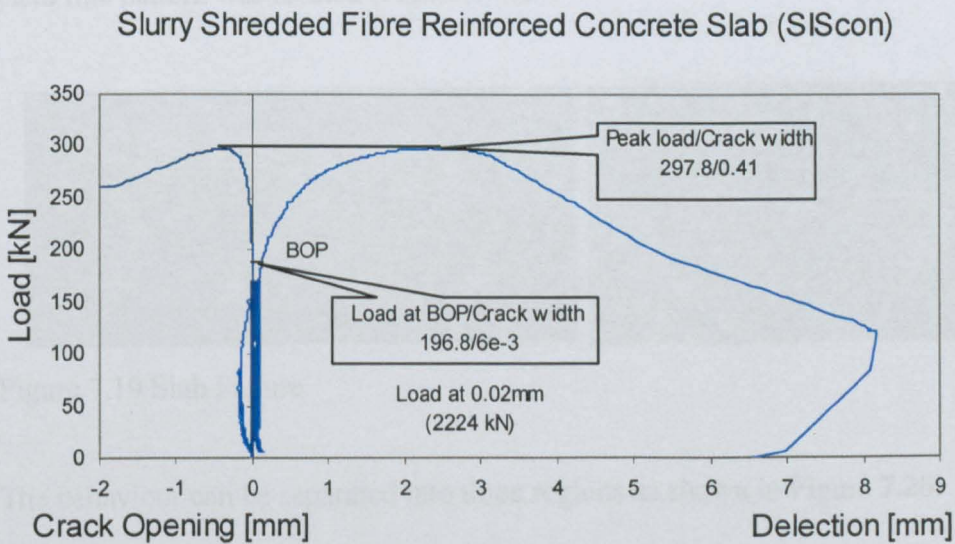


Figure 7.17 Applied load versus slab deflection and crack opening

At collapse, the slab cracked in two parts along the edge of the ribs as shown in Figure 7.18 and Appendix E. The first crack formed in the middle on the bottom of

the slab at a load of around 197 kN, which is the highest of all slabs investigated. As more load was applied, the crack propagated along the slab until a yield line was formed parallel to the support. The slab collapsed at a peak load of 298 kN. Because of the vibration of the slab mould, a concrete cover without fibre of about 2 cm was formed at the bottom of the slab (Figure 7.13b). This may have reduced the flexural capacity of the slab.



Figure 7.18 Crack propagation in a SIScon slab

7.3.3 FLEXURAL BEHAVIOUR OF RCON SLABS

The first significant crack formed in the concrete at the bottom of the slab, at the edge of the holes in the central area, as shown in Figure 7.19a. These cracks increased in length and propagated to the support as more load was applied until a yield line pattern was formed (Figure 7.19a).



Figure 7.19 Slab Failure

The behaviour can be separated into three regions as shown in Figure 7.20:

Elastic behaviour in region I: the load-carrying capacity and deflection can be described by elastic theory.

Elastic plastic behaviour in region II: cracks propagate from the applied load to the boundary of the slab.

Plastic yield lines in region III: radial cracks increase in length until a yield pattern is formed. Final failure in this case was due to punching shear.

Conventional Reinforced Concrete Slab (RC2)

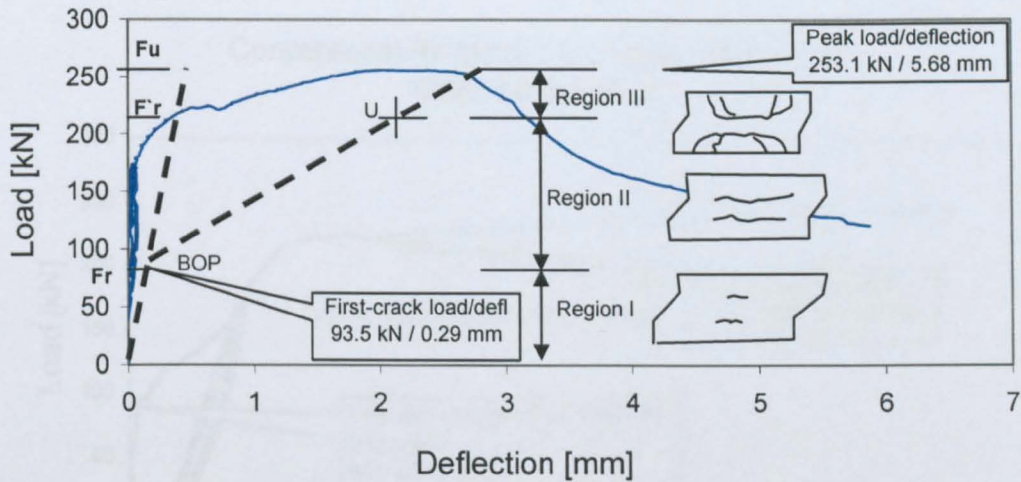


Figure 7.20 Absolute load-displacement relationship for RC2 slab

The peak load was measured at a value of 253.1 kN (Fig. 7.20). The relative load-deflection curve (excluding support deflection) is presented in Figure 7.21.

Conventional Reinforced Concrete Slab (RC2)

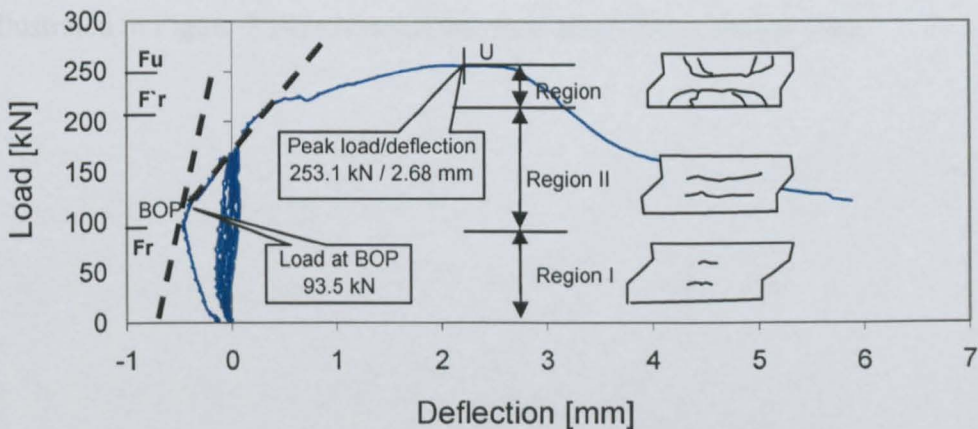


Figure 7.21 Relative load-deflection curve

The influence of the flexible support is reflected through the initial shape of the curve. The load-strain behaviour measured by strain-gauge No.3 (in Figure 7.14) shows that the steel re-bars were close to yielding at service load (Figure 7.22). Hence, though the slab passed the test for class C250, it did so very marginally. However, it is noted that as a result of the recess in the slabs, the loading was not as well distributed as would be expected in practice.

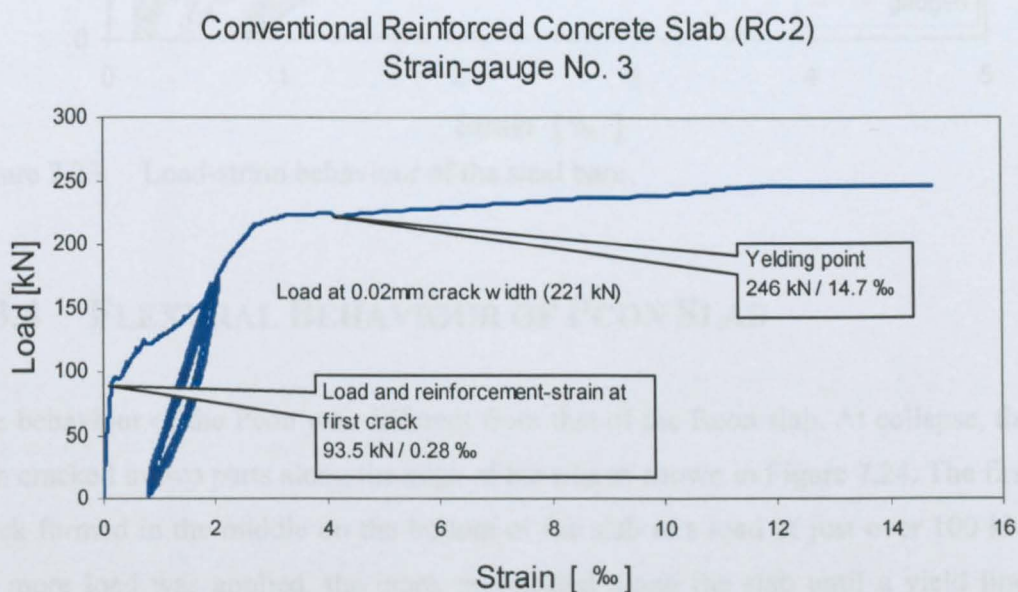


Fig 7.22 Load-strain relationship for the Rcon slab for gauge No. 3

Figure 7.23 shows that most of the strain-gauges fixed on the steel bars (numbers, as illustrated in Figure 7.14) exceeded the yield strain at the design load.

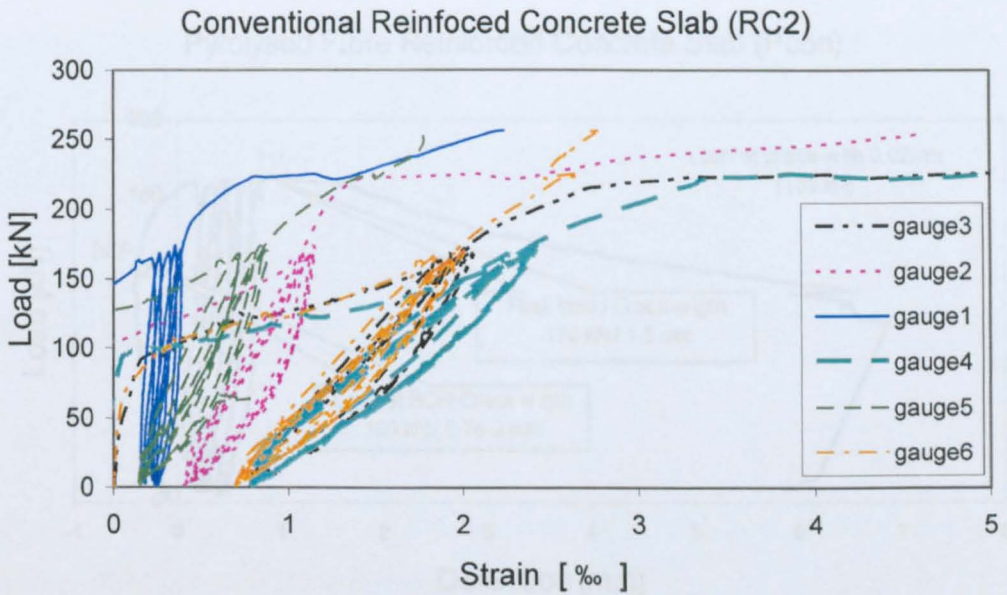


Figure 7.23 Load-strain behaviour of the steel bars

7.3.4 FLEXURAL BEHAVIOUR OF PCON SLAB

The behaviour of the Pcon was different from that of the Rcon slab. At collapse, the slab cracked in two parts along the edge of the ribs as shown in Figure 7.24. The first crack formed in the middle on the bottom of the slab at a load of just over 100 kN. As more load was applied, the crack propagated along the slab until a yield line, parallel to the support developed.



Figure 7.24 Failure of the Pcon slab

The location of the crack confirms that many of the fibres did not penetrate in the narrow gaps of the diagonal beams. However, as can be deduced from Figure 7.25,

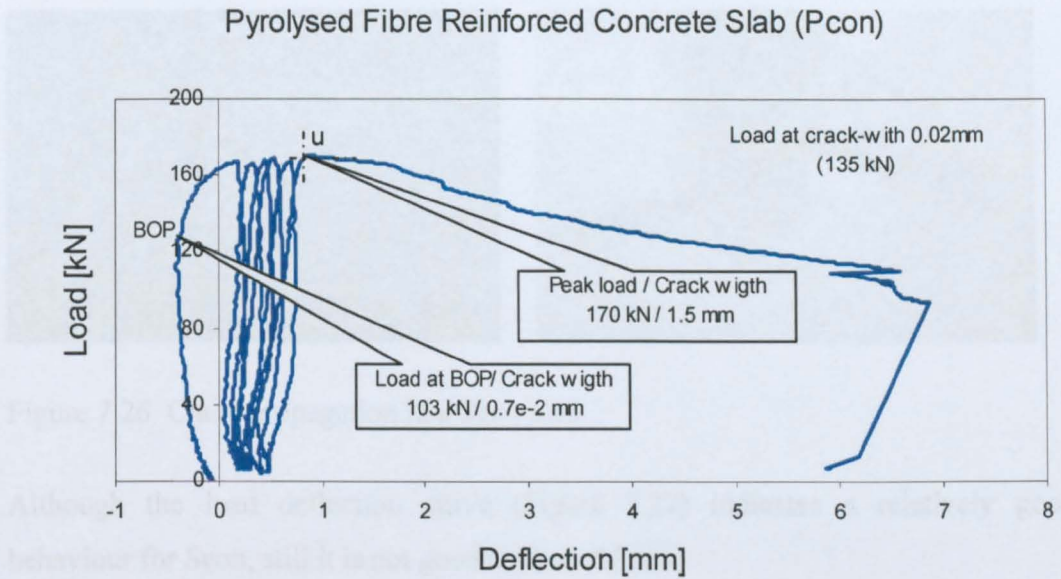


Figure 7.25 Load-deflection behaviour of the Pcon slab

The slab was subjected to five load cycles at around 167 kN. Though, this slab did not make the C250 class, it passed the B125 test.

7.3.5 FLEXURAL BEHAVIOUR OF SCON SLAB

The Scon slab was tested successfully for class B125 loading condition of BS 124 (1994). The slab failed at an ultimate load of 141 kN. Although, the crack propagation in the bottom of the slab is similar to the Rcon slab (Figure 7.26), the shape of the load-deflection curve is very similar to that of Pcon.

As in the case of Pcon slab, the crack location indicates that the fibre did not penetrate completely in the slot region. However, since the fibres, are smaller the penetration is much better. Hence, the relatively low capacity is more a function of the small amount of fibre penetration into the slot region.



Figure 7.26 Crack propagation in a Scon slab

Although the load deflection curve (Figure 7.27) indicates a relatively good behaviour for Scon, still it is not good as that of Pcon.

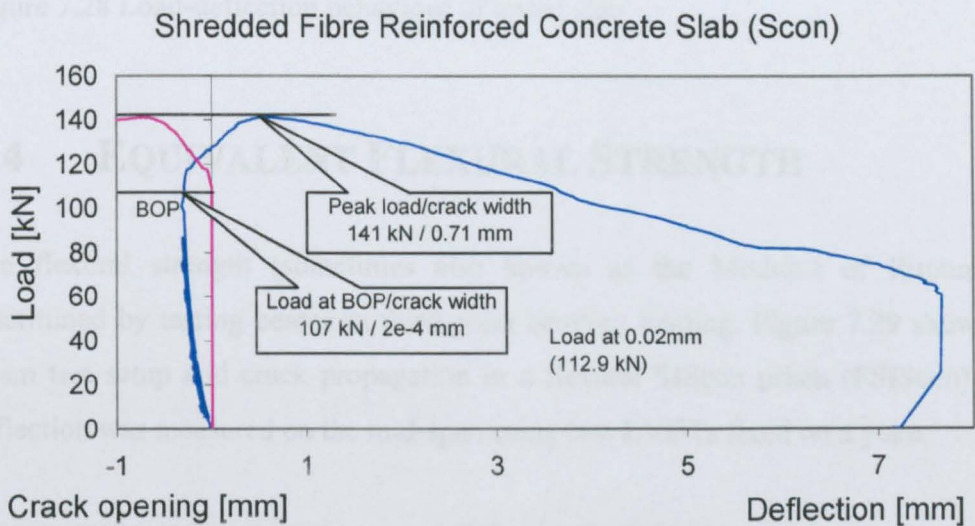


Figure 7.27 Applied load versus slab relative deflection and crack opening

Figure 7.28 and Table 7.6 indicate that the Rcon slab had the lowest bend-over-point BOP since it had no fibres. The SIScon slab exhibited the best behaviour. All SFRC slabs resisted higher loads after cracking, which is a sign of controlled crack development and good anchoring of the fibres. Ultimately, the SFRC slabs failed when the fibres were pulled out from the concrete.

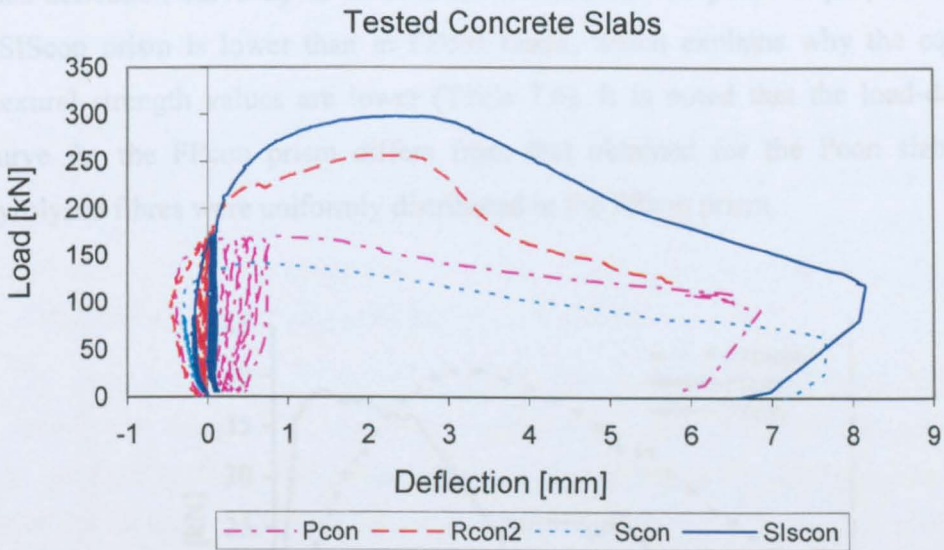


Figure 7.28 Load-deflection behaviour of tested slab

7.4 EQUIVALENT FLEXURAL STRENGTH

The flexural strength (sometimes also known as the Modulus of Rupture) is determined by testing beams in third-point bending loading. Figure 7.29 shows the prism test setup and crack propagation in a flexural SIScon prism (FSIScon). The deflection was measured on the mid-span using two LVDTs fixed on a yoke.

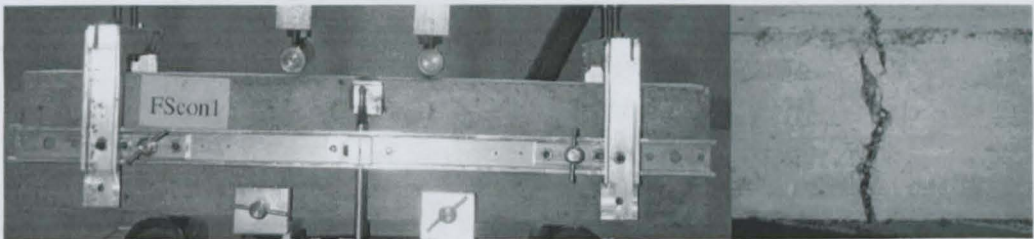


Figure 7.29 Bending test and crack propagation for SIScon prism

Figure 7.30 indicates that the initial load mid-span deflection of the FPcon prism is stiffer than that of FScon and FSIScon, while the FSIScon prism is more ductile. The RILEM (2000) equivalent flexural strength values ($f_{e,2}$, $f_{e,3}$) reflect the strength that an elasto-plastic, prism of the same energy-absorption capacity as that defined by the

load-deflection curve up to an assumed deflection. The point of proportionality in FSIScon prism is lower than in FPcon beam, which explains why the equivalent flexural strength values are lower (Table 7.6). It is noted that the load-deflection curve for the FPcon prism differs from that obtained for the Pcon slab, as the pyrolysed fibres were uniformly distributed in the FPcon prism.

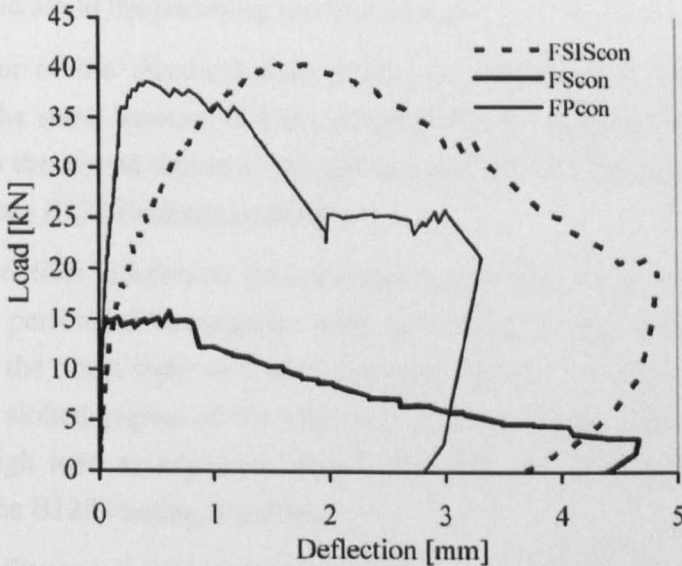


Figure 7.30 Applied load versus mid-span deflection curve for tested beams

Table 7.6 Equivalent flexural strengths

Code	Fibre content [%]	Slab test		Prism tests	
		BOP load [kN]	Peak load [kN]	fe,2 [kN/mm ²]	fe,3 [kN/mm ²]
Rcon	-	93.5	253	-	-
Pcon	6	103	170	13.5	11.4
Scon	2	107	141	5.0	3.6
SIScon	17.5	196.8	299	8.99	10.8

7.5 CONCLUSIONS

This chapter deals with the work on testing of line supported drainage lids with incline slots in the centre, using conventional reinforcement and steel fibres from recycled tyres.

Six slabs were tested having different mix designs, type and amount of reinforcement.

The experiments demonstrated that steel fibres from recycled tyres can be successfully used to reinforce structural elements.

The reinforced concrete slab (Rcon) passed the test for class C250 (BS EN 124, 1994), but it did so very marginally. The slab's eventual failure was due to punching shear. The Rcon slab had the lowest bend-over-point (BOP) of all slabs. Even small amounts of fibre reinforcement could improve the performance of this slab and avoid the punching mode of failure.

The behaviour of the shredded fibre reinforced concrete slab was very good considering the small amount of fibre included (2% by weight). The penetration of the fibre in the slotted region of the slab was not perfect. The Scon slab passed the test for class B125 loading condition.

The pyrolysed fibre reinforced concrete slab had a high ratio of fibre (6% by weight) and performed reasonably well, with high energy absorption. This indicates that the fibres were very well anchored. However, the penetration of the fibres in the slotted region of the slab was poor and, hence, the slab did not achieve as high load as expected. Hence, the slab can be considered to have passed only the B125 loading condition.

The slurry infiltrated shredded FRC Slab had a very high amount of shredded fibre (17.5% by weight). The fibre was placed in the mould without any processing and had a high amount of rubber. The cement slurry pretreated the bundled fibres well and hence, a good result was obtained. The slab exhibited extremely high strength and ductility, even higher than Rcon and passed the test for C250 comfortably.

It is concluded that the fibres extracted from waste tyres can be used to produce successfully pre-cast-concrete structural elements.

8. CONCLUSIONS AND RECOMMENDATIONS

A summary of the general conclusions of this thesis and recommendations for further work are presented in this chapter. The conclusions are presented in two parts. The first part deals with the four test programmes undertaken as part of the experimental investigations and the second part deals with the analytical and design studies.

8.1 CONCLUSIONS

8.1.1 PART 1: EXPERIMENTAL INVESTIGATIONS

8.1.1.1 Fibre characterisation, Concrete Mix Development and Optimisation

Two different types of recycled steel fibres (shredded and pyrolysed), fibres chopped from virgin tyres cord and two types of industrial fibres were investigated. The shredded fibres were obtained from the third stage of the shredding process and hence, contained rubber particles and carbon black. The density of the recycled fibres was determined. Different concrete mixes were developed for each fibre type and volume ratio by using different mix methods.

The conclusions of this part of the study are:

- To maximise the benefit of using fibre in concrete the shredded and pyrolysed fibres have to be cleaned from rubber or carbon black. No more than 10% rubber by volume is recommended.
- Shredded fibres in general affect the workability more adversely than PRSF fibres.

- Using “sieved” shredded fibres improves the concrete workability up to 50%.
- Using 30% superpozzolan (by cement weight) and superplasticizer (0.2%, 0.4% and 0.75% (by cement weight) for fibre ratios 1.5%, 3% and 6%, respectively) leads to high workability and better concrete compaction.
- Fibres should be added at the end of the mix and the mix duration should be about one minute.
- The maximum fibre content, which does not result in fibre balling, was 2% and 6% for shredded and pyrolysed fibres, respectively.
- A high strength concrete (120 MPa) was achieved by adding 5% of PRSF and 1.5% superplasticizer. The resulting slump was 60 mm.

8.1.1.2 Pull-out Tests

The aim of these tests was to study the bond behaviour of different fibre types and to determine the fibre critical length. Pull-out tests were developed to pull single and multi fibres embedded in an uncracked concrete using single and double-sided pull-out tests.

The main conclusions are as follows:

- The single-sided tests allowed the fibre pull-out response to be recorded only up to peak load, due to the difficulty of controlling the displacement speed of the test machine.
- The peak loads for the PRSF fibres with all embedded lengths occur at a fibre slip less than 2 mm, whilst in the case of ISF fibres this takes place after 2 mm. The tensile strength of PRSF fibre is about 1500 MPa (based on nominal diameter).
- The debonding phase on the pull-out response for SRSF fibre is relatively short compared with the linear phase and the tensile strength is about 1150 MPa, due to damage on the fibres. Undamaged fibres have strength about 2400 MPa.

- The displacements from single-sided pull-out tests were affected by fibre slip from the grip of the test machine.
- It was found that the peak load increases with the embedment length. Higher matrix strength increases the fibre bond and the pull-out response is better when the fibre is pulled from a matrix containing fibres, especially shredded fibres. Such increase can be related to the effect of shredded fibres in bridging the micro cracking around the pulled fibre at the early stage.
- The pull-out response can be characterised by two modes: fibre pull-out, (such as in the case of PRSF, ISF-1 and shredded fibre with an embedded length less than 10 mm) or fibre fracture, (such as for PRSF fibre with a blob at the end and shredded fibre with an embedded length greater than 10mm).
- The results obtained from double-sided pull-out tests were more stable than single sided pull-out tests. The double-sided test method eliminated the inaccuracies associated with the single-sided tests.
- The pull-out behaviour of the PRSF shows a stiffer initial response and a larger plateau at peak load than ISF-1. This is because the PRSF has bond distributed along all its length whilst the ISF-1 anchored only at the end (smooth surface).
- An analytical model for PRSF and ISF-1 pull-out is proposed.
- The critical fibre length for PRSF fibres and shredded fibre is found to be 60mm and 20mm, respectively.

8.1.1.3 Flexural Toughness Tests Using Unnotched Beams

The aim of these tests was to study the effect of fibre content, fibre type, matrix strength, testing methods for the flexural toughness of SFRC and establish how the recycled steel fibres behave in bending compared with industrial fibres. Fibre ratios ranged between 1.0% (by weight) and 6% were tested with four different matrix strengths. The flexural toughness was performed and calculated using 100mmx100mmx500mm prisms under four point-loading tests according to ASTM C1018 and JSCE-SF4 recommendations.

The main conclusions can be summarised as follows:

- It was found that an increase in the fibre ratio, not only increases the peak load capacity, but also the residual capacity in the post-peak region. For example the flexural toughness factor calculated for OPC50 mix reinforced with PRSF (1.0%, 2% and 6% fibre ratio) and SRSF (0.5%, 1.0% and 2% fibre ratio) are 1.69, 4.43 and 9.45 for PRSF and 2.55, 2.43 and 3.14 for SRSF.
- The use of the yoke, recommended by JSCE-SF4, led to much better results at the early stages of the recorded load-deflection curve.
- It was found that the method proposed for the determination of the flexural toughness recommended by the Japanese standards (JSCE-SF4) avoids the possible errors made in the ASTM C1018 which calculates the toughness index I_5 in the unstable region of the post-peak.
- For the ASTM procedure, it was recommended to calculate the flexural toughness by subtracting the area in the “unstable” region.
- The positive effect of the PRSF fibre length on the flexural toughness factor is demonstrated when the fibre length increases from 15mm (2.83 for 5% fibre ratio) to 25mm (4.83 for 5% fibre ratio) and then 50mm (9.45 for 6% fibre ratio).
- The flexural toughness factor increases up to 20% when sieved SRSF fibres are used.
- The strength high concrete (120 MPa) achieved a much higher flexural capacity and toughness (11.4 for 5% PRSF) compared to OPC50 (9.45 for 6% PRSF).

8.1.1.4 Flexural Toughness Tests Using Notched Beams

These tests aimed to study the parameters affecting crack propagation to determine the location of the neutral axis depth and to collect data for use in FE analysis and design tools. Notched prisms, of size 150mmx150mm x550mm, were subjected to four point loading according to RILEM. A single mix was reinforced with different fibre types (PRSF, VSF, SSF-1, ISF-2 and SRSF). The load-deflection response at

the centre and the crack width at different locations on the central vertical axis were recorded.

The main conclusions are listed as follows:

- It was found out that the flexural toughness of notched beams is affected by the same parameters that influence the flexural behaviour of unnotched beams.
- Even for the same fibre amount, the crack propagation is not always vertical, indicating high variability in material properties.
- The load deflection response of the PRSF fibres is comparable with that of the industrial fibre used in this study.
- The equivalent flexural strength of the VSF fibres is about 15% higher than that of the PRSF fibres, due to the effect of carbon black.
- In the case of shredded fibres the load deflection response was dominated by an unstable region at the post-peak load. The short fibre length and the smooth surface of the SRSF fibres result in sudden drops of the load.

8.1.1.5 Concrete Slab Tests

To demonstrate the use of fibres as reinforcement in a practical application, full-scale drainage cover slabs were tested under cycling point load acting in the centre of the slab. Four types of reinforcement were used: a) normally reinforced with ordinary bars (Rcon), b) reinforced with 6% PRSF fibres (Pcon), c) reinforced with 2% SRSF fibres (Scon), d) slurry infiltrated slab reinforced with 17% shredded fibres. The deflections were measured along the line support, support edge and slab centre.

The main conclusions are as follows:

- The experiments demonstrated that the Rcon slab passed the test for class C250 and failure of this slab was due to punching shear.
- The Scon slab passed only the B125 loading condition, due to the low fibre content and poor fibre penetration in the slotted region of the slab.

- The Pcon slab passed only the B125 loading condition, due to poor fibre penetration in the slotted region of the slab.
- The best results were achieved by the SIScon slab. The high volume of shredded fibres and good penetration of the cement slurry in the fibres resulted in extremely high strength and ductility, even higher than for the Rcon slab and passed the C250 loading condition comfortably.

8.1.2 PART 2: ANALYTICAL STUDY AND DESIGN

An Inverse analysis using FE package “ABAQUS” was undertaken to determine the SFRC stress-strain characteristics.

In the following the main conclusions are presented:

- The hinge length of $0.5h_{sp}$ was used to calculate the strains from the experimentally measured crack width. The resulting load-strain relationship agrees with results obtained by FEA.
- The normalised neural axis depth varied between 0.8 - 0.9 at peak and 0.84-0.97 at deflection of 3mm (depending on fibre ratio and type).
- It was found out that the determination of parameter $f_{eq,2}$ is unreliable (due to the inaccuracy in calculating the limit of proportionality) and can lead to inaccurate estimation of flexural capacity.
- The result of an initial FE analysis using the RILEM design parameters as tensile stiffening for a simulated notched beam indicated that using the RILEM design parameters can overestimate the load-carrying capacity of SFRC.
- The inverse analysis implemented in this study provided optimised softening stress-strain curves for each fibre type and content ratio. It was found out that the tensile strength of SFRC is a function of tensile strength of plain concrete and fibre ratio. However, the stress reduction after cracking is influenced only by the fibre type.

- The σ - ϵ behaviour can be described in three phases; 1) A linear elastic phase up to the first crack, 2) a concrete cracking phase with fibre debonding which results in the stress drop. 3) a phase during which the concrete main crack is developed, but dominated by fibre pull-out.
- The results of FE analysis using the newly developed σ - ϵ models indicate that the numerically obtained deflection-strain relationship and the position of the neutral axis agreed with the experimental results.
- The mesh sensitivity can be considered in the way that strains in the σ - ϵ model are scaled inversely to the element length.
- For practical design, the obtained stress-strain curves are simplified by proposing a bi-linear softening stress-strain model.
- Charts and equations for design moment vs fibre ratio are proposed. Size effect and stress and safety reduction factors are considered.
- In a case study, the design moments calculated for a slab on grade using the proposed moment-fibre ratio are in agreement with results obtained by using the Bekaert design manual.

8.2 RECOMMENDATION FOR FURTHER STUDY

A number of interesting questions still remain unanswered, new topics of research have been opened for investigation and several propositions require validation. The subject of SRSF is very wide and this study has contributed a significant part of knowledge hoping that further investigations will continue toward the better understanding of the subject. It is believed that further development is required in the following:

8.2.1 IMPROVING THE RECYCLING PROCESSES AND THE QUALITY OF THE RECYCLED FIBRES

- A mechanical and chemical process has to be developed to obtain cleaner and demagnetised SRSF fibres.
- A mechanical process should be developed to clean, sort and chop the PRSF fibres in any required length and finally a packaging process is needed to produce the PRSF as engineered fibres. To improve the anchoring and avoid the separating the wires that form a PRSF, a mechanical process is needed to produce a blob at both ends of the fibres.

8.2.2 IMPROVING THE EXPERIMENTAL DATA

- Industrially applicable mixing processes need to be developed to enable the recycled steel fibres to be used by industry.
- More study on fibre reinforced high strength concrete is needed, since an initial test with 6% PRSF fibres showed very promising results.
- The single fibre pull-out tests need to be significantly re-engineered to achieve more accurate pull-out response.
- The double-sided pull-out tests need to be improved to be able to test very thin fibres, such as the shredded fibres, and to eliminate the friction between the plate and concrete. The complete pull-out response can be improved by testing multi fibres.
- To understand the pull-out behaviour of fibres in flexural tests, single and multi inclined fibres need to be tested.
- Finally, a greater number of flexural tests need to be undertaken using different beam sizes, concrete strength and fibre content to provide further data relating to the shape and magnitude of the strain-crack width profiles. To calculate the external work done, the deflection should also be measured at the load locations.

8.2.3 IMPROVING THE ANALYTICAL INVESTIGATION AND THE PROPOSED DESIGN METHOD

- The inverse analysis undertaken can be expanded to determine the optimum stress-crack width relationship. From that, the characteristic length can be calculated. Fracture mechanics principles should be used to calculate the height and length of the fracture zone.
- To test the reliability of the proposed model, uniaxial tensile tests with different fibre content, fibre types and concrete strength need to be performed.
- Further research should be concentrated on the design tools such the moment-fibre ratio relationship proposed in this study. A parametric study on the influence of concrete strength and size effect on the proposed relationship should be undertaken.
- For design of slabs on grade it is necessary to undertake FE analysis using the proposed stress-strain curves and experimental investigations have to be undertaken to compare the FE results with experimental results.

REFERENCES

- Abbot, G.M.P. (2001) The use of crumb rubber from end of life tyres in sport and play. *Proceedings of the international symposium on recycling and reuse of used tyres*, Thomas Telford, pp. 203 -211.
- ACI 544.IR-XX (1995) *Committee report on fibre reinforced concrete. American Concrete Institute Committee 544, Response to TAC Comments July 1995*, Detroit, USA.
- ACI 544 (1988) Measurements of properties of fibre reinforced concrete. *ACI Materials Journal*, 85(6), pp. 583-593.
- ACI 544-4R (1988) *Design Considerations for Steel Fibre Reinforced Concrete. American Concrete Institute*, Detroit, USA.
- AMAT, (2003) *Advanced Molecular Agitation Technology Ltd*, <<http://www.amat-ltd.com>>
- Armelin, H.S. and Banthia, N.B. (1977) Predicting the flexural post-cracking performance of steel fibre reinforced concrete from the pullout of single fibres. *ACI Materials Journals*, 94(1), pp. 18-31.
- ASTM C1018-94b (1995) *Standard test method for flexural toughness and first-crack strength of fibre-reinforced concrete (using beam with third-point loading). American society of testing and materials, ASTM Annual Book of Standards 4.02*, Philadelphia, USA, pp. 509-516.
- ASTM C494-82 Type F, (1982) *Specification for chemical admixture for concrete, American Society for Testing and Materials, ASTM annual book of standard, 1.05*, Philadelphia, USA.
- ASTM 311-94 (1994) *Specification for chemical admixture for fly ash. American Society for Testing and Materials, ASTM annual book of standards 1.05*, Philadelphia, USA.
- ASTM A820 (1994) *Standard Specifications for Steel Fibers for Fiber Reinforced Concrete*.
- ASTM C 143/C 143M (1998) *American Society for Testing Materials: Standard Test Method for Slump of Hydraulic-Cement Concrete*.
- Banthia, N. and Trottier, J.F. (1995) Test methods for flexural toughness characterization of fibre reinforced concrete: some concerns and a proposition. *ACI Materials Journals*, 92 (1), pp. 48-57.
- Banthia, N., Trottier, J.F., Beaupre, D. and Wood, D. (1994) Properties of steel fibre reinforced shotcrete. *Canadian Journal of Civil Engineering*, 21 (4), pp. 564-575.

-
- Banthia, N. (1990) A study of some factors affecting the fibre-matrix bond in steel fibre reinforced concrete. *Canadian Journal of Civil Engineering*, 17(4), pp. 10-620.
- Banthia, N. and Trottier, J.F. (1994) Concrete reinforced with deformed steel fibres, part1: bond-slip mechanisms, *ACI Material Journal*, 91(5), pp. 435-446.
- Barr, B., Gettu, R., Al-Oraimis, K.A. and Bryars, L.S. (1996) Toughness measurement- the need to think again. *Cement and Concrete Composites*, 18 (4), pp. 281-297.
- Barr, B. and Lee, M.K. (2001) Definition of round robin test, preparation of specimens. Execution and evaluation of round robin testing cylinders. *Report of sub-task 2.1 and 2.2. Report - Test and Design Methods for Steel Fibre Reinforced Concrete. BRPR-CT98-813.*
- Barr, B. and Lee, M.K. (2002) Interpretation in the procedure of calculating RILEM TC-162 beam design Parameters. Definition of round robin test, preparation of specimens, execution and evaluation of round Robin testing - report of subtasks 2.1 and 2.2, Brite-Euram project BRPR-CT98-0813: Test and Design Methods for Steel Fibre Reinforced Concrete, *Project funded by the European Community under the Industrial & Materials Technologies Programme (Brite-Euram II)*.
- Baumann A. and Weisgerber F.M. (1983) Yield line analysis of slab on grade. *Journal of structural engineering ASCE*, 109(7), pp. 1553-1568.
- Bayasi Z., Kaiser H. and Gonzales M. (2001) Composite slabs with corrugated SIMCON deck as alternative for corrugated metal sheets. *Journal of Structural Engineering*, 127(10), pp. 1198-1205.
- Bazant, Z.P. (2002) Concrete fracture model: testing and practice, *Engineering Fracture Mechanics*, 69, pp. 165-205.
- Bazant, Z.P. and Oh, B.H. (1983) Crack band theory for fracture of concrete, *Material and Structure*, 16, pp. 155-157.
- Bazant, Z.P. and Pijaudier-Cabot, G. (1989) Measurement of characteristic length of non-local continuum. *Journal of Engineering Mechanics (ASCE)*, 115(4), pp. 755-767.
- Bekaert (1999) Steel fibre reinforced industrial floors, *design in accordance with the Concrete Society TR34*, Zwevegem, Belgium.
- Bekaert (2003) *Concrete reinforcement*. <<http://www.bekaert.com/building>>
- Bindiganavile, V. and Banthia, N. (2001) Polymer and steel fibre reinforced cementitious composites under impact loading - part 01:00 bond-slip response. *ACI Materials Journal*, 98(1), pp. 10-16.
- Bonzel, J. and Schmidt, M. (1984) Distribution and orientation of steel fibres in concrete and their influence on the quality of steel fibre concrete. *Beton*, 34(12), pp. 501-504 (in German).
-

-
- BRC Ltd UK (2003). <<http://www.brc-uk.co.uk>>
- Brite-Euram, (2002) Subtask 7.2 Final Report, Brite-Euram BRPR-CT98-0813: Test and Design Methods for Steel Fibre Reinforced Concrete, *Project funded by the European Community under the Industrial & Materials Technologies Programme (Brite-Euram II)*, pp. 1 -209.
- BS 12 (1996) *British standard for concrete: method for determination of compressive strength of concrete cubes*, British Standards Institute, London.
- BS 812-Part 1 (1975) *British standard for aggregate: sampling, shape, size and classification*, British Standards Institute, London.
- BS 5075-Part 3 (1995) *British standard for admixtures: specification for superplasticising admixtures*, British Standards Institute, London.
- BS 1881-111 (1983) *Testing concrete. Method of normal curing for test specimens (20 °C method)*. British Standards Institute, London.
- BS 1881-116 (1983) *Testing concrete. Method for determination of compressive strength of concrete cubes*. British Standards Institute, London.
- BS EN 124 (1994) *Dully tops for vehicular and pedestrian areas-Design requirements, type testing, marketing, quality control*. British Standards Institute, London
- Burakiewicz, A. (1998) Testing of fibre bond strength in cement matrix. *Institute of Fundamental Technological research*, Polish Academy of Science, Warsaw, Poland, pp. 355-364.
- Casanova, P. and Rossi, P. (1996) Analysis of metallic fibre reinforced concrete beams submitted to bending. *Material and Structure*, 29, pp. 354-361.
- Casanova, P. and Rossi, P. (1997) Analysis and design of steel fibre reinforced beams. *ACI Structural Journal*, 94(5), pp. 595-602.
- CEB, (1993) CEB-FIP Model Code (1990) *Bulletin d'information no. 203-205*, Thomas Telford, London, England.
- Chanvillard, G. and Aitcin, P.C. (1996) Pullout behaviour of corrugated steel fibres. *Advanced Cement Based Materials*, 4(1), pp. 28-41.
- Charles Lawrence Recycling Ltd (2004) <<http://recycling.clgplc.co.uk>>
- Chen, L., Mindess, S., and Morgan, D.R. (1994) Specimen geometry and toughness of steel-fibre reinforced concrete. *Journal of Materials in Civil Engineering*, 6(4), pp. 529-541.
- Chen, L., Mindess, S., Morgan, D.R., Shah, S.P., Johnston, C.D. and Pigeon, M. (1995) Comparative toughness of fibre reinforced concrete. Testing of fibre reinforced concrete, SP 155-4, *American Concrete Institute*, Detroit, pp. 41-75.
-

-
- Concrete Society (2003) *Concrete industrial ground floors-A guide to design and construction. Technical Report No. 34*, Uk
- Copalaratnam, V.S., and Gettu, R., On the characterisation of flexural toughness in FRC, *Cement Concrete Composites*, 17(1995), pp. 249-254.
- Council Directive (1999/31) of 26 April 1999 on the landfill of waste, *Official Journal of the European Communities*, L 182, 16/07/1999, pp. 1-19.
- Council Directive 1999/31/EC of 26 April 1999 on the landfill of waste, *Official Journal L 182*, (European Commission, Brussels, 1999), pp. 1 – 19.
- Cox, H.L. (1952) The elasticity and strength of paper and other fibrous materials. *British Journal of Applied Physics*, 3, pp. 72-79.
- Davies R.W. and Worthington G.S. (2001) Use of scrap tyres as a fuel in the cement manufacturing process. Proceedings of the international symposium on recycling and reuse of used tyres. Thomas Telford, pp. 93–106.
- DBV (1996) Grundlagen zur Bemessung von Induriefussboeden aus Stahlfaserbeton (in German) Basis for evaluation of steel fibre concrete for use in industrial floors. *Deutscher Beton Verein*, pp. 258-273.
- DBV (1992) Design recommendation for fibre concrete in tunnel construction, *Deutschen Beton Vereins*.
- DVB (2001) Merkblatt “Stahlfaserbeton”. *Deutscher Beton-Verein*. Germany
- Department of the Environment and the Welsh Office (1995) *A strategy for sustainable waste management in England and Wales, making waste work*. The Stationary Office, London.
- DFT (2002) *Transport statistics Great Britain 2002 edition. 28th edition, published by The Stationary Office, Department for Transport*, pp. 206, London.
- DFT (2003) *Traffic in Great Britain Q4 2002 data. Transport statistics bulletin -3 5*, Department for Transport, pp. 17, London.
- DTI (2001) *Tyre waste arisings and recycling rates. URN 01/608, Department of Trade and Industry*, pp. 4, London.
- Dupont D. and Vandewalle, L.(2002) A practical proposal to drive a stress-strain relation with residual tensile strengths. *Brite-EuRam Project BRPR-CT98-0813*, Annex 5.1.3, (2002).
- Dupont, D. and Vandewalle, l. (2002a) Recommendations for Finite Element Analysis of FRC. *Brite-EuRam Project BRPR-CT98-0813*, Subtask 3.5.
- Edgington J. (1977) Economic fibrous concrete.in Institution of Civil Engineers *Proceedings:conference on fibre-reinforced materials, London, UK*. Pp. 115-126.
-

-
- ENV 1992-1-1, 1992 Eurocode 2 - Design of Concrete Structures, Part 1-6; *General Rules and Rules for Buildings, European Prestandard, European Committee for Standardisation.*
- Environment Agency (2003) *Tyres in the environment. Environment Agency's.* <<http://www.environment-agency.gov.uk>>
- Erdem E, (2003) *The Flexural Behaviour of SFRC Beams and Slabs: Bending with s-e Method, Test and Design Methods for Steel Fibre Reinforced Concrete – Background and Experiences, Proceedings of the RILEM TC 162 – TDF Workshop, edited by B. Schnütgen and L. Vandewalle. Bochum: RILEM Publications S.A.R.L.*
- ETRA (2001) Boost for European tyre recycling, *European Tyre Recycling Association*, <<http://www.tirestyres.com>>
- EUELV (2000) Directive 2000/53/EC of the European parliament and of the council of 18 September 2000 on end-of life vehicles. *Official journal of the European Communities L269*, 21 October 2000, pp. 9.
- EULD (1999) Council Directive 1999/31/EC of 26 April 1999 on the landfill of waste. *Official journal of the European Communities L 182*, 16 July 1999, pp. 19.
- European Commission (1999) Council Directive of 26 April 1999 on the landfill of waste, *Official Journal of the European Communities, L 182*, 16 July 1999, pp. 1-19.
- European Committee for Standardisation, BS EN 124 - Dully tops for vehicular and pedestrian areas-Design requirements, type testing, marketing, quality control' *BSI, (1994)* London.
- EUWD (2000) Directive 2000/76/EC of the European parliament and of the council of 4 December 2000 on the incineration of waste. *Official journal of the European Communities L332*, 28 December 2000, pp. 22.
- Falkner H. and Henke V. (1998) Application of steel fibre concrete for underwater concrete slabs. *Cement and composites*, 20(5), pp. 377-385.
- Falkner H., Teutsch, M. and Huang (1995) Investigation of the bearing-load capacity and deformation of fibre reinforced industrial flooring No. 117. *Institute fuer Baustoffe, Massivebau und brandschutz IBMB, TU Branschweig, Germany.*
- Fanella D.A. and Naaman A. E. (1985) Stress-strain properties of fiber reinforced mortar in compression. *Journal of the American Concrete Institute*, 82(4), pp. 475-483.
- Fantilli, A.P. and Vallini, P. (2003) Bond-slip relationship for smooth steel reinforcement. in Euro-C Conference *Proceeding: Computational Modelling of Concrete Structures*, edited by Bicanic, N., de Brost, R., Mang, H. and Meschke, G.St. Johann im Pongau, Austria, pp. 215-223.
-

-
- Fibermesh (2003) Fiber reinforcement: making concrete better®.
<<http://www.fibermesh.com>>
- Gettu, R., Barragan, B.E., Martin, M.A, Zerbino, R.L. (2001) A parametr study of the uniaxial tensile behaviour of SFRC. *Report of tests performed at the university politecnica de Catalunya within sub-task 2.3 of Bite project: Test and design method for SFRC (BRPR.CT98.0813)*, Barcelona, Spain.
- Glinicki, M.A. (1994) Toughness of Fibre Reinforcement mortar at hgth Tensile Rates. *ACI Materials Journal*, 91(2), pp. 161-166.
- Gopalaratnam, V. and Gettu, R. (1995), On the characterization of flexural toughness in fibre reinforced concrete. *Cement and concrete composites*, 17(3), pp. 239-254.
- Gopalaratnam, V.S. and Cheng, J. (1987) On the modelling og inelastic interfaces in fibrous composites. Symposium Proceeding, *Materials Research Society*, 114, pp. 225-231.
- Gopalaratnam, V.S. and Shah, S.P. (1987) Tensile failure of steel fibre-reinforced mortar. *Journal of engineering mechanics, ASCE*, 113(5), pp. 635-652.
- Groth, P. (1996) Cracking in concrete - Crack prevention with air and crack distribution with steel fibre reinforcement. Luleå University of Technology, *Division of Structural Engineering, Licentiate Thesis 1996:37L*, Nov 1996.
- Hannant D.J. (1978) *Fibre Cement and Fibre Concretes*. Published by John Wiley and Sons Ltd, New York.
- Hartwich K. (1986) *Zum riss und verformungsverhalten von stahlfaservesaerkten stahlbetonstaeben unter laengszug*. Ph.D. Thesis (in German), TU Braunschweig.
- Hemmy, O. (2002) Recommendations for Finite Element Analysis of FRC, Report of Subtask 3.5, Brite-EuRam Project BRPR-CT98-0813: Test and Design Methods for Steel Fibre Reinforced Concrete, Project funded by the European Community under the Industrial & Materials Technologies Programme (*Brite-Euram II*).
- Hibbitt, Karlsson and Sorensen (2000) ABAQUS User's Manual, II, version 6.1.
- Hillerborg A. (1985) Determination and significance of the fracture toughness of steel fibre concrete. Steel Fibre Concrete, Proceedings of US-Sweden joint seminar (NSF-STU), edited by Shah S.P. and Skarendahl A. *Swedish Cement and Concrete Research Institute*, Stockholm, pp. 257-271.
- Hillerborg A. (1980) Analysis of fracture by means of fictitious Crack model, particularly for Fibre reinforced Concrete. *The international Journal for Cement Composites*, 2(4), pp. 177-184.
- Hillerborg A., Modeer M. and Peterson P. E. (1976) Analysis of crack growth in concrete by means of fracture mechanics and finite elements. *Cement Composites*, Michigan, USA.
-

-
- Hillerborg, A. (1983) *Analysis of one single crack, in Fracture Mechanics of Concrete*. Elsevier Science Publishers B.V., Amsterdam.
- Hird A.B., Griffiths P.J. and Smith R.A. (2002) Tyre waste and resource management: *A mass balance approach. Viridis Project*, <<http://www.viridis.co.uk>>
- Hodkin and Jones Decathlon (2003) High performance drainage systems, <<http://www.decathlon-drainage.com>>
- Hoff G.C. (1985) Use of steel fiber reinforced concrete in bridge decks and pavements. *in Swedish Cement and Concrete Research Institute Proceedings of steel fiber concrete US-Sweden joint seminar (NSF-STU)*, pp. 67–108.
- Imam M., Vandewalle L. and Mortelmans F. (1995) Are current concrete strength test suitable for high strength concrete. *Materials and Structures*, 28(181), pp. 384-391.
- INTEC (2003) RC 400/5 - INTEC'S high technology plant for the production of ultra fine rubber powders. <<http://www.intec-industries.com>>
- Japan Society of Civil Engineers-SF4 (1994). *Methods of tests for flexural strength and flexural toughness of steel fibre reinforced concrete. Concrete Library of JSCE*, pp. 58-61.
- Japan Society of Civil Engineers, JSCE-SF1 (1994) *Recommendation for design and contraction steel fibre reinforced concrete*, *JSCE Concrete Library*, 3, pp. 5-29.
- Jenq Y.S. and Shah S.P. (1985) Two parameter fracture model for concrete. *ASCE Journal of Engineering Mechanics Division*, 11(10), pp. 1227-1241.
- Jenq Y.S. and Shah S.P. (1986) Crack propagation in fibre reinforced concrete. *Journal of Structural Engineering*, 112 (1), pp. 19-34.
- Johnston C.D. (1977) Steel fibre reinforced mortar and concrete – a review of mechanical properties. *Publication SP-44, American Concrete Institute, Detroit*.
- Johnston C.D. (1995) Deflection measurement considerations in evaluating fibre reinforced concrete performance using ASTM C1018. Testing of fibre reinforced concrete, Publication SP 155-4, *American Concrete Institute, Detroit*, pp. 1-22.
- Karihaloo, B.L. (1995) *Fracture Mechanics and Structural Concrete*, Longman Scientific and Technical, Harlow, UK.
- Kandie, B.K.T. (2001) *Effect of Super-Classified Pulverized Fuel Ash on Strength and Durability of Concrete*, Ph.D. Thesis, University of Sheffield.
- Kelly, A. (1966) *Strong solids*. Clarendon Press, Oxford.

-
- Kohler (1996) Cryogenic processing of scrap tyres. *Polymer recycling*, 2(2), pp. 83 – 88.
- Krenchel H. (1964) *Fibre reinforcement*. Akadamisk Forly, Copenhagen.
- Krstulovic-Opara N. and Al-Shannag M. J. (1999) Slurry infiltrated mat concrete (SIMCON)-based shear retrofit of reinforced concrete members. *ACI Structural Journal*, 96 (1), pp. 105-114.
- Krstulovic-Opara, N. and Al-Shannag, M.J. (1999) Slurry infiltrated mat concrete (SIMCON)-based shear retrofit of reinforced concrete members, *ACI Structural Journal*, 6, pp. 105-114.
- Kupfer, H., Hilsdorf, H. K. And Rusch, H. (1973) Behaviour of Concrete under Biaxial Stress, *ACI*, 99(8), pp. 656-666.
- Landfill Directive (1999) Council Directive of 26 April 1999 on the landfill of waste, *Official Journal of the European Communities*, L 182, 16 July 1999, pp. 1-19.
- Lankard D.R. (1984) Slurry infiltrated fibre concrete (SIFCON). *Concrete International: Design and Construction*, 6(12), pp. 44-47.
- Lee, M.K. and Barr, B.I.G. (2003) Strength and fracture properties of industrially prepared steel fibre reinforced concrete. *Cement and Concrete Composites*, 25, pp. 221-332.
- Leibengood, L.D., Darwin, D. And Dodds, R.H. (1986) Parameters affecting FE analysis of concrete structures, *Journal of Structural Engineering*, ASCE, 12(2), pp. 326-341.
- Li. V.C., Stang, H. and Krenchel, H. (1993) Micromechanics of Crack Bridging in Fibre Reinforcement Concrete. *Materials and Structures*, 26, pp. 486-494.
- Lok T. S. and Xiao J. R. (1999) Flexural Strength Assessment of Steel Fiber Reinforced Concrete, *Journal of Materials in Civil Engineering*, 11(3), pp. 188–196.
- Maalej M. and Li V. C. (1994) Flexural strength of fibre cementitious composites. *Journal of Material in Civil Engineering*, 6(3), pp. 390-406.
- Maidl B. R. (1995), *Steel fibre reinforced concrete*. Berlin: Ernst and Sohn.
- Mandel J.A. (1985) Micromechanical modelling of steel fiber reinforced cementitious materials. in Swedish Cement and Concrete Research Institute *Proceedings of steel fiber concrete US-Sweden joint seminar (NSF-STU)*, pp. 219-256.
- Mangat P.S. and Swamy R.N. (1974) Compactibility of steel fibre reinforced concrete. *Concrete*, 8(5), pp. 34-35. London.
- Manouselis, I. (2002) *Use of Recyled Steel Fibres from Tyres in Concrete*. MSc. Thesis, University of Sheffield. UK.
-

-
- Mechtcherine, V. and Mueller, H.S. (2003) Analysis of concrete fracture using a heterogeneous continuum model. *Computational Modelling of Concrete Structures*. Edited by Bicanic et al. 2003 Swets and Zeitlinger, Lisse, Netherlands.
- Metso Minerals (2003) Scrap-tire pyrolysis – the impossible dream, <<http://www.scrap.org>>
- Meyerhof G.G. (1962) Load carrying capacity of concrete pavements. *Journal of the soil mechanics and foundations division ASCE*, 88(3), pp. 89-115.
- Morgan D.R. (1995) *Special sprayed concrete sprayed concrete-properties, design and applications*. Editors Austin S.A. and Robin P.J., Ehhittles Publishing, Caihness, pp. 229-265.
- Morgan D.R., Chen L. and Beaupre D. (1995) Toughness of fibre reinforced shotcrete. *Proceedings of Engineering Foundation Conference Shotcrete for Underground Support VII, ASCE*, pp. 66-87.
- Morris J.W., Glazer J. and Chan J.W. (1990) Metallurgical determinants of toughness at cryogenic temperature. *Advances in cryogenic engineering*, 36, pp. 777-785.
- Murguia, J.L. (2001) *Recycled Tyre Reinforcing Steel Fibres as Reinforcement for Pumped and Sprayed Concrete*. MSc Thesis, University of Sheffield. UK.
- Naaman, A.E. and Shah, S.P. (1976) Pullout mechanism in steel fibre reinforced concrete, *Journal of the Structural Division, ASCE*, 102, pp. 1537-1548.
- Naaman, A.E., Namur, G., Alwan, J.M. and Najm, H. (1991) Fibre pull-out and bondslip I: analytical study. *Journal of Structural Engineering, ASCE*, 117(9), pp. 2769-2790.
- Naaman, A.E., Namur, G., Alwan, J.M. and Najm, H. (1991a) Fibre pull-out and bondslip II: Experimental Validation. *Journal of Structural Engineering, ASCE*, 117(9), pp. 2791-2800.
- Namur G.G., Naaman A.E. and Clark S.K. (1987) Analytical prediction of the pull-out behaviour of steel fibre in cementitious matrices. *in Research Society Proceedings of Symposium on bonding in cementitious composites, materials*, 114, pp. 217-224.
- Namur, G.G. and Naaman, A. E. (1989) A bond model for fibre reinforced concrete based on bond stress slip relationship. *ACI Material Journal*, 86(1), pp. 45-57.
- Nemegeer D. (1996) Design Guidelines for Dramix Steel Wire Fibre Reinforced Concrete, *The Indian Concrete Journal*, 70(10), pp. 575 – 584.
- Neocleous, K., Pilakoutas, K. and Tlemat, H. (2003) *Design of concrete slabs reinforced with waste-tyre steel fibres, DTI partners in innovation project: Demonstrating steel fibres from waste tyres as reinforcement in concrete*,

Technical report no CCC/03/0102D, Centre for Cement and Concrete, The University of Sheffield, UK, 23 pp, <<http://www.shef.ac.uk/tyre-recycling>>

- Neocleous K., Pilakoutas K. and Tlemat H. (2004) Design considerations on the use of steel fibres from waste tyres, as reinforcement in concrete. *Proceedings of the first international conference on innovative materials and technologies for construction and restoration*, Lecce - Italy, June 6-9 2004, ed. by A. La Tegola and A. Nanni, pub. by Linguori Editore, Vol.1, pp 611-619, ISBN 88-207-3678-8.
- Neville, A.M. (1995) *Properties of Concrete*. Longman Scientific and Technical, Harlow, UK.
- Neville, A.M. and Brooks, J.J.(1990) *Concrete Technology*, Longman Group, pp. 8. London, UK.
- Ngo, D and Scordelis, A. C. (1967) Finite element analysis of reinforced concrete beams, *ACI*, 64(3), pp. 152-163.
- Ogilvie S.M. and Poll A.J. (1999) Developing markets for recycled material. Report no AEAT-5538, *Department of Trade and Industry*, pp. 40. London. UK
- Olesen, J.F. (2001) Fictitious Crack Propagation in Fibre-Reinforced Concrete Beams. *Journal of Engineering Mechanics, ASCE*, 127(3), pp. 272-280.
- Ostergaard, Olesen, J.F., Stang, H. and Lange (2002) A method for fast and simple interpretation and inverse analysis of the wedge splitting test. *Brite-EuRam Project BRPR-CT98-0813, Subtask 3.5*.
- Padmarajaiah, S.K. and Ramaswamy, A. (2002) A finite element assessment of flexural strength of prestressed concrete beams with fibre reinforcement. *Cement and Concrete Composites*, 24, pp. 229-241.
- Parviz, S. and Cha-Don, L. (1990) Distribution and Orientation of Fibres in Steel Fibre Reinforced Concrete. *ACI Materials Journal*, 87(5), pp. 433-439.
- Pilakoutas K. and Strube R, (2001) *Re-use of tyre's fibres in concrete. Proceedings of the international symposium on recycling and reuse of used tyres*, Thomas Telford, Dundee Scotland, pp. 225-236.
- Philips, D.V. and Binshenge, Z. (1993) Direct tension test on notched and unnotched plain concrete specimens. *Magazine of Concrete Research*, 45(162), pp. 25-35.
- Ramakrishnan V. (1985) Steel fiber reinforced shotcrete, a state-of-the-art report. in Swedish Cement and Concrete Research Institute *Proceedings of steel fibre concrete US-Sweden joint seminar (NSF-STU)*, pp. 7-24.
- Ramakrishnan, V. (1987) Materials and Properties of Fibre Concrete. in Madras India *Proceeding of the international Symposium of Fibre Reinforced Concrete*, 1, pp. 2.3-2.23.

-
- Rashid, Y.R. (1968) Analysis of prestressed concrete vessels', *Nuclear Eng. And Design*, pp. 334-344.
- Recycling (2001) Mountains to climb before the UK can achieve tyre targets. *Recycling week materials*.
- Resplendino, J. and Petitjean, J. French recommendations for ultra-high performance fibre-reinforced concretes. Test and Design Methods for Steel Fibre Reinforced Concrete –Background and Experiences- *Proceedings of the RILEM TC 162-TDF Workshop*. Edited by B. Schnetgen and L. Vandewalle. Germany.
- RILEM (1972) *Fibre concrete materials. Report prepared by the RILEM technical committee 19-FRC - fibre reinforced cement composites*, pp. 103-120.
- RILEM TC 162-TDF (2002) *Test and design methods for steel fibre reinforced concrete: bending test. Materials and Structures*, 35(253), pp. 579-582.
- RILEM TC 162-TDF (2000) *Test and design methods for steel fibre reinforced concrete: σ - ϵ design method, Materials and Structures*, 33, pp. 75-81.
- RILEM TC 162-TDF (2001) *Test and design methods for steel fibre reinforced concrete: Uniaxial tension test for steel fibre reinforced concrete, Materials and Structures*, 34, 3-6.
- RILEM TC 162-TDF (2002) *Test and Design Methods for Steel Fibre Reinforced Concrete, Design of steel fibre reinforced concrete using the σ - w method: principles and applications, Materials and Structures*, 35, pp. 262-278.
- Robins, p., Austin, s. and Jones, p. (2002) Pull-out behaviour of hooked steel fibres. *Material and Structures*, 35, pp. 434-442.
- Robinson C., Colasanti A. and Boyd G. (1991) Steel fibre reinforced auto assembly plant floor. *Concrete International*, 13(4), pp. 30-35.
- Rodriguez I.M., Lasegoiti M.F., Cabrero M.A., Torres A., Chomon M.J. and Caballero (2001) Pyrolysis of scrap tyres. *Fuel processing technology*, 72, pp. 9-22.
- Rossi P., Acker P. and Malier Y. (1987) Effect of steel fibres at two different stages; the material and the structure. *Materials and Structures*, 20(120), pp. 436-439.
- Schnuetgen B.(1981) Bemessung von Stahlfaserbeton und ihre Problematic. Konstruktiver Ingenieur Bericht, Heft 37 (in German), *Ruhr-University Bochum*, Bochum, Germany.
- Schnuetgen, B. Dams, S. (1994) Stahlfaser im Tunnelbau, Beton-informationen, Heft 5-94, Beton-Verlag Duesseldorf.
- Shommakhi A.A. (2000) Re-use of tyre steel fibres in concrete construction. MSc (Eng) Dissertation, The University of Sheffield, UK.
-

-
- Skatun O. and Spigerverk C. (1986) Application of wet process steel fibre reinforced Shotcrete in Scandinavia. Developments in fibre reinforced cement and concrete, in Rimel Technical Committee 49-TFR *Proceedings of the RILEM symposium FRC*, 2(86).
- Smorgon ARC (1998) *Pavement and Floor Design Technical Manual. Technical Report*. <<http://www.smorgonarc.com.au>>
- Stang, H. (2002) Finite Element Modelling using Discrete Crack Elements. *Brite-EuRam Project BRPR-CT98-0813, Subtask 3.5*.
- Stang, H. (2000) *Analysis of 3 Point Bending Test*. Technical University of Denmark.
- Stoeven Y.M. de Haan, Bouter C. and Shah S.P. (1978) Pull-out tests of steel fibres. in *The Construction Press Proceedings of the RILEM symposium 78*, edited by R.N. Swamy, Lancaster, England, pp. 345-352.
- Strategy Unit (2002) *Waste not, want not: a strategy for tackling the waste problem in England*. Published by Strategy Unit, Cabinet Office, London, pp. 155.
- STWG (1997) *Second report to ministers. Scrap tyre working group, cited in Environment Agency (2003), Tyres in the environment. Environment Agency's* <<http://www.environment-agency.gov.uk>>
- Swamy R.N. (1974) Technology of steel fibre reinforced concrete for practical applications. *Proceedings of the Institution of Civil Engineers, Part 1- Design and Construction*, 56(1), pp. 143-159. London, UK.
- Swamy R.N. and Fattuhi N.J. (1974) Mechanics and properties of steel fibre reinforced concrete. *Proceedings of first Australian conference on engineering materials*, pp. 351-368.
- Swamy R.N. and Mangat P.S. (1974) Influence of fibre-aggregate interaction on some properties of steel fibre reinforced concrete. *Materials and Structures*, 7 (41), pp. 307-314.
- Swamy, R.N. and Stavrides, H. (1975) Some properties of high workability steel fibre concrete, *RILEM Symposium: Fibre Reinforced Cement and Concrete*, UK, pp. 197-208.
- Swift, D.G. and Smith, R.B.L. (1978) *The Physical Significance of the flexural Test for Fibre Cement Composites. RILEM Symposium*, Edited by R.N. Swamy. The construction Press, Lancaster, UK, pp. 463-478.
- SYEP (2001) *Dealing with waste tyres. South Yorkshire environmental partnerships*, <<http://www.syep.org.uk>>
- Tada H., Paris P.C. and Irwin G.R. (1985) *The Stress Analysis of Cracks Handbook*, 2nd Edition, Paris Productions Inc., St. Louis USA.
- Timoshenko S.P. and Goodier J.N. (1970) *Theory of Elasticity*. McGraw Hill. New York.

-
- Tlemat, H. Pilakoutas, K. (2002a) *Literature review of DTI partners in Innovation Project: Demonstrating steel fibres from waste tyres as reinforcement in concrete*, Technical report no CCC/02/0102A, Centre for Cement and Concrete, The University of Sheffield, UK, 79 pp, <<http://www.shef.ac.uk/tyre-recycling>>
- Tlemat, H. and Pilakoutas K. (2002b) *Steel fibre testing, DTI partners in innovation project: Demonstrating steel fibres from waste tyres as reinforcement in concrete*, Technical report no CCC/02/0102B, Centre for Cement and Concrete, The University of Sheffield, UK, <<http://www.shef.ac.uk/tyre-recycling>>
- Tlemat, H., Pilakoutas, K. and Neocleous, K. (2003a) Pullout behaviour of steel fibres recycled from used tyres', *Proceedings of International Symposia on Celebrating Concrete: People and Practice (in Role of Concrete in Sustainable Development)*, Dundee UK, Sept. 2003, Thomas Telford Ltd, London, pp.175-184.
- Tlemat H., Pilakoutas K. and Neocleous K. (2003b) Flexural Toughness of SFRC Made with Fibres Extracted from Tyres, in Recycling and Reuse of Waste Materials', *Proceedings of International Symposium on Advances in Waste Management and Recycling*, Dundee, September, 2003, Thomas Telford Ltd, London, pp. 365-374.
- Tlemat, H., Pilakoutas, K. and Neocleous, K. (2003c) *Concrete element design and testing, DTI partners in innovation project: Demonstrating steel fibres from waste tyres as reinforcement in concrete*, Technical report no CCC/03/0102C, Centre for Cement and Concrete, The University of Sheffield, UK. <<http://www.shef.ac.uk/tyre-recycling>>
- Tlemat, H., Pilakoutas, K. and Neocleous, K. (2004a) Stress-strain characteristic of SFRC using recycled fibres. *Materials and Structures*. Paper submitted in March 2004.
- Tlemat, H., Pilakoutas, K. and Neocleous, K. (2004b) Finite Element Analysis of SFRC. *Materials and Structures*. Paper submitted in April 2004.
- Tlemat, H., Pilakoutas K. and Neocleous, K. (2004c) Demonstrating Steel Fibres from waste Tyres as reinforcement in Concrete-Characteristics. *International Conference in Innovation Materials and Technologies for construction and Restoration*, Lecce, Italy, June 6-9 2004, ed. by A. La Tegola and A. Nanni, pub. by Linguori Editore, Vol.1, pp 172-185, ISBN 88-207-3678-8.
- Tlemat, H., Pilakoutas, K. and Neocleous, K. (2004d). Slurry infiltrated shredded fibre reinforced concrete (SIScon) for pre-cast applications. *Sixth International RILEM Symposium on Fibre Reinforcement Concrete (BEFIB 2004)*, 20-22 September 2004, Varenna-Lecco, Italy (Paper submitted in January 2004)
- Toutanji, H.A. and El-Korchi, T. (1994) Uniaxial Tensile Strength of Cementitious Composites. *Journal Testing and Evaluation, ASTM*, 22(3), pp. 226-232.
-

- Toutanji H.A. and Bayasi Z. (1998) Effects of manufacturing techniques on the flexural behaviour of steel fibre reinforced concrete. *Cement and Concrete Research*, 28(1), pp. 115-124.
- Trefil-Arbed (2003) *Fibre selection*. <<http://www.trefilarbed.com>>
- Tsartsari, A. (2001) *Optimisation of Ultra-high-strength Concrete using particle packing technology, super-calssified PFA and microsical*. MSc Thesis, University of Sheffield, UK.
- TWRC (2001) Thin wire reinforcement for concrete. British patent application no 130852.7 filed by the University of Sheffield on 24/12/01.
- Ulfjar, J., Krenk, S. and Brincker, R. (1995) Analytical model for fictitious crack propagation in concrete beam. *Journal of Engineering Mechanics, ASCE*, 121(1), pp. 7-15.
- UTWG (2001) *Fifth annual report of the used tyre working group*. Published in *used tyre working group's*, <<http://www.tyredisposal.co.uk>>
- UTWG (2003) *Tyre recycling companies*. Published in *used tyre working group's*, <<http://www.tyredisposal.co.uk>>
- Van Mier J.G.M., Stang H. and Ramakrishnan V. (1996) Practical structural applications of FRC and HPFRCC. *Proceedings of the second international RILEM workshop on high performance fiber reinforced cement composites*. pp. 450–459.
- Vandewalle L. (2003) Design with σ - ϵ method, Test and Design Methods for Steel Fibre Reinforced Concrete – Background and Experiences, *Proceedings of the RILEM TC 162 – TDF Workshop*, edited by B. Schnütgen and L. Vandewalle. Bochum, Germany: RILEM Publications S.A.R.L.
- Vandewalle L. and Dupont D. (2003) Bending Test and Interpretation, Test and Design Methods for Steel Fibre Reinforced Concrete – Background and Experiences, *Proceedings of the RILEM TC 162 – TDF Workshop*, edited by B. Schnütgen and L. Vandewalle. Bochum, Germany: RILEM Publications S.A.R.L.
- Wang, Y., Li, V. C. and Backer, S. (1987) Analysis of synthetic fibre pullout from a cement matrix. Symp. Proc., *Materials Research Society*, 114, pp. 159-165.
- Wang, Y., Li, V. C. and Backer, S. (1988) Modelling of fibre pull-out from a cement matrix, *The international journal of cement composites and light-weight concrete*, 10(3), pp. 143-149.
- Waste Guide (2003) *The stakeholders' guide to sustainable waste management*. The Environment Council, <<http://www.wasteonline.org.uk>>
- Wei S., Mandel J. and Said S. (1986) Study of the interface strength in steel fiber-reinforced-cement based composites. *Journal of the American Concrete Institute*, 83(4), pp. 597-605.

- Williams P.T., Bottrill R.P., Brindle A.J. and Cunliffe A. M. (2001) The potential of pyrolysis for recycling used tyres. *in* Thomas Telford *Proceedings of the international symposium on recycling and reuse of used tyres*, pp. 187–202.
- WS-2000 (2000) *Waste strategy 2000 for England and Wales. Report no 4693-1/2*, Department of the Environment, Transport and the Regions, London, pp. 199.
- Yang C.C., Mura T. and Shah S.P. (1991) Micromechanical theory and uniaxial tensile tests of fibre reinforced cement composites. *Journal of Material Research*, 6(11), pp. 2463-2473.

APPENDIX

APPENDIX A MIX OPTIMISATION

A.1 FRESH AND HARDENED PROPERTIES

Table A.1 Results of mix optimisation and hardened properties for the unnotched beams

Mix type	w/c ratio %	Aggregate mm	Fibre ratio % by weight	Fibre type	SP % by cement	Slump mm	Comp. (7d)	Comp. (28 d) MPa	First crack KN	I ₅	I ₁₀	I ₂₀
OPC40	0.52	<10	0.00	-	0.00	170	39.5	42.0	-	-	-	-
	"	"	0.75	SRSF	0.00	20	-	-	-	-	-	-
	"	"	1.00	SRSF	0.20	25	34.4	40.4	14.46	4.17	6.44	9.8
SPFA 40/30	0.46	<10	0.00	-	0.00	170	39.5	42.6	-	-	-	-
	"	"	1.00	SRSF	0.00	65	30.6	48.8	10.70	4.33	7.34	12.26
	"	"	1.50	SRSF	0.00	45	27.7	44.9	12.38	3.48	5.41	8.95
	"	"	1.50	SRSF	0.40	75	22.0	-	14.90	4.72	9.7	17.24
	"	"	1.50	Sieve SRSF	0.20	90	27.4	-	17.42	4.85	8.36	12.34
	"	"	1.50	PRSF	0.00	90	27.8	-	16.05	4.87	10.9	20.63
	"	"	1.50	ISF-1	0.00	100	26.1	-	14.33	5.69	11.9	24.2
OPC 50	0.45	<20	0.00	-	-	-	41.7	52.5	12.50	1.93	-	-
	"	"	1.00	SRSF	-	-	-	38.3	15.00	4.98	9.95	17.87
	"	"	1.50	SRSF	-	-	-	40.8	-	-	-	-
	"	"	2.00	SRSF	-	-	-	43.0	14.80	4.84	9.08	19.11
	"	"	1.00	PRSF	0.08	75	44.1	55.7	16.00	4.64	8.34	16.73
	"	"	2.00	PRSF	-	-	41.0	51.7	20.00	5.12	9.94	18.67
	"	"	4.00	PRSF	0.60	35	-	-	-	-	-	-
	"	"	5.00	PRSF	1.00	-	-	-	-	4.91	8.87	15.1
	"	"	5.50	PRSF	1.00	60	-	-	-	-	-	-
	"	"	6.00	PRSF	1.00	40	-	-	34.00	4.94	8.69	15.08
"	"	2.00	ISF-1	-	-	-	-	15.00	-	-	-	

Table A.2 Concrete mix used in notched beam and slab tests

Fibre type	Fibre ratio [% by weight]	Mix proportions for mix code SP 40/30 [kg/m ³]											Water reduced [%]		
		OPC	Fibre	SP	Cement	W	W/B	W/C	Aggregates					Total Mass	Total Volume
									20mm	10mm	Sand	Total			
Plain	-	236	-	101	94	155	0.46	0.66	690	345	865	1900	2392	1000	0.10
PRSF	1.5	236	36.21	101	94	155	0.46	0.66	690	345	851	1886	2414	1000	0.30
	3.0	236	73.1	101	94	155	0.46	0.66	690	345	837	1872	2437	1000	0.40
	6.0	236	148.9	101	94	155	0.46	0.66	690	345	807	1842	2483	1000	0.75
VSF	1.5	236	36.24	101	94	155	0.46	0.66	690	345	853	1888	2416	1000	0.30
	3.0	236	73.2	101	94	155	0.46	0.66	690	345	841	1876	2441	1000	0.40
	6.0	236	149.5	101	94	155	0.46	0.66	690	345	815	1850	2492	1000	0.75
ISF-1	6.0	236	149.5	101	94	155	0.46	0.66	690	345	815	1850	2492	1000	0.75
ISF-2	6.0	236	149.5	101	94	155	0.46	0.66	690	345	815	1850	2492	1000	0.75
SRSF	0.5	236	12.0	101	94	155	0.46	0.66	-	1035	860	1895	2399	1000	0.30
	1.0	236	24.1	101	94	155	0.46	0.66	-	1035	8.55	1890	2406	1000	0.50
	2.0	236	48.4	101	94	155	0.46	0.66	-	1035	844	1879	2420	1000	0.75

APPENDIX B PULL-OUT TESTS

B.1 DATA FROM PULL-OUT TESTS

Table B1 Pull-out response for single-sided pull-out tests using load spring

PESF code	Fibres [%]	Length l [mm]	Diameter d [mm]	Slip (mm) s [mm]	Peak load [N]	Bond t [MPa]	Tensile σ [MPa]
A5-10-2%	2%	10	0.96	0.96	179.6	5.95	248.1
A3-10-2%	2%	10	1.01	4.38	191.7	6.00	239.4
A2-10-2%	2%	10	1.04	4.18	189.5	5.80	223.1
A6-10-2%	2%	10	1.10	0.56	214	6.20	225.6
A7-10-2%	2%	10	1.10	0.64	290.7	8.40	305.9
A4-10-2%	2%	10	1.11	0.77	291.4	8.36	301.2
A4-20-2%	2%	10	1.24	0.61	335.8	8.57	276.4
Average			1.08	1.73	241.81	7.04	259.96
A6-20-2%	2%	20	0.88	0.56	369.1	6.67	607.0
A1-20-2%	2%	20	0.97	0.78	372.9	6.20	504.7
A1-10-2%	2%	20	1.04	1.08	366	5.60	430.8
A2-20-2%	2%	20	1.10	0.77	440.9	6.38	464.1
A5-20-2%	2%	20	1.19	1.54	455.9	6.09	410.0
A3-20-2%	2%	20	1.20	0.66	662.8	8.79	585.3
A3-30-2%	2%	20	1.38	2.30	677.5	7.81	452.9
A7-30-2%	2%	20	1.51	1.11	737.8	7.81	417.0
A6-30-2%	2%	20	1.55	1.08	825	8.47	437.2
Average			1.20	1.10	545.32	7.09	478.78
A9-30-2%	2%	30	1.05	5.24	776.3	7.84	896.5
A5-30-2%	2%	30	1.09	0.69	567.5	5.52	608.2
A2-30-2%	2%	30	1.09	1.87	1030.5	10.03	1104.4
A1-30-2%	2%	30	1.33	0.45	1733	13.80	1501.3
A4-30-2%	2%	30	1.33	1.12	876.3	7.00	630.7
Average			1.18	1.87	996.72	8.84	948.22

Table B2 Pull-out response for single-sided pull-out tests using load spring, (SRSF)

SRSF	Fibres	Length	Diameter	Aspect	Slip (mm)	Peak load	Bond	Tensile
code	[%]	l [mm]	d [mm]	ratio l/d	s [mm]	[N]	t [MPa]	σ [MPa]
S5-10-1%	1%	10	0.15	66.67	2.17	17.35	3.68	982.1
S7-10-1%	1%	10	0.20	50.00	1.69	14.8	2.36	471.3
S1-10-1%	1%	10	0.20	50.00	1.09	25.36	4.04	807.4
S6-10-1%	1%	10	0.30	33.33	4.04	97.22	10.30	1375.4
S2-10-1%	1%	10	0.30	33.33	2.15	95.65	10.15	1353.2
S3-10-1%	1%	10	0.35	28.57	1.83	79.62	7.24	827.6
S4-10-1%	1%	10	0.35	28.57	0.63	12.45	1.13	129.4
Average			0.26	41.50	1.94	48.92	5.56	849.49
S4-20-0.5%	0.5%	20	0.35	57.14	1.69	45.3	2.06	470.6
S1-20-2%	2%	20	0.35	57.14	1.65	46.2	2.10	480.5
S3-20-2%	2%	20	0.35	57.14	1.91	101.2	4.60	1051.7
S8-20-2%	2%	20	0.35	57.14	0.72	29.5	1.34	306.5
S10-20-2%	2%	20	0.35	57.14	0.71	29.5	1.30	306.5
S13-20-2%	2%	20	0.31	64.52	1.54	57.8	2.97	766.2
S6-20-0.5%	0.5%	20	0.30	66.67	1.25	49	2.30	692.9
S3-20-0.5%	0.5%	20	0.30	66.67	2.03	103.8	5.51	1469.2
S2-20-2%	2%	20	0.30	66.67	4.86	27.4	1.46	388.1
S5-20-2%	2%	20	0.30	66.67	6.33	67.4	3.57	953.2
S7-20-2%	2%	20	0.30	66.67	1.37	75.3	4.00	1064.7
S9-20-2%	2%	20	0.30	66.67	1.64	33.79	1.80	478.0
S11-20-2%	2%	20	0.30	66.67	2.36	74.09	3.90	1050.2
S14-20-2%	2%	20	0.30	66.67	1.16	15.7	0.83	222.0
S1-20-0.5%	0.5%	20	0.25	80.00	1.25	40.36	2.57	822.3
S5-20-0.5%	0.5%	20	0.25	80.00	1.41	42.1	2.67	857.6
S4-20-2%	2%	20	0.25	80.00	1.37	15.2	0.97	309.5
S12-20-2%	2%	20	0.25	80.00	2.31	84.8	5.40	1728.2
S15-20-2%	2%	20	0.25	80.00	3.83	11.8	0.75	241.0
S7-20-0.5%	0.5%	20	0.20	100.00	1.73	33.6	2.67	1069.1
S6-20-2%	2%	20	0.20	100.00	2.06	57	4.53	1813.8
S16-20-2%	2%	20	0.20	100.00	0.71	37.4	3.00	1200.7
Average			0.29	71.98	2.00	49.01	2.74	908.48
S1-25-2%	2%	25	0.35	71.43	2.56	128.3	4.67	1333.1
S2-25-2%	2%	25	0.35	71.43	2.14	70.4	2.56	731.6
S3-25-2%	2%	25	0.35	71.43	2.34	219.7	8.00	2283.7
S4-25-2%	2%	25	0.35	71.43	1.27	122.1	4.44	1268.6
S5-25-2%	2%	25	0.35	71.43	2.16	102.4	3.73	1064.4
S7-25-2%	2%	25	0.30	83.33	4.13	219.8	9.33	3110.2
S9-25-2%	2%	25	0.30	83.33	1.07	70.6	3.00	999.2
S6-25-2%	2%	25	0.20	125.00	3.16	87.88	5.60	2797.3
S8-25-2%	2%	25	0.20	125.00	2.10	99.1	6.31	3155.8
Average			0.29	90.14	2.32	131.65	5.77	2097.03
S6-30-1%	1%	30	0.60	50.00	1.91	201.4	3.56	712.3
S4-30-1%	1%	30	0.35	85.71	1.73	234.6	7.11	2437.9
S5-30-1%	1%	30	0.35	85.71	0.79	297.2	9.00	3088.7
S11-30-1%	1%	30	0.35	85.71	2.91	221.1	6.70	2297.4
S2-30-1%	1%	30	0.30	100.00	2.47	231.4	7.01	2405.0
S3-30-1%	1%	30	0.30	100.00	2.10	133.4	4.72	1886.5
S10-30-1%	1%	30	0.30	100.00	1.72	155.7	5.51	2202.8
S1-30-1%	1%	30	0.20	150.00	0.76	90.5	4.80	2879.8
S7-30-1%	1%	30	0.20	150.00	1.55	88.7	4.71	2824.9
S8-30-1%	1%	30	0.15	200.00	0.62	43.3	3.06	2448.0
S9-30-1%	1%	30	0.15	200.00	0.90	61.5	4.35	3480.8
Average			0.30	118.83	1.59	159.89	5.50	2424.01

Appendix

Table B3 Pull-out response for single-sided pull-out tests using load spring, (ISF-1)

ISF-1 code	Fibre ratio [%]	Length l [mm]	Diameter d [mm]	Aspect ratio l/d	Slip (mm) s [mm]	Peak load [N]	Bond t [MPa]	Tensile σ [MPa]
I3-10-2%	2%	10	1.00	10.00	1.52	361.6	11.51	460.4
I2-10-2%	2%	10	1.00	10.00	2.15	391	12.40	497.8
I1-10-2%	2%	10	1.00	10.00	2.45	416	13.24	530.0
Average			1.00	10.00	2.04	389.53	12.38	496.07
I2-20-2%	2%	20	1.00	20.00	4.08	534.7	8.50	680.8
I3-20-2%	2%	20	1.00	20.00	3.29	673.9	10.72	858.1
I1-20-2%	2%	20	1.00	20.00	4.35	528.3	8.40	672.6
Average			1.00	20.00	3.91	578.97	9.21	737.17
I2-30-2%	2%	30	1.00	30.00	3.71	724.6	7.69	922.6
I3-30-2%	2%	30	1.00	30.00	6.95	722.1	7.66	919.4
I1-30-2%	2%	30	1.00	30.00	8.75	793	8.41	1009.7
Average			1.00	30.00	6.47	757.55	8.04	964.55

Table B4 Pull-out response for Double-sided tests, (ISF-1)

ISF-1 code	Length l [mm]	Diameter d [mm]	Aspect ratio l/d	Slip (mm) s [mm]	Peak load [N]	Bond t [MPa]	Tensile σ [MPa]
I1-10-1	10	1.00	10.00	3.88	310	9.87	394.7
I1-10-2	10	1.00	10.00	4.48	208	6.62	264.8
I1-30-1	10	1.00	10.00	5.06	176	5.60	224.1
I1-30-2	10	1.00	10.00	4.90	181	5.76	230.5
Average			10.00	4.47	231.33	7.36	294.54
I1-20-1	20	1.00	20.00	The data was not converted			
I-20-2	20	1.00	20.00	10.60	370	5.89	471.1
Average			20.00	10.60	370	5.89	471.10

Table B5 Pull-out response for Double-sided tests, (one PRSF)

PRSF code	Length l [mm]	Diameter d [mm]	effective d d(eff) [mm]	Aspect ratio l/d	Aspect ratio l/d(eff)	Slip (mm) s [mm]	Peak load [N]	Bond t [MPa]	Tensile σ [MPa]
A1-10-1	10	1.55	1.19	6.45	8.42	4.39	316	6.49	285.2
A1-20-1	10	1.55	1.19	6.45	8.42	1.01	118	2.42	106.5
Average				8.60	8.42	2.50	335	4.46	195.82
A1-20-1	20	1.55	1.19	12.90	16.84	0.75	600	6.16	541.4
A1-20-2	20	1.55	1.19	12.90	16.84	2.10	570	5.85	514.4
Average				12.90	16.84	0.75	600	6.01	527.90
A1-30-1	30	1.55	1.19	19.35	25.26	1.05	614	4.20	554.1
A1-30-2	30	1.55	1.19	19.35	25.26	1.83	692	4.74	624.5
Average				19.35	25.26	1.44	653	4.47	589.26

Appendix

Table B6 Pull-out response for Double-sided tests, (three PRSF)

PRSF code	Length l [mm]	Diameter d [mm]	effective d [mm]	Aspect ratio		Slip s [mm]	Peak load [N]		Bond t [MPa]	Tensile σ [MPa]
				l/d (eff)	ratio l/d		Single			
A3-10-1	10	1.55	1.19	6.45	8.42	0.94	980	327	6.71	294.8
A3-10-2	10	1.55	1.19	6.45	8.42	0.55	620	207	4.24	186.5
Average				6.45	8.42	0.75	800	267	5.48	240.64
A3-20-1	20	1.55	1.19	12.90	16.84	1.39	1480	493	5.07	445.2
A3-20-2	20	1.55	1.19	12.90	16.84	1.76	1800	600	6.16	541.4
Average				12.90	16.84	1.58	1640	547	5.61	493.31
A3-30-1	30	1.55	1.19	19.35	25.26	0.18	1920	640	4.38	577.5
A3-30-2	30	1.55	1.19	19.35	25.26	0.19	2110	703	4.81	634.7
Average				19.35	25.26	0.19	2015	672	4.60	634.68

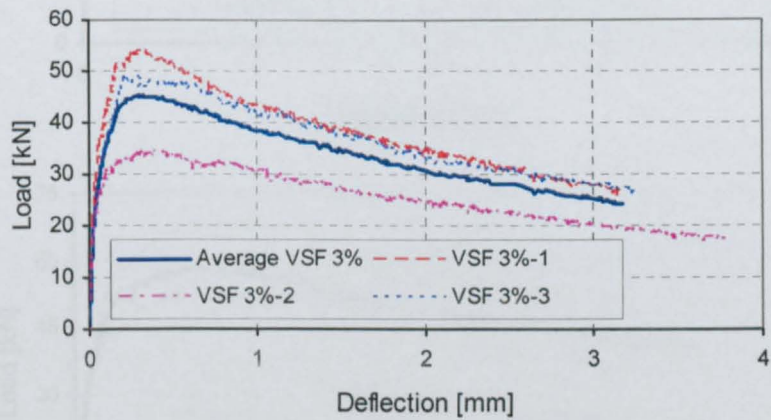
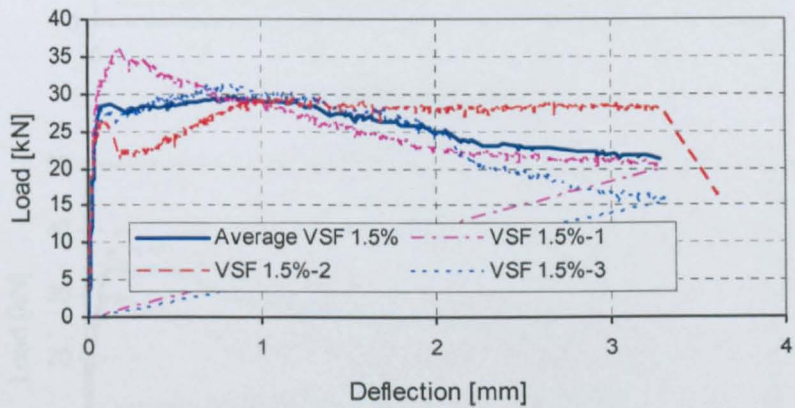
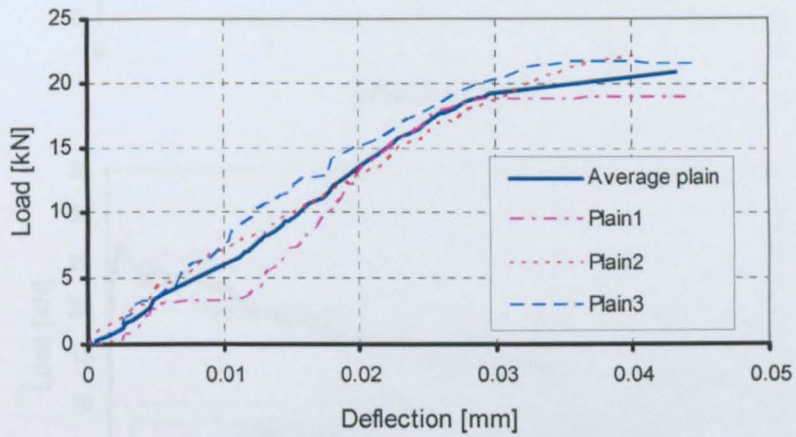
Table B7 Pull-out response for Double-sided tests, (one PRSF with a blob)

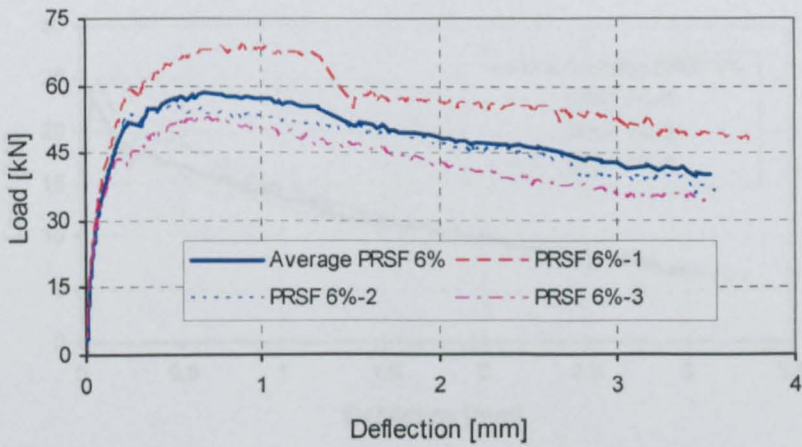
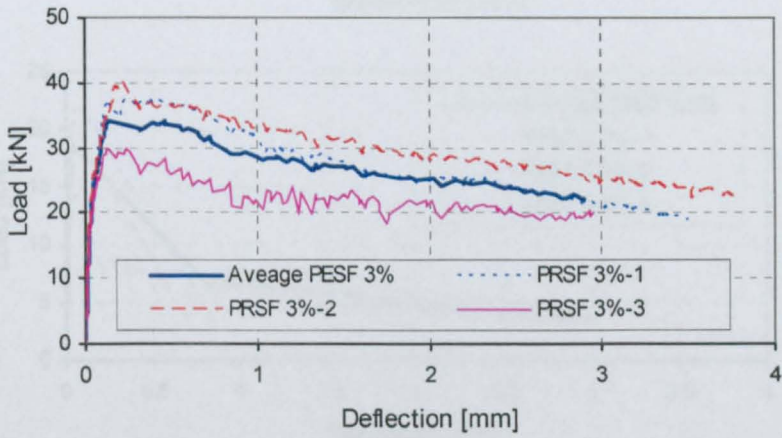
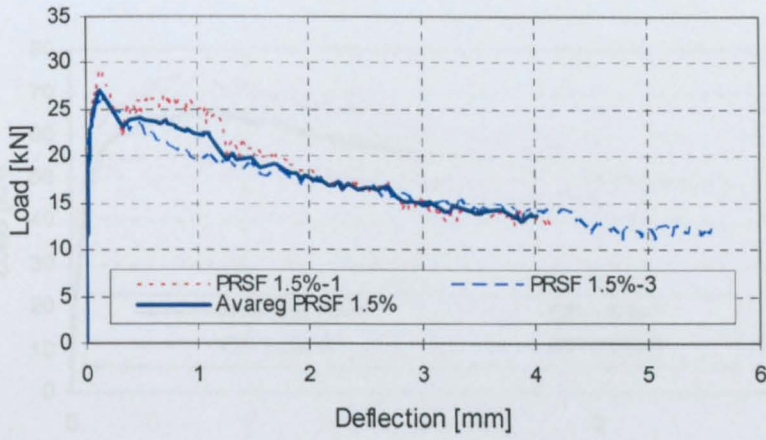
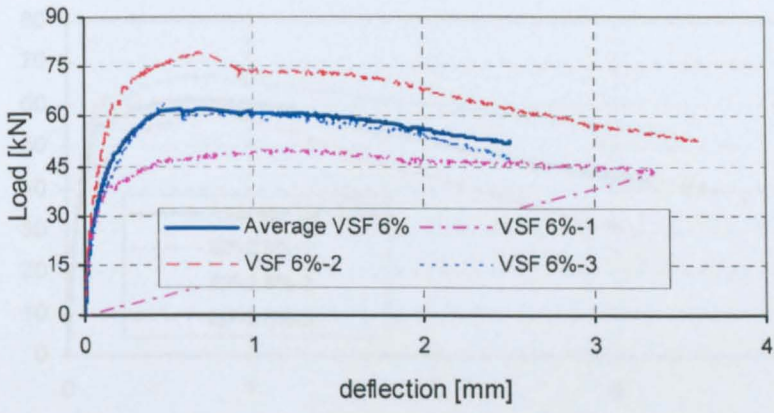
PRSF fibres	Length l [mm]	Diameter d [mm]	effective d [mm]	Aspect ratio		Slip s [mm]	Peak load [N]	d (cone) [mm]	Bond t [MPa]	Tensile σ [MPa]
				l/d (eff)	l/d					
A1-10-1d	10	1.55	1.19	6.45	8.42	0.60	1139	2.54	23.39	1027.8*
A1-10-2d	10	1.55	1.19	6.45	8.42	0.55	610	2.54	12.53	550.5*
Average				6.45	8.42	0.58	875	2.54	17.96	789.14
A1-20-1d	20	1.55	1.19	12.90	16.84	1.53	1290	2.87	13.25	1164.1*
A1-20-2d	20	1.55	1.19	12.90	16.84	problem with the clamp		2.03		
Average				12.90	16.84	1.53	1290	2.45		
A1-30-1d	30	1.55	1.19	19.35	25.26	0.96	1180	3.88	8.08	1064.8*
A1-30-2	30	1.55	1.19	19.35	25.26	0.69	1570	2.94	10.75	1416.8*
Average				19.35	25.26	0.83	1375	3.41	9.41	1240.79

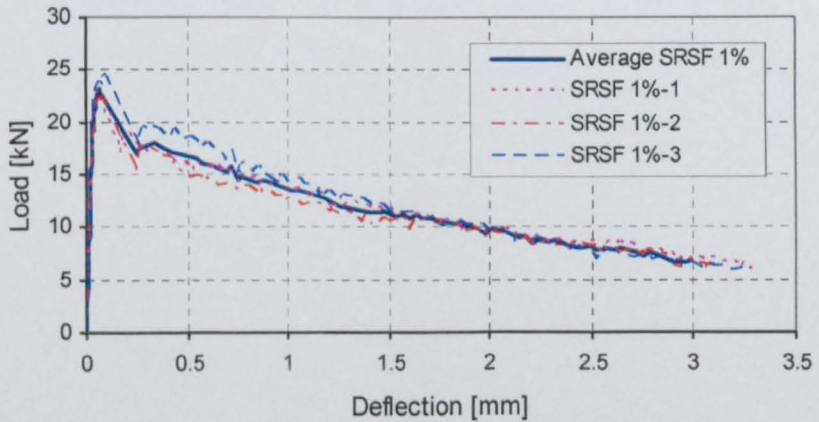
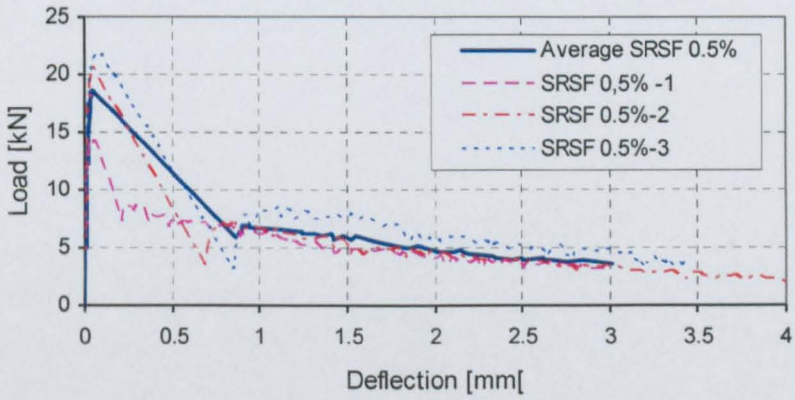
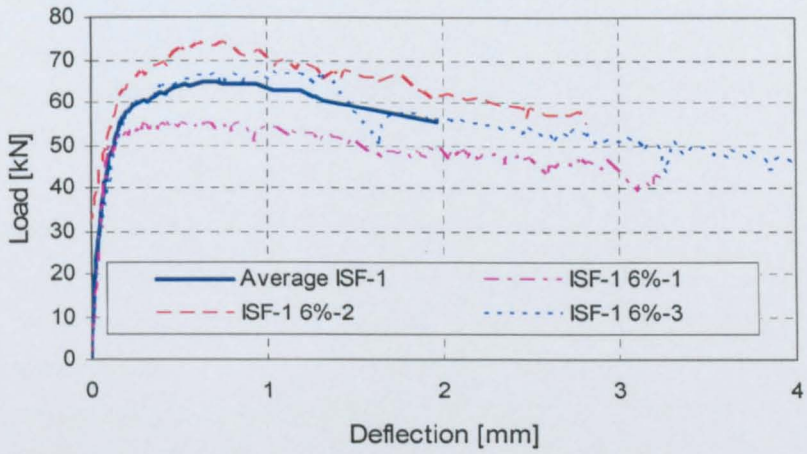
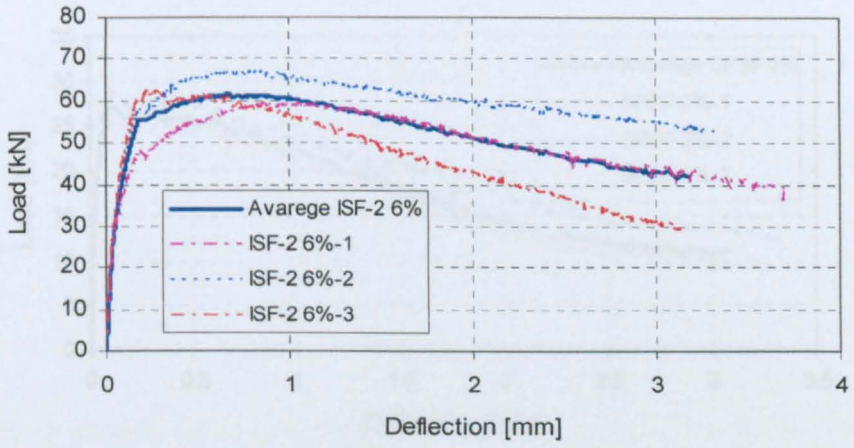
*The blob was broken

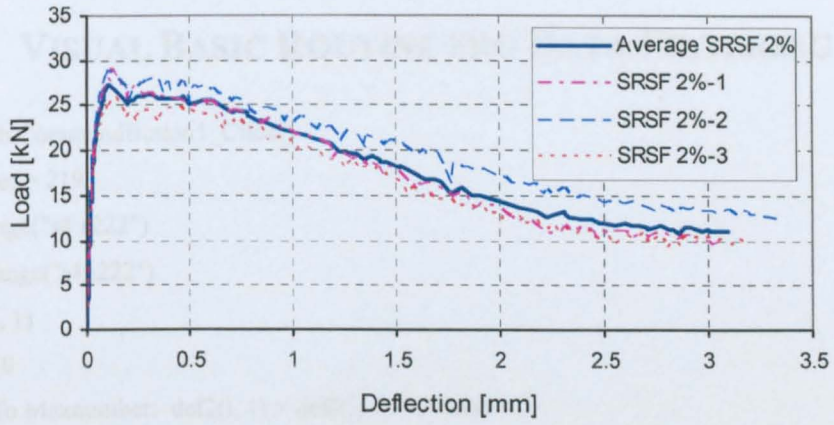
APPENDIX C FLEXURAL TOUGHNESS TESTS

C.1 LOAD-DEFLECTION RESPONSES OF THE NOTCHED BEAM TESTS









```

For i = 1 To MaxNumber - def(2) - 1
    For j = 1 To MaxNumber - def(2) - 1
        k = 1
        While (def(2), i) <= def(2) - 1, i)
            def(2), i) = 0
            k = k + 1
            If k > MaxNumber Then Goto Nextj
        Wend
        level2:
        CountX = CountX + (k - 1)
        If CountX > MaxNumber - def(2) - 1 Then Goto Nextj
        For j = 1 To MaxNumber - def(2) - 1
            def(2), i) = def(2) - (k - 1) * i
            level(2), i) = level(2) + (k - 1) * i
        Nextj
    Nexti
    level3:
    For j = 1 To i - 1
        Show("row", Cells(2, 2) = def(2))
        Show("row", Cells(2, 3) = level(2))
    Nextj
    Show("row", Cells(3, 2) = "def")
    Show("row", Cells(3, 3) = "Load")
End Sub
    
```

C.2 VISUAL BASIC ROUTINE FRO DATA FILTERING

```
Private Sub CommandButton1_Click()
Maxnumber = 219
def2 = Range("s4:s222")
load1 = Range("j4:j222")
c = def2(1, 1)
CountX = 0
For i = 1 To Maxnumber: def2(i, 1) = def2(i, 1) - c: Next
For i = 2 To Maxnumber
k = i
While (def2(k, 1) <= def2(i - 1, 1))
def2(k, 1) = 0
k = k + 1
If k > Maxnumber Then GoTo level2
Wend
level2:
CountX = CountX + (k - i)
If CountX > (Maxnumber - i) Then GoTo level3:
For j = i To Maxnumber - (k - i)
def2(j, 1) = def2(j + (k - i), 1)
load1(j, 1) = load1(j + (k - i), 1)
Next j
Next i
level3:
For j = 1 To i - 1
Sheets("real").Cells(j + 3, 2) = def2(j, 1)
Sheets("real").Cells(j + 3, 1) = load1(j, 1)
Next j
Sheets("real").Cells(3, 2) = "def2"
Sheets("real").Cells(3, 1) = "Load"
End Sub
```

C.3 VISUAL BASIC ROUTINE TO CALCULATED THE AVERAGE OF THREE CURVES

```
Private Sub CommandButton1_Click()
Dim load(1500)
Dim def(1500)
numberoftest = 3
' change only maximum number (number of nodes) and tol
maxnumber = 1035
tol = Cells(1, 11)
Range("N1:O999").ClearContents
For i = 1 To numberoftest
  For j = 2 To maxnumber + 1
    Cells(j - 1 + (i - 1) * maxnumber, 16) = Cells(j, 2 * i)
    Cells(j - 1 + (i - 1) * maxnumber, 17) = Cells(j, 2 * i - 1)
    Cells(j - 1 + (i - 1) * maxnumber, 18) = i
  Next
Next
Range(Cells(1, 16), Cells(maxnumber * numberoftest, 18)).Select
Selection.Sort Key1:=Cells(1, 16), Order1:=xlAscending, Header:=xlGuess, _
  OrderCustom:=1, MatchCase:=False, Orientation:=xlTopToBottom, _
  DataOption1:=xlSortNormal
countx = 1
For i = 2 To maxnumber * numberoftest - 1
  If (Abs(Cells(i, 16) - Cells(i - 1, 16)) < tol) And (Abs(Cells(i, 16) - Cells(i + 1, 16)) < tol) Then
    If (Cells(i, 18) + Cells(i - 1, 18) + Cells(i + 1, 18) = 6) And (Cells(i, 18) * Cells(i - 1, 18) * Cells(i + 1, 18) = 6) Then
      def(countx) = (Cells(i, 16) + Cells(i - 1, 16) + Cells(i + 1, 16)) / 3
      load(countx) = (Cells(i, 17) + Cells(i - 1, 17) + Cells(i + 1, 17)) / 3
      countx = countx + 1
    End If
  End If
Next
For i = 1 To countx
  Cells(i, 14) = def(i)
  Cells(i, 15) = load(i)
Next
End Sub
```

C.4 RESULTS OF COMPRESSIVE TESTS FOR NOTCHED BEAMS

Mix type	fibre ratio % by weight	$f_{cm,cube}$ MPa	ave $f_{cm,cube}$ MPa	$f_{cm,cyl}$ MPa	E_{cm} MPa	$f_{ck,cyl}$ MPa
Plain	0	49.8	51.3	43.6	35253	35.6
		54.5				
		49.6				
ISF-1	6%	50.5	52.9	45.0	35615	37.0
		56				
		51.3				
	1.50%	53.8	44.0	37.4	33496	29.4
		45.5				
		44.5				
PESF	3%	42.7	38.6	32.8	32067	24.8
		43.3				
		38.3				
	6%	39.2	50.0	42.5	34953	34.5
		50.6				
		49.6				
SRSF	0.50%	49.8	49.4	41.9	34801	33.9
		47				
		49.9				
	1.0%	46.6	50.0	42.5	34953	34.5
		53.9				
		48.4				
2%	53.1	44.7	38.0	33681	30.0	
	47.4					
	51.1					
VSF	1.5%	49.1	54.2	46.0	35897	38.0
		41.4				
		43.7				
	3%	44.4	62.1	52.8	37562	44.8
		55				
		54.3				
6%	53.2	66.2	56.3	38382	48.3	
	64.3					
	58.6					
ISF-2	6%	63.3	63.9	54.3	37928	46.3
		64.5				
		75.3				
		61				
		64.1				
		67.3				
		63.5				
		63.5				

APPENDIX D FE ANALYSIS

D.1 RESULTS OF THE FE ANALYSIS

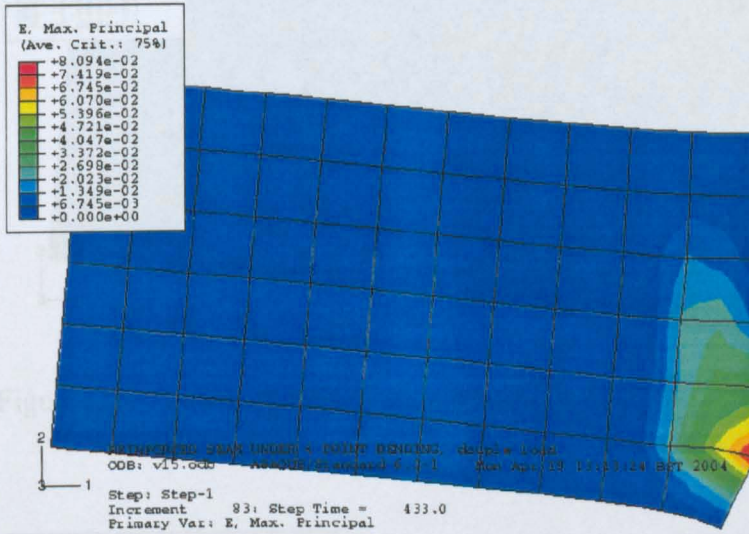


Figure D1 Maximal principal strain distribution for VSF 1.5%

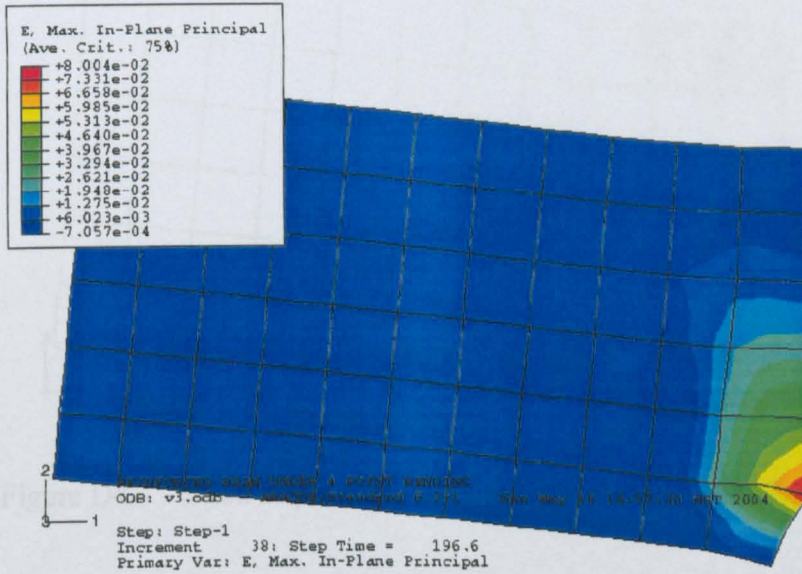


Figure D2 Max. principal strain distribution for VSF 3%

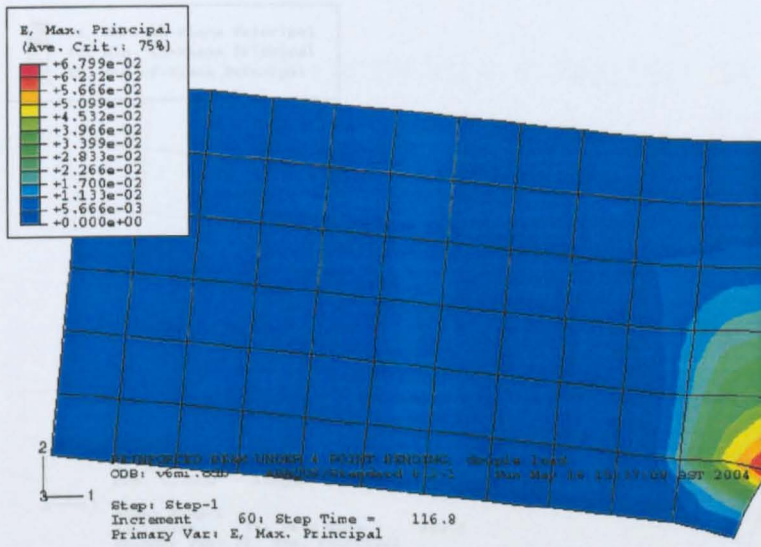


Figure D3 Max. principal strain distribution for VSF 6%

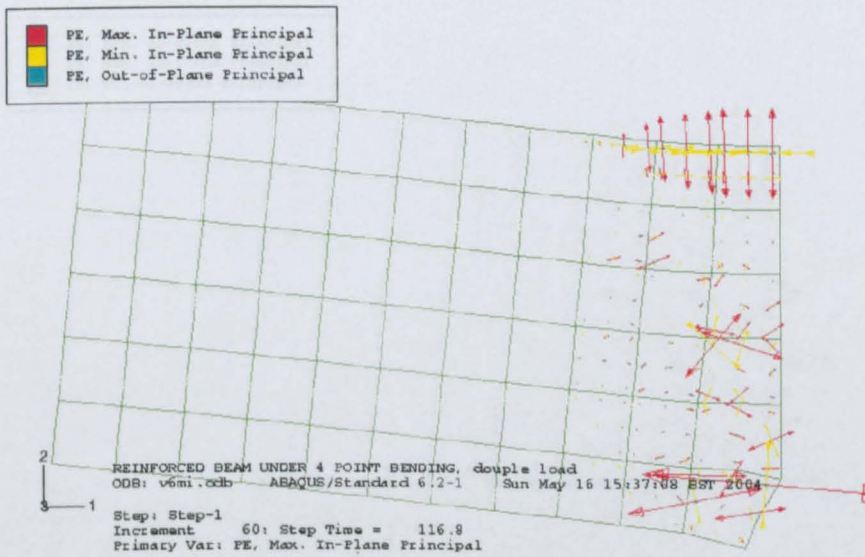


Figure D4 Max. in-plane principal plastic strain distribution for VSF 6%

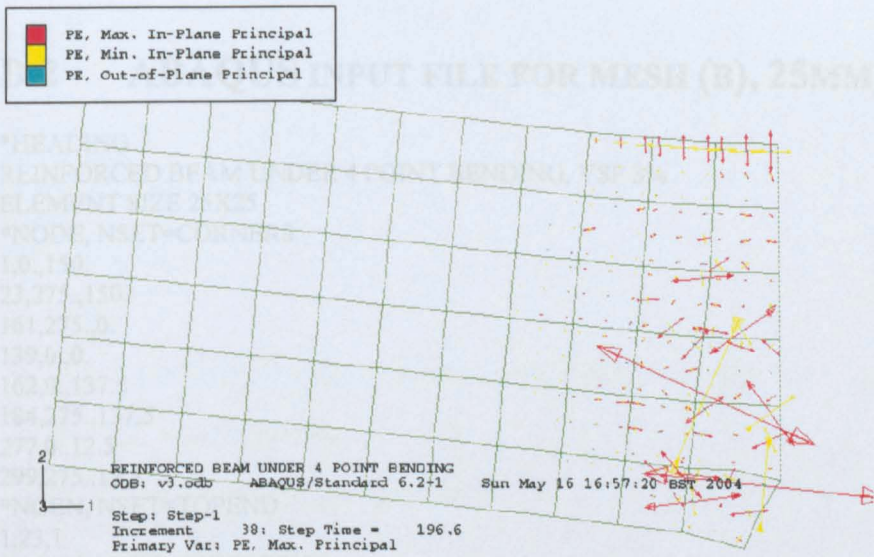


Figure D5 Max. in-plane principal plastic strain distribution for VSF 3.0%

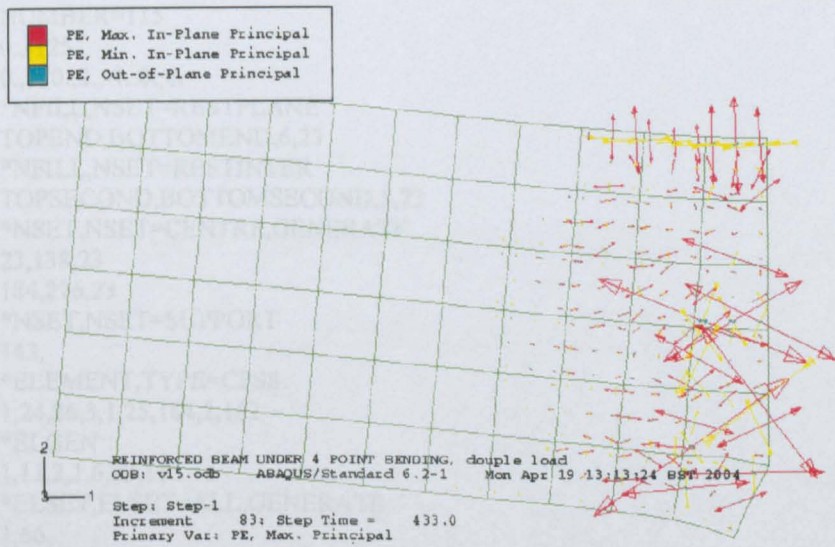


Figure D6 Max. in-plane principal plastic strain distribution for VSF 1.5%

D.2 ABAQUS INPUT FILE FOR MESH (B), 25MM

```
*HEADING
REINFORCED BEAM UNDER 4 POINT BENDING, VSF 3%
ELEMENT SIZE 25X25
*NODE, NSET=CORNERS
1,0.,150.
23,275.,150.
161,275.,0.
139,0.,0.
162,0.,137.5
184,275.,137.5
277,0.,12.5
299,275.,12.5
*NGEN, NSET=TOPEND
1,23,1
*NGEN, NSET=TOPSECOND
162,184,1
*NCOPY,SHIFT, OLDSET= TOPEND, NEWSET= BOTTOMEND,CHANGE NUMBER= 138
0.,-150.
0.,1.,0.,0.,-1.,0.,0.
*NCOPY,SHIFT, OLDSET= TOPSECOND, NEWSET= BOTTOMSECOND,CHANGE
NUMBER=115
0.,-125.
0.,1.,0.,0.,-1.,0.,0.
*NFILL,NSET=RESTPLANE
TOPEND,BOTTOMEND,6,23
*NFILL,NSET=RESTINTER
TOPSECOND,BOTTOMSECOND,5,23
*NSET,NSET=CENTRE,GENERATE
23,138,23
184,276,23
*NSET,NSET=SUPPORT
143,
*ELEMENT,TYPE=CPS8
1,24,26,3,1,25,164,2,162
*ELGEN
1,11,2,1,6,23,11
*ELSET,ELSET=ALL,GENERATE
1,66
*SOLID SECTION, ELSET=ALL, MATERIAL=FIBRECON
150.
*MATERIAL,NAME=FIBRECON
*ELASTIC
36297.,0.2
*CONCRETE
19.5,0.
25.8,.0002
31.1,.0004
35.6,.0006
39.2,.0008
41.9,.001
43.7,.0012
44.7,.0015
*FAILURE RATIOS
1.15,.095
*TENSION STIFFENING, TYPE=STRAIN
1.,0.
```

```

.7,.001
.33,.01
.05,.025
.0,.05
*BOUNDARY
SUPPORT,2
CENTRE,1
*STEP
*STATIC,RIKS
0.05,1,,,,,138,2,-3.
*CLOAD
17,2,-4000.
*EL PRINT, POSITION=AVERAGED AT NODES, SUMMARY=YES
S11,E11
*NODE FILE, NSET=CENTRE
U,CF,RF
*OUTPUT,FIELD,VARIABLE=PRESELECT
*ELEMENT OUTPUT
*OUTPUT,HISTORY
*NODE OUTPUT, NSET=SUPPORT
RF2
*NODE OUTPUT,NSET=CENTRE
U2
*ELEMENT OUTPUT, ELSET=ALL
E11, S11
*END STEP

```

D.3 CRITICAL LENGTHS

Table D3.1 Critical lengths of tested notched beams

Fibre type	Fibre ratio	A_{oe} [N/mm ²]	A_F [Nmm x 10 ⁻³]	G_{F2} [N/mm]	l_c [mm]	Average l_c [mm]
VSF	1.5	0.032	58.4	2.28	68.7	
	3.0	0.061	103.7	4.05	64.3	
	6.0	0.080	141.3	5.52	66.9	
PRSF	1.5	0.030	57.8	2.26	72.4	69.0
	3.0	0.043	81.1	3.17	71.7	
	6.0	0.077	135.6	5.30	66.6	
ISF-1	6.0	0.087	160.5	6.27	69.7	
ISF-2	6.0	0.083	158.3	6.19	72.3	
SRSF	0.5	0.013	21.4	0.84	58.8	65.0
	1.0	0.021	35.9	1.40	64.7	
	2.0	0.028	54.6	2.13	71.8	

D.4 ABAQUS INPUT FILE FOR MESH (C), 12.5 MM

```
*HEADING
REINFORCED BEAM UNDER 4 POINT BENDING, 1.5% VSF
ELEMENT SIZE 12.5X12.5
*NODE, NSET=CORNERS
101,0.,150.
145,275.,150.
1345,275.,0.
1301,0.,0.
1446,0.,143.75
1490,275.,143.75
2546,0.,6.25
2590,275.,6.25
*NGEN, NSET=TOPEND
101,145,1
*NGEN, NSET=TOPSECOND
1446,1490,1
*NCOPY,SHIFT, OLDSET= TOPEND, NEWSET= BOTTOMEND,CHANGE NUMBER= 1200
0.,-150.
0.,1.,0.,0.,-1.,0.,0.
*NCOPY,SHIFT, OLDSET= TOPSECOND, NEWSET= BOTTOMSECOND,CHANGE
NUMBER=1100
0.,-137.5
0.,1.,0.,0.,-1.,0.,0.
*NFILL,NSET=RESTPLANE
TOPEND,BOTTOMEND,12,100
*NFILL,NSET=RESTINTER
TOPSECOND,BOTTOMSECOND,11,100
*NSET,NSET=CENTRE,GENERATE
145,1145,100
1490,2390,100
*NSET,NSET=SUPPORT
1309,
*ELEMENT,TYPE=CPS8
1,201,203,103,101,202,1448,102,1446
*ELGEN
1,22,2,1,12,100,22
*ELSET,ELSET=ALL,GENERATE
1,264
*SOLID SECTION, ELSET=ALL, MATERIAL=FIBRECON
150.
*MATERIAL,NAME=FIBRECON
*ELASTIC
36297.,0.2
*CONCRETE
19.5,0.
25.8,.0002
31.1,.0004
35.6,.0006
39.2,.0008
41.9,.001
43.7,.0012
44.7,.0015
*FAILURE RATIOS
1.15,.07
*TENSION STIFFENING, TYPE=STRAIN
1.,0.
```

Appendix

.57,.003
.5,.015
.2,.0375
*BOUNDARY
SUPPORT,2
CENTRE,1
*STEP
*STATIC,RIKS
0.05,1,,,,,1145,2,-3.
*CLOAD
133,2,-4000.
*EL PRINT, POSITION=AVERAGED AT NODES, SUMMARY=YES
S11,E11
*NODE FILE, NSET=CENTRE
U,CF,RF
*OUTPUT,FIELD,VARIABLE=PRESELECT
*ELEMENT OUTPUT
*OUTPUT,HISTORY
*NODE OUTPUT, NSET=SUPPORT
RF2
*NODE OUTPUT,NSET=CENTRE
U2
*ELEMENT OUTPUT, ELSET=ALL
E11, S11
*END STEP

D.5 ABAQUS INPUT FILE FOR MESH (A), 50MM

```
*HEADING
REINFORCED BEAM UNDER 4 POINT BENDING, 15% VSF
ELEMENT SIZE 50X50
*NODE, NSET=LEFTTOP
1,0.,150.
2,12.5,150.
14,0.,100.
15,12.5,100.
27,0.,50.
28,12.5,50.
40,0.,0.
41,12.5,0.
*NODE, NSET=LEFTSECOND
53,0.,125.
54,12.5,125.
66,0.,75.
67,12.5,75.
79,0.,25.
80,12.5,25
*NODE, NSET=RIGHT
3,25.,150.
55,25.,125.
81,25.,25.
42,25.,0.
13,275.,150.
65,275.,125.
91,275.,25.
52,275.,0.
*NGEN, NSET=TOPRIGHT
3,13,1
*NGEN, NSET=TOPSECOND
55,65,1
*NCOPY,SHIFT, OLDSET= TOPRIGHT, NEWSET= BOTTOMRIGHT,CHANGE NUMBER= 39
0.,-150.
0.,1.,0.,0.,-1.,0.,0.
*NCOPY,SHIFT, OLDSET= TOPSECOND, NEWSET= BOTTOMSECOND,CHANGE
NUMBER=26
0.,-100.
0.,1.,0.,0.,-1.,0.,0.
*NFILL,NSET=RESTPLANE
TOPRIGHT,BOTTOMRIGHT,3,13
*NFILL,NSET=RESTINTER
TOPSECOND,BOTTOMSECOND,2,13
*NSET,NSET=CENTRE
13,26,39,65,78,91
*NSET,NSET=SUPPORT
43
*ELEMENT,TYPE=CPS8
1,14,16,3,1,15,55,2,53
2,27,29,16,14,28,68,15,66
3,40,42,29,27,41,81,28,79
4,16,18,5,3,17,57,4,55
*ELGEN
4,5,2,1,3,13,5
*ELSET,ELSET=ALL,GENERATE
1,18
```

Appendix

```
*SOLID SECTION, ELSET=ALL, MATERIAL=FIBRECON
150.
*MATERIAL,NAME=FIBRECON
*ELASTIC
36297.,0.2
*CONCRETE
19.5,0.
25.8,,0002
31.1,,0004
35.6,,0006
39.2,,0008
41.9,,001
43.7,,0012
44.7,,0015
*FAILURE RATIOS
1.15,,055
*TENSION STIFFENING, TYPE=STRAIN
1.,0.
.55,,0035
.25,,025
0.,.05
*BOUNDARY
SUPPORT,2
CENTRE,1
*STEP
*STATIC,RIKS
0.05,1,,,,,91,2,-3.
*CLOAD
10,2,-4000.
*EL PRINT, POSITION=AVERAGED AT NODES, SUMMARY=YES
S11,E11
*NODE FILE, NSET=CENTRE
U,CF,RF
*OUTPUT,FIELD,VARIABLE=PRESELECT
*ELEMENT OUTPUT
*OUTPUT,HISTORY
*NODE OUTPUT, NSET=SUPPORT
RF2
*NODE OUTPUT,NSET=CENTRE
U2
*END STEP
```

D.6 ABAQUS INPUT FILE FOR BEAM ELEMENT

```
*HEADING
REINFORCED BEAM UNDER 4 POINT LOAD, 6% PRSF, 150x150x550mm
*NODE
1,,,,1.
23,550.
*NGEN, NSET=NALL
1,23,1
*NSET,NSET=SUPPORT
3,
*NSET,NSET=CENTRE
12,
*ELEMENT,TYPE=B21
1,1,2
*ELGEN,ELSET=EALL
1,22,1,1
*BEAM SECTION,SECTION=RECT,MATERIAL=FIBRECON,ELSET=EALL
150.,125.
*MATERIAL,NAME=FIBRECON
*ELASTIC
30500.,0.2
*CONCRETE
12.86,0.
16.97,.0002
20.5,.0004
23.44,.0006
25.79,.0008
27.5,.001
28.78,.0012
29.4,.0015
*FAILURE RATIOS
1.15.,18
*TENSION STIFFENING, TYPE=STRAIN
1.,0.
.7,.001
0.,.04
*STEP
*STATIC,RIKS
0.2,1,,,,12,2,-4.
*BOUNDARY
3,2
21,1,2
*CLOAD
9,2,-4000
15,2,-4000
*EL PRINT, POSITION=AVERAGED AT NODES,SUMMARY=YES
SF1,SM1,SK1
*NODE FILE, NSET=NALL
U,RF
*NODE PRINT
U,RF
*OUTPUT,FIELD,VARIABLE=PRESELECT
*ELEMENT OUTPUT
*OUTPUT,HISTORY
*NODE OUTPUT,NSET=SUPPORT
RF2
*NODE OUTPUT,NSET=CENTRE
U2
*ELEMENT OUTPUT, ELSET=EALL
SM1,SK1
*END STEP
```

APPENDIX E TESTS IMAGES

E.1 IMAGES RELATED TO CHAPTER FLEXURAL TESTS



Timber moulds 150mm x15mm 550mm



VSF fibre mixed with concrete



6% VSF fibre concrete after mixing



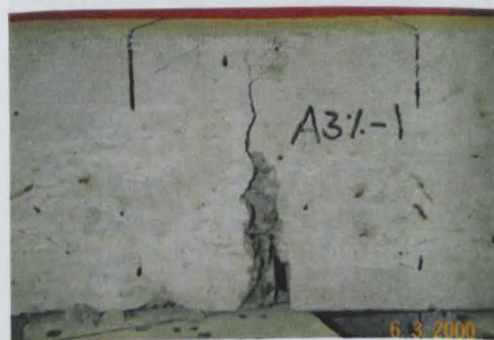
Crack propagation, 1.5% PRSF



Crack propagation, 1.5% PESF



Crack propagation, 3% PESF



Central Crack propagation, 3% PRSF



Inclined crack propagation, 3% PRSF



Central crack propagation, 6% PRSF



Central crack propagation, 3% PRSF



Inclined crack propagation, 6% PRSF



Incline crack propagation, 6% PRSF



Inclined crack propagation, 1.5% PRSF



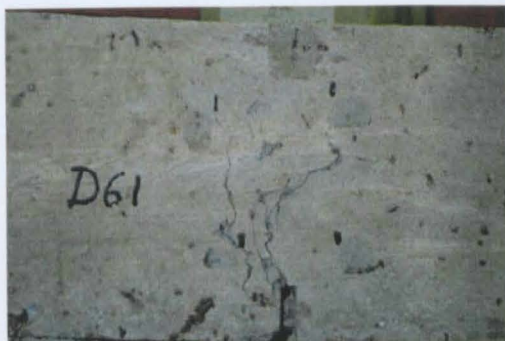
Multi cracking, 6% ISF-1



Inclined crack propagation, 6% ISF-1



Inclined crack propagation, 6% ISF-1



Multi crack propagation, 6% ISF-2



Single crack propagation, 6% ISF-2



Multi crack propagation, 6% ISF-2



Crack outside the notch, 3% VSF



Inclined crack propagation, 3% VSF



Multi crack propagation, 3% VSF



Central crack propagation, 6% VSF



Crack outside the notch, 6% VSF



Incline crack propagation, 1.5% VSF



Crack outside the notch, 1.5% VSF



Central crack propagation, 0.5% SRSF



Central crack propagation, 0.5% SRSF



Inclined crack propagation, 1% SRSF



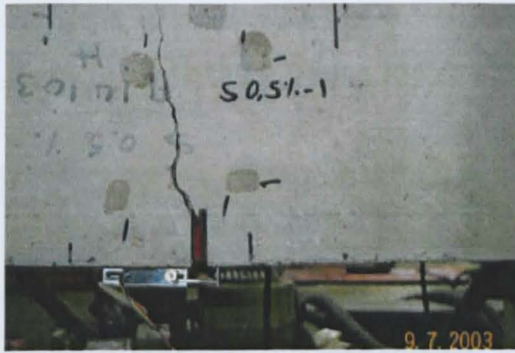
Central crack propagation, 2% SRSF



Inclined crack propagation, 2% SRSF



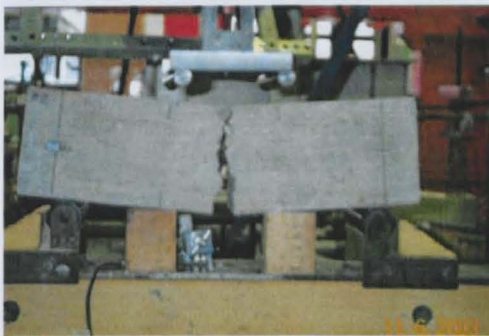
Inclined crack propagation, 2% SRSF



Inclined crack propagation, 0.5% SRSF



Inclined crack propagation, 1.0% SRSF



Failure of plain concrete prism



Failure of plain concrete prism

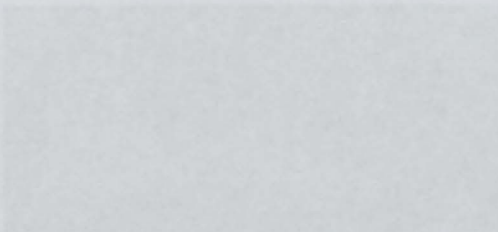
LVDT's location on slab underside



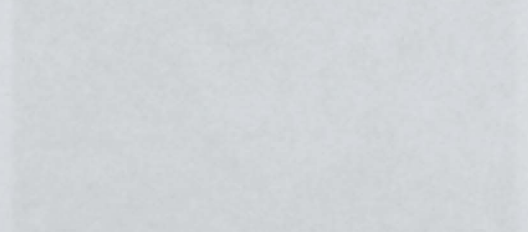
Failure at rib edge



Failure at rib edge



Failure of floor slab

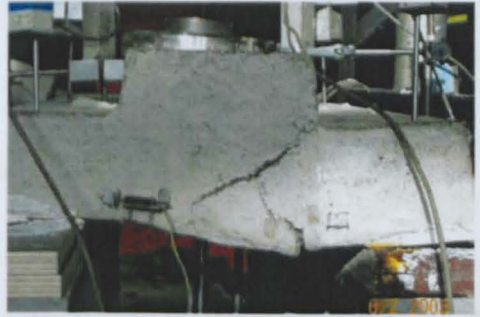


Failure of floor slab at supports

E.2 IMAGES RELATING TO SLAB TESTS



Casting of Scon slab, 2% SRSF



Testing of Scon slab, 2% SRSF



LVDT's located on slab underneath



Measurement of deflection and crack width



Failure at rib edge



Failure at slab rib centre



Failure of Rcon slab



Failure of Rcon slab at support

APPENDIX F SECTIONAL ANALYSIS



Incline cracks in 100x100x500mm prism reinforced with 6% PRSF



Crack, 2% SRSF

Crack outside the central axis, 2% SRSF



Crack in a SIScon beam

Crack at the bottom of a SIScon beam



Figure F1 Proposed stress-strain model

APPENDIX F SECTIONAL ANALYSIS

The aim of this analysis is to determine the σ - ε curve, the stress reduction factor $\phi = \sigma_1 / \sigma_i''$ and the normalised moment capacity for a beam reinforced with a fibre type that has not been tested within this work. The parameters needs are only the area under load-deflection curve up to 3mm and the compressive strength of the beam.

$$A_{\sigma-\varepsilon} = \frac{G_{F2}}{l_c} \quad (F1)$$

$$G_{F2} = A_{P-\delta} / b \cdot yh \quad (F2)$$

where

$A_{\sigma-\varepsilon}$ Area under the stress-strain curve for the new SFRC beam [N/mm²]

G_{F2} Energy released by unit area [N/mm]

$A_{P-\delta}$ Area under the load deflection curve obtained by four-point bending test [Nmm]

b Beam sectional width [mm]

yh Neutral axis position [mm]

l_c Critical length (Table D.1)

Given $A_{\sigma-\varepsilon}$, the stress reduction factor can be calculated using the Figure F1

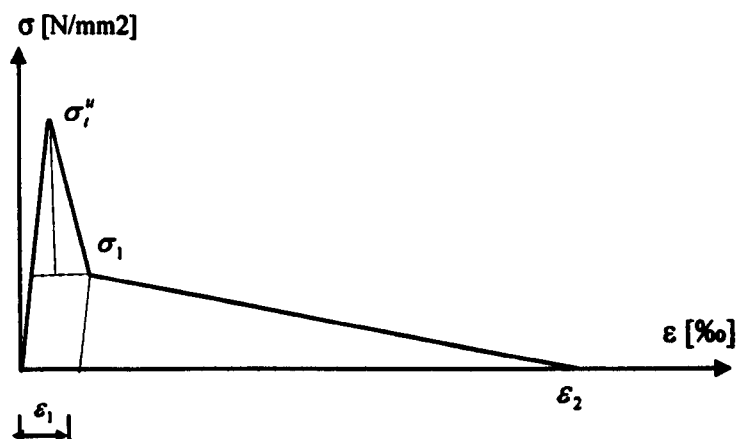


Figure F1 Proposed stress-strain model

$$A_{\sigma-\varepsilon} = \frac{(\sigma_i^u - \sigma_1) \cdot \varepsilon_1 + \sigma_1 \cdot (\varepsilon_2 - \varepsilon_1)}{2} + \sigma_1 \cdot \varepsilon_1 \tag{F3}$$

$$\phi_{cal} = \frac{\sigma_1}{\sigma_i^u} = \frac{2A_{\sigma-\varepsilon}}{\sigma_i^u \cdot \varepsilon_2} - \frac{\varepsilon_1}{\varepsilon_2}$$

To test the reliability of the equation (F2), the stress reduction factors for the fibres investigated in this work were also calculated by using the average l_c and the corresponding $A_{\sigma-\varepsilon}$. It can be seen that the result were satisfied in comparison to that by FE analysis (Table 6.1) and proposed model (Table 6.2) determined values.

Table 6.3 Calculation of Φ_{cal} factors

Fibre type	Fibre ratio [%]	G_{F2} [N/mm]	Aver l_c [mm]	$A_{\sigma-\varepsilon}$ [N/mm ²]	Φ_{cal} [-]	Φ_{FEA} [-]	Φ_{model} [-]
VSF	1.5	2.28		0.033			
	3.0	4.05	66.6	0.059	0.66	0.65	0.7
	6.0	5.52		0.080			
PESF	1.5	2.26		0.033			
	3.0	3.17	70.2	0.046	0.61	0.61	0.6
	6.0	5.30		0.077			
ISF-1	6.0	6.27	69.7	0.091	0.71	0.7	0.73
ISF-2	6.0	6.19	72.3	0.090	0.74	0.7	0.71
SRSF	0.5	0.84		0.012			
	1.0	1.40	65.1	0.020	0.38	0.4	0.38
	2.0	2.13		0.031			

The normalised design moment at the ultimate limit state can be determined using the internal equilibrium condition as shown in Figure F2 as follows.

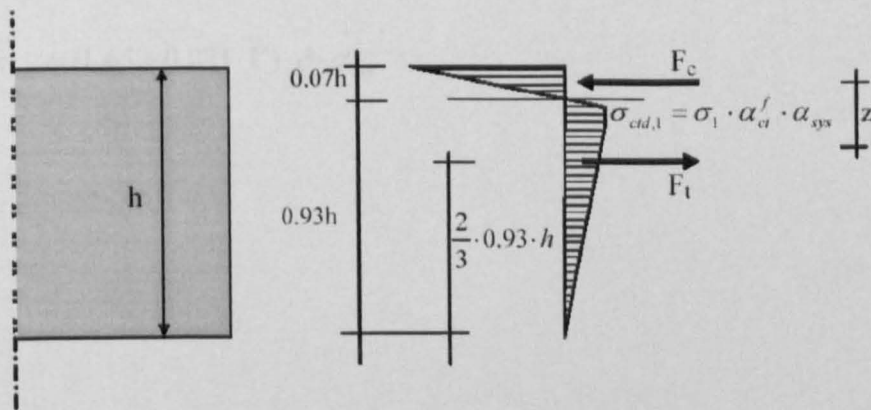


Figure F2 Internal forces at ultimate limit state

$$F_i = \sigma_{cd} \cdot \frac{0.93h}{2} b$$

$$\sigma_{cd} = \sigma_1 \cdot 0.85 \cdot \alpha_{sys} / 1.3 = 0.65 \cdot \sigma_1 \cdot \alpha_{sys} \quad (F4)$$

$$\sigma_1 = \sigma_i^u \cdot \phi$$

$$\sigma_i^u = \sigma_{i,p} (1 + 0.32 \cdot v)$$

$$\sigma_{i,p} \approx 0.1 \cdot f_{ck}$$

$$V = v / D$$

where

v Fibre ratio by weight

D Concrete density = 25 kN/m³

$$\sigma_1 = 0.1 \cdot f_{ck} \cdot (1 + 0.32 \cdot V / 25) \cdot \phi = 0.1 \cdot f_{ck} (1 + 0.0128 \cdot V) \cdot \phi$$

$$z = \frac{1}{3} \cdot 0.93h + \frac{2}{3} \cdot 0.07h = 0.36h \quad (F5)$$

$$M_{cd} = F_i \cdot z \quad (F6)$$

Using equations (F5) and (F6) with respect to Figure 6.24 and the safety and reduction factors, the design moment can be expressed as

$$M_{cd} = 0.65 \cdot ((0.1 \cdot f_{ck} (1 + 0.0128 \cdot V) \cdot \phi) \cdot \alpha_{sys} \cdot (\frac{0.93h}{2} \cdot h \cdot b)) \cdot 0.36h$$

$$\frac{100M_{cd}}{1.5 \cdot f_{ck} \cdot h^2 \cdot b} = \frac{m_{cd}}{1.5} = (1.1 + 0.014 \cdot V) \cdot \phi \cdot \alpha_{sys}$$

$$m_{cd} = (1.65 + 0.021 \cdot V) \cdot \phi \cdot \alpha_{sys}$$